

University of Bath



PHD

Construction of an equivalent circuit for induction motors used with variable supply frequency, including inverter-fed applications.

Pouya, Firouz

Award date:
1979

Awarding institution:
University of Bath

[Link to publication](#)

General rights

Copyright and moral rights for the publications made accessible in the public portal are retained by the authors and/or other copyright owners and it is a condition of accessing publications that users recognise and abide by the legal requirements associated with these rights.

- Users may download and print one copy of any publication from the public portal for the purpose of private study or research.
- You may not further distribute the material or use it for any profit-making activity or commercial gain
- You may freely distribute the URL identifying the publication in the public portal ?

Take down policy

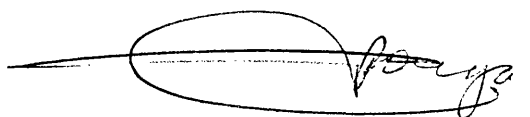
If you believe that this document breaches copyright please contact us providing details, and we will remove access to the work immediately and investigate your claim.

CONSTRUCTION OF AN EQUIVALENT CIRCUIT FOR
INDUCTION MOTORS USED WITH VARIABLE SUPPLY
FREQUENCY, INCLUDING INVERTER-FED APPLICATIONS

submitted by Firouz Pouya C.Eng. MIEE
for the degree of PhD
of the University of Bath
1979

COPYRIGHT

Attention is drawn to the fact that copyright of this thesis rests with its author. This copy of the thesis has been supplied on condition that anyone who consults it is understood to recognise that its copyright rests with its author and that no quotation from the thesis and no information derived from it may be published without the prior written consent of the author. This thesis may be made available for consultation within the University Library and may be photocopied or lent to other libraries for the purpose of consultation.

A handwritten signature in black ink, appearing to read 'F. Pouya', is written over a horizontal line.

F. Pouya

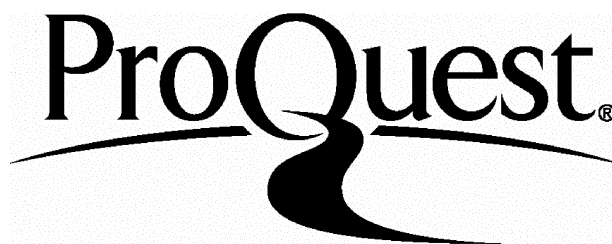
ProQuest Number: U442887

All rights reserved

INFORMATION TO ALL USERS

The quality of this reproduction is dependent upon the quality of the copy submitted.

In the unlikely event that the author did not send a complete manuscript and there are missing pages, these will be noted. Also, if material had to be removed, a note will indicate the deletion.



ProQuest U442887

Published by ProQuest LLC(2015). Copyright of the Dissertation is held by the Author.

All rights reserved.

This work is protected against unauthorized copying under Title 17, United States Code.
Microform Edition © ProQuest LLC.

ProQuest LLC
789 East Eisenhower Parkway
P.O. Box 1346
Ann Arbor, MI 48106-1346

CONTENTS

Page

Abstract.

Acknowledgements.

List of Symbols.

List of Figures.

CHAPTER 1 OBJECT OF THE THESIS

- | | | |
|-----|---|---|
| 1.1 | Introduction. | 1 |
| 1.2 | Effect of frequency variation on the circuit parameters. | 2 |
| 1.3 | Effect of the parameter variations and voltage saturation on the performance characteristics. | 3 |
| 1.4 | Determining the exact additional losses in the induction motors due to harmonic frequencies. | 5 |

CHAPTER 2 THE CONSTRUCTION OF AN EQUIVALENT CIRCUIT FOR INDUCTION MOTORS USED WITH VARIABLE SUPPLY FREQUENCY, INCLUDING INVERTER-FED APPLICATIONS

Summary.

- | | | |
|-------|--|----|
| 2.1 | Introduction. | 7 |
| 2.2 | The induction motor equivalent circuit. | 9 |
| 2.3 | Measurement of experimental results. | 13 |
| 2.4 | Evaluation of the magnetising branch parameters for variable speed applications. | 14 |
| 2.4.1 | Experimental results. | 15 |
| 2.5 | Evaluation of the primary and secondary equivalent circuit parameters for variable speed applications. | 16 |
| 2.5.1 | Program description and experimental results. | 17 |

	<u>Page</u>
2.6 Application of the new equivalent circuit for superimposed modulation frequencies.	19
2.6.1 Experimental results.	20
2.7 Errors introduced in the performance calculations, when the fixed frequency equivalent circuit is used in variable frequency applications.	22
2.7.1 Comparison of results.	22
2.8 Conclusions.	23
Bibliography.	25

CHAPTER 3 ANALYSIS OF THE NEW EQUIVALENT CIRCUIT
AND CONSTRUCTION OF A NON-LINEAR MODEL
FOR INDUCTION MOTORS USED IN VARIABLE
SPEED APPLICATIONS

Summary.

3.1 Introduction.	27
3.2 Literature review.	29
3.3 Part one.	37
3.3.1 Analysis of the new linear equivalent circuit.	37
3.3.2 The actual rotor circuit per phase.	38
3.3.3 The equivalent rotor circuit.	39
3.3.4 Calculation of performance.	41
3.3.5 Starting torque.	42
3.3.6 Torque speed characteristics.	43
3.3.7 Measurement of experimental results.	48
3.3.8 Digital program description of torque speed characteristics.	50
3.3.9 Experimental results.	52
3.4 Part two.	53
3.4.1 The construction of a non-linear model for induction motors in variable speed applications.	53

	<u>Page</u>
3.4.2 Effect of saturation on leakage reactances.	53
3.4.3 Experimental results.	55
3.4.4 Effect of saturation on the magnetising branch parameters.	56
3.4.5 Model representation of magnetising branch parameters.	59
3.4.6 Program description of the non-linear model.	60
3.4.7 Reduction in the shaft torque due to voltage saturation.	63
3.5 Discussion of results.	63
3.6 Conclusions.	70
Bibliography.	71

CHAPTER 4 COMPARISON AND HARMONIC ANALYSIS OF THE PULSE WIDTH MODULATED INVERTERS WHEN FEEDING INDUCTION MOTORS

Summary.

4.1 Introduction.	75
4.2 Literature review.	80
4.3 General technique of harmonic analysis for stepped wave output inverters.	90
4.3.1 Analysis of three-phase stepped wave output inverters.	93
4.4 Analysis of inverters with adjustable output voltage by chopping technique, also known as "sub-oscillation".	93
4.5 Analysis of inverters operating in linear sub-oscillation.	94
4.6 Analysis of inverters operating in sinusoidal sub-oscillations.	97
4.6.1 Analysis of inverters using triangular wave forms to generate the modulation pulses.	99
4.6.2 Analysis of inverters using inductive load currents and boundary limits to generate modulation pulses.	108

	<u>Page</u>
4.7 Program description of inverters using triangular waveforms as reference.	110
4.7.1 Discussion of results.	112
4.8 Program description of inverters using load current and boundary limits to generate the modulation pulses.	113
4.8.1 Discussion of results.	115
4.9 Effect of a variable frequency induction motor equivalent circuit on the inverter efficiency calculations (harmonic losses only are considered).	116
4.9.1 Efficiency calculation of inverter type using triangular waveforms as reference.	117
4.9.2 Efficiency calculation of inverter type using load current as reference.	119
4.10 Comparison of inverters using triangular waveform and load current as the reference signals.	120
4.11 Conclusions.	121
Bibliography.	125
<u>CHAPTER 5</u> <u>CONCLUSIONS AND SUGGESTIONS FOR FURTHER WORK</u>	
5.1 Conclusions.	131
5.2 Suggestions for further work.	132
<u>APPENDIX A</u>	
A.1 Part one.	A1
A.1.1 Checking the meter readings at different frequencies.	A1
A.1.2 Examination of the sensitive phase meter readings.	A5
A.2 Part two.	A6
A.2.1 Determination of the rated applied volts-per-hertz.	A6
A.2.2 Calculation of the equivalent circuit parameters.	A7

	<u>Page</u>
A.3 Part three.	A9
A.3.1 Evaluation of equivalent RL network from frequency response, using circle fit technique.	A9
A.4 Part four.	A11
A.4.1 Modulation technique.	A11

APPENDIX B DESIGN DETAILS OF INERTIA MACHINE FOR
PLOTTING TORQUE SPEED CHARACTERISTICS
OF HIGH SPEED INDUCTION MOTORS

B.1 Introduction.	B1
B.2 Design of the inertia disc.	B3
B.3 Transverse vibrations and whirling speeds.	B4
B.4 The transverse vibration of a beam with two concentrated masses.	B6
B.5 The determination of whirling of the circular shaft with gyroscopic effects.	B10
B.5.1 Determination of L_{11} .	B12
B.5.2 Determination of L_{12}, L_{21} .	B13
B.5.3 Determination of L_{22} .	B14
B.6 The torque transducer.	B16
B.7 Digital tacho design.	B18
B.8 Results and conclusions.	B19
Bibliography.	B20

ABSTRACT

The following chapters give details of the construction of a new equivalent circuit for induction motors used in variable and modulated frequency supplies and one of its advantages for the determination of the additional losses in the machine due to harmonic frequencies.

Chapter 1 includes the aim of the work and briefly explains the reason for obtaining such a model and its applications.

In Chapter 2 the technique of constructing the new equivalent circuit is given. This is done as follows. With the aid of a digital computer and circle fit technique the frequency responses of the open and short circuit test results taken at various supply frequencies are used to find the values of the new equivalent circuit parameters. The new equivalent circuit takes care of the parameter changes arising from different supply frequencies and produces the correct input and output performance characteristics. The new equivalent circuit also produces the exact responses for mixed and modulated frequencies.

In Chapter 3 the new equivalent circuit is analysed and performance equations are derived. This enables changes in the performance characteristics at different supply frequencies to be calculated directly from the performance equations.

Using a digital computer the non-linear model of the induction motor is constructed from the test results for variable speed applications. The magnitude of the errors introduced in calculating the machine's performance characteristics are determined using the linear model in the non-linear region. Their magnitude becomes greater with the increasing value of the rotor speed or the supply frequency.

An accurate torque speed plotting machine for extremely high speed induction machines is designed and constructed. Highly accurate results are achieved by sensing the rotor torque and speed without any physical contact with the rotor.

In Chapter 4 the Fourier series analysis is used to analyse and derive the output harmonic contents of two popular types of inverter. The additional losses in the machine due to these harmonic frequencies of both inverter types are determined and compared. The new equivalent circuit is used to determine the magnitude of the errors induced in the calculation of these additional losses if the standard equivalent circuit is used.

ACKNOWLEDGEMENTS

The author would like to thank all those concerned in the work involved in this thesis.

In particular to thank my supervisor, Professor K.V. Diprose, without whose help and guidance this thesis would not have been possible.

I would also like to express my gratitude to Professor B.M. Bird for his permission to use the generator sets at Bristol University, and to the staff there for assistance in providing the necessary test facilities. I must also thank Mr. R.C. Eyre for his permission to use the air tunnel variable frequency generator in the Aerospace Department, Royal Aircraft Establishment, Farnborough, and the staff for their kind assistance.

Finally the author would like to extend his gratitude to all in the Department of Electrical and Electronic Engineering, University of Bath, for their help throughout the period of his research.

LIST OF PRINCIPLE SYMBOLS

A	Constant.
B	Flux density (Chapter 2) and temperature rise per hertz (Chapter 3).
B_{mm}	Maximum flux density.
C	Capacitance.
DZ	Slit width.
E	d.c. supply voltage and Young's elastic modulus (Appendix B).
E_1	Gap voltage.
E_2	Modulus of the line frequency voltage induced in the secondary circuit.
\bar{E}_2	Line frequency voltage induced in the secondary circuit.
e	Phase voltage (Appendix A).
F_1	Stator frequency.
F_m	Modulation frequency.
F_r	Rotor frequency.
f_1, f_2	Force.
H_n	Angular momentum.
I	Second moment of area.
I_L	Load current.
$I_{L(0)}$	Initial load current.
I_m	Magnetising branch current.
$I_{O/c}$	Open circuit line current.
$I_{S/c}$	Short circuit line current.
I_S	Starting current

I_{xx}	Second moment of inertia in x direction.
I_{yy}	Second moment of inertia in y direction.
$I_{1,2,3}$ and $i_{1,2,3}$	Line currents.
J	Integer number.
K, K', K_e K_h, K_2	Constants.
L	Inductance.
L_{11}	Maximum deflection at the end of the shaft due to force f_1 .
L_{12}	Maximum deflection at the end of the shaft due to moment M .
L_{21}	Maximum slope at the end of the shaft due to force f_1 .
L_{22}	Maximum slope at the end of the shaft due to moment M .
m	Number of motor phases (Chapters 2 and 3) and number of chops per cycle (Chapter 4).
m_1, m_2	Mass.
n	Harmonics order.
n_s	Synchronous speed.
P_e	Eddy current loss.
P_h	Hysteresis loss.
P_g	Power transferred across the airgap.
P_n	n th harmonic power.
$P_{o/c}$	Open circuit per phase power.
$P_{s/c}$	Short circuit per phase power.

R_1	Stator resistance.
R_2	Rotor resistance.
R_L	Resistive part of the load impedance.
R_m	Resistive part of the magnetising impedance.
RP_1	Stator correction resistor.
RP_2	Rotor correction resistor.
R_{mech}	Mechanical shaft load.
R_{v_1}, R_{v_2}	Moment.
$R_1(t)$	Temperature dependent stator resistance.
r	Ratio of the saw tooth to sine wave voltage.
S	Rotor slip due to supply frequency and number of sub-oscillations (Chapter 4).
S_m	Rotor slip due to modulation frequency and rotor slip at maximum torque (Chapter 3).
T	Shaft torque (Chapters 2 and 3) and the period of the fundamental voltage (Chapter 4).
T_L	Load time constant (Chapter 4).
T_S	Starting torque (Chapter 3).
T_m	Maximum torque (Chapter 3).
T_o	Period of sub-oscillations.
t	Lamination thickness (Chapter 2) and temperature (Chapter 3).
t_1	Initial temperature (Chapter 3) and conduction period (Chapter 4).
t_2	Off period (Chapter 4).
V_A, V_B and V_C	Referred voltages.

V_n	nth harmonic voltage.
V_1	Input terminal voltage.
$V_{o/c}$	Open circuit phase voltage.
$V_{s/c}$	Short circuit phase voltage.
V_C	Amplitude of the sine wave voltage.
V_S	Amplitude of the saw tooth voltage.
$W_{1,2}$	Wattmeter readings.
X_1	Stator reactance.
X_2	Rotor reactance.
X_m	Magnetising reactance.
X_L	Reactive part of the load impedance.
$X_{o/c}$	Open circuit phase reactance.
Y_1, Y_2	Deflection.
Z_m	Magnetising branch impedance.
Z_2	Secondary impedance.
Z_2'	Equivalent magnetising and rotor impedance.
Z_{22}	Rotor impedance transferred to primary.
Z_L	Load impedance.
Z_p	Phase impedance.
Z_s	Per-phase source impedance.
$Z_{o/c}$	Open circuit impedance.
$Z_{s/c}$	Short circuit impedance.

α_1, α_2 and α_3	Phase angles.
ϕ_m	Magnetising circuit phase angle.
ϕ_2	Rotor phase angle.
ϕ_{22}	Equivalent rotor phase angle transfer to primary.
θ	Sine wave phase angle.
ϵ	Small error.
ω_s	Supply frequency.
ω_n	Synchronous speed, and in Appendix B the transverse vibration frequency.

LIST OF FIGURES

- 2.1 Standard induction motor equivalent circuit.
- 2.2 New frequency dependent induction motor equivalent circuit.
- 2.3 Locus diagram of the magnetising branch at rated volts-per-hertz for a given applied volts per hertz.
- 2.4 Locus diagram of short circuit test results at rated line current.
- 2.5 Flow diagram of the search technique.
- 2.6 Locus diagram of the rotor circuit at unity slip.
- 2.7 Locus diagram of the per phase impedance obtained from modulation frequencies.
- 2.8 Locus diagram of phase input impedance.
- 2.9 Starting and maximum torque at various frequencies.

- 3.1 Flux density characteristic of the iron.
- 3.2 Power flow diagram in equation form.
- 3.3 Typical torque speed curve for a three-phase induction motor.
- 3.4 Temperature rise during acceleration of a given load versus supply frequency.
- 3.5 Flow diagram of the linear model for determination of torque speed characteristics.
- 3.6-3.14 Torque versus slip at supply frequencies from 10 Hz up to 320 Hz in steps of 40 Hz.
- 3.15 Short circuit characteristics.
- 3.16 Starting torque versus volts-per-hertz squared.
- 3.17 Effect of saturation on the shape of the airgap flux wave.
- 3.18 Open circuit characteristics.
- 3.19 Open circuit per phase impedance per hertz versus magnetising current.

- 3.20 $\cos\psi_m$ versus magnetising current.
- 3.21 Phase impedance per hertz versus supply frequency in the non-linear region.
- 3.22 Flow diagram of the non-linear model.
- 3.23 Percentage of reduction in torque due to the non-linearity of the machine versus rotor slip.
- 3.24 Torque speed characteristics on a three dimensional axis.
- 3.25 Locus diagram of the magnetising branch.

- 4.1 Circuit diagram of a basic stepped wave inverter system.
- 4.2 Voltage waveforms obtained from a basic inverter system.
- 4.3 Circuit diagram of a three-phase basic inverter system.
- 4.4 Modulated waveform obtained from a three-phase basic inverter system.
- 4.5 Typical pulse width modulated waveform.
- 4.6-7 Typical control waveform of a PWM system.
- 4.7a The frequency spectrum of the symmetrical and asymmetrical PWM techniques.
- 4.8 Typical PWM waveform obtained from a slit width modulation technique.
- 4.9 Flow diagram of a predetermined PWM technique.
- 4.10 Fundamental output voltage versus reference sine wave, inverters using triangular wave as reference.
- 4.11 Fundamental output voltage versus the number of pulses per cycle, inverters using triangular wave as reference.
- 4.12 Level of the harmonic content versus the number of pulses per cycle, inverters using triangular wave as reference.
- 4.13 Efficiency versus the number of pulses per cycle, inverters using triangular wave as reference.
- 4.14 Total power in pulses over a half cycle versus sine wave amplitude, inverters using triangular wave as reference.

- 4.15 Harmonic content versus reference sine wave amplitude, inverters using triangular wave as reference.
- 4.16 Flow diagram for the determination of DZ.
- 4.17 Flow diagram of slit width inverter.
- 4.18 Fundamental frequency versus number of pulses in a half cycle and normalised fundamental voltage, inverters using slit width technique.
- 4.19 Inverter output frequency versus output harmonic content, inverters using slit width technique.
- 4.20 Efficiency versus the number of pulses per cycle, inverters using slit width technique.
- 4.21 Slit width versus the number of pulses, inverters using slit width technique.
- 4.22 Harmonic content versus the number of pulses, inverters using slit width technique.
- 4.23 Total power pulses over a half cycle versus the number of pulses, inverters using slit width technique.
- 4.24 Inverter efficiency (harmonic losses only) versus the rotor slip with slit width proportional to line current.
- 4.25 Inverter efficiency (harmonic losses only) versus the output fundamental frequency, inverters using triangular wave as reference.
- 4.26 Inverter efficiency (harmonic losses only) versus amplitude of sine wave with frequency dependent model as load.
- 4.27 Inverter efficiency (harmonic losses only) versus fundamental output frequency, inverters using slit width technique.
- 4.28 Load current versus the fundamental output frequency, both inverters driving the same load.
- 4.29 Efficiency of both types of inverters when supplying the same load versus fundamental output frequency.

- A(1) Two-wattmeter method of measuring three-phase power.
- A(2) Vector diagram of the two-wattmeter method.

- A(3) Series, parallel RL network.
- A(4) Locus diagram of RL network.
- A(5) Open circuit characteristics at 50 Hz.
- A(5a) Per phase equivalent circuit.
- A(6) Parallel RL circuit.
- A(7) Locus diagram of parallel RL circuit.
- A(8) Circuit diagram of the modulation technique.
- A(9) Equivalent circuit seen by the modulation signal.

- B(1) Photograph of the torque speed plotting machine.
- B(2) Photograph of the inertia discs.
- B(3) Deflection diagram of simple beam.
- B(4) Deflection diagram of a beam due to concentrated mass at one end.
- B(5) A phase rectifier and sampling circuit diagram.
- B(6a) Standard Wein bridge oscillator.
- B(6b) Modified Wein bridge oscillator.
- B(7) Temperature characteristic of the oscillator outputs.
- B(8) Transducer output versus the angle of rotation.
- B(9) Circuit diagram of the digital tacho.
- B(10) Digital tacho output voltage versus the rotor speed.
- B(11) - Torque speed characteristics from 10 Hz up
B(31) through 100 Hz in steps of 10 Hz and from
100 Hz to 320 Hz inclusive in steps of 20 Hz.

CHAPTER 1

OBJECTS OF THE THESIS

1.1 Introduction

After the announcement of the silicon controlled rectifiers in the late 1950's, attention was immediately focussed on the application of this device in the power inverters for variable speed drives. One area of the application was speed control of induction motors normally classified as constant speed drives.

Before the arrival of the power SCR's, induction motors were designed to run from constant frequency supplies, although the Ward Leonard system was employed in some cases. Thus an equivalent circuit is introduced for constant frequency applications. This equivalent circuit can easily relate the output characteristics of the motor to some small number of identifiable circuit parameters at the design frequency. The circuit parameters are normally determined at the design frequency and do not necessarily represent the exact behaviour of the machine with other supply frequencies.

The main object of this thesis is to investigate the behaviour of the circuit parameters with different applied frequencies. This investigation is not introduced to aid the design of induction motors for variable speed applications. It is designed to point out the changes in the circuit parameters arising from different applied frequencies and to give a simple technique of modifying the standard equivalent circuit

model into a frequency dependent form, which will represent the exact behaviour of a given motor at any applied frequency. A three-phase, three horsepower induction motor is used as an example to illustrate the proposed method.

The effect of non-linearities on the performance characteristic and technique of modelling them from test results is also investigated. The errors introduced in the performance characteristic using the linear model in this region are determined and given. A similar analysis of the standard equivalent circuit is applied to the new frequency dependent model to derive the performance equations. One of the applications of such a model in determining the additional losses due to harmonic frequencies is allowing the efficiency of any type of inverter to be calculated.

1.2 Effect of Frequency Variation on the Circuit Parameters

From an inverter designer's point of view, the equivalent circuit parameters must represent all the required characteristics with any applied frequency. Two different experiments are set to find out these parameter variations.

(a) The standard equivalent circuit parameters are determined at various supply frequencies, using the standard locked rotor and light running tests. The locus diagram of the magnetising branch parameters is

plotted. Then, the circle fit technique is employed to form an RL network to represent the behaviour of the magnetising branch at any applied frequency. Also with the aid of a digital computer similar forms of RL networks are found to replace the primary and secondary reactances. During the process of searching for the equivalent RL networks, the exact ratio of primary and secondary leakage reactances are determined.

(b) The second experiment is set to determine the relationship between modulation frequency and equivalent circuit parameters. A known modulation frequency is injected into the line current. The injected frequency is then varied and the response of the circuit parameters to this frequency alone is observed, with the machine operating under various load conditions. The technique employed to inject the modulation frequency and determine the parameter variations is fully detailed in Chapter 2, Section 6.

From the results of the above investigations a linear equivalent circuit model is constructed.

1.3 Effect of the parameter variations and voltage saturation on the performance characteristics

In order to investigate the effect of changes in the parameters with different supply frequencies on the performance calculations, the new equivalent circuit is analysed and performance equations are derived. With the aid of a digital computer the performance characteristics are computed from these equations and compared

with the experimental results. This confirms that the effect of parameter variations on the performance characteristics can be calculated directly from the new equivalent circuit.

All the experimental results are obtained by the design and development of an extremely accurate torque speed plotting machine. It is important to achieve highly accurate results, because the changes in the machine performance due to parameter variations are very small. Therefore the introduction of sizeable errors in the results would swamp the required variations. The effect of temperature rises during the acceleration of the load on the stator resistance is observed and accounted for on the computer program.

The non-linear model of the machine is also constructed to determine the magnitude of errors introduced in the performance calculations if the linear model is used. Various experiments are then designed to identify the nature of changes in the equivalent circuit parameters with voltage saturation. The results are used to produce the non-linear relationship between the parameters and applied volts-per-hertz and frequency. A digital program is developed which alters the values of the parameters according to the applied voltage, frequency and load condition. The torque speed characteristics are computed from the non-linear model when the applied volts-per-hertz is above the rated value. These characteristics are then compared with the linear model characteristics to determine the amount of reduction in the rotor torque.

The reduction in torque in the non-linear region is mainly due to the saturation of the machine's yoke and it becomes greater when the rotor speed approaches the synchronous speed and also with higher values of the supply frequencies.

1.4 Determining the exact additional losses in the induction motors due to harmonic frequencies

The output waveform of the inverter supplies contains the fundamental frequency plus additional switching frequencies. The fundamental voltage sets the main energising current through the machine. The harmonic voltages set additional currents through the windings resulting in additional losses in the form of heat or pulsation torques which are damped out by the load inertia. With higher orders of the harmonics the relative rotor slip approaches unity. Therefore the majority of the additional losses are dissipated in the form of heat in the resistive part of the machine. Only a small portion of these losses are converted to mechanical power. The magnitude and sign of these harmonic torques depend on the order of the harmonics. The standard equivalent circuit is normally used with various assumptions to determine these additional losses. This introduces errors which become especially large with higher orders of the harmonics. This is because the resistive and inductive part of the machine no longer remain constant. The resistive part becomes larger and the inductive part becomes smaller with the higher applied

frequencies. In this way the changes in the load impedance produce higher additional losses at higher harmonic frequencies compared with those obtained from frequency independent loads such as the standard equivalent circuit. Therefore the new equivalent circuit no longer has this drawback and produces the exact figures at any frequency.

The Fourier series analysis is applied to analyse the output waveforms of two popular types of inverters. The additional harmonic losses are then calculated, firstly by employing the standard induction motor equivalent circuit as the load, and secondly by employing the new equivalent circuit. The difference between the two sets of results gives one of the advantages of the new equivalent circuit for determining the realistic figures. Finally Fourier series analysis is applied to compute the efficiency of two popular inverters operating under the same conditions, for example running from the same supply rails, producing an equal number of pulses per cycle, the same fundamental frequency output and delivering equal amounts of power into the load.

All the efficiency calculations are based on the magnitude of additional harmonic losses only. The losses in the inverter system such as switching losses in the power devices, commutation networks etc. are not considered, because these losses have no relation to the nature of the load when delivering a given amount of output power.

CHAPTER 2

THE CONSTRUCTION OF AN EQUIVALENT CIRCUIT FOR INDUCTION MOTORS USED WITH VARIABLE SUPPLY FREQUENCY, INCLUDING INVERTER-FED APPLICATIONS

Summary

In this chapter the effect of changes in the supply and modulation frequencies on the induction motor equivalent circuit parameters are identified. Using a circle fit technique, the frequency responses of the short and open circuit test results are used to determine the frequency dependent RL networks and hence construct the new equivalent circuit for variable speed applications. This equivalent circuit produces the exact responses for mixed and modulated frequencies. The errors involved in the performance calculations, using the fixed frequency equivalent circuit in variable frequency applications, are also given.

2.1 Introduction

Since the introduction of the induction motor equivalent circuit for constant frequency applications, all the design data and performance equations have been based around its parameters. The standard induction motor equivalent circuit is shown in figure 2.1. If each phase of a polyphase induction motor is identical, then the equivalent circuit is taken to represent one such phase. Most standard electrical machine text books ^{2.1}, develop the performance equations from the standard equivalent circuit; although the simplified equivalent is often used. Many other complex equivalent circuits ^{2.2,2.3,2.4}, have been developed to allow for all the space harmonics present in the motors.

In variable speed applications, the equivalent circuit parameters are assumed to remain constant and their values are obtained at the designed supply frequency ^{2.5,2.6}, (50 Hz in the U.K.). These fixed parameters are then used to obtain the necessary design and performance data over the operating frequency range.

In fact, the equivalent circuit parameters are frequency dependent, so that using them as fixed values at any supplied frequency will result in some errors in the calculated characteristics. The magnitude of these

errors depend on the frequency deviation. Changes in the machine parameters with supply frequency are well known, and mainly occur in the rotor circuit ^{2.7,2.8}. Errors introduced in the starting torque are especially noticeable because the rotor frequency is at its maximum and reduces as the rotor accelerates. Their values at any supply frequency can be calculated by knowing the machine geometry as represented in ALGER ^{2.1}.

The engineers who are involved in designing control systems for variable speed induction motors are not usually familiar with machine design. They base all their control laws around the induction motor equivalent circuit model which produces correct characteristics at all supply frequencies and which can easily be constructed from simple tests on the motor itself. This thesis represents a technique of obtaining such a model from open circuit and short circuit test results, taken at various supply frequencies.

The open circuit results are used to construct the complex frequency response of the magnetising branch elements for a given applied volts per hertz. Short circuit results are used to construct the complex frequency response of the input impedance for the locked rotor condition. With the aid of a digital computer, circle fitting and other search techniques are used to determine the elements of the new equivalent circuit shown in figure 2.2. The parallel resistors shown across the leakage reactances do not have any physical meanings, but are used to alter the primary and secondary impedances

with supply frequency. A further advantage of this new equivalent circuit is that it produces the correct characteristics for modulated waveforms as well as a main supply frequency.

That is, the new model not only produces all the correct values of the parameters at any supply frequency, but also produces all the necessary changes in the impedances for any superimposed modulation frequency.

2.2 The Induction Motor Equivalent Circuit

In order that the motor can be treated as one entity the equivalent electric circuit is then introduced. The electrical equivalent circuit of an induction motor is an electrical network that represents the electrical and magnetic circuit of the motor.

Many assumptions have been adopted with regard to equivalent circuit parameters. One such assumption is that the equivalent circuit parameters are constant and are not slip dependent. Other assumptions are that the stator resistance and magnetising branch losses can be neglected. The output of an induction motor can be defined in terms of its diameter and length. The relationship between these dimensions and its output will depend on how the motor is rated. Because of the correlation between equivalent circuit parameters and performance characteristics of an induction motor, the per unit resistance and reactance of an induction motor become very important in terms of output performance. A relationship

between the motor size, per unit resistance and reactance can be established, and hence any assumptions on the neglect of equivalent circuit parameters have to be made with regard to the size of the motor in question 2.9.

As the physical dimensions of the induction motor largely dictate the type of characteristics it will present; three groups of induction motors are described, related according to their characteristics and diameter.

(i) Large Power Induction Motors These motors are designed to operate at high efficiencies with low magnetising currents, hence the reduction of iron losses leading to a value of R_m large enough to be ignored. With large diameter motors the series stator impedance is mainly inductive. The stator resistance may be neglected since it is small compared with the stator leakage reactance.

(ii) Medium and Fractional Horsepower Motors
Between the large power induction motors and the very smallest of miniature induction motors lie the medium and fractional horsepower motors. These motors are not capable of high efficiencies. Because of their size, the resistive elements of their impedances cause high copper losses and hence lower efficiencies. For an approximate analysis, R_m may still be neglected, although the stator resistance must be included in all but the most superficial of investigations.

(iii) Subminiature Induction Motors Among the dimensionally smallest of induction motors are the subminiature induction motors often used in servo-systems. The assumption of infinite R_m may be sufficiently accurate for most purposes, but because of its size the stator resistance must now be included. Stator leakage reactance is also small compared to stator resistance.

One of the advantages to be gained from using the equivalent circuit is that the output characteristics of a motor can be related to a small number of easily identifiable circuit parameters. An alteration to the electric or magnetic circuit of an induction motor can be related to one or more of the equivalent circuit parameters. In turn these will alter the performance characteristics of the motor. For example, an increase in the length of the airgap of an induction motor will decrease the magnetising reactance, producing a higher magnetising current and a lower power factor. At the same time the stator and rotor gap leakages are decreased causing a corresponding increase in starting torque and current coupled with an increase in pull out torque.

Because both the stator and rotor usually have slotted boundaries there will be non-uniformity in the airgap flux and space harmonics will be present. In order to allow for all the space harmonics present in the motor, several authors ^{2.2,2.3,2.4}, have presented complex equivalent circuits based on a ladder network. Although computers can largely solve the problem of the manipula-

tion of the large matrices involved, it becomes increasingly difficult to relate any circuit parameters to a physical or real quantity. The circuits become more complex if time harmonics are also considered, as each time harmonic is responsible for numerous space harmonics.

In a design office, induction motor design engineers have a standard design available and in order to meet a particular requirement will alter the dimensions of a motor until this requirement can be best met ^{2.10}. This technique requires a combination of trial and error, and experience. An alternative method is to replace the lengthy error method by a computational direct search technique ^{2.11}. This entails feeding the required motor characteristics into a computer program and thereby obtaining the necessary mechanical and electrical parameters to achieve that performance ^{2.12}. In such a method it would also be possible to allow for extra constraints, such as the use of standard frame sizes and wire gauges, or to allow for various economic variations (eg. the price of copper) therefore producing a realistic design ^{2.13}. These constraints will vary not only between manufacturers but also with market price fluctuations.

Although the use of direct search techniques in the design of induction motors is not new ^{2.14,2.15}, the majority of methods contain an optimum design for a given performance ^{2.16}.

If the equivalent circuit is kept as simple as possible and the number of equivalent circuit parameters kept as small as possible, then any change in the actual

machine can easily be related to the output characteristics via the circuit parameters. In this way a mathematical model that relates the physical motor quantities to the output characteristics can be defined.

2.3 Measurement of Experimental Results

The changes in the equivalent circuit parameter with frequency are very small, therefore all the necessary precautions are taken to obtain the true readings. In order to achieve this, all the readings are taken with the machine at its normal running temperature (45°C). Furthermore all the apparatus used in the experiments are checked for correct readings within the frequency range. The majority of standard equipment is designed and calibrated for 50 Hz supply systems, and outside this frequency range the readings are likely to be inaccurate. The method used to examine the meter readings is given in Appendix A, part one. The following three standard tests are used to obtain the required results.

(i) D.C. Test A d.c. current equal to the motor rated is set through one of the motor phase windings via a d.c. source. The d.c. voltage and current are then used to determine the stator resistance (R_1).

(ii) Open Circuit Test The rotor of the machine is kept at synchronous speed by means of another motor. The three phase supply voltage is set to its rated volts per hertz. The determination of the rated value of the applied volts-per-hertz of this

particular machine is given in Appendix A, part two. The total input power and current are then measured with various supply frequencies.

(iii) Short Circuit Test The rotor of the machine is locked such that it cannot rotate. The line current is kept at its rated value and total input power and phase voltage are measured with various supply frequencies.

The results obtained from the above three tests are used to calculate the values of the equivalent circuit parameters. The calculations and formulae are given in Appendix A, part two (A.2.2).

2.4 Evaluation of the Magnetising Branch Parameters for Variable Speed Applications

The parallel or series form of the magnetising elements represented in the well known standard equivalent circuit is normally determined at a given supply frequency. This simple form generally represents the complex networks of the magnetising elements. The resistive part mainly represents core losses. Such losses consist of hysteresis and eddy current arising from changing flux densities in the iron of the machine in both stator and rotor when energised ^{2.17}. Eddy current loss is dependent on the squares of flux density, frequency and thickness of the laminations. Under normal machine conditions, it may be expressed to a sufficiently close approximate as:-

$$P_e = K_e (B_{\max} \cdot F \cdot t)^2 \quad \text{--- (2.1)}$$

where K_e is a constant, its value depends on the units, volume and resistivity of the iron. Hysteresis loss can be expressed in equation form only on an empirical basis as:-

$$P_h = K_h \cdot F(B_{\max})^n \quad \text{--- (2.2)}$$

where n ranges from 1.5 to 2.5 with the value 2.0 often used, and K_h is constant depending on the characteristics and volume of the iron and units used. These losses are flux and frequency dependent. In variable speed applications the magnitude of the flux density remains almost constant when the machine is operating under given applied volts per hertz. Thus, it is evident that the evaluation of the magnetising branch parameters at a particular supply frequency can no longer be applied at other supply frequencies.

To obtain the frequency dependent equivalent network, the open circuit results at various supply frequencies can be used to plot the complex frequency response of the magnetising parameters. The curve fitting techniques can be employed to search for some form of RL networks which have the same frequency response. The determined new network will represent the exact values of the magnetising parameters at any supply frequency for a given volts per hertz.

2.4.1 Experimental Results

A three horsepower, high speed, three phase induction motor is used to produce the required experimental results. The open circuit results (rotor running

at synchronous speed) are taken with a given applied volts-per-hertz at various supply frequencies up to 400 Hz. At each step the rotor is driven into its synchronous speed by means of another motor. From these results the values of R_m and X_m at each step of the supply frequency are calculated and plotted in figure 2.3. It is evident that this complex frequency response shown in figure 2.3 belongs to a simple parallel RL network. The inductive and resistive parts of this RL network can easily be calculated by using a circle fit technique. Full details of the circle fit technique are given in Appendix A, part three. The frequency response of this RL network is also plotted and shown in figure 2.3, confirming the true representation of the magnetising branch parameters at any supply frequency for a given applied volts per hertz.

2.5 Evaluation of the Primary and Secondary Equivalent Circuit Parameters for Variable Speed Applications

The leakage reactance of the induction motor consists of eight distinct components ^{2.1}.

- (a) The primary reactance.
- (b) The secondary slot reactance.
- (c) Stator-end-winding leakage.
- (d) Stator-end-ring leakage.
- (e) Stator differential leakage.
- (f) Rotor differential leakage.
- (g) Stator reactance due to skew.
- (h) Rotor reactance due to skew.

The primary and secondary leakage reactances are a composite of the above components. Due to the complex construction of squirrel-cage induction motors, the rate of change with frequency in the inductive and resistive parts of the rotor circuit will be greater than the stator elements. The change in the rotor resistive part is much larger because the deep bar effect forces the current to flow towards the rotor surface. In other words if the squirrel-cage rotor circuit is represented by a series of "n" identical mutually coupled loops ^{2.18}, the equivalent inductive and resistive parts of such a complex mesh will not remain constant at varying supply frequencies. The variation in the stator parameters arising mainly from skin effect is slight and can be neglected in many applications. The results obtained from the standard short circuit test (locked rotor) at various supply frequencies contain the variations of all the primary, secondary and magnetising branch parameters. Therefore, it is not easy to determine their equivalent RL networks directly from the short circuit frequency response without the aid of a digital computer and by the use of various assumptions. These assumptions are given in full detail in the following section.

2.5.1 Program Description and Experimental Results

A digital program is designed and developed to compute the input impedance of the new equivalent circuit model in real and imaginary numbers. The program is

initially supplied with the following data.

- (a) The values of the magnetising branch parameters obtained from circle fit technique.
- (b) All the short circuit test results taken at various supply frequencies.
- (c) The value of the stator d.c. resistance.

The flow diagram of this search technique is shown in figure 2.5. The values of the parameters obtained from this technique for the motor under experimentation are also given in figure 2.2. These values of the new equivalent circuit parameters confirm that the changes are mainly occurring within the secondary circuit.

A reasonably close model can also be constructed without the aid of a digital computer. This can be done by assuming that the impedance of the magnetising branch parameters is very large compared with primary and secondary parameters obtained from short circuit tests and can be neglected in this particular test. The stator parameters can be assumed to have negligible frequency variations. The ratio of the primary and secondary leakage reactances can also be determined according to their starting torque characteristics from published tables ^{2.19}, or the rotor can be removed and search coils can be inserted in the stator slots. Then the components of the stator leakage reactance can be determined by simply energising one of the phases of the machine and observing the voltages induced in the search coils ^{2.20}. This allows the secondary circuit parameters to be

separated from the test results and plotted on a complex frequency axis. The value of the rotor series resistance R_2 and leakage reactances X_2 and its parallel resistance RP_2 can be calculated (by use of circle fit technique). Using these assumptions, the secondary parameters of the machine under experimentation are separated and shown in figure 2.6. However, the digital search technique has the advantage of giving greater accuracy and the ability to calculate the ratio of X_1 to X_2 from the data.

2.6 Application of the New Equivalent Circuit for Superimposed Modulation Frequencies

Up to this point the supply frequency only has been considered in the construction of the new equivalent circuit. In this section the validity of such a model for superimposed frequencies is examined. The standard equivalent circuit used for induction motors is usually obtained at one frequency only. The application of this model in determining the design figures for inverter systems could result in serious errors. Advancements in semiconductor technology have resulted in the design of inverters with much higher switching frequencies. The changes in the equivalent circuit parameters with high switching frequencies can no longer be ignored since they cause errors in many design figures, eg. calculating losses, efficiencies and machine time constant etc.

The amplitude of the current harmonics resulting from switching frequencies are much smaller than the current at the main supply frequency. In particular the magnetising branch currents are so small that they can be neglected. When the modulation frequency is very high compared with the supply frequency, the relative rotor slip remains almost at unity. However, when the modulation frequency approaches the main supply frequency, the relative rotor slip cannot be taken as unity. Its value varies according to rotor speed and can be presented as:-

$$S_m = \frac{F_m - F_r}{F_m} \quad \text{--- (2.3)}$$

where F_m and F_r are the modulation and rotor frequencies respectively and S_m is the corresponding value of the slip.

2.6.1 Experimental Results

The line currents of the machines fed from inverter supplies contain the main frequency and all the harmonics of the switching frequencies. A technique of modulating one of the lines of the machine is developed to investigate the changes in the equivalent circuit parameters with respect to each of these harmonic frequencies.

Modulation frequencies of up to 3 kHz are injected into one line while the motor is running with mains supply frequency (50 Hz). The current at modulation frequencies is then measured in the same line and used to observe the changes in machine parameters due to

these frequencies only. The technique developed to carry out the observations is given in full detail in Appendix A, part four.

A phase sensitive meter is used to measure the magnitudes and phase angles of the injected and extracted signals which are then used to calculate the complex frequency response of one of the phases of the machine. The experiment is repeated with several values of the rotor slip and the frequency responses are shown in figure 2.7. When the modulation frequencies are much higher than the main driving supply frequency the impedances are independent of slip but, as expected, the resistive part of the locus diagrams (complex frequency responses) are not identical when the modulation frequency approaches the main supply frequency. This is because at low modulation frequencies the relative rotor slip does not remain at unity... Thus secondary resistance becomes more slip dependent and varies with load conditions. The locus diagram of the input impedance taken at one of the phases of the machine, using a phase sensitive meter for frequencies up to 10 kHz; and those computed from the new equivalent circuit are identical and are shown in figure 2.8. Figures 2.7 and 2.8 confirm that the new equivalent circuit model represents the exact behaviour of the machine parameters for superimposed modulation frequencies as well as the main supply frequencies.

2.7 Errors Introduced in the Performance Calculations, when the Fixed Frequency Equivalent Circuit is used in Variable Frequency Applications

The performance characteristics of the induction machines are generally determined from the torque equation given in standard text books ^{2.21} as:-

$$T = m(I_2)^2 \cdot \frac{R_2}{S} \quad \text{--- (2.4)}$$

where T = shaft torque,

m = number of phases, and

I_2 = current, in the secondary circuit.

Because of the changes in the machine parameters in variable frequency applications, the magnitude of (I_2) no longer remains constant, when the machine is operating with a given applied volts-per-hertz and load condition. The value of R_2 also varies with the supply frequency as shown in figure 2.6. In order to achieve the precise performance calculations, the values of I_2 and R_2 must be determined at the frequency of operation. This can be done directly from the new equivalent circuit model. Use of this model alters the parameter values according to the frequency of operation.

2.7.1 Comparison of Results

The starting and maximum torques are calculated from the standard equivalent circuit of the induction motor obtained using a supply frequency of 50 Hz and torque equation 2.4 of section 2.7. The applied volts-per-hertz is kept constant and frequency is varied from

50 Hz to 400 Hz inclusive. A similar performance equation for the new equivalent circuit is derived and used to calculate the starting and maximum torque for the same applied volts-per-hertz and frequency range.

The actual values of the starting and maximum torque are also measured experimentally for the same operating conditions. All three sets of results are plotted and shown in figure 2.9. This figure clearly shows the magnitude of the errors involved in the above performance figures, if the equivalent circuit of 50 Hz is used instead of the new variable equivalent circuit. The magnitude of errors depend on the frequency deviation and rotor slip. But as the rotor accelerates, its frequency reduces and its parameters approach low frequency values. This results in a reduction in errors as the rotor speed approaches the synchronous speed. The maximum torque characteristics are given in figure 9.

2.8 Conclusions

It is shown that the new equivalent circuit model of the induction motor for variable supply frequency applications can be constructed from short- and open-circuit test results. The accuracy of the resultant equivalent circuit depends on the technique employed to replace the frequency dependent elements with equivalent RL networks.

It is also shown that the new model can be applied for both mixed and main supply frequencies. This is another advantage of using such a model for harmonic

analysis of any inverter type. The level of power distributed in each harmonic depends on the load impedance. As this model is able to produce the correct load impedance at any applied frequency, it becomes a very important tool in determining and comparing the efficiency of the inverters operating under the same conditions.

In speed control systems with large frequency deviations, the application of the fixed frequency equivalent circuit results in serious errors in the performance calculations. When the equivalent circuit parameters obtained at a lower frequency range are used to calculate the performance characteristics at the higher end, the magnitude of errors involved maximise, especially at unity slip. Errors reduce as the rotor accelerates towards the synchronous speed. The effect of high frequency on the rotor resistive part becomes very similar to the deep bar effect used in some rotor construction.

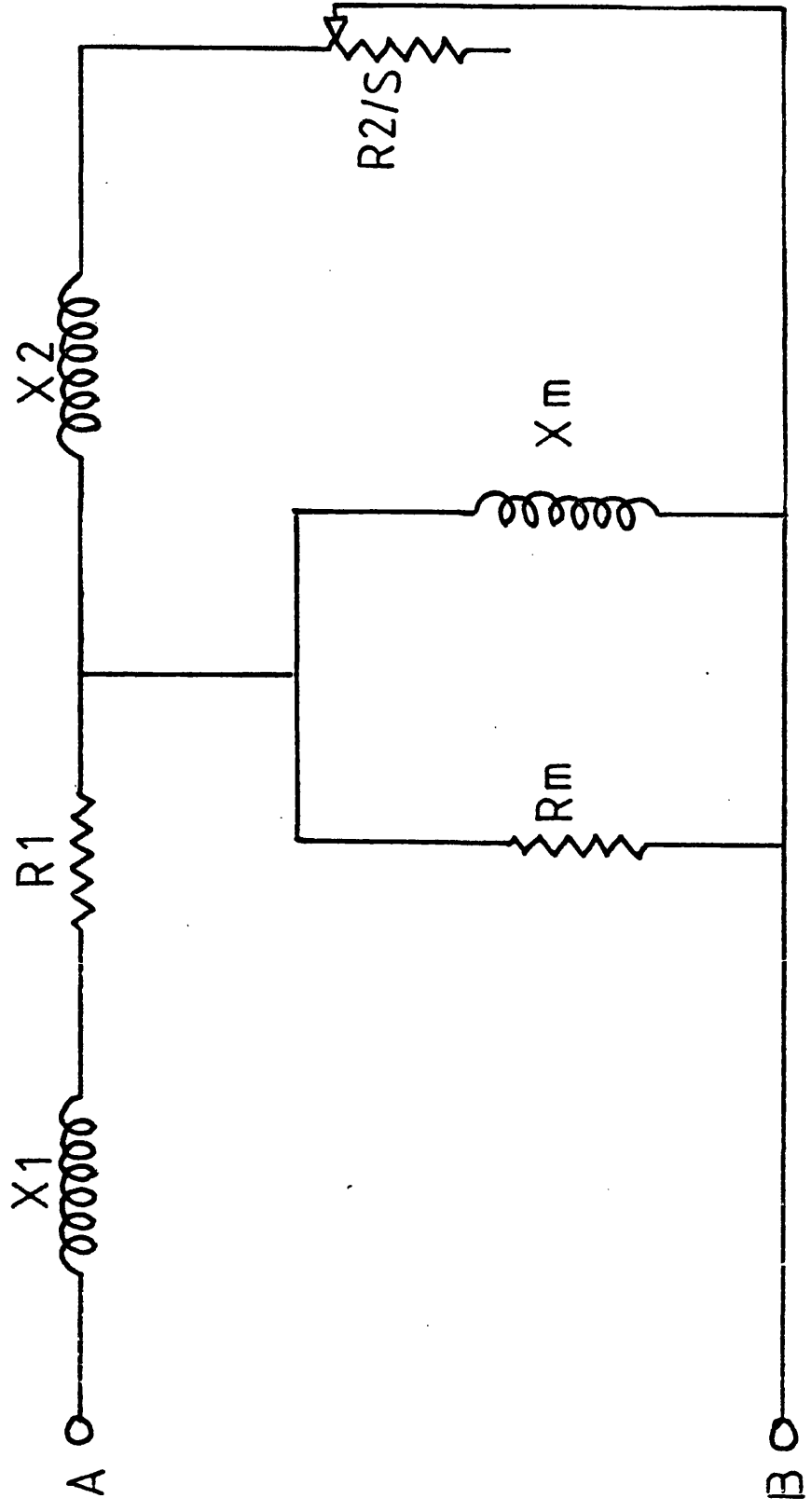
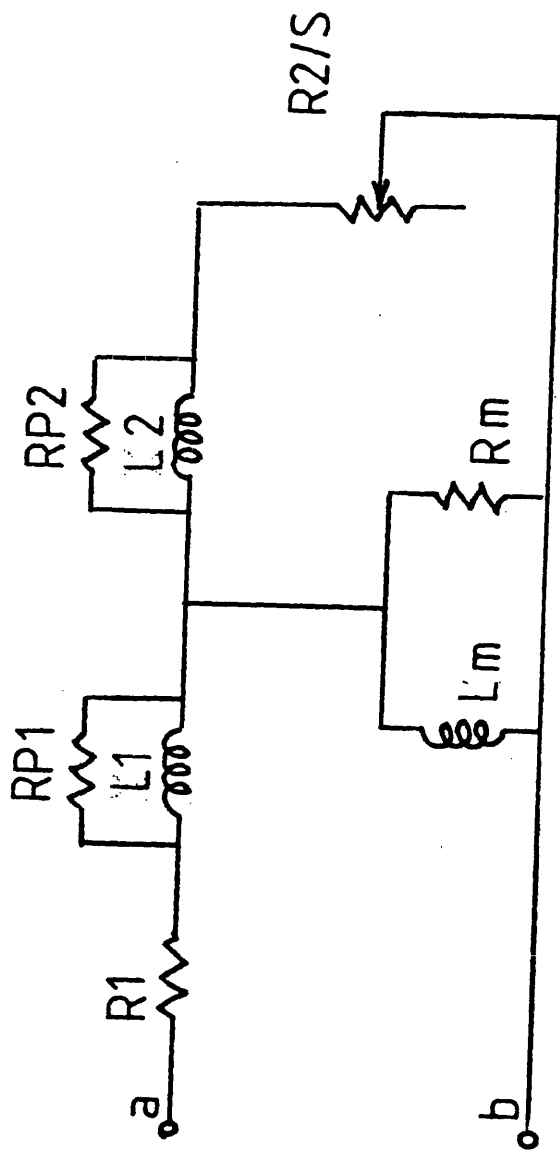


FIG. 2.1 Standard Induction Motor Equivalent Circuit



- R1 = 2.25 (OHMS)
- RP1 = 900 (OHMS)
- L1 = 2.3 (mHS)
- R2 = 2.0 (OHMS)
- RP2 = 10 (OHMS)
- L2 = 1.2 (mHS)
- Rm = 500 (OHMS)
- Lm = 30 (mHS)

FIG. 2.2 New Freq. Dependent Induction Motor Equivalent Circuit

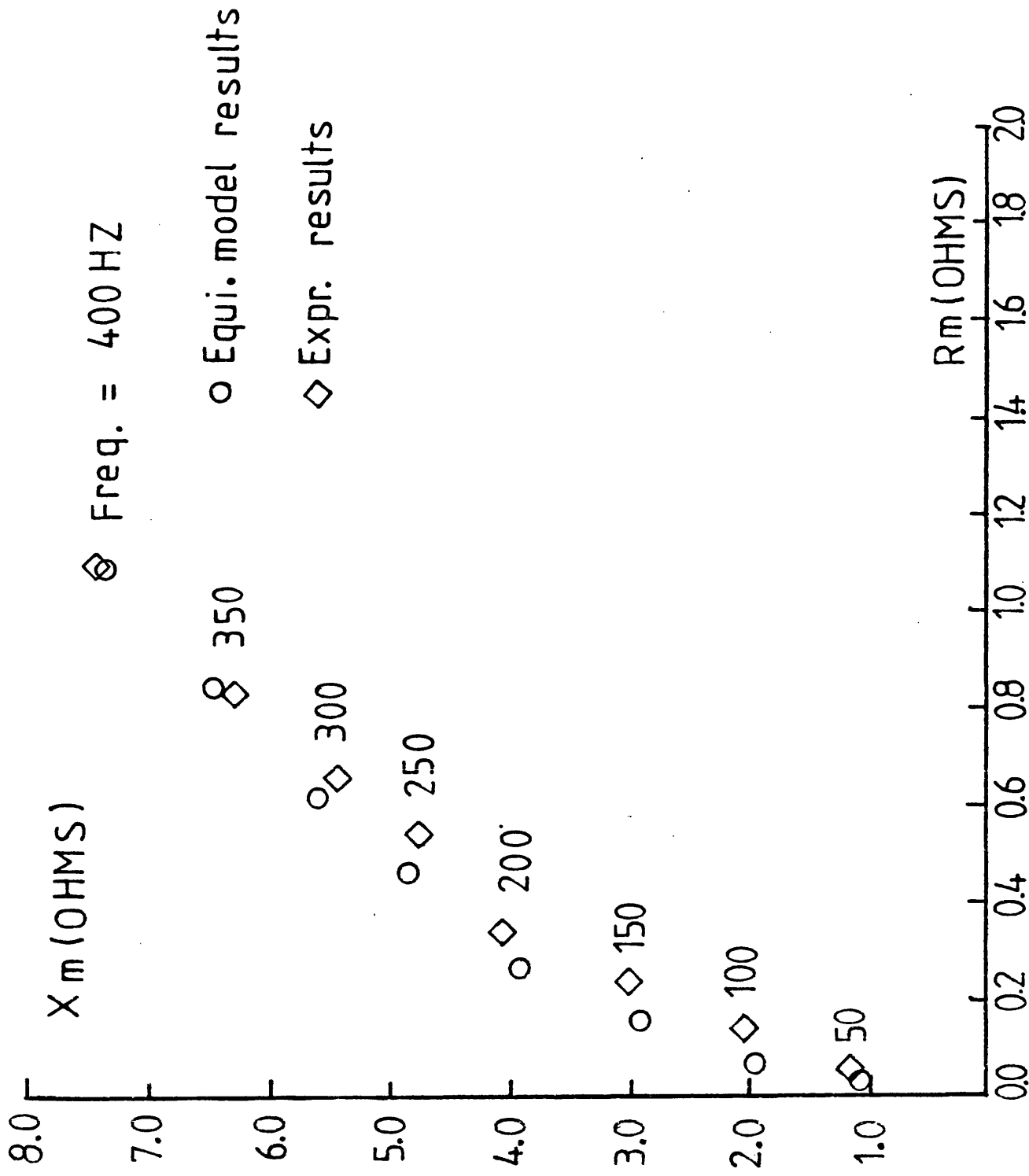


Fig. 2.3 Locus Dia. of Mag. Branch at Rated V / Hz

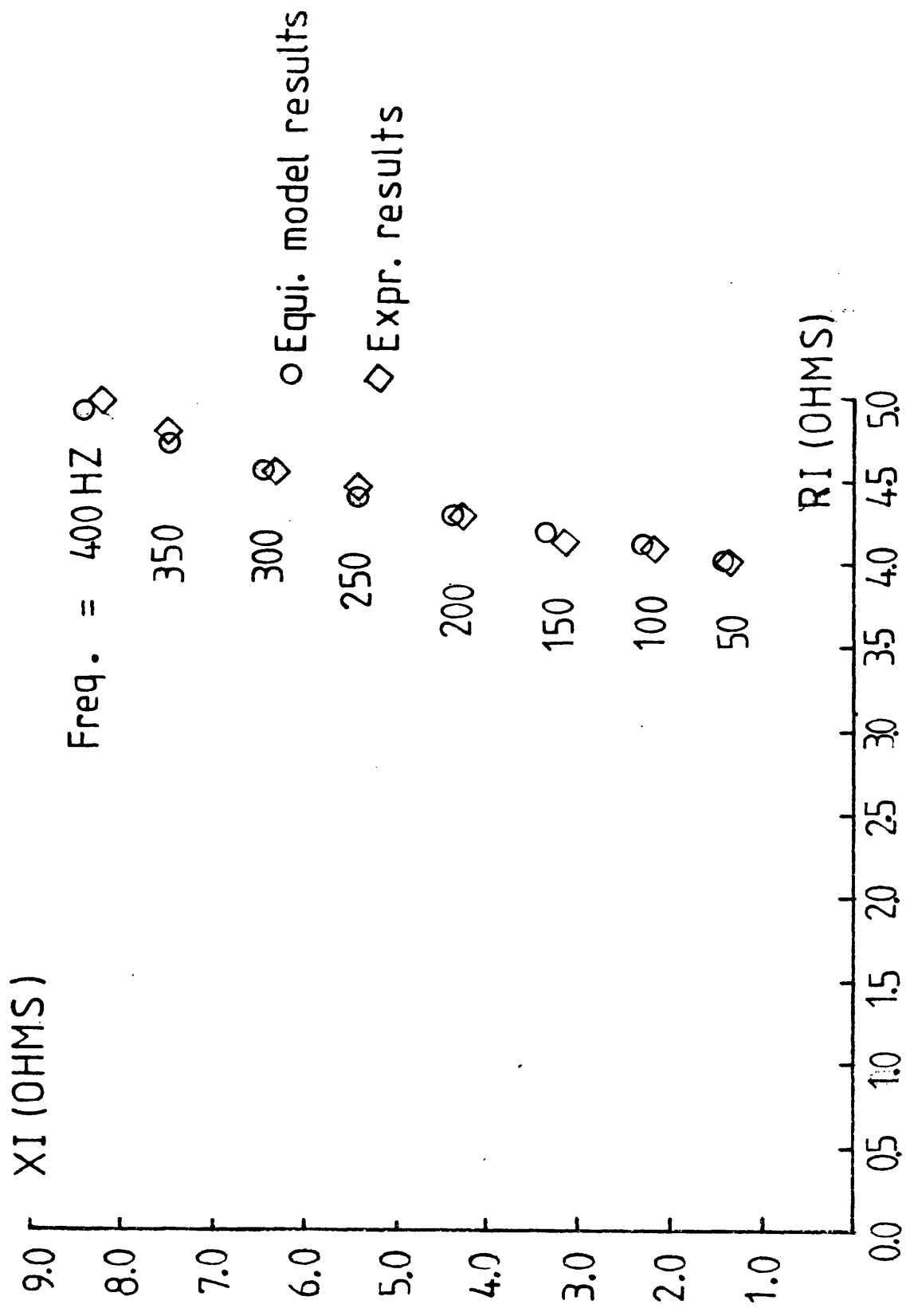


Fig. 2.4 Locus Dia. of Short Circuit Test Results
At Rated Line Current

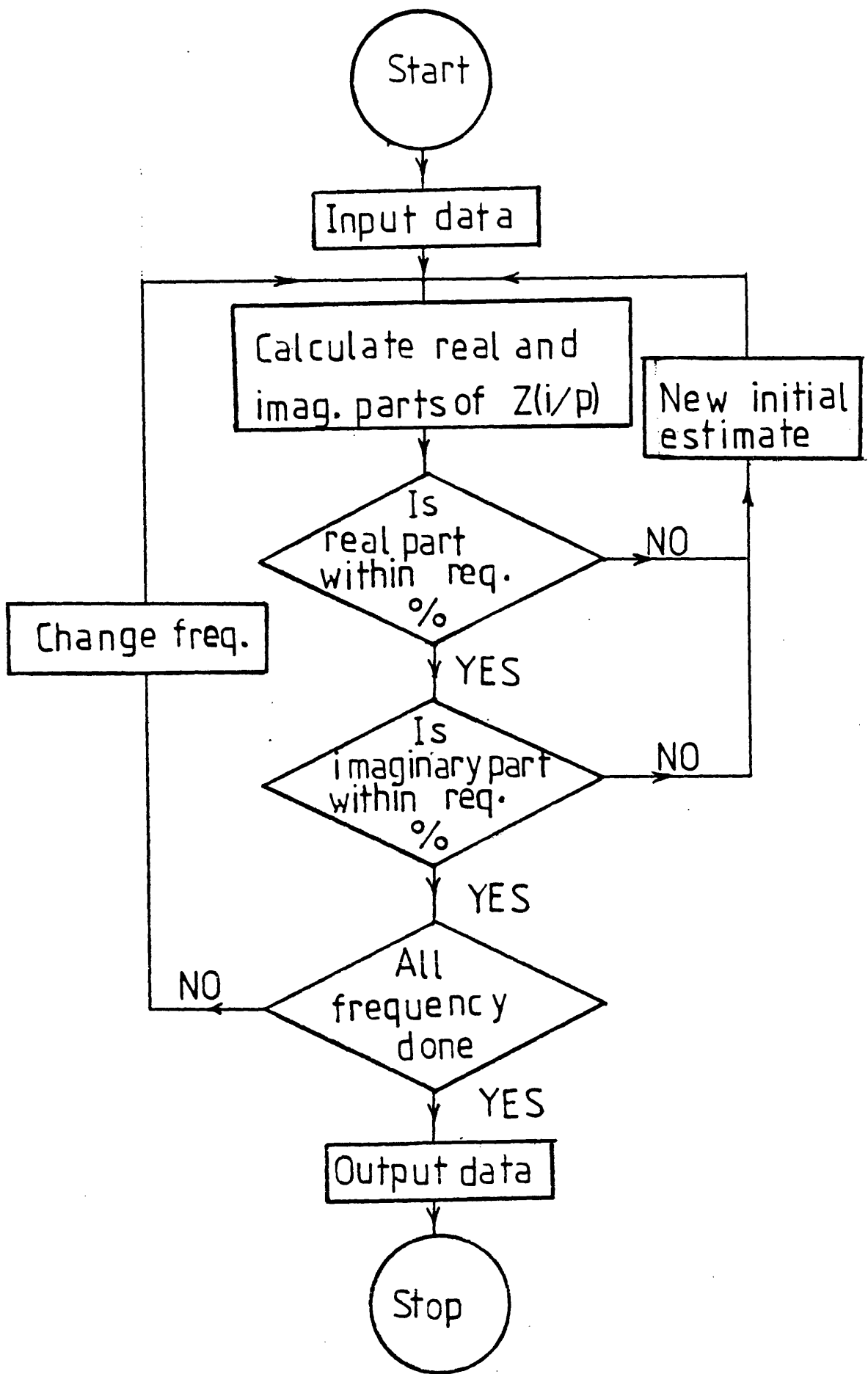


Fig. 2.5 Flow Dia. of Search Technique

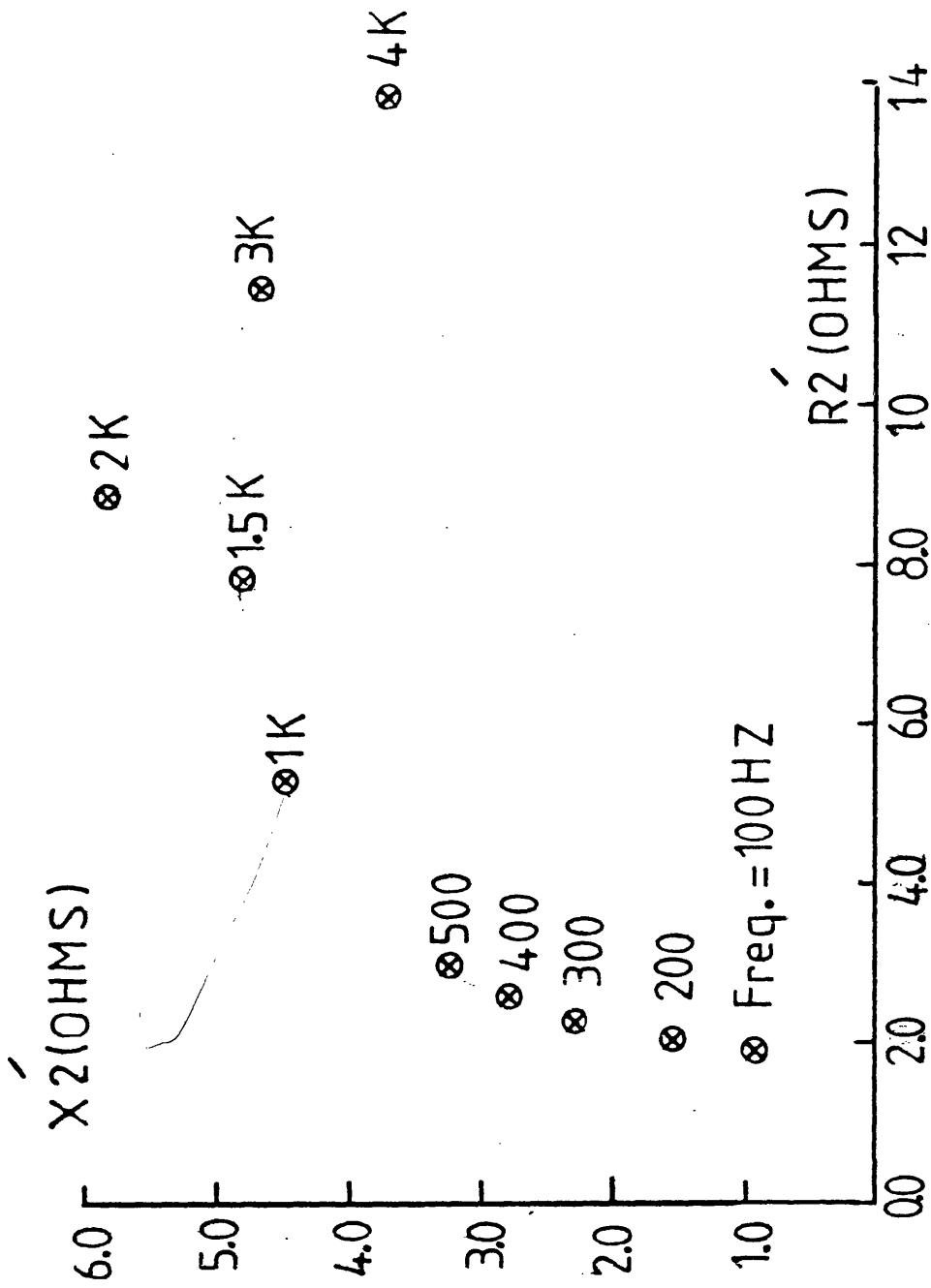


Fig.2.6 Locus Dia. of Rotor Circuit at Unity Slip

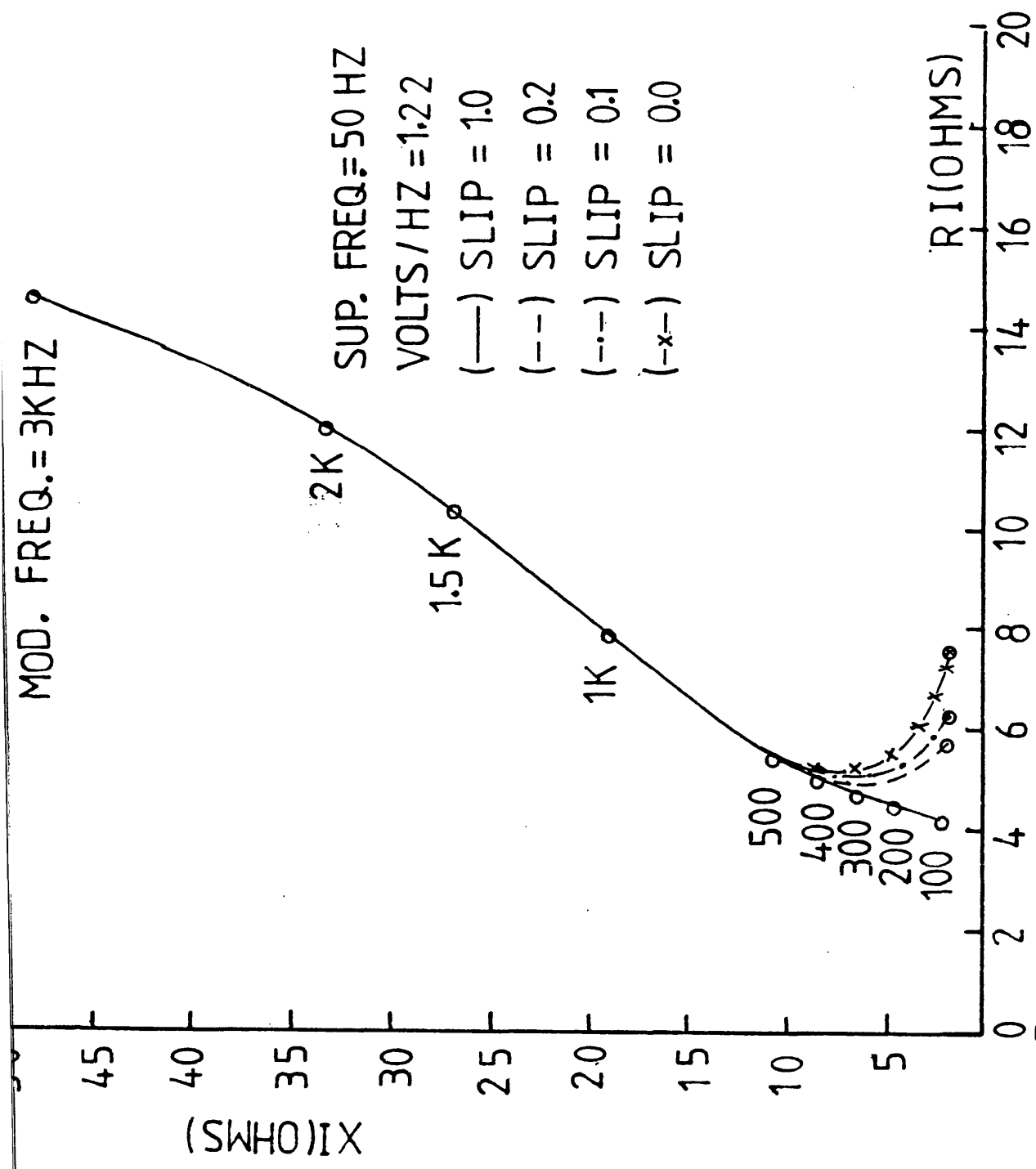


Fig. 2.7 Locus Dia. of Per Phase Impedance Obtained

From Modulation Freq.

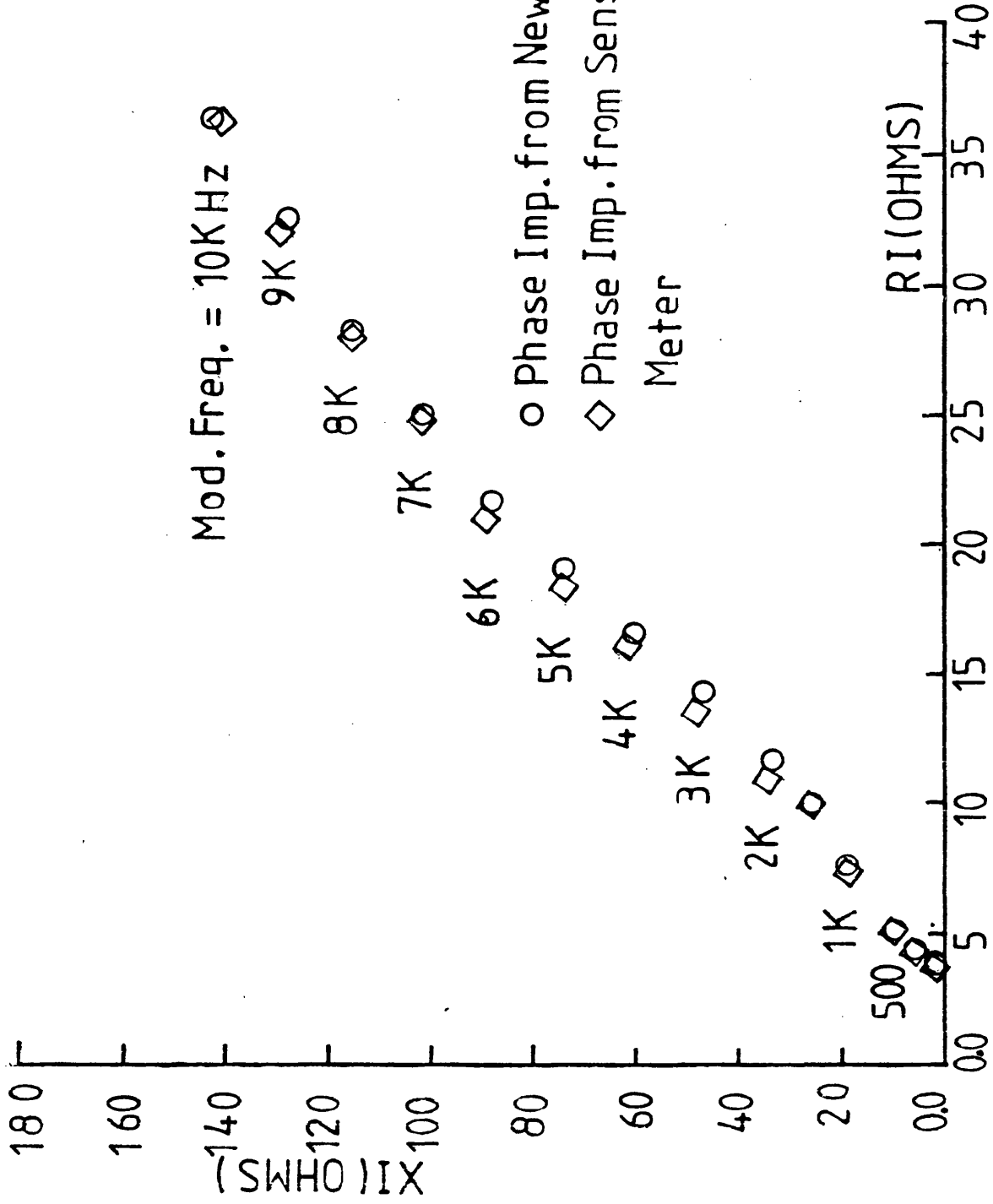


Fig. 2.8 Locus Dia. of Phase Input Impedance

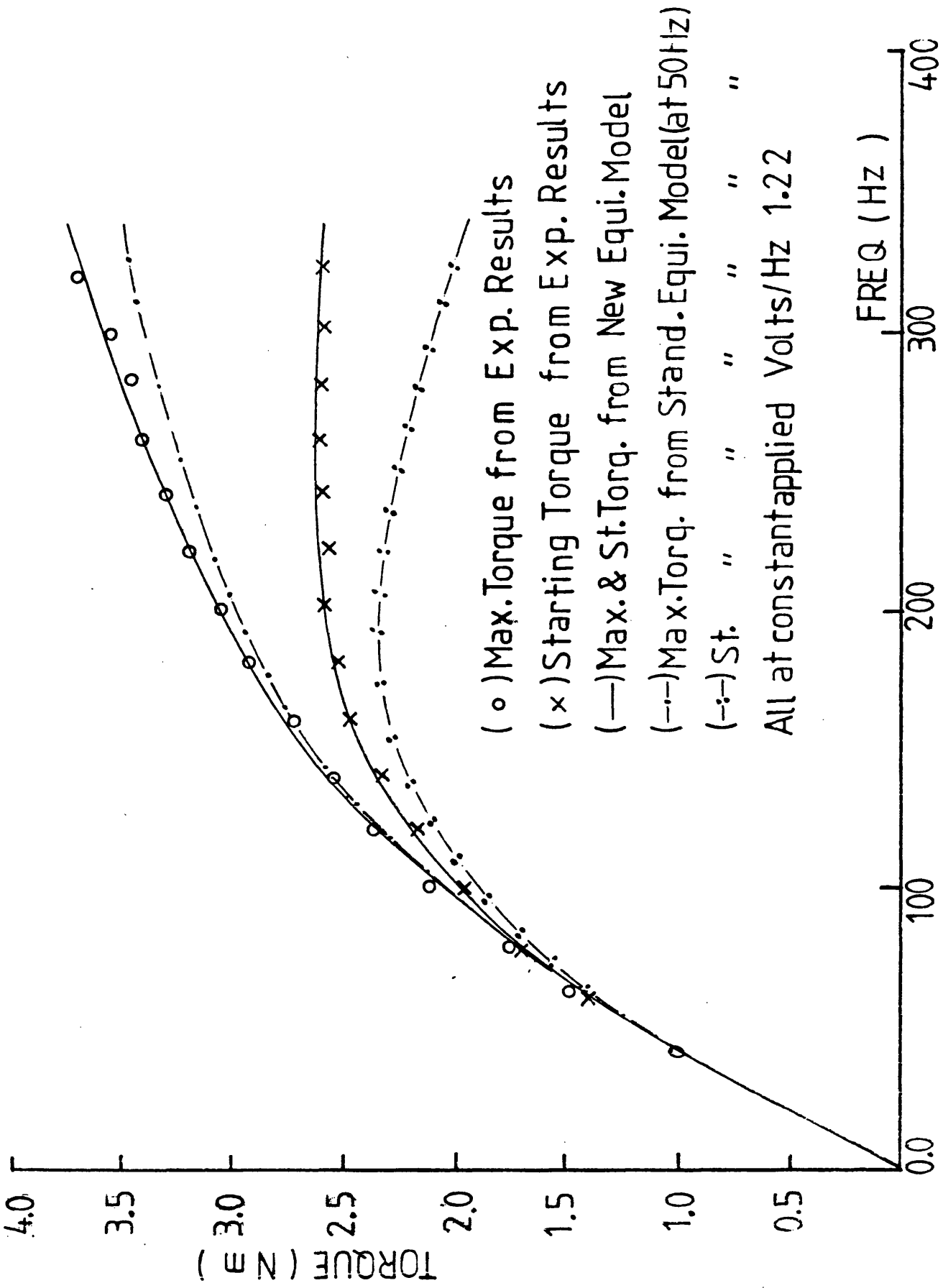


Fig. 2.9 Starting & Max. Torque at Various Frequencies

Bibliography

- 2.1 ALGER, P.L.: "The nature of induction machines", (Gordon & Breach), New York, 1965.
- 2.2 LI, K.Y.G.: "Analysis and operation of an inverter fed variable speed induction motor", Proc. IEE, Vol. 116, No. 9, 1969, pp. 1571.
- 2.3 HANCOCK, N.N. and KARAKRADDI, B.H.: "The physical realisation of induction motor equivalent circuits", Proc. IEE, Vol. 108, Part 16, 1961, pp. 145.
- 2.4 KLINGSHIRN? E.A. and JORDAN, H.E.: "Losses on non-sinusoidal voltage sources", Trans. IEEE, PAS Vol. 87, No. 3, 1968, pp. 624.
- 2.5 JAIN, C.G.: "The effect of voltage shape on the performance of a three-phase induction motor", IEEE Trans. on Power Apparatus and Systems", PAS Vol. 84, June 1964, pp. 561-566.
- 2.6 JACOVIDES, L.J.: "Analysis of induction motor drives with a non-sinusoidal supply voltage using Fourier analysis", Trans. IEEE on Ind. App., Vol. 1A-9, No. 6, Nov/Dec 1973, pp. 741-746.
- 2.7 MURPHY, J.M.D.: "Thyristor control of a.c. motors", Vol. 6, 1973.
- 2.8 LARGIADER, H.: "Design aspects of induction motors for traction applications with supply through static frequency changes", (Brown Boveri), 57, 152, 1970.
- 2.9 BONE, J.C.H. and SCHWARZ, K.K.: "Large a.c. motors", Proc. IEE, Vol. 120, October 1973, pp. 1111.
- 2.10 LLOYD, T.C.: "Some aspects of electric motor design-polyphase induction motor design to meet fixed specifications", AIEE, PAS Vol. 63, January 1944, pp. 14.
- 2.11 CHALMERS, B.J. and BENNINGTON.: "Digital computer program for design synthesis of large squirrel-cage induction motors", Proc. IEE, Vol. 114, No. 2, February 1967, pp. 261.
- 2.12 VEINOTT, C.G.: "Synthesis of induction motor designs by digital computer", Trans. AIEE, PAS Vol. 79, 1960, pp. 12.

- 2.13 APPELBAUM, J. and ERLICKI, M.S.: "A problem of economic optimisation of electrical equipment design", Trans. IEEE, Com. and Elec., Vol. 83, November 1964, pp. 773.
- 2.14 VEINOTT, C.G.: "Induction machinery being revolutionised by the digital computer", Trans. AIEE, PAS Vol. 75, Part III, February 1956, pp. 150.
- 2.15 LLOYD, M.R.: "Some aspects of solid salient pole synchronous motors", PhD Thesis, University of Southampton, October 1976.
- 2.16 APPELBAUM, J. and ERLICKI, M.S.: "Optimised parameter analysis of an induction machine", IEEE Trans., PAS Vol. 84, No. 11, 1965, pp. 1017.
- 2.17 LINDSAY, J.F. and BARTON, T.H.: "A modern approach to induction machine parameter identification", Trans. IEEE on Power Apparatus and Systems, PAS Vol. 91, July 1972, pp. 1493.
- 2.18 WALLACE, A.K. and WRIGHT, A.: "Novel simulation of cage winding based on mesh circuit model", Trans. IEEE on Power App. and Sys., PAS Vol. 93, 1974, pp. 377.
- 2.19 LANGSDORF, A.S.: "Theory of alternating-current machines", (2nd Edition, McGraw-Hill).
- 2.20 BOBLIO, G., PESSINA, G. and ZIMAGLIA, C.: "The choice of law $V(F)$ for motors fed by sinusoidal voltage, variable frequency in relation obtaining functional charge, fixed previously", Sicme Motori. Str. Del. Francese 126, Torino, 1977.
- 2.21 DANIELS, A.R.: "The performance of electrical machines", (McGraw-Hill).

CHAPTER 3

ANALYSIS OF THE NEW EQUIVALENT CIRCUIT AND THE CONSTRUCTION OF A NON-LINEAR MODEL FOR INDUCTION MOTORS USED IN VARIABLE SPEED APPLICATIONS

Summary

The new equivalent circuit of the previous chapter is analysed and all the performance equations are derived in Part One indexed as 3.3. With the aid of a digital computer, the performance characteristics are computed and compared with the experimental results.

Part Two indexed as 3.4 contains the discussion on, and construction of the non-linear model of the induction motors from test results, used in variable speed applications. The errors introduced in the performance calculations using the linear model in the non-linear region are then given.

3.1 Introduction

To confirm the validity of the new equivalent circuit for calculating the output performance, it is analysed and performance equations are derived. These equations are then used to compute and compare the torque speed characteristics of the new equivalent circuit with the experimental results.

The vast majority of the work done in the past for modelling various saturation effects in the machine parameters represented in the literature review involves having the machine geometry. This is done by calculating the flux in each path individually and then introducing the saturation factor. Engineers in industry who are involved in inverter design for speed control of induction motors usually have very limited knowledge of machine design. Thus there is a need for a simple technique of determining the non-linearities of the machine from test results as well as a method for their inclusion in the equivalent circuit parameters.

Hysteresis and eddy current losses change considerably with the supply frequency ^{3.1}, beyond the knee of the saturation curve and because of this the operating point varies with the supply frequency. The relationship between the rated value of the operating

volts-per-hertz and the supply frequency can then be determined either from the non-linear model or directly from the test results for constant flux applications.

Using a digital computer, the non-linear model of the induction motor is constructed from test results. This is done as follows. The open and short circuit test results at several values of the applied voltages and frequencies in the saturation region are used as the necessary data for modelling. In the linear region the new equivalent circuit of the previous chapter is used to obtain the required characteristics. In the non-linear region the computer model alters the values of the equivalent circuit parameters according to values of the applied volts-per-hertz and load conditions.

Calculation of the performance characteristics in the non-linear region from the linear equivalent circuit introduces errors in shaft torque proportional to the supply frequency and rotor speed. The magnitude of the errors are determined by comparison of the torque speed characteristics obtained from linear and non-linear equivalent circuit models. The modelling of the stray load losses ^{3.2,3.3}, and saturation harmonics is not within the scope of this thesis. The effect of these appears to produce plateaus, peaks and troughs on the experimental torque speed characteristics.

An accurate method of obtaining torque speed characteristics is achieved by the design and development of a special torque speed plotting machine for

extremely high speed applications. This is done by measuring the machine torque and speed, without actual physical contact with the rotor, during the acceleration of a given inertia load.

3.2 Literature Review

Saturation Effect on Equivalent Parameters

The influence of saturation on the performance of electrical machines has been appreciated by engineers for many years. However the precise evaluation of its effects has remained a somewhat intractable problem. Early papers ^{3.4}, presented a method which attempted to calculate separately the saturation effects due to tooth-tip and zigzag leakage fluxes.

It was assumed that the zigzag flux was the main source of saturation, and began by calculating the average m.m.f. per slot driving zigzag flux across two airgaps and the iron path. The length of the iron path was taken as the sum of the stator, and rotor, slot pitches. The magnetisation characteristic of the iron was represented for high flux densities by a straight line on the logarithmic scale as in figure 3.1(a) and the iron area was assumed to be equal to the airgap area. The saturation factor for the zigzag reactance was calculated as the ratio of the m.m.f. in the airgap to the total m.m.f. The tooth-tip leakage reactance was then estimated for an increased slot opening, the increase being a function of the degree of saturation of the zigzag flux. Designs in which the prime source of saturation is the tooth-tip leakage flux could not be treated by this method.

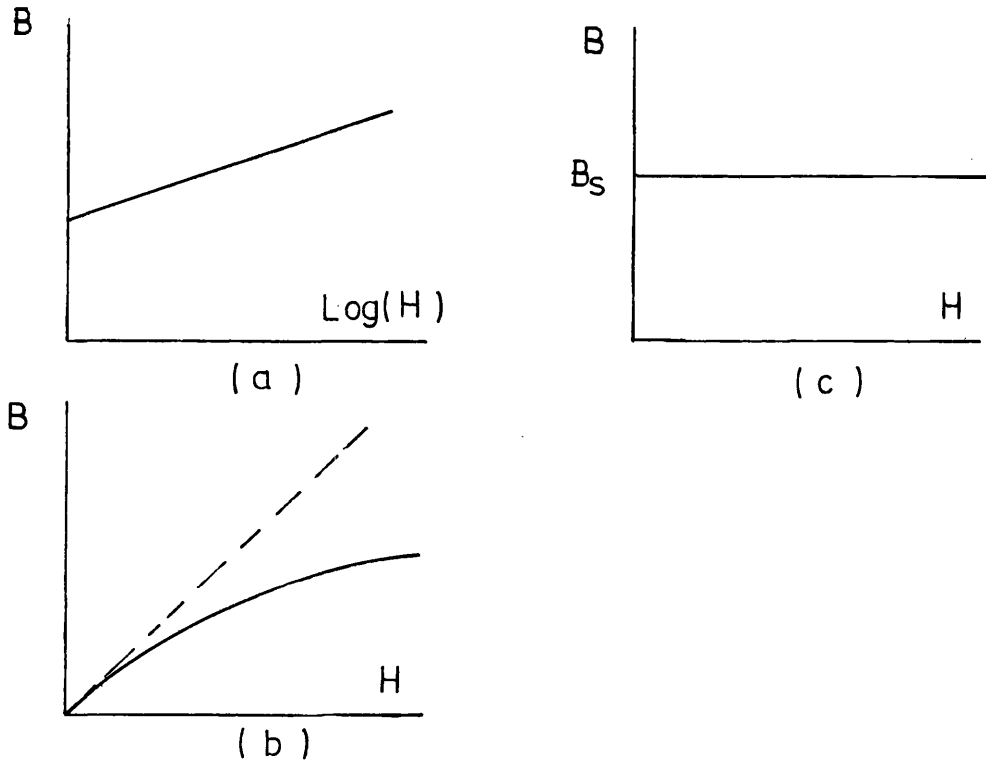


Figure 3.1 Flux Density Characteristic of the Iron

The semi-empirical method published ^{3.5} in 1949 still treated the tooth-tip and zigzag fluxes separately. The basis of this method was to select the iron area most likely to saturate, and then to calculate the flux at that point. An unsaturated flux was first calculated on the assumption that all the m.m.f.'s were applied to the relevant air-path length. This flux was then used to calculate a flux density in the iron, which was assumed to be the density which would occur if the iron retained its initial characteristic, shown by the broken line in figure 3.1(b). Once this fictitious

density was found, the actual density was read off the true magnetisation curve, to give the leakage flux and hence the saturation factor.

In 1961, AGARWAL and ALGER^{3.6} produced a simple method which combined the tooth-tip and zigzag-leakage fluxes. It was assumed that no m.m.f. was consumed in the iron until the flux density reached an arbitrary level of 125,000 lines/in², after which the density remained constant regardless of any further increase in m.m.f., as shown in figure 3.1(c). A single iron area was assumed to offer the greatest constriction to the total flux, and was used to calculate an unsaturated flux density in the iron. The saturation factor was then unity until the density reached the limiting value, after which it became the ratio of this maximum density to the unsaturated value. All the above methods ignored the effect of skew-leakage flux. ANGST extended the work of AGARWAL and ALGER in 1963^{3.7} to include the effect of skew-leakage flux on the saturation of the leakage paths. Simplifications were still made to produce formula amenable to manual calculation, and only one saturable area was considered.

In 1969, B.J. CHALMER and R. DODGSON^{3.8} also adopted the rectangular magnetisation characteristic, as used by AGARWAL and ALGER to compute the combined saturation factors. Their study was conducted in three stages. The first stage covers the calculation of the elements of resistance and leakage reactance of the

motor, assuming that there are no saturation effects. In the second stage, the magnitude and phase of each saturable reactance flux is calculated, and a picture of the combined leakage fluxes over a pole pitch is constructed. In the final stage, the effects of the combined leakage fluxes is determined, and the saturation factors are computed. Specific attention is devoted to the identification of saturable areas in the magnetic circuit.

The only components of leakage flux which are assumed not to saturate are the end-winding and slot-body leakage fluxes.

Similarly as the flux density rises above the knee of the saturation curve, the effective frequency of the voltage induced in the core laminations rises rapidly ^{3.1}. The combined increases in frequency and flux density cause the eddy-current losses to rise much faster than the square of the density.

The phenomenon of flux penetration in solid ferromagnetic cores has been analysed under various simplifying assumptions, and the results have been used in such practical applications as the solid pole shoes of self-starting synchronous motors, eddy-current brakes and couplings, and induction motors with solid iron secondaries. POHL's ^{3.9} graphical treatment of the problem extended the results of the linear theory beyond the knee of the magnetisation curve. The B/H curve is divided into several linear segments, and the linear analysis is applied step by step. The effect of hysteresis

was included in POHL's work, but the end effect due to finite length of the rotor was neglected. Another attempt to extend the linear theory to the non-linear range was made by GIBBS ^{3.10}, who introduced a quadratic equation for the B/H curve in the results obtained under the assumption of constant permeability. This equation, though an approximate fit, was found to be unsuitable for the B/H curve of cast iron. The effect of finite length was included in GIBBS' paper by increasing the resistivity of the rotor material. Several authors ^{3.11,3.12, 3.13}, have made use of the limiting theory in which the B/H curve was idealised as a step function of excitation. McCONNEL and SVERDRUP ^{3.11}, applied the solution of the one dimensional field problem to the two dimensional field existing in the rotor, ignoring the end effect. KESAVAMURTHY and RAJAGOPALAN ^{3.12} have analysed the flux penetration due to alternating and rotating magnetic fields, including finite axial length. However since this analysis was based on constant permeability, the results were applicable only to the linear range. In another investigation ^{3.13} using the limiting B/H curve, they analysed the phenomenon in the non-linear range also, taking the limiting value of the flux density B_s at any instant as the value of B corresponding to the H acting at that instant. The limiting theory was later used by ANGST ^{3.14} who also derived a complex end effect by a three-dimensional linear analysis.

In all these analytic methods, the B/H curve as a whole was not introduced into the field problem at the initial state. Further, according to the linear and limiting theories, the rotor power factor is obtained as a constant, independent of slip, voltage or rotor material.

In 1969 PILLAI ^{3.15,3.16}, attempted to develop a theoretical treatment of the problem in solid and hollow rotors, by introducing the non-linear nature of the B/H curve into the analysis at the initial stage of solution, and to account theoretically for the variation of the rotor power factor with slip. He included the end effect simply by increasing the resistivity of the rotor material and also by neglecting the hysteresis effect. A Fourier analysis of the output voltage wave shapes of low-frequency sources shows that, depending upon the order, the harmonic component of the voltage may contribute either positive or negative torque ^{3.17}. Synchronous torques occurring in squirrel-cage induction motors may be due to a variety of causes, one of which is the interaction between pairs of stator and rotor harmonics ^{3.18}.

In 1971 CHALMERS and DODGSON presented ^{3.19} a new method for determining the wave shape of airgap flux density in induction motors taking into account the effect of saturation in the magnetic circuit. They considered the m.m.f. in the airgap at no-load as a fundamental sinusoid. Then, the waveform of the airgap flux density

due to this m.m.f. is first determined by using the magnetic properties and dimensions of the magnetic circuit, and then used to find its fundamental component and saturation harmonics. LEE and TINDALL^{3.20} used the assumptions, that the saturation harmonics in induction machines are greatest at no-load and evaluated the amplitudes of saturation harmonics by performing a non-linear field calculation over a radial cross section of the machine. The over-relaxation technique was used to solve the necessary field equations. In 1976 ROGERS^{3.21} produced a mathematical model which included the effects of both m.m.f. and permeance harmonics and allowed standard circuit techniques to be used. He employed a new method of field analysis^{3.22} to the problem of the three-phase cage-rotor induction motors. The method unifies the field and circuit theories of machines^{3.23}. A realistic airgap geometry is assumed and the field within the airgap and within each slot are calculated separately in terms of the assumed distribution of tangential magnetic-field strength at their common boundaries. From the vector potential in each slot, the flux linking any stator coil can be calculated and its terminal voltage equation obtained.

The vast majority of induction motors have skewed slots, and one of the reasons for employing skew is to reduce the cogging tendency. A cogging torque is the component of the torque output of a machine that varies with rotor position with respect to stator, and if very

large can cause the rotor to lock at standstill. A high cogging torque is always undesirable in an induction motor since although it may not prevent the machine from starting, it can cause vibrations in the machine frame. In 1968 BINNS ^{3.24} described an accurate method of analysis of the cogging phenomenon and gave a method by which the cogging torque variations can be determined from simple airgap leakage flux and magnetising flux equations. In 1970 BINNS and DYE ^{3.25} described the effect of slot skewing on the cogging torques and produced a simple equation which describes the effect of skew on these torques. It is important in certain cases to avoid slot skewing, which increases losses and leakage reactance resulting in lower efficiency ^{3.25,3.26}, particularly in polyphase motors. ALGER ^{3.1} discusses cogging torques, and gives some conditions under which the torques are appreciable. The effect of the cogging tendency can also be eliminated by considering the stator and rotor slot numbers without the use of skewed slot ^{3.27}. Certain practical changes in the equivalent circuit parameters of a cage induction motor due to skewing the rotor can be derived mathematically from fundamental principles for predicting its performance characteristics ^{3.28}. Digital and mathematical models have been constructed for predicting changes in the equivalent circuit parameters and performance characteristics arising from the effects of:-

- (a) saturation harmonics,

- (b) high frequency losses due to open stator slots with and without skewed rotor slots ^{3.29}, and,
- (c) machines employing double-cage rotors ^{3.30}.

3.3 Part One

3.3.1 Analysis of the New Linear Equivalent Circuit

Considering the equivalent circuit of figure 2.2, all the parameters of this equivalent circuit are expressed on a per phase basis. This applies whether the stator winding is Y- or Δ - connected. In the latter case the values refer to the equivalent Y- connection. Appearing in this figure is the positive of the equivalent circuit that has reference to the stator (or primary) winding. Note that it consists of:

- (i) a stator phase winding resistance R_1 ,
- (ii) a stator phase leakage reactance X_1 , and,
- (iii) a parallel RP_1 which takes care of all changes in the stator winding when supplied with different frequencies.

The magnetising impedance is made up of the core-loss resistance R_M and the magnetising reactance X_M . The form of magnetising impedance is the same as the standard one, but values of R_M and X_M are obtained from a circle diagram whereas in a standard case the values of the magnetising branch parameters are determined from a motor running light test with fixed supply frequency. The latter case does not include any changes which would arise at different supply frequencies, as mentioned in Chapter 2.

The secondary consists of the rotor phase leakage reactance X_2 , rotor phase resistance R_2 and RP_2 which takes care of any changes in the secondary elements. RP_1 and RP_2 have no physical significance, in other words they cannot be referred to any physical elements within the machine. They can only be justified if the parallel networks are converted into series equivalent form. Then the resistive parts add to stator and rotor d.c. resistances to represent the a.c. resistances at any applied frequency. The reactive parts are also frequency dependent and represent the primary and secondary leakage reactances at any applied frequency. In the following sections the frequency dependent model is analysed to obtain the necessary performance equations.

3.3.2 The Actual Rotor Circuit Per Phase

For any specified load condition which calls for a particular value of slip, the rotor current per phase may be expressed as:

$$\bar{I}_2 = \frac{S\bar{E}_2}{Z_2} \quad \text{--- (3.1)}$$

$$\text{but } \bar{Z}_2 = \frac{X_2^2(R_2 + RP_2) + R_2(RP_2)^2}{(RP_2)^2 + (X_2)^2} + jS \frac{(RP_2)^2 \cdot X_2}{(RP_2)^2 + (X_2)^2} \quad \text{--- (3.2)}$$

$$\text{or } \bar{Z}_2 = Z_2 \angle \phi_2$$

$$\text{where } \phi_2 = \text{Tan}^{-1} \frac{S \cdot X_2 (RP_2)^2}{X_2^2 (R_2 + RP_2) + R_2^2 (RP_2)^2} \quad \text{--- (3.3)}$$

$$\text{thus } \bar{I}_2 = \frac{S \bar{E}_2}{Z_2 (\text{Cos} \phi_2 + j S \cdot \text{Sin} \phi_2)} \quad \text{--- (3.4)}$$

where \bar{E}_2 and X_2 are the stand still values. I_2 is a slip-frequency current produced by the slip-frequency induced emf SE_2 acting in a rotor circuit having an impedance per phase of equation (3.2). In other words, this is the current that would be seen by an observer riding with the rotor winding. Furthermore, the amount of real power involved in this rotor circuit is the current squared, times the real part of the rotor impedance. In fact, this power represents the rotor copper loss per phase. Hence the total rotor copper loss may be expressed as:

$$P_{CU2} = m \cdot I_2^2 \cdot Z_2 \cdot \text{Cos} \phi_2 \quad \text{--- (3.5)}$$

where m is the number of rotor phases.

3.3.3 The Equivalent Rotor Circuit

By dividing both the numerator and denominator of equation (3.4) by the slip S , we get:

$$\bar{I}_2 = \frac{\bar{E}_2}{\bar{Z}_2 \left(\frac{1}{S} \text{Cos} \phi_2 + j \text{Sin} \phi_2 \right)} \quad \text{--- (3.6)}$$

$$\begin{aligned}\bar{z}_{22} &= z_{22} / \phi_{22} \\ &= \bar{z}_2 \left(\frac{1}{s} \cos\phi_2 + j \sin\phi_2 \right) \quad \text{--- (3.7)}\end{aligned}$$

$$\phi_{22} = \phi_2$$

where \bar{z}_{22} is the rotor impedance transferred to the primary. Note that the magnitude and phase angle of \bar{I}_2 remains unaltered by this operation. However there is a clear difference between equation (3.4) and (3.6). In the latter case \bar{I}_2 is produced by a line-frequency voltage \bar{E}_2 acting in the rotor circuit having an impedance per phase of:

$$z_2 \cdot \left(\frac{1}{s} \cos\phi_2 + j \sin\phi_2 \right) \quad \text{--- (3.8)}$$

Hence the \bar{I}_2 of equation (3.6) is a line-frequency current, whereas the \bar{I}_2 of equation (3.4) is a slip-frequency current. Now, the real power associated with the equivalent rotor circuit is clearly:

$$P_g = I_2^2 \cdot \frac{1}{s} \cdot z_2 \cdot \cos\phi_2 \quad \text{--- (3.9)}$$

Hence the total power transferred the airgap from the stator to the rotor for

$$P_g = m \cdot I_2^2 \cdot \frac{1}{s} \cdot z_2 \cdot \cos\phi_2 \quad \text{--- (3.10)}$$

A comparison of this expression with equation (3.5) indicated that the power associated with the equivalent

circuit is considerably greater. This means that the point of reference has changed from the rotor to the stator. In other words the observer changes his point of reference from the rotor to the stator. This shift is important because now, upon looking into the rotor, the observer sees not only the rotor copper loss but the mechanical power developed as well. The equation (3.10) can be rewritten in a manner that indicates this fact.

$$P_g = m \cdot I_2^2 \left[Z_2 \cdot \cos\phi_2 + \frac{1}{s} \cdot Z_2 \cdot \cos\phi_2 (1 - s) \right] \quad \text{--- (3.11)}$$

In other words the variable slip dependent resistor may be replaced by the actual rotor winding resistance, (real part of equation (3.2)) and a variable resistance R_{mech} which represents the mechanical shaft load. That is:

$$R_{\text{mech}} = \frac{1}{s} \cdot Z_2 \cdot \cos\phi_2 (1 - s) \quad \text{--- (3.12)}$$

This expression is useful in analysis because it allows any mechanical load to be represented in the equivalent circuit by a resistor.

3.3.4 Calculation of Performance

When the three-phase induction motor is running at no-load, the slip has a value very close to zero. Hence the mechanical load resistor R_{mech} has a very large value, which in turn causes a small rotor current to flow. The corresponding electromagnetic torque

assumes a value which is required to overcome the rotational losses consisting chiefly of friction and windage. If a mechanical load is now applied to the motor shaft, the initial reaction is for the shaft load to drop the rotor speed slightly and thereby increase the slip. The new value of slip causes I_2 to increase, consequently increasing rotor power to yield sufficient torque to provide a balance of power to the load. Thus equilibrium is established and the operation proceeds at a particular value of S . In fact there is a unique value of slip for each value of load horse power.

3.3.5 Starting Torque

Consider the power-flow diagram shown in figure 3.2. The total power transferred across the airgap (ie. rotor input power supplies the rotor copper loss and mechanical output power). The resultant shaft torque of this transferred airgap power is:

$$T_S = m \cdot I_2^2 \cdot \frac{1}{S} \cdot Z_2 \cdot \cos\phi_2 \quad \text{--- (3.13)}$$

or

$$= m \cdot I_2^2 \cdot \frac{1}{S} \cdot Z_{22} \cos\phi_{22}$$

The value of torque at any slip is determined by the real part of the rotor impedance. In some applications where high starting torque is essential, the rotor resistance has a high value to start with, and this reduces as slip increases. One way to do this is to

design the squirrel-cage with deep bars or with two distinct rotor bars separated by a flux-leakage path. In either case, the effective secondary resistance is high at starting, when the rotor frequency is high, and low at full speed.

Another way is to provide an insulated secondary winding, similar to the primary, which is brought out to slip rings and connected to an external resistance between the slip rings at starting. The resistance may be adjusted to give the desired torque at standstill, decreased as the speed rises, and short-circuited at full speed. This method allows minimum starting current, and permits longer duration of the starting period, or prolonged operation at low speeds without overheating the motor, and so is generally used for large and adjustable speed motors.

3.3.6 Torque-speed Characteristics

The torque-speed characteristics of the induction motor can be explained from equation (3.4). As slip is allowed to increase from nearly zero to about 10%, the rotor current increases almost linearly. Moreover, for this same range of slip the rotor power factor angle ψ_2 varies over a range of about zero to 10° . This means that the rotor power factor $\cos \psi_2$ remains practically invariant over this range and so torque increases almost linearly in this region.

As slip is allowed to increase still further, the rotor current continues to increase, but much less than at first. The reason for this lies in the increasing importance of the product of slip times the imaginary term of rotor impedance. In addition, the angle ϕ_2 now begins to increase at a rapid rate which makes the $\cos \psi_2$ diminish more rapidly than the current increases. Since the torque equation now involves two opposing factors, it is reasonable to expect that a point will be reached beyond which torque will decrease for any increases in slip, so the torque-speed curve takes on a form similar to that shown in figure 3.3.

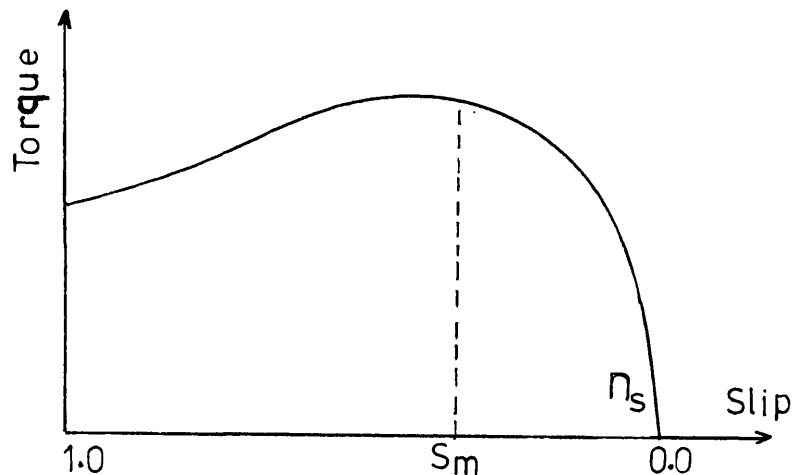


Figure 3.3 Typical torque-speed curve for a three-phase induction motor

The starting torque is the torque developed when slip is unity, ie. the speed n is zero. The starting torque of induction motors has a value usually somewhat in excess of rated torque, and its value is

calculated in the same manner as torque is computed for any value of slip, simply by substituting the value of S by unity. Thus the magnitude of the rotor current at standstill becomes:

$$I_S = \frac{V_1}{[(R_1 + R_2')^2 + (X_1 + X_2')^2]^{\frac{1}{2}}} \quad \text{--- (3.14)}$$

$$\text{where } \bar{Z}_2' = \frac{Z_m \cdot Z_{22} / \phi_m + \phi_{22}}{Z_m / \phi_m + Z_{22} / \phi_{22}} \quad \text{--- (3.15)}$$

$$\text{thus } R_2' = Z_2' \cdot \cos \phi_2' \quad \text{--- (3.16)}$$

$$X_2' = Z_2' \cdot \sin \phi_2' \quad \text{--- (3.17)}$$

The corresponding power transferred across the airgap is then:

$$P_g = m \cdot I_2^2 \cdot Z_{22} \cdot \cos \phi_{22} \quad \text{--- (3.18)}$$

$$\text{where } \bar{I}_2 = \frac{\bar{E}_2}{Z_{22} \cdot \phi_{22}} \quad \text{--- (3.19)}$$

$$\text{but } \bar{E}_2 = \frac{V_1 \cdot Z_2' / \phi_2'}{Z_1 / \phi_1 + Z_2' / \phi_2'} \quad \text{--- (3.20)}$$

$$\text{where } \bar{Z}_1 = Z_1 / \phi_1'$$

$$= \frac{X_1^2 (R_1 + RP_1) + R_1 (RP_1)^2}{X_1^2 + (RP_1)^2} + j \frac{X_1 (RP_1)^2}{X_1^2 + (RP_1)^2} \quad \text{--- (3.21)}$$

$$\text{and } \phi_1 = \text{Tan}^{-1} \frac{X_1 (RP_1)^2}{X_1^2 (R_1 + RP_1) + R_1 (RP_1)^2} \quad \text{--- (3.22)}$$

$$\text{thus } P_g = m \cdot \left[\frac{V_1 \cdot Z_2' / \phi_2'}{Z_{22} / \phi_{22} (Z_1 / \phi_1 + Z_2' / \phi_2')} \right]^2 \cdot Z_{22} \cdot \text{Cos} \phi_{22} \quad \text{--- (3.23)}$$

It is interesting to note that the higher starting torques result from increased rotor copper losses at standstill.

Another important torque quantity of the three-phase induction motor is the maximum developed torque. This quantity is so important that it is sometimes the starting point in the design of the induction motor. The maximum (breakdown) torque is a measure of the reserve capacity of the machine. It frequently has a value of 200 to 300% of the rated torque. It permits the motor to operate through momentary peak loads. However this maximum torque cannot be delivered continuously; excessive currents would destroy the insulation, and the machine is very unstable in this region, ie. any small changes in load would result in much variation in the rotor speed. It is also possible to stall the machine.

Since the developed torque is directly proportional to the gap power, the torque is maximum when the gap power is maximum. But the gap power has a maximum value when there is a maximum transfer of power to the equivalent rotor resistor. Applying the maximum power transfer theorem to the equivalent circuit we have:

$$\frac{R_{22}}{S_m} = [R_1'^2 + (X_1 + X_2)^2]^{1/2} \quad \text{--- (3.24)}$$

$$\text{where } z_1' = \frac{z_1 \cdot z_m \cos \phi_1 + \phi_m}{z_1 \cos \phi_1 + z_m \cos \phi_m} \quad \text{--- (3.25)}$$

$$\text{thus } R_1' = z_1' \cos \phi_1' \quad \text{--- (3.26)}$$

$$X_1' = z_1' \sin \phi_1' \quad \text{--- (3.27)}$$

That is, maximum power is transferred to the gap power resistor R_{22}/S when this resistor is equal to the impedance looking back into the source. Thus the corresponding value of S_m for T_m is:

$$S_m = \frac{R_{22}}{[R_1'^2 + (X_1 + X_2)^2]^{1/2}} \quad \text{--- (3.28)}$$

Note from equation (3.28), that the maximum torque can occur at any speed depending on the value of rotor resistance. Some induction motors are in fact designed to have maximum torque at starting. With the slip S_m known, the corresponding rotor current can be found and then inserted into the torque equation to yield the final form for the breakdown torque. Thus by neglecting the magnetising branch we have:

$$T_m = \frac{1}{2\omega S} \cdot \frac{mV_1^2}{[R_1 + \sqrt{R_1^2 + (X_1 + X_{22})^2}]^2} \quad \text{--- (3.29)}$$

Therefore maximum torque is independent of the rotor resistance, ie. different values of rotor resistance would only determine the value of slip in which the maximum torque will occur.

3.3.7 Measurement of Experimental Results

In order to examine the validity of the new equivalent circuit for performance calculations, the experimental torque speed characteristics are required. One method of obtaining these characteristics is to plot the shaft torque versus its speed while the machine is accelerating a given inertia mass from zero to maximum velocity. The machine has to be robust and 100% safe for speeds up to 20,000 RPM. The torque transducer is not used in the load shaft for measuring the amount of twist. This is because the available torque transducers normally carry brushes and therefore they are liable to introduce errors into the readings at higher speeds. Also any failure in the bearings can easily damage the transducer unless it is provided with a special clutch. The application of load cells is not considered either, due to economic reasons. Instead, the torque is measured directly from the case of the main drive induction motor, which is equal and in an opposite direction to rotor torque. The rotor speed is measured by a slotted disc and an infra-red photo-cell. The speed and torque transducers, without physical contact with the rotor, allow extremely accurate results

to be obtained at any rotor speed. All the necessary calculations are carried out when designing the inertia disc, drive shaft and bearings to avoid the coincidence of the transverse vibration frequency with operation frequency.

The coincidence of these two frequencies can lead to failure in the system. The gyroscopic effects are also taken into consideration to make sure that the shafts whirling speeds are well outside the operating range. Highly accurate electronic circuitry is designed and developed for the torque and speed transducers. The design and development of the whole plotting machine is given in full detail in Appendix B. This test rig is then used to plot the torque-speed characteristic of the machine with supply frequencies from 10 Hz up through 100 Hz with steps of 10 Hz, and from 100 Hz to 320 Hz inclusive with steps of 20 Hz. In addition at each step of the operations the machine terminal voltage is kept at the following volts-per-hertz, 1.34, 1.24, 1.16, 1.1, 1.00, 0.908 (or 110%, 100%, 97%, 91%, 83%, 75%, of the rated volts per hertz) and plots are shown in figures B.11 to B.31 in Appendix B. Because the changes in the machine parameters at various supply frequencies are very small, and the purpose of these torque-speed characteristics are to investigate the validity of these small changes, it is necessarily essential to observe any possible changes arising from temperature in parameters or reduction in terminal

voltages at starting currents. Thus, the terminal voltages are also plotted while the machine is accelerating the inertia disc and are shown on the torque-speed characteristic curves. In addition, the temperature rises at each step of the frequency operation, while the machine is accelerating the inertia disc from zero velocity to maximum velocity during six different applied volts-per-hertz, are plotted and shown in figure 3.4. These six different voltage operations are carried out immediately one after the other in descending order, and the total temperature rise at each step of the supplied frequencies are plotted and shown in figure 3.4. The temperature characteristic is incorporated in the computer program in section (3.7) to allow for the changes in the stator resistance (R_1) during the acceleration.

3.3.8 Digital Program Description of Torque Speed Characteristics

A digital program is developed which uses the torque equation (3.13) to plot the torque speed characteristics. This program includes two major loops. The first loop plots the characteristics for six given applied volts per hertz. These six steps are chosen to obtain the same results as the experiments for the purpose of comparison. The second loop adjusts the changes in the resistive parts according to the temperature rise characteristics. This also provides the same

conditions as the experimental results. The program adjusts the value of stator resistance R_1 according to the relationship given in equation (3.30).

$$R_1(t) = R_1(\text{d.c.}) + A.t \quad \text{--- (3.30)}$$

$$R_1(\text{d.c.}) = 2.0\Omega$$

$$A = 18.8\text{m}\Omega/\text{C}^\circ$$

Where R_1 is the d.c. stator resistance per phase, taken at room temperature, and constant A is the increase in the resistance for each degree of temperature rise in centigrade. But average temperature rise in the machine for accelerating a given load and given supply frequency from figure 3.4 is:

$$t = t_1 + B.F \quad \text{--- (3.31)}$$

where t_1 is the initial machine temperature and constant B is the temperature rise per hertz during the acceleration of the given load. Thus:

$$R_1 = R_1(\text{d.c.}) + A(t_1 + B.F) \quad \text{--- (3.32)}$$

Because all six torque-speed characteristics are plotted immediately in descending order of applied volts-per-hertz, this program uses the room temperature as the initial value of t_1 for the first plot, and then the average temperature rise of this as the initial value of t_1 for the next plot, and so on. At the end of each supply frequency operation the program again starts the

initial value of t_1 as the room temperature. The flow diagram of the program is shown in figure 3.5.

In addition when the applied volts-per-hertz is 110% of the rated value, the non-linear program of section (3.4) is used to determine the torque speed characteristics.

3.3.9 Experimental Results

The internal impedance of the generator set used to produce the experimental curves causes the terminal voltage across the induction motor to vary with rotor speed as shown in figures B.11 - B.31 in Appendix B. The voltage drop is maximum when the rotor speed is zero and is restored to pre-set value as rotor speed approaches synchronous speed. Within this operating range there is no saturation in the leakage reactances, and this is discussed in later sections. Therefore the linear voltage square law is applied to make the necessary corrections in the experimental torque speed curves due to this voltage drop. The corrected experimental curves and those obtained directly from the new equivalent circuit are shown in steps of 40 Hz in figures 3.6 - 3.14. In the linear region results are identical except when the applied volts-per-hertz is 110% of the rated value which appears to have the effect of load losses and saturation harmonics on the experimental curves. However the calculated curves obtained from the new equivalent circuit do not contain these

effects. This is because the modelling of the load losses and saturation harmonics are not included in the equivalent circuit as mentioned before.

3.4 Part Two

3.4.1 The Construction of a Non-Linear Model for Induction Motors in Variable Speed Applications

In the following sections the effect of voltage saturation on the machine parameters is discussed. Various experiments are designed to identify the changes in the parameters with saturation. The test results are then used to produce the non-linear relationship between the parameters, applied voltage and frequency. A digital program is then developed which alters the values of the parameters according to the applied voltage and frequency and produces the required characteristics. The torque speed characteristics are obtained from the non-linear model when the applied volts-per-hertz is 110% of the rated value. These characteristics are then used to determine the magnitude of error which would have been involved if the linear model was used. A 110% of the rated value is chosen which is approximately equal to the gap voltage when the machine is operating in the regenerative mode.

3.4.2 Effects of Saturation on Leakage Reactances

It is well known that the leakage reactance of an induction motor varies with the operating conditions. The principal cause of this variation is the magnetic

saturation of the leakage flux path, which increases with current and reduces the leakage reactance. Many manufacturers have developed formulae for the machine reactances, and empirical factors are often included, particularly for the estimation of saturation. If the design of a new machine differs from the previous standards, the empirical factors may no longer be applicable.

The total leakage reactance of a cage induction motor is the sum of the primary and secondary leakage reactances, and this total is subdivided into eight principal components as listed in Chapter 2, Section 5. Components (a) to (d) are caused by leakage fluxes at the locations mentioned. These fluxes obviously link only one winding. Components (e) and (f) are reactances due to the m.m.f. harmonics of the stator and rotor fields in the airgap.

If the stator or rotor slots are skewed, the load m.m.f. of the skewed member is displaced in time phase along the core length. This produces an m.m.f. in the airgap which is a function of the phase difference between the stator and rotor fundamental m.m.f. waves, and which drives skew leakage flux around the magnetic circuit. Skewing may be visualised as a reduction of the magnetic coupling between the primary and secondary windings by a shift of the magnetic axis of the skewed member, its effect is to reduce the mutual reactance, thus adding leakage reactances (g) and (h) to the respective members.

3.4.3 Experimental Results

To investigate the changes in the leakage reactance of the machine under the experiment, arising from saturation, various readings of phase volts, currents and power are taken with rotor locked. Bristol University's generator sets were used to obtain the necessary supply frequencies. Then the per phase volts-per-hertz and current characteristics with various supply frequencies with rotor locked are plotted and shown in figure 3.15. Due to the limited power capability of these generator sets, it was not possible to obtain any results above the phase currents of ten amperes. (Induction machines normally have starting currents of about five times the rated value. In the case of this particular machine, generators capable of supplying 15 amps or more were required). Within the limited ranges of these experiments there was no indication of any saturation in the iron of the machine.

The experimental results of the starting torques and applied volts-per-hertz squared obtained previously using the generator sets at the Royal Aircraft Establishment, Farnborough, are also linearly related and are shown in figure 3.16. This confirms that there is no sign of saturation in the flux paths with starting currents of up to 110% of the rated values. Therefore the non-linear model does not make any alterations in the leakage reactances for the determination of the required performance characteristics.

3.4.4 Effect of Saturation on the Magnetising Branch Parameters

The magnetic flux in both stator and rotor is carried by alloy-steel laminations, usually containing 1 to 3% silicon. The lamination thickness usually compromises between the cost and the eddy current loss, which later increases as the square of the thickness. Economy requires use of the highest flux density compatible with moderate core losses and magnetising ampere turns, making a steel of high magnetic quality desirable. The laminations are, therefore, annealed at a high temperature and are insulated with core plate enamel. In the smaller sized motors and with controlled atmosphere anneal however, the oxide scale on the laminations may provide sufficient insulation. Partly closed slots are also used in smaller motors because they increase the effective gap area giving a lower magnetising current for a given size of motor, and allowing the use of fewer turns in the winding with lower resistance. The width of opening is chosen to permit easy assembly of the coils and to avoid magnetic saturation of the tooth-tips at high currents. Larger motors designed for voltages greater than 600 volts are normally made with open slots to permit the use of form-wound coils insulated before assembly.

Since the flux density in the teeth varies in proportion to the airgap flux density, magnetic saturation will be reached by the teeth at the centre of the

flux wave before it is reached elsewhere. The magnetising current drawn from the line is nearly sinusoidal however and the impressed main flux wave preserves its sinusoidal space distribution at all currents.

Therefore the airgap flux wave has a flat top, the flattening becoming more pronounced as the flux is increased (figure 3.17).

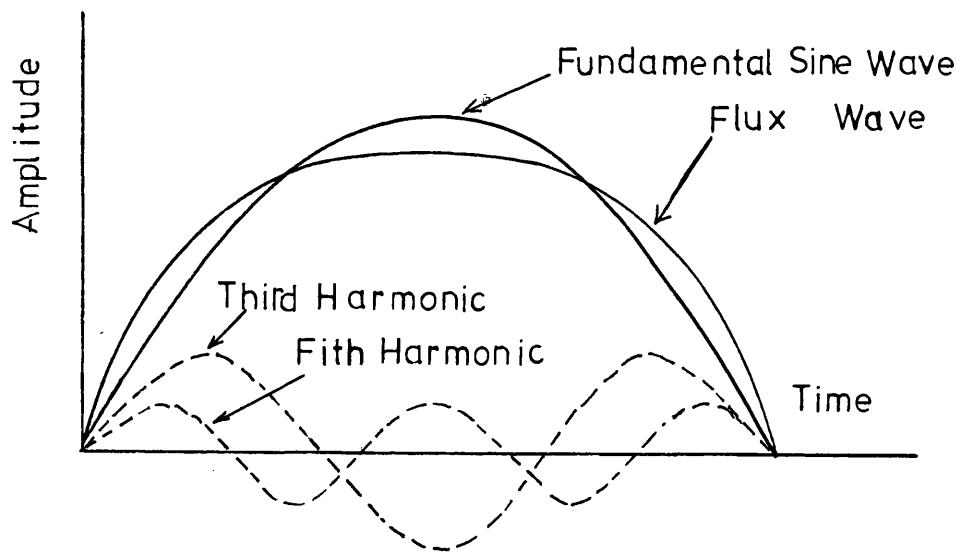


Figure 3.17 Effect of Saturation on the Shape of the Airgap Flux Wave

The flux density in the core, behind the teeth is at a maximum at 90 electrical degrees away from the peak of the airgap flux density wave, since the core flux is the space integral of the airgap flux. Hence the peripheral distribution of core ampere turns is 90° displaced from that for the teeth. A saturated core therefore tends to result in a peaked airgap flux wave, offsetting in part the flattening effect of saturation in the teeth. The flux distribution curve retains its

fixed shape as the field revolves, so that the saturation harmonics in the airgap flux wave revolve at the same speed as the fundamental, and produce rotor voltages at multiples of the slip frequency. At high values of slip, they induce rotor currents which damp them out completely, restoring the sinusoidal flux wave shape and the decreased airgap flux and saturation at increasing values of load current make these harmonics of no importance with respect to breakdown torque or starting performance.

The resistive part of the magnetising branch represents the sum of the core loss, the stray-load losses, friction loss and windage loss. The core loss rises much faster than the square of the density as the flux density rises above the knee of the saturation curve. This is because of the rapid rise in the effective frequency of the voltages induced in the core laminations. The stray-load losses are additional core loss, caused by the increase in the airgap leakage fluxes with load, and by the high frequency pulsations of these fluxes. Also a large part of the stray-load loss is due to induced harmonic currents in the rotor circuit.

The values of the resistive and the reactive parts of the magnetising branch are usually determined from the running light test. This equivalent network represents the magnetising branch, when the motor is running light, with flux density at the knee of the saturation curve. A series of experiments are carried

out to investigate the behaviour of the magnetising parameters well before and after the knee of the saturation curve. To do this the induction machine is mechanically coupled to an a.c. series-connected commutator machine (Appendix B, figure B.1). The induction motor is fed with supply frequencies from 50 Hz up through 200 Hz. At each step the rotor is driven into its corresponding synchronous speed by means of the a.c. commutator machine. Then the phase voltage is increased from 0.2 to 2.0 volts-per-hertz inclusive, and corresponding values of phase current and total input power are recorded. The saturation curves at various supply frequencies are then plotted and shown in figure 3.18. In Section 3.4.6 these curves together with input power are broken down into various other characteristics to obtain an equivalent circuit model of the magnetising branch for below and above the knee of the saturation curve.

3.4.5 Model Representation of Magnetising Branch Parameters

In Chapter 2, the circle fit technique is employed to determine the parallel RL network to represent the magnetising branch equivalent circuit parameters. This RL network represents all the changes in the magnetising branch arising from different supply frequencies with constant volts-per-hertz operating point. Due to non-linear characteristics of the iron of the machine, the values of the parallel RL network

elements will be different with different applied volts-per-hertz across the input terminals. The voltage drop across the primary impedance will differ at different values of the rotor slip for a given applied volt per hertz. This makes the operating point of the magnetising branch slip dependent as well as the applied voltage. Now it is required to form a model which would be frequency, applied voltage and rotor slip dependent. Similar techniques could be employed to find some forms of parallel and series combinations of RL networks to give the required characteristics. Instead a digital computer program is developed which produces the required characteristics of the magnetising branch, depending on the value of these variables.

3.4.6 Program Description of the Non-Linear Model

The program is developed to compute a complex number whose magnitude and phase angle are dependent on values of the operating conditions, that is supply frequency, magnitude of applied voltage and rotor slip. Any changes either in applied voltage or slip will result in changes in the magnitude of the magnetising current, hence the latter is used as a reference to search for values of the required complex number.

From the experimental results, the magnitude of the input impedances and cosines of phase angles ($\cos \phi_m$) of the magnetising branch with different supply frequencies are calculated and plotted with various line currents and are shown in figures 3.19 and 3.20.

The change in $\text{Cos } \phi_m$ with different supply frequencies for a given volts-per-hertz is not very significant due to the fact that the resistive part of the magnetising circuit is frequency dependent as well as the reactive part. This is also confirmed in the locus diagram of R_m versus X_m shown in Chapter 2, figure 2.3. Thus the results obtained from this experiment when the machine is running from a 150 Hz supply frequency are used to calculate the values of $\text{Cos } \phi_m$. The values of $\text{Cos } \phi_m$ versus line current are plotted and shown in figure 3.20. However the magnitudes of the input impedance per hertz change very significantly with different supply frequencies as the applied volts-per-hertz rises above the knee of the saturation curve (see figure 3.19).

The changes in magnitude of the input impedance in the saturation region with different supply frequencies are also calculated and shown in figure 3.21. Then by inspection this non-linearity of the input impedance with supply frequency is fitted with equation (3.33).

$$(\text{ZI/HZ})_F = 0.15 + 0.175e^{-F/50} \quad \text{--- (3.33)}$$

Similarly the non-linear region of figure 3.20 is fitted with equation (3.34).

$$(\text{Cos } \phi_m)_{I_m} = 0.08 + 0.002I_m^2 \quad \text{--- (3.34)}$$

Finally from equation (3.33) and figure 3.19 the value of the per phase input impedance within the saturation region is given by equation (3.35).

$$(ZI/HZ)_{I_m, F} = (ZI/HZ)_F + [0.65 - (ZI/HZ)_F] e^{-\frac{I_m - 1.2}{2.5}}$$

Substituting $(ZI/HZ)_F$ from equation (3.33) we obtain:

$$(ZI/HZ)_{I_m, F} = 0.15 + 0.175e^{-F/50} + e^{-\left(\frac{F+20I_m-24}{50}\right)} - 0.65e^{-\left(\frac{I_m-1.2}{2.5}\right)} \quad \text{--- (3.35)}$$

The computer program uses the equivalent parameters of figure 2.2 of Chapter 2 as the initial starting data. For any given terminal voltage, supply frequency and rotor slip, it calculates the magnitude of the current taken by the magnetising branch. If the modulus of this current lies within the linear region of operation it continues to compute the required output without making any changes in the given values of magnetising branch elements. But if it lies within the non-linear region, then using this value of I_m , and equations (3.34) and (3.35) it computes the new values of the magnetising circuit elements. The computed results are then used to find the corresponding new value of I_m . If the difference between the new value of Z_m and the

one used immediately before, is within the given accuracy it jumps out of the loop and uses the new computed values of the magnetising branch elements to carry out the rest of the operations. See figure 3.22 for the flow diagram. The resultant model is then used to compute all the required characteristics with the rotor at synchronous speed.

3.4.7 Reduction in the Shaft Torque due to Voltage Saturation

The torque speed curves of the linear and non-linear model applied with 110% of the rated volts-per-hertz are used to determine the effect of voltage saturation. The reduction in the torque is calculated as a percentage and shown in figure 3.23. With rotor slip greater than 0.4, the gap voltage is well within the linear region for the given volts per hertz. However as the slip falls below 0.4, the gap voltage rises above the linear region. This increases the magnetising current and reduces the rotor current which causes a subsequent reduction in the output torque. The magnitude of error for a given volts-per-hertz increases further with the supply frequency as shown in figure 3.23.

3.5 Discussion of Results

The investigation into the effects of variable supply frequency on the three-phase induction machine performance clearly shows the important role of rotor parameters in torque-speed characteristics. Because

of the increasing value of the rotor resistive part with higher supply frequency (due to various losses and non-uniform distribution of current at high frequencies) the starting torque also increases correspondingly when the machine is applied with a given volts per hertz.

The value of rotor slip at which the maximum breakdown torque occurs, decreases as the supply frequency increases. This is mainly because of the increasing value of X_2 with frequency.

In an ideal machine having equal stator and rotor parameters (ie. $X_1 = X_2$, $R_1 = R_2$), the starting torque will increase from zero to a maximum value as the supply frequency increases from zero until a value when the reactive and the resistive parts of the machine are equal. Any further increase in the frequency after this point will result in lower values of the starting torque. But the starting torque characteristic of the induction motors rise to a maximum point and then stays almost constant. This is because the rotor resistance is not constant and increases as the supply frequency rises, at the same time the actual rotor inductance falls with frequency.

Thus the resistive and reactive parts of the rotor circuit, appear to behave in such a manner that after reaching the maximum it continues to produce constant starting torques for any further increases in the supply frequency. The width of this frequency band which produces almost constant starting torques for a given volts-per-hertz depends on the type of rotor construction used.

Another important point to be considered is the behaviour of the normal operating point on the torque speed characteristics with various supply frequencies. The value of slip at this point is usually taken to be less than 10% depending on the machine type. The position of this point depends on the maximum allowed load variations and it is always taken as a percentage of maximum breakdown torque. The maximum breakdown torque variations of this particular machine with supply frequency with rated volts-per-hertz applied is plotted in figure 2.9 in Chapter 2.

The value of slip for a given operating point similar to that of maximum torque also decreases as the supply frequency increases. Or, in other words, for a given value of the slip the corresponding value of the torque becomes greater at higher supply frequencies. This can be seen on the three-dimensional torque speed characteristic of the machine, when applied with rated volts-per-hertz (constant flux) shown in figure 3.24. As a result the machine becomes more efficient at higher supply frequencies when operating near synchronous speed. The rotor frequency also approaches to zero, and consequently any increase in the resistive part of the rotor due to higher frequency losses reduces towards d.c. value. Therefore the effect of running the machine with higher supply frequency virtually has a similar effect to that of the deep bar used in rotor construction.

Even though saturation of any region of the iron would result in changes in the leakage reactances, the experiment results obtained from locked rotor tests do not indicate any sign of saturation in the iron of this particular machine. Also the limited output power of the generator sets of Bristol University did not allow the machine to be driven well above the saturation region with the rotor locked. However there was enough power to carry on the investigation within the operating conditions. This is also confirmed by the torque characteristic results in Section 3.3.9, figure 3.16. Thus the effect of saturation on the leakage reactances are neglected and therefore this effect is not included in the resultant model.

The magnetising parameters begin to alter in a non-linear fashion as soon as the magnetising current rises above the linear region. One might argue that in normal operating conditions the magnetising current never reaches the non-linear region. However in some variable frequency applications it is necessary to keep the torque constant over ranges of speed. This would require the machine to be driven above the designed volts-per-hertz characteristics especially in the lower frequency ranges. Also when the machine is operating in regenerative mode, the gap voltage may rise well above the normal operating level and result in voltage saturation.

The difference in the element values of the magnetising circuit in the linear operating region mainly arises from changes in the rotor frequency as its slip

changes with the applied voltage. The amount of variation in this region is not significant enough to produce serious effects on the machine performance equations. However as the terminal voltage rises above the operating knee point of the saturation curve, the magnetising elements start to change very rapidly as mentioned before. This consequently results in a serious effect on the machine performance, such as a reduction in the shaft torque. Therefore the resistive and inductive parts of the magnetising branch become dependent on both the applied volts-per-hertz and the supply frequency.

These variations are calculated from the computer program and are shown in figure 3.25. Because of these variations the value of the operating applied volts-per-hertz can no longer be taken as a constant value in variable frequency applications. Therefore the operating volts-per-hertz should be related to the gap voltage. This relationship can be determined from the ~~new~~ equivalent circuit.

Since the airgap flux is proportional to the E_1/F_1 (E_1 = gap voltage, F_1 = stator frequency) the electromagnetic torque is proportional to the square of the airgap flux at a given rotor frequency F_2 . Consequently if the airgap flux is maintained constant under all operating conditions, the induction motor torque is determined solely by the absolute rotor frequency (F_2) and is independent of the supply frequency (F_1). A control scheme in which the airgap flux is constant and the rotor

slip frequency is directly controlled, thus permits a precise adjustment of motor torque at any speed, provided that the ratio of E_1/F_1 is kept constant throughout all the supply frequencies. Generally in constant flux applications the ratio of the terminal voltage to the supply frequency V_1/F_1 is kept constant. But this is not adequate enough in wide frequency range applications. Because of the frequency dependent elements of the machine the ratios of V_1/F_1 and E_1/F_1 do not follow directly and some adjustment has to be made in the ratio of V_1/F_1 in order to keep E_1/F_1 constant at any applied frequency. If this non-linear relationship between V_1/F_1 and E_1/F_1 is not clearly identified, it can result in serious problems at higher frequency ranges, ie. the operating volts-per-hertz can become much higher than the rated value. This can easily run into saturation harmonics and hence distort the torque speed characteristics. This is clearly apparent in the experimental results (obtained from the machine under test) when the supply frequency is above 150 Hz and the applied volts-per-hertz exceeds the rated value. This is because the ratio of the input terminal voltage to the supply frequency is kept constant rather than the gap voltage.

In variable speed applications, the inverter designer must be aware of all the non-linearities arising from voltage saturation in order to achieve the best results. In the majority of inverter designs it is not required to have the non-linear model of the machine. But

perhaps it may help towards a better understanding of the machine performance when the machine's operating frequency and number of pulses per cycle are very low. Under these conditions, because of higher supply rail voltages than the rated value and longer time constants of switching pulses, the flux in the airgap will rise from the initial value into saturated value during each switching mode. Thus the average flux in the airgap will be a combination of fundamental and saturation harmonics. This results in a considerable amount of distortion on the shaft torque which may stall the machine. Also considerable amounts of heat are generated in the windings and rotor bars which can damage the machine. Thus, having the non-linear model or at least being aware of these non-linearities due to voltage saturation can help the inverter designer to calculate or predict the required minimum number of pulses per cycle for given frequency and supply rail voltages without running into serious problems.

Once all these behaviour patterns of the machine are clear for any speed control circuitry designer, he can simply include all the necessary changes in his controller to obtain any torque speed characteristics from an induction machine most efficiently.

Finally the experimental and computed torque speed characteristics confirm the validity of such a frequency dependent model and the technique used to obtain individual equivalent circuit parameters.

Another important point to notice is the constant slip frequency operation characteristic of the machine. Under this condition when the machine is operating with a constant applied volts per hertz, the rotor parameters are no longer dependent on the supply frequency. This results in a constant shaft torque as long as the rotor frequency remains unaltered. Consider plane M in parallel with plane XOZ in figure 3.24. Plane M intersects the torque speed characteristics at points indicated by $\tau_1, \tau_2 \dots$. Since plane M and plane XOZ are in parallel all points on this plane correspond to a constant torque, including those points indicated by $\tau_1, \tau_2 \dots$. All these points ($\tau_1 \dots$) correspond to a constant slip frequency. However their corresponding rotor slip depends on the supply frequency. For example, when the machine is operating from a 50 Hz supply with the rated volts per hertz producing a 1.25 Nm rotor torque, the rotor slip is 0.5 corresponding to a slip frequency of 25 Hz. However with a 300 Hz supply for the same rotor torque and running condition the rotor slip becomes 0.083. This also corresponds to a slip frequency of 25 Hz. Therefore in the constant torque application a parallel plane similar to M can be used to determine the value of the rotor slip at any supply frequency.

3.6 Conclusions

Similar performance equations to those used in the standard equivalent circuit can be derived and applied for the new equivalent circuit. All the changes in the equivalent circuit parameters at different supply frequencies can therefore be related to the output performance characteristics. The effect of the saturation of the yoke of the machine on the performance characteristics up to 110% of the rated applied volts-per-hertz results in a reduction in the output torque. This reduction in torque increases as the rotor speed approaches the synchronous speed and increases even further with higher values of the supply frequency.

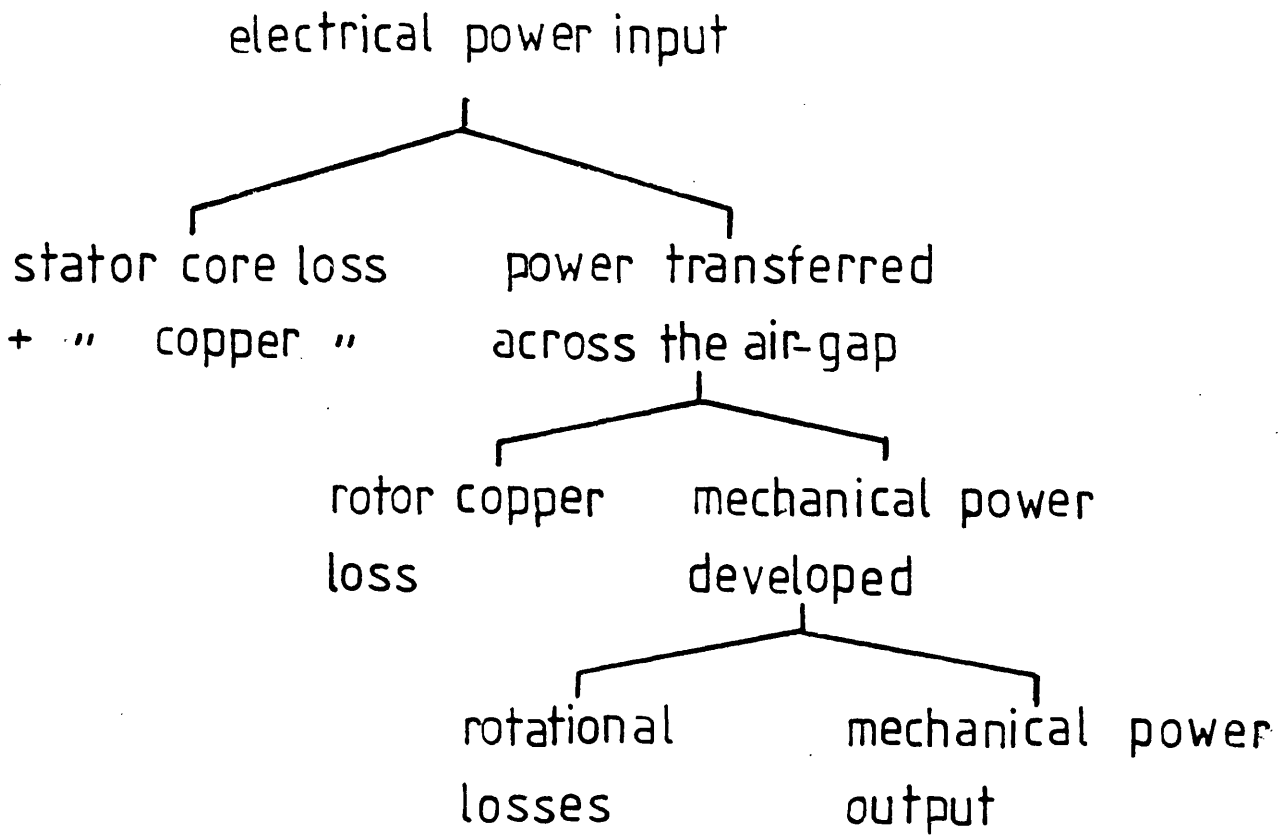


Fig.3.2a. power flow dia. in statement form

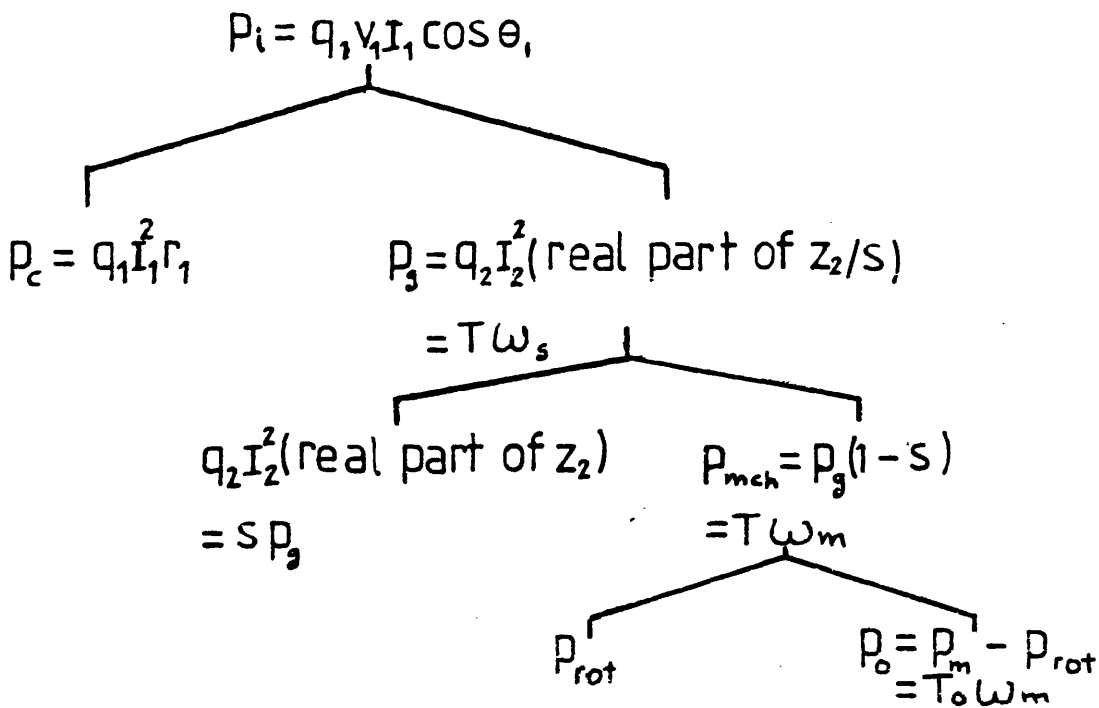


Fig.3.2b power flow dia. in equation form

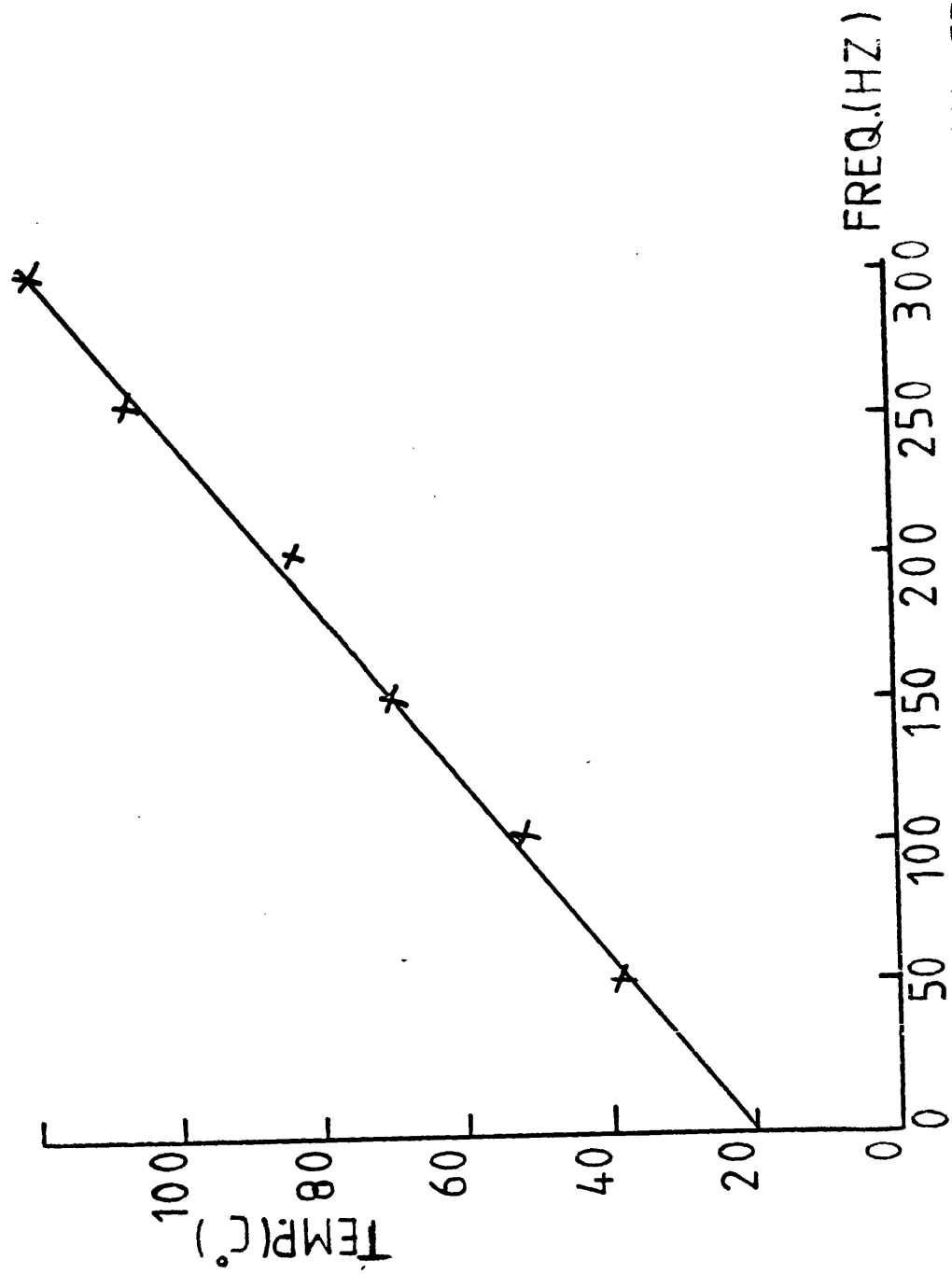


Fig 3.4 TEMP. RISE DURING ACCE. A GIVEN LOAD V SUP. FREQ.

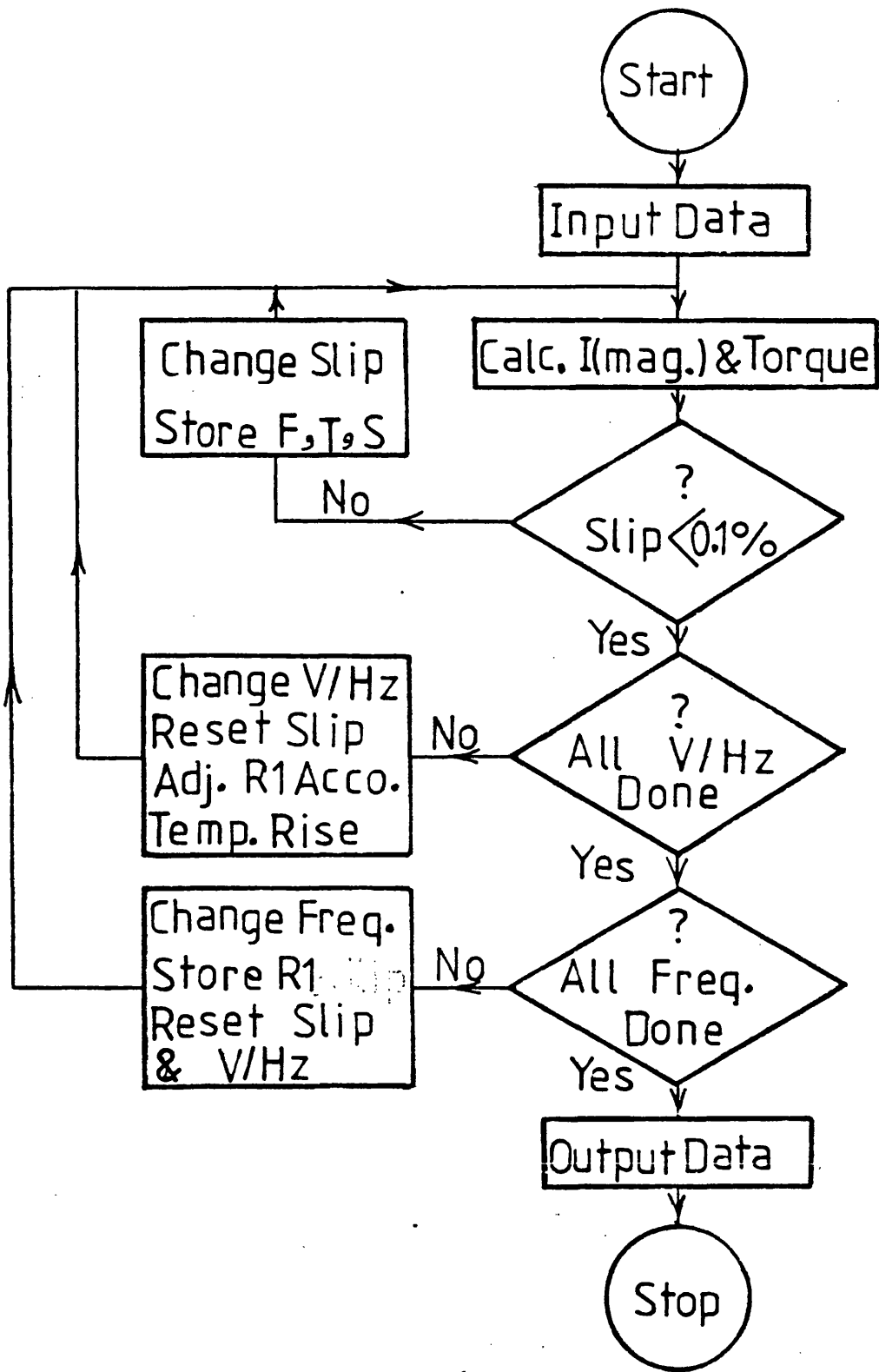


Fig. 3.5 Flow Dia. Of Linear Model For Det. Of Torque Speed Chara.

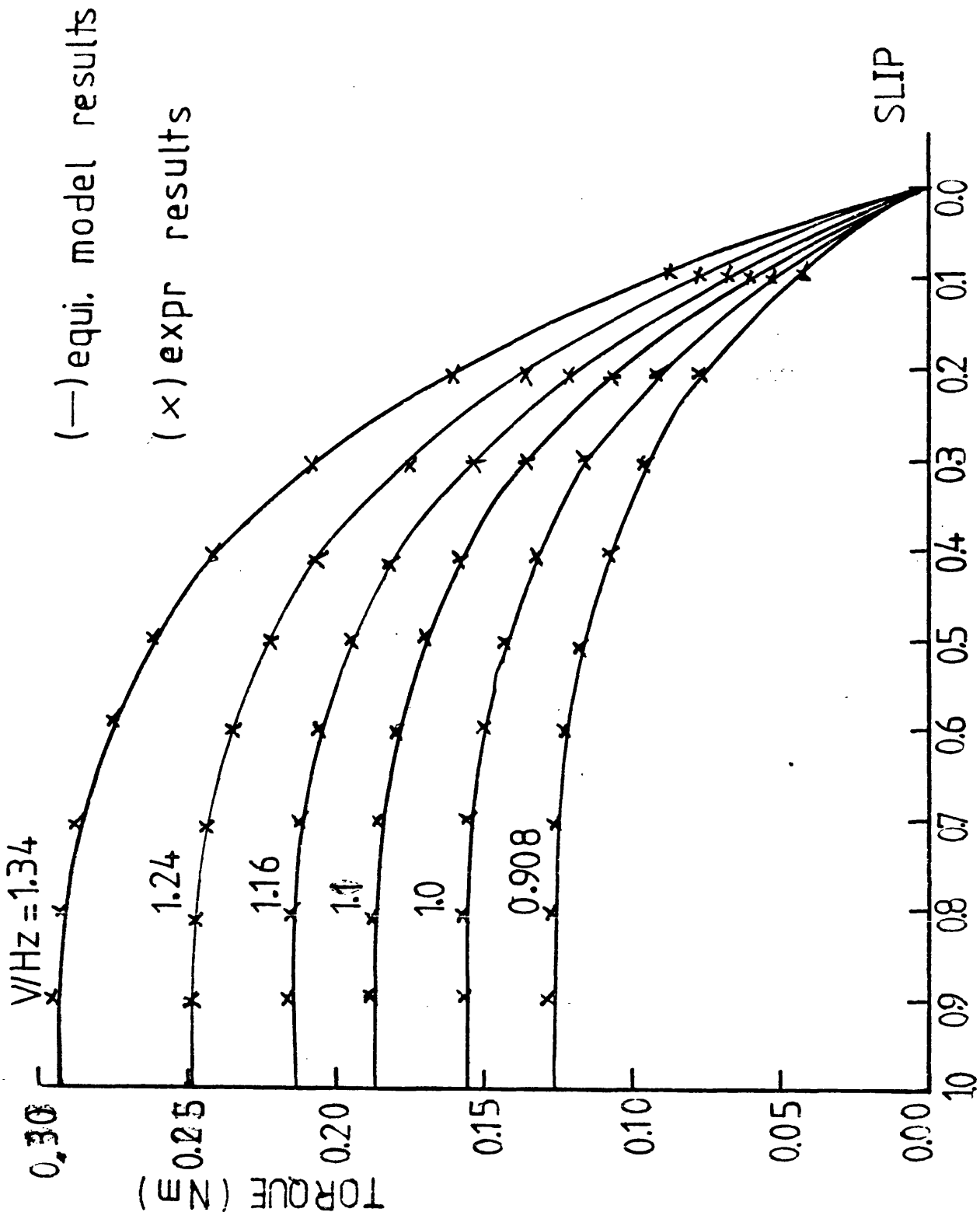


Fig. 3.6 TORQUE V SLIP F= 10HZ

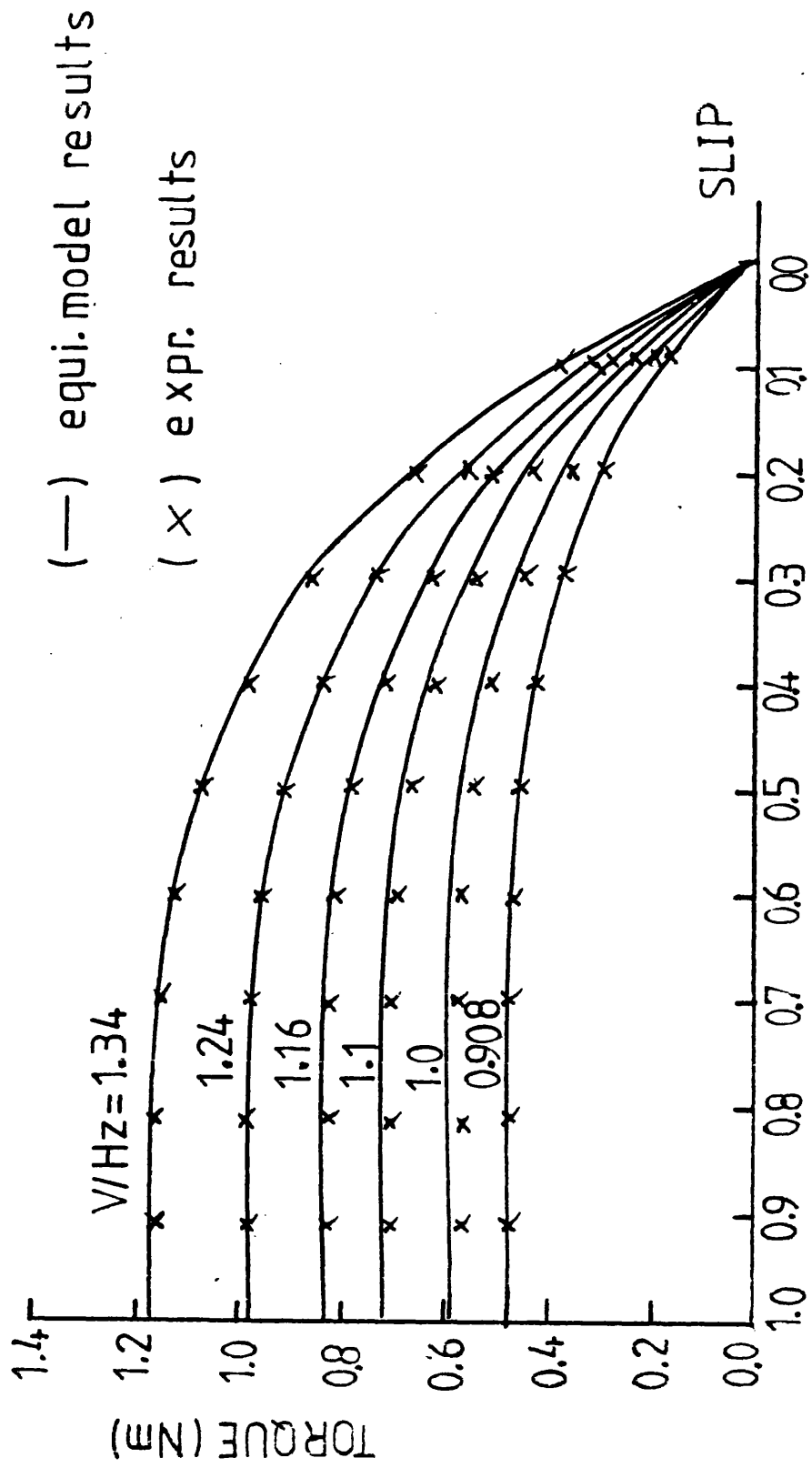


Fig 3.7 TORQUE V SLIP F = 40 HZ

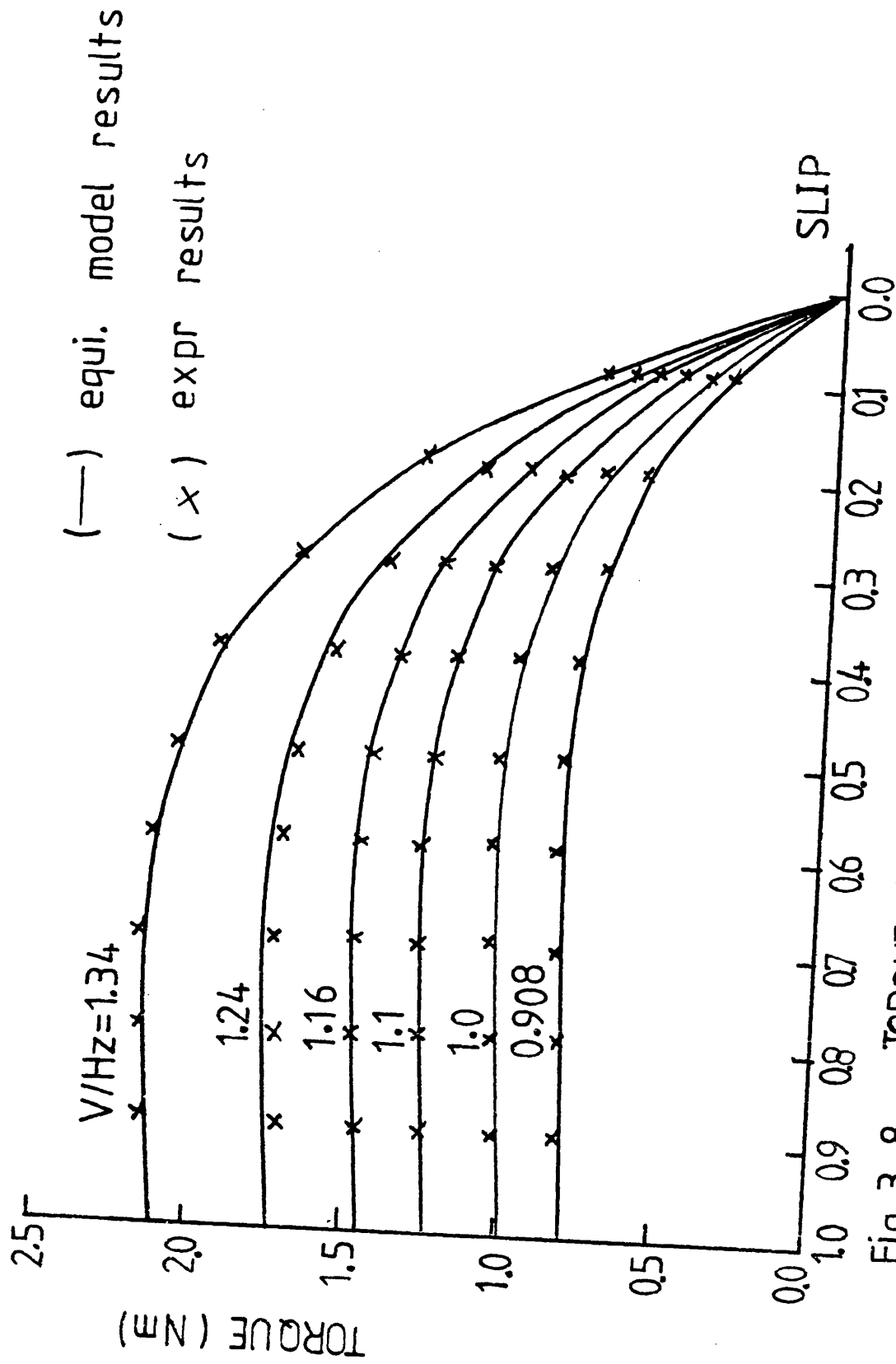


Fig. 3. 8 TORQUE V SLIP F= 80 HZ

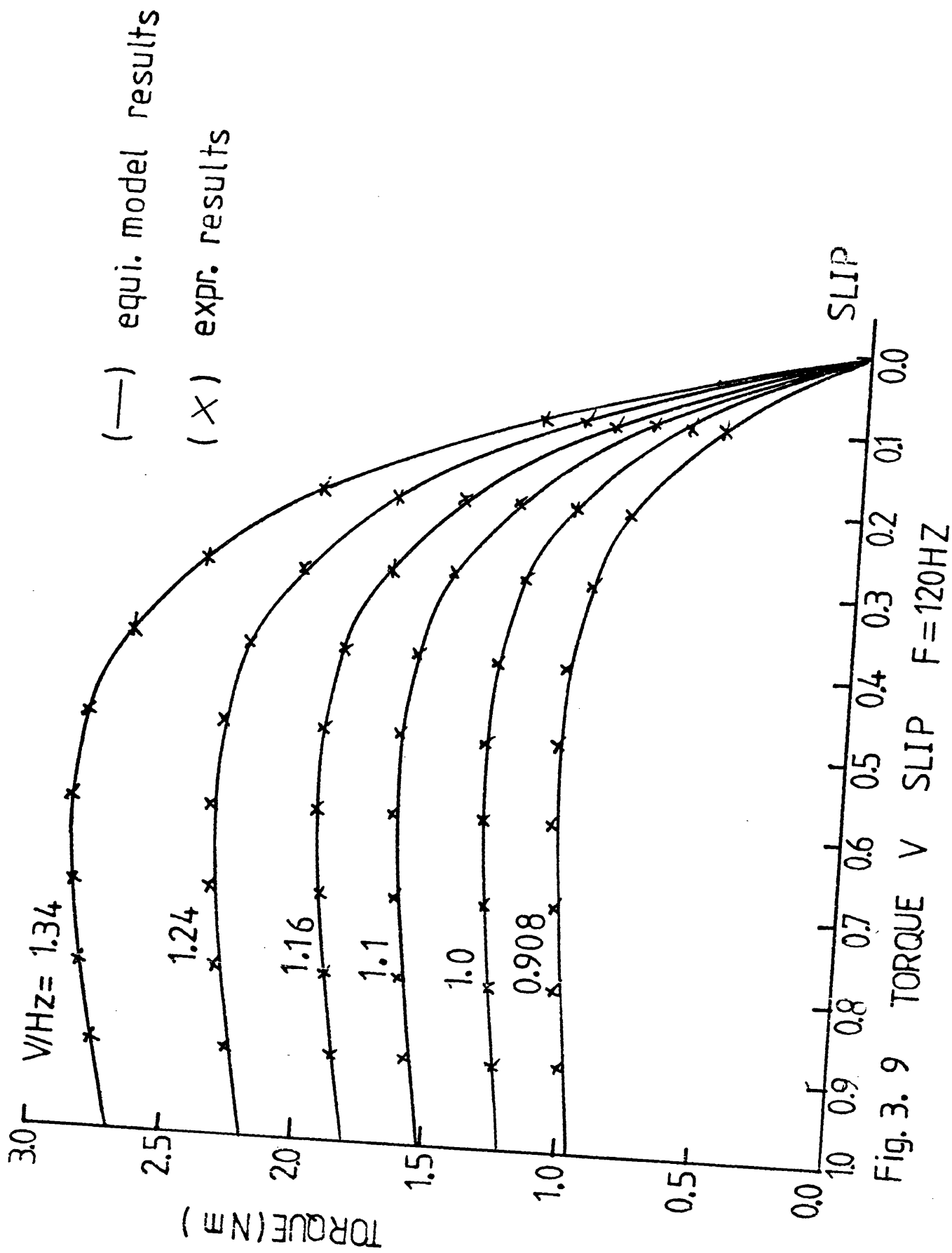


Fig. 3. 9 TORQUE V SLIP F=120HZ

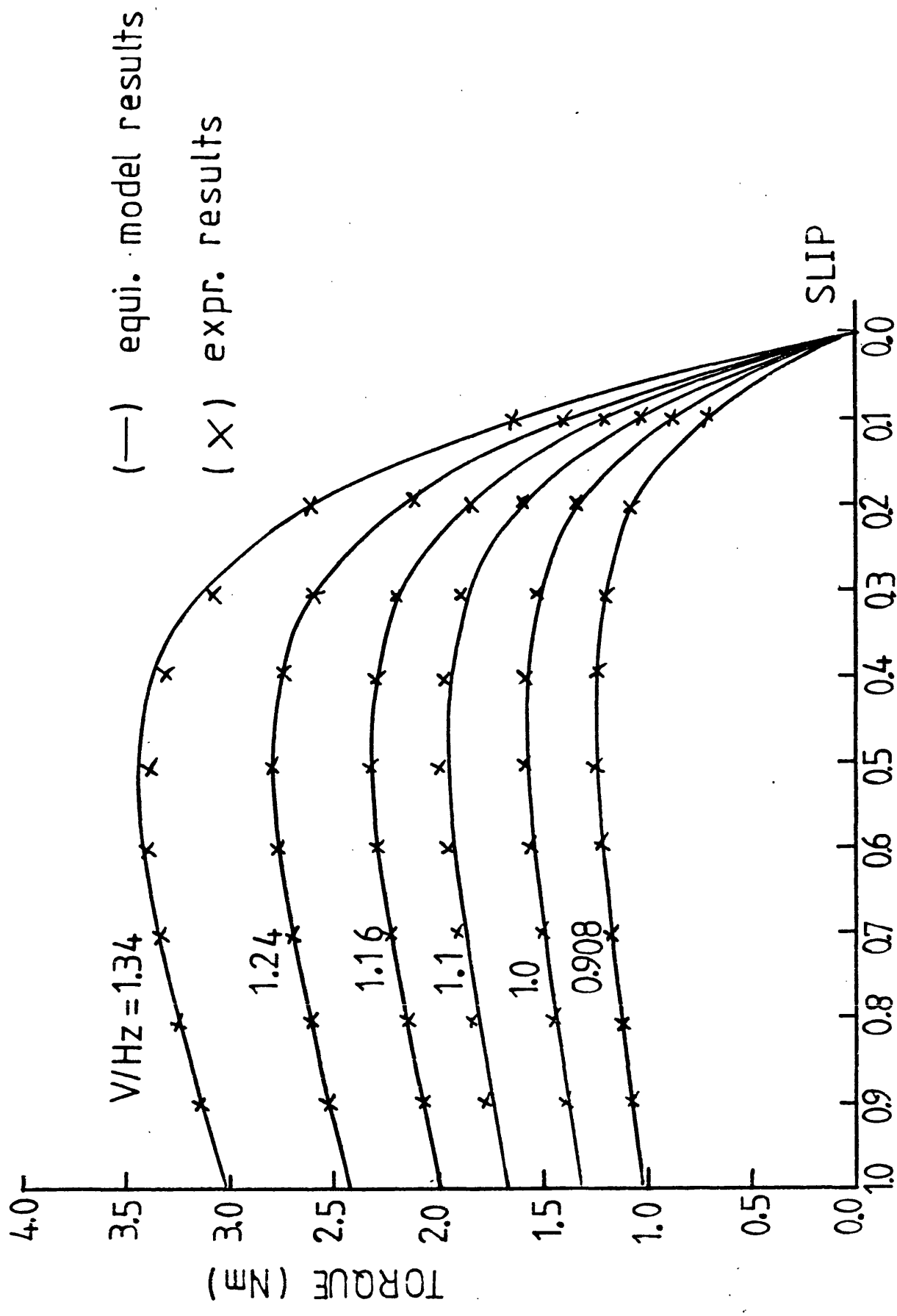


Fig. 3.10 TORQUE V SLIP F=160HZ

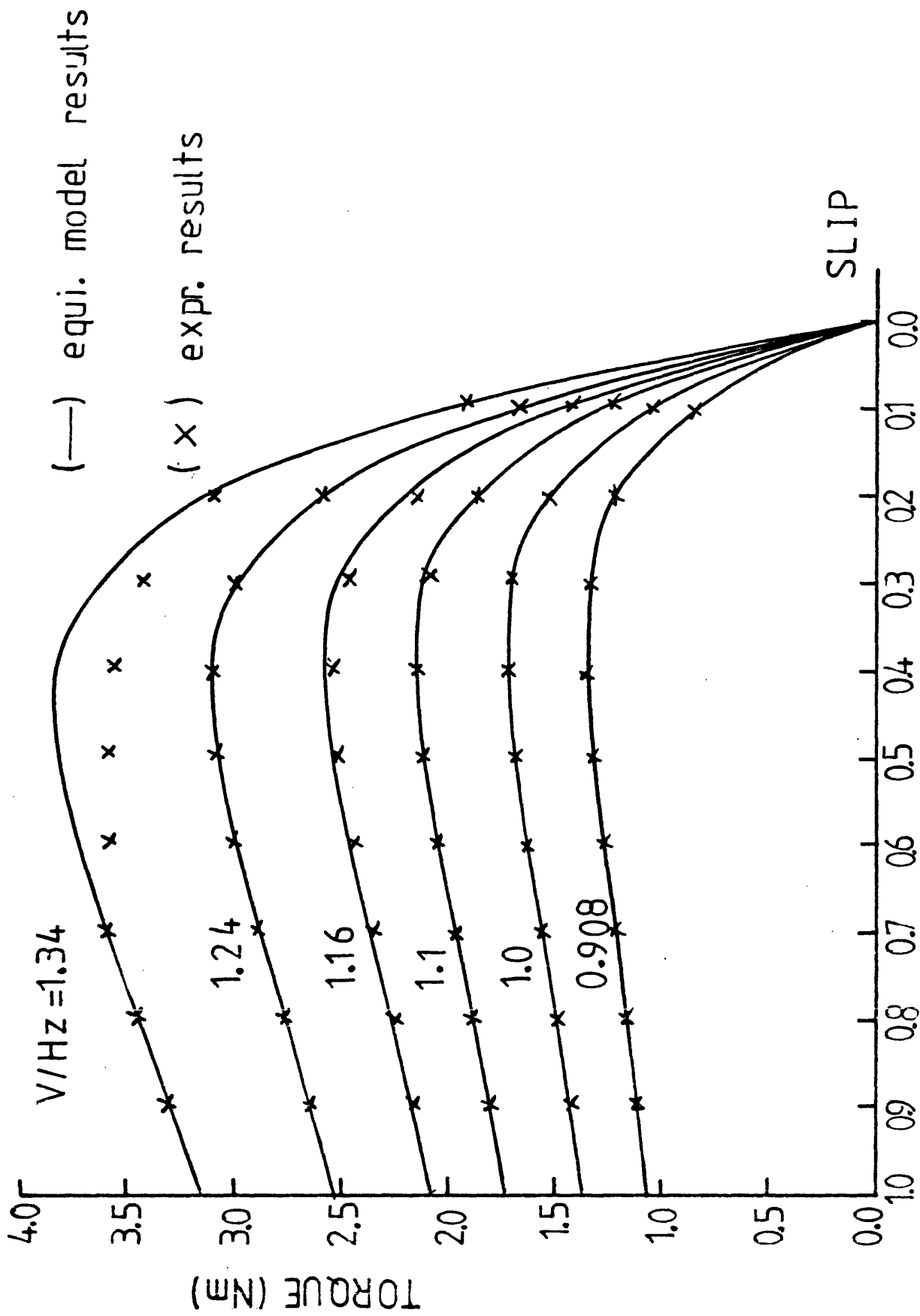


Fig. 3.11 TORQUE V SLIP $F = 200 \text{ HZ}$

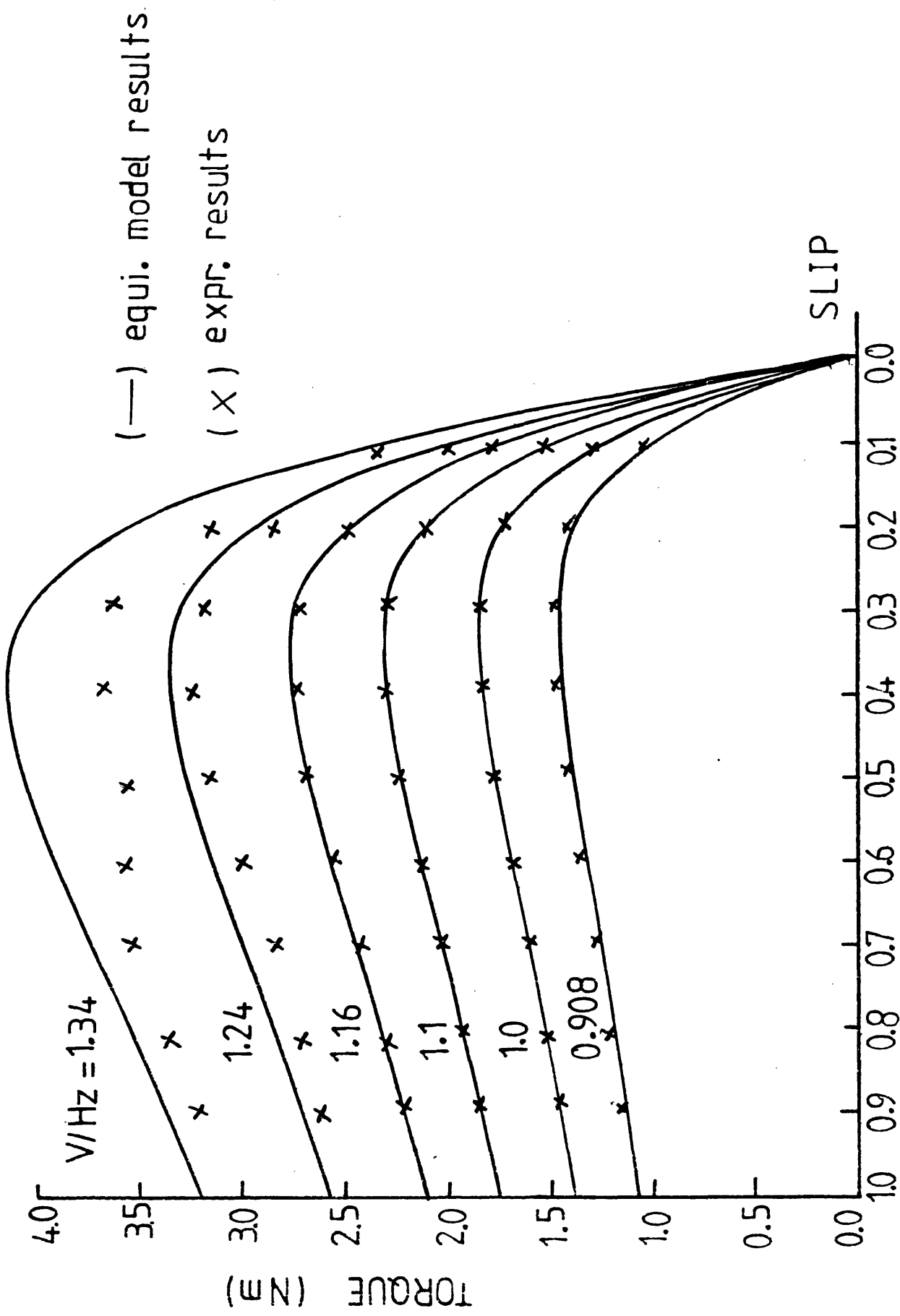


Fig. 3.12 TORQUE V SLIP F = 240HZ

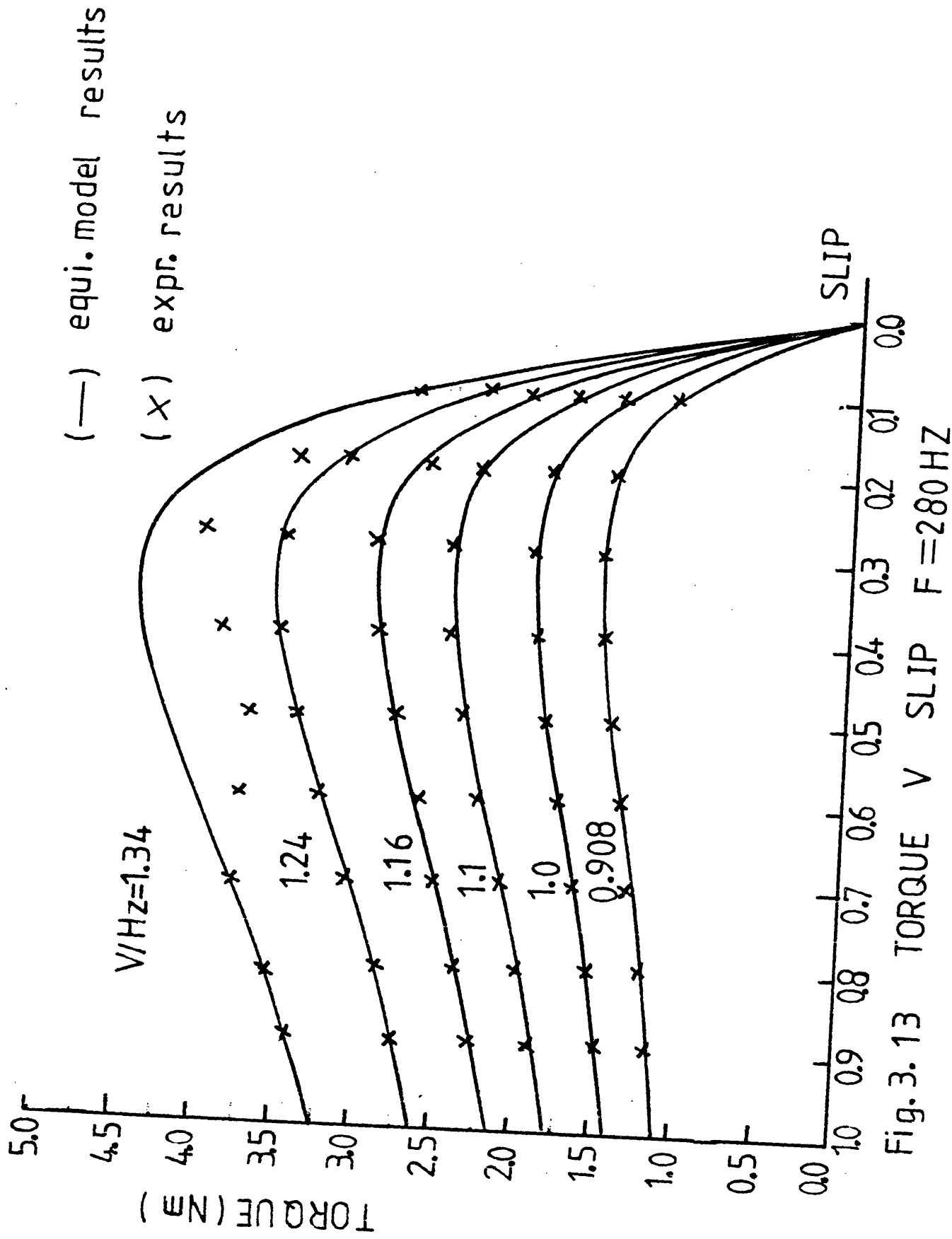


Fig. 3.13 TORQUE V SLIP F=280HZ

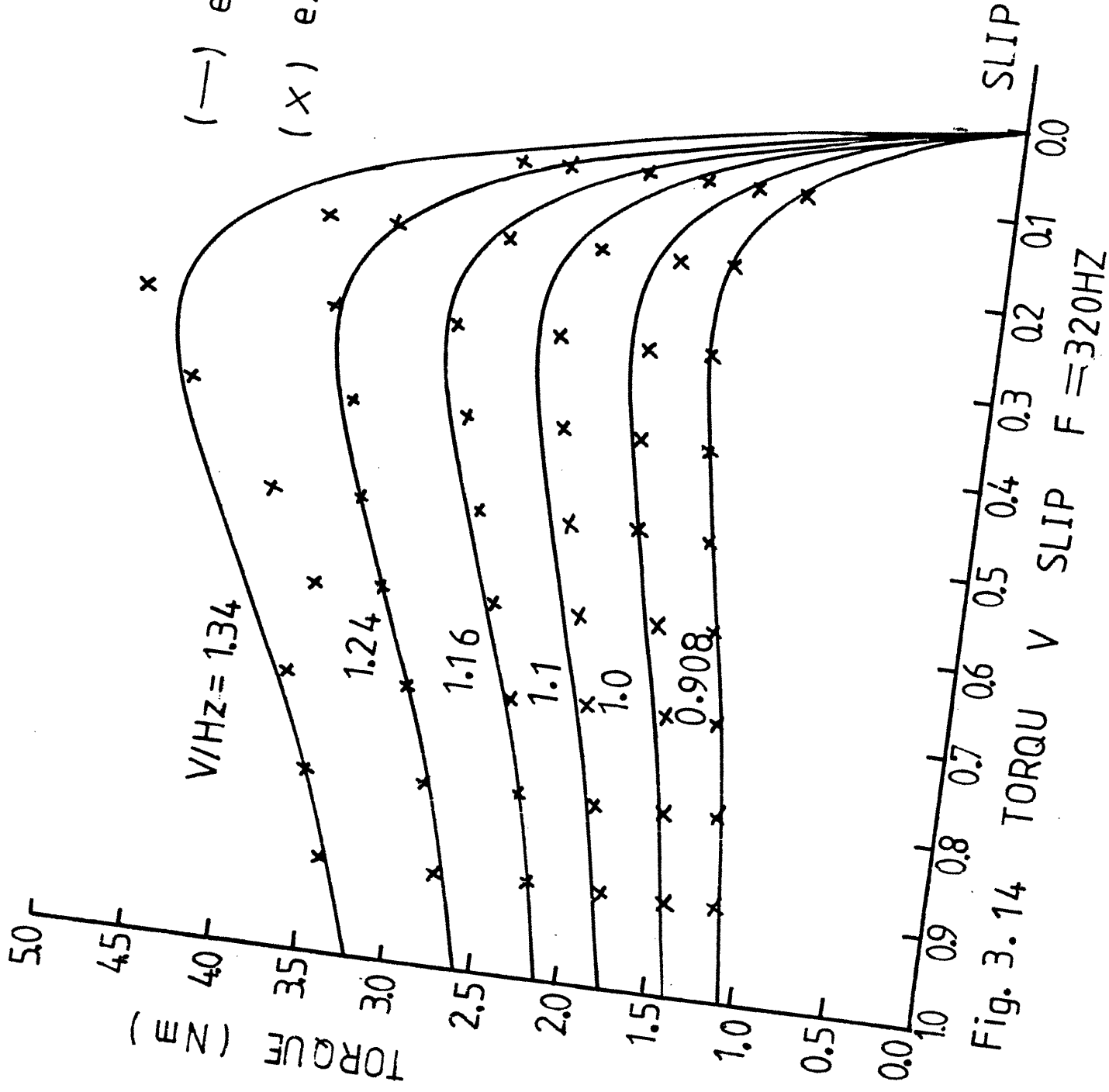


Fig. 3.14 TORQUE V SLIP F = 320HZ

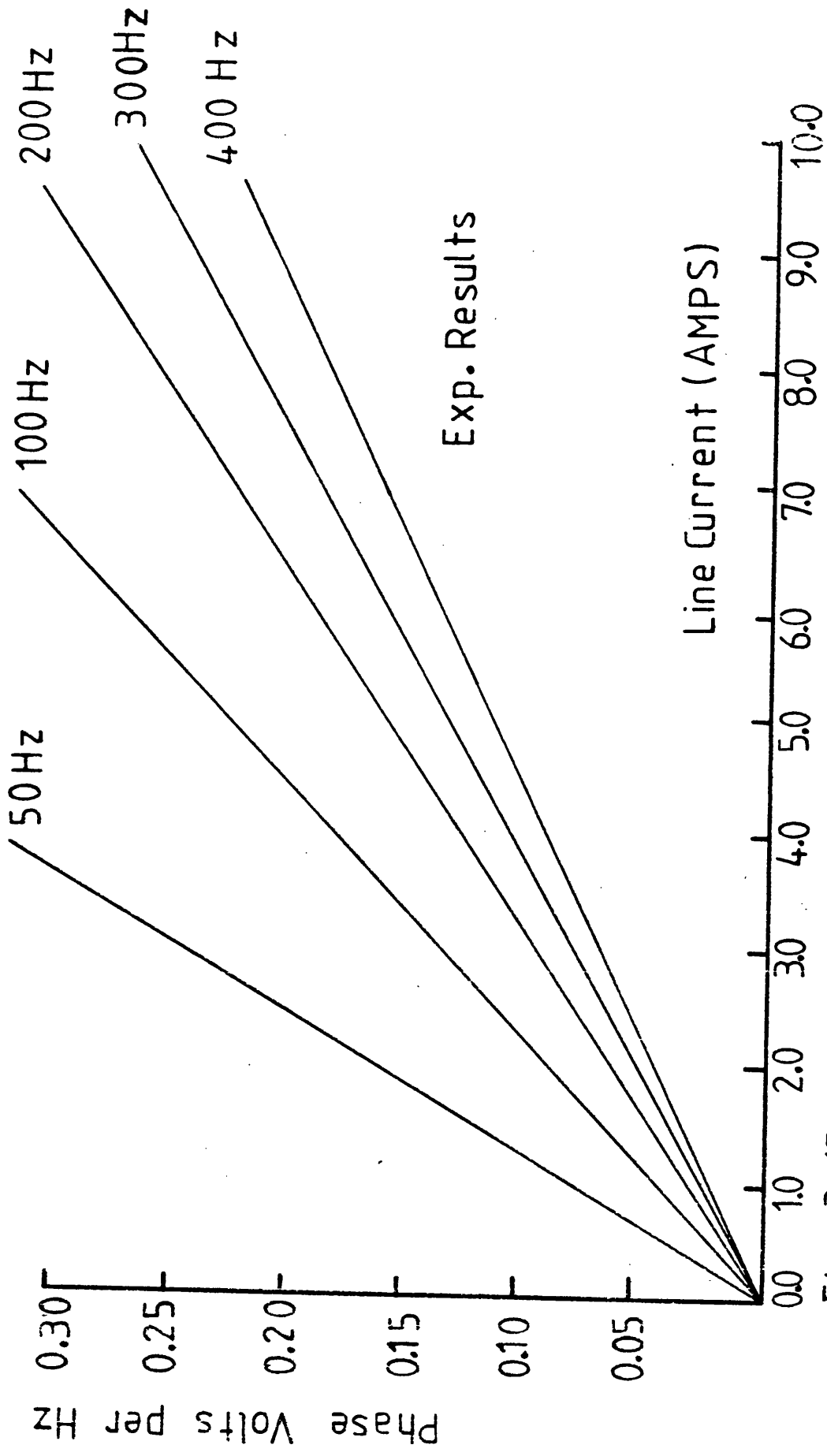


Fig. 3.15 Short Circuit Chara.

(*) Exp. Results

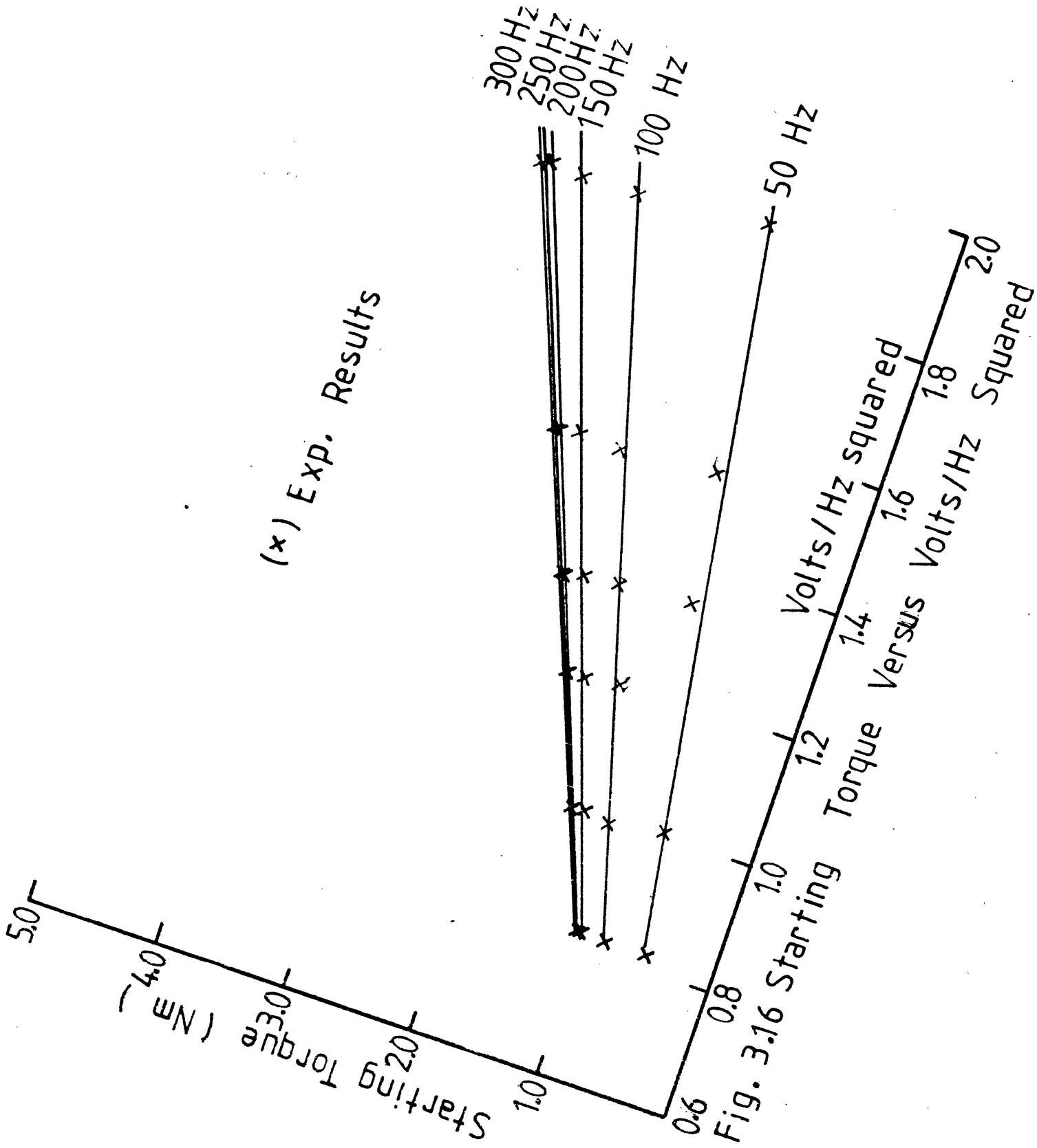


Fig. 3.16 Starting Torque Versus Volts/Hz Squared

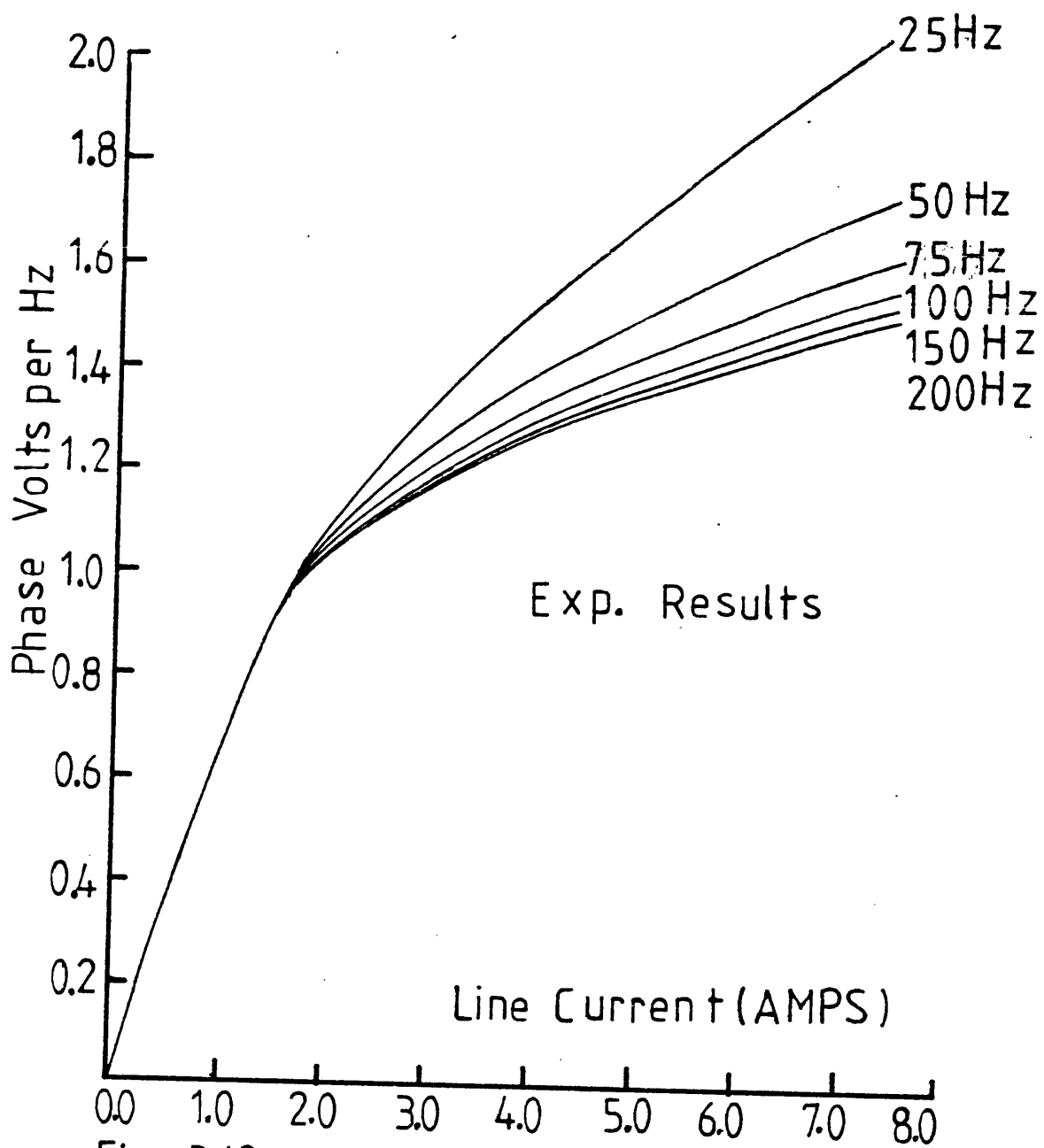


Fig. 3.18 Open Circuit Chara.

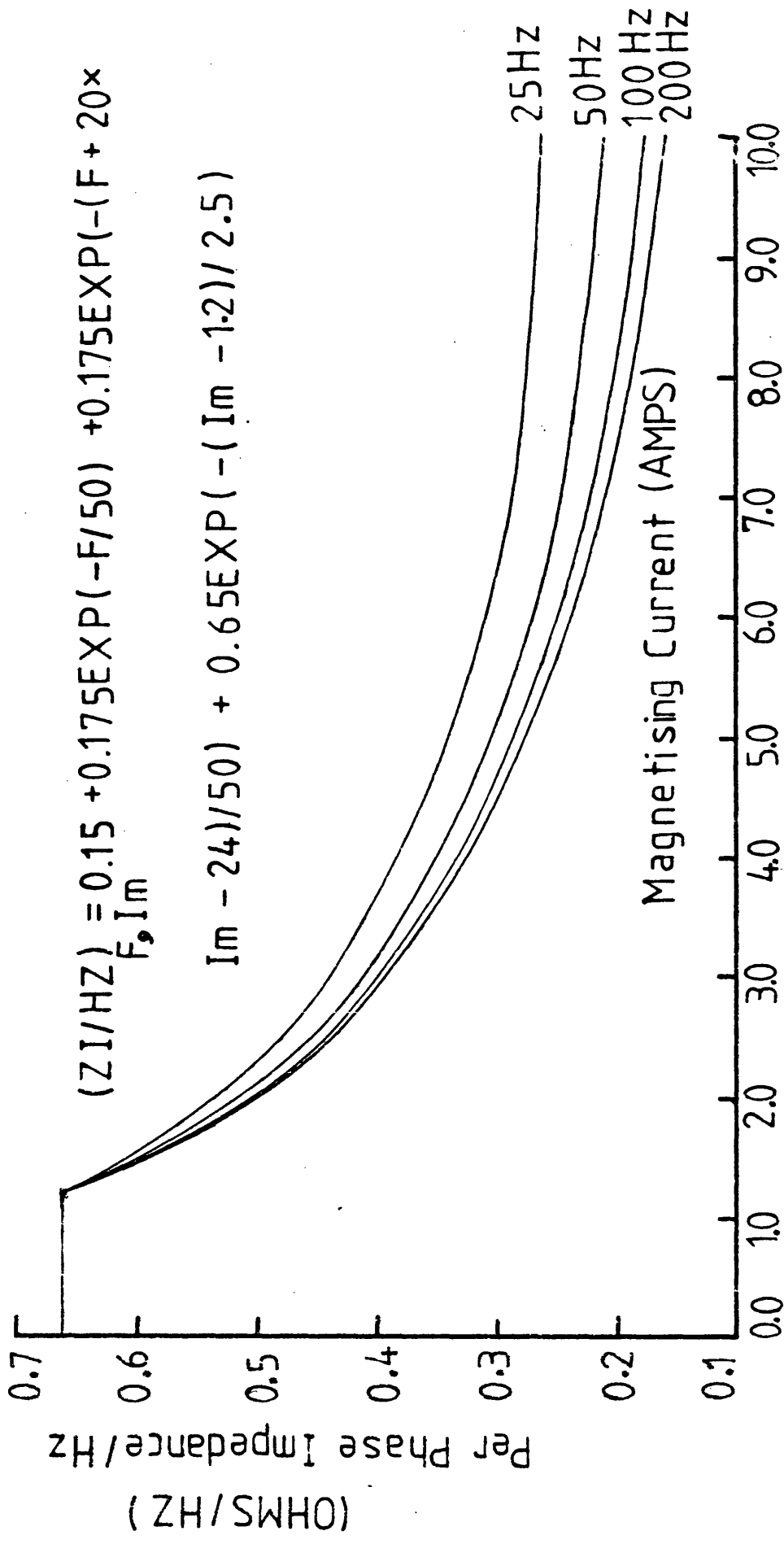


Fig. 3.19 O/C-Per Phase Impedance / Hz Versus Mag. Current

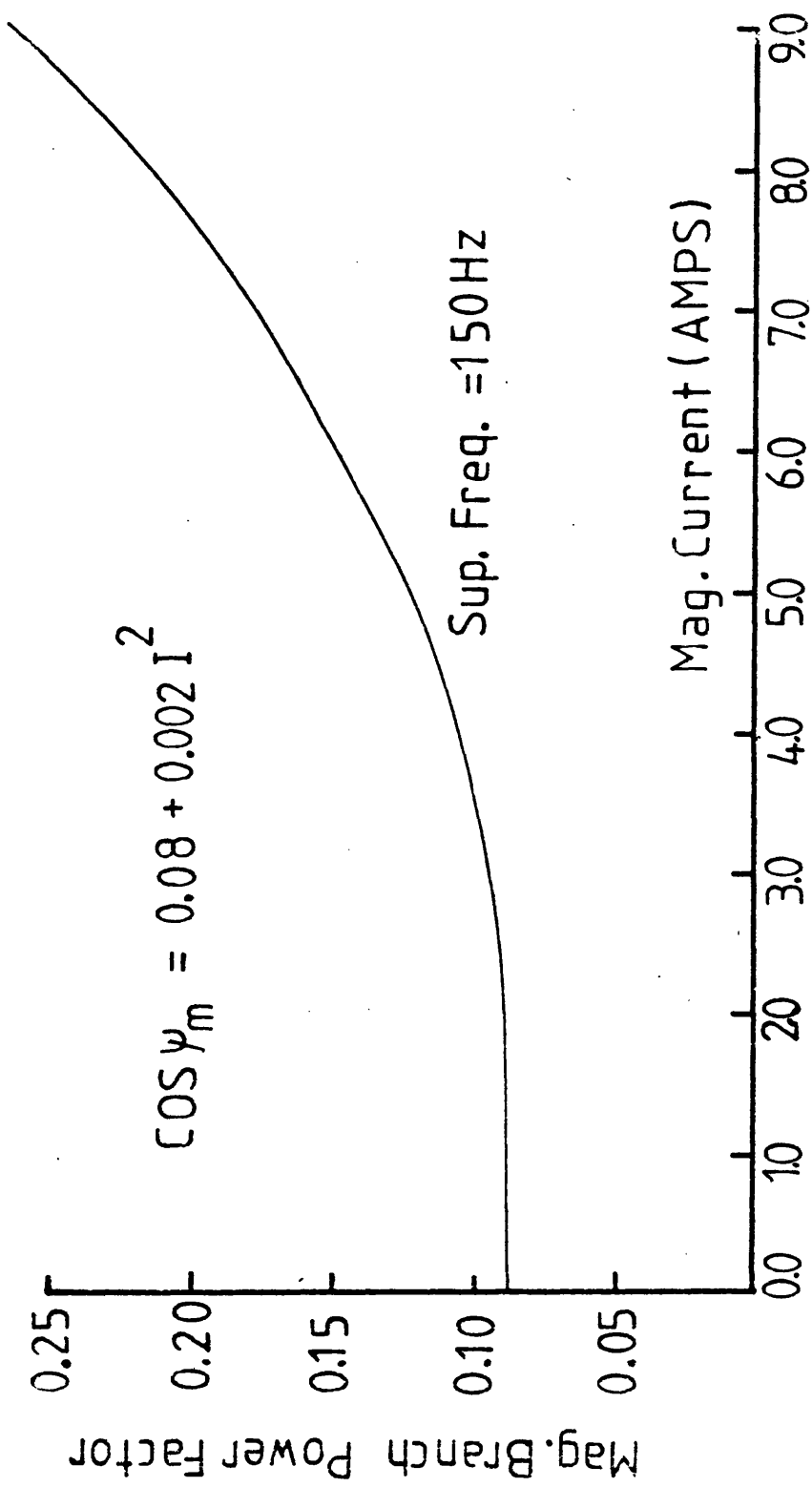


Fig. 3.20 $\text{COS } \psi_m$ Versus Mag. Current

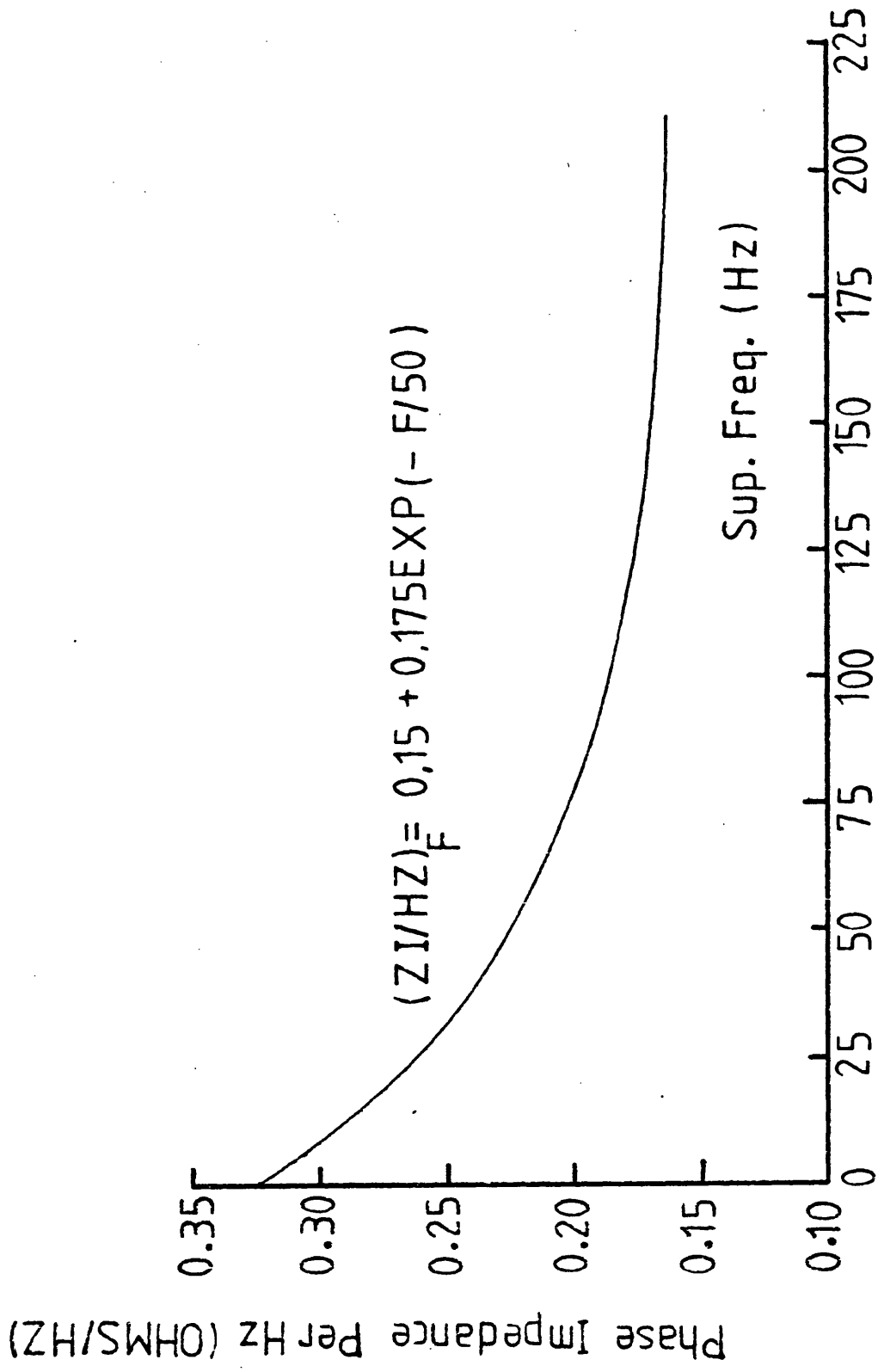


Fig. 3.21 Phase Imp. per Hz Versus Sup. Freq. in Non-linear Region

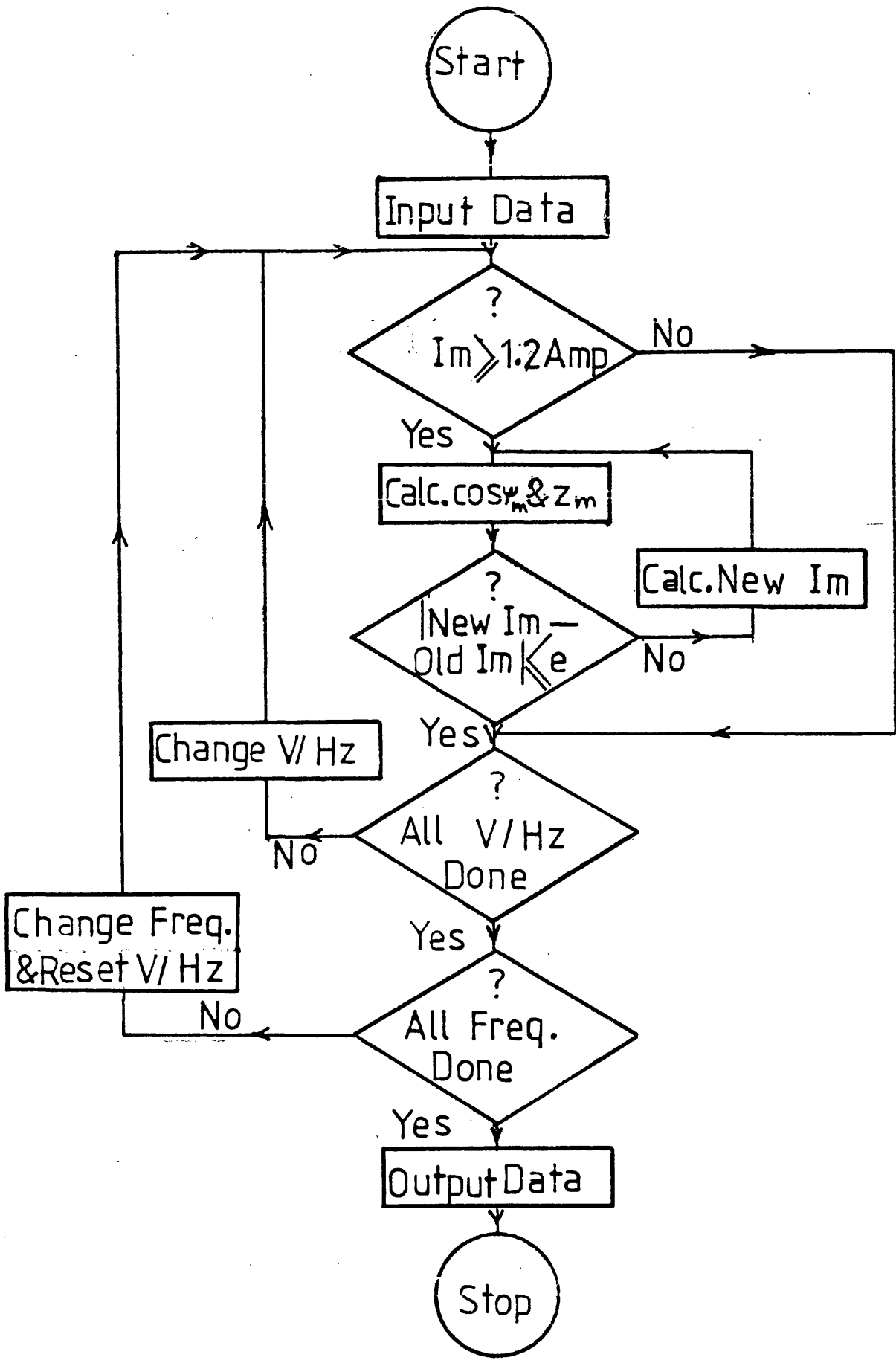


Fig. 3.22 Flow Dia. Of Non-linear Model

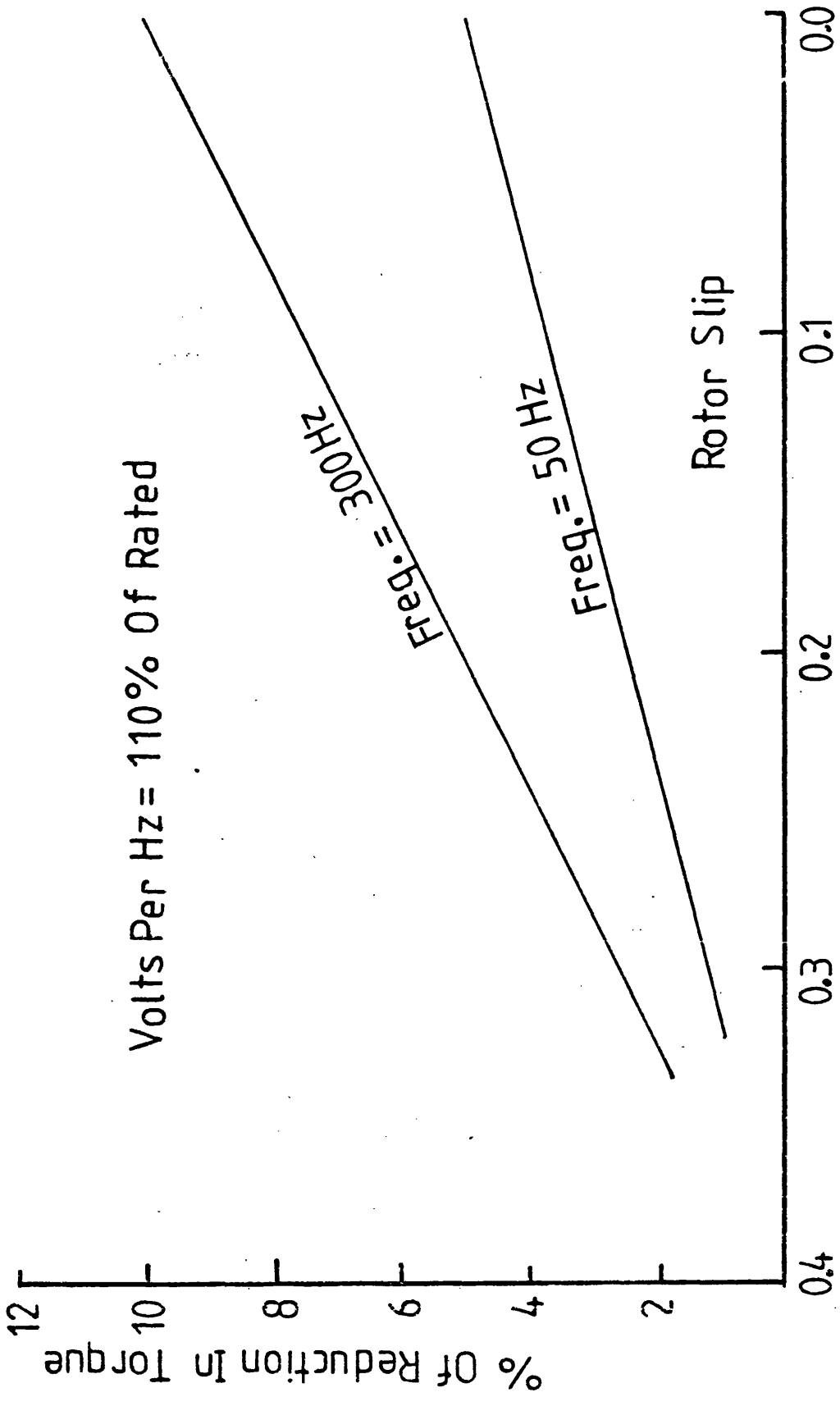


Fig. 3.23 %Of Reduction In Torque due to Non-linearity Of Machine Versus Rotor Slip

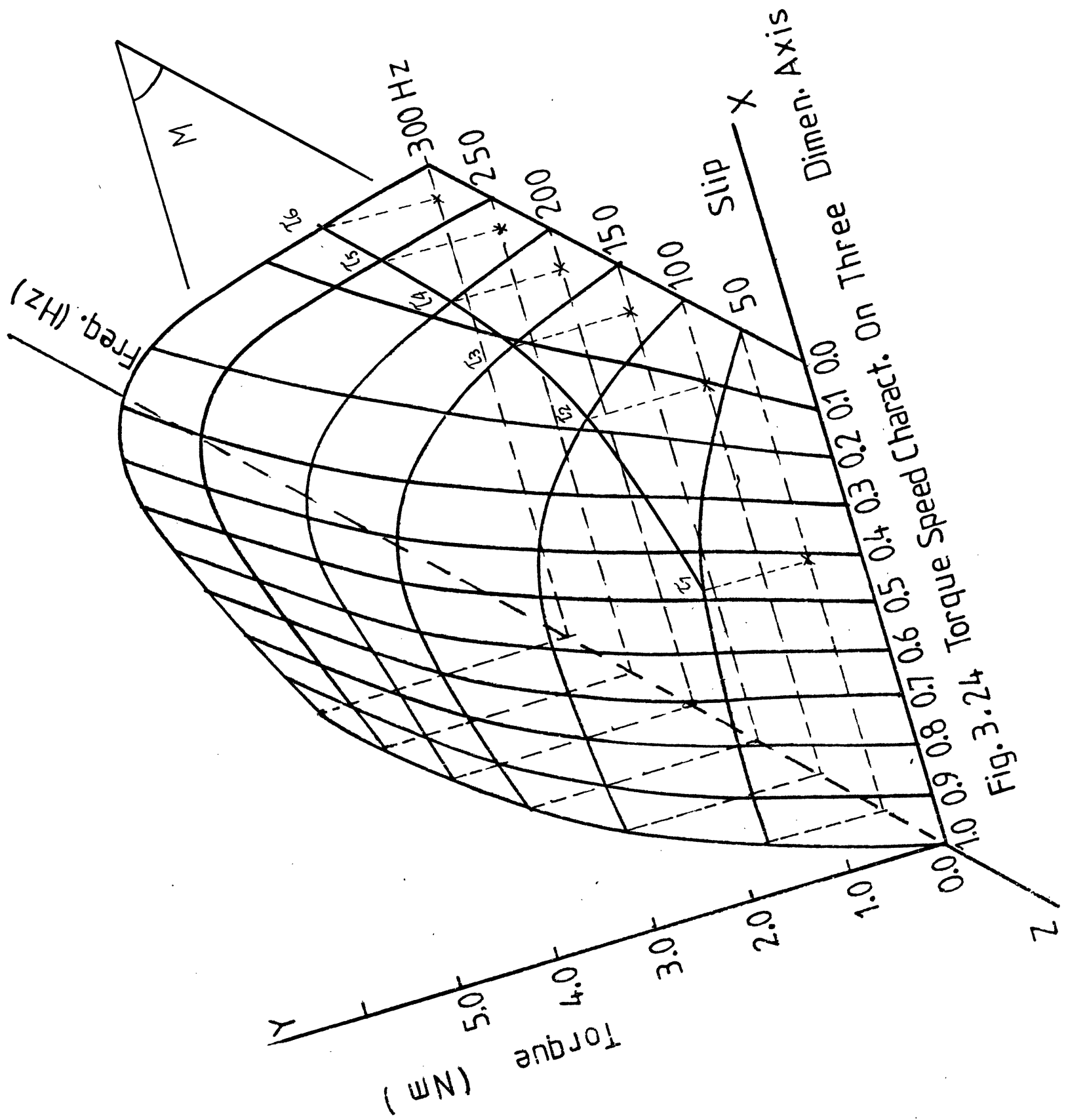


Fig. 3.24 Torque Speed Character. On Three Dimen. Axis

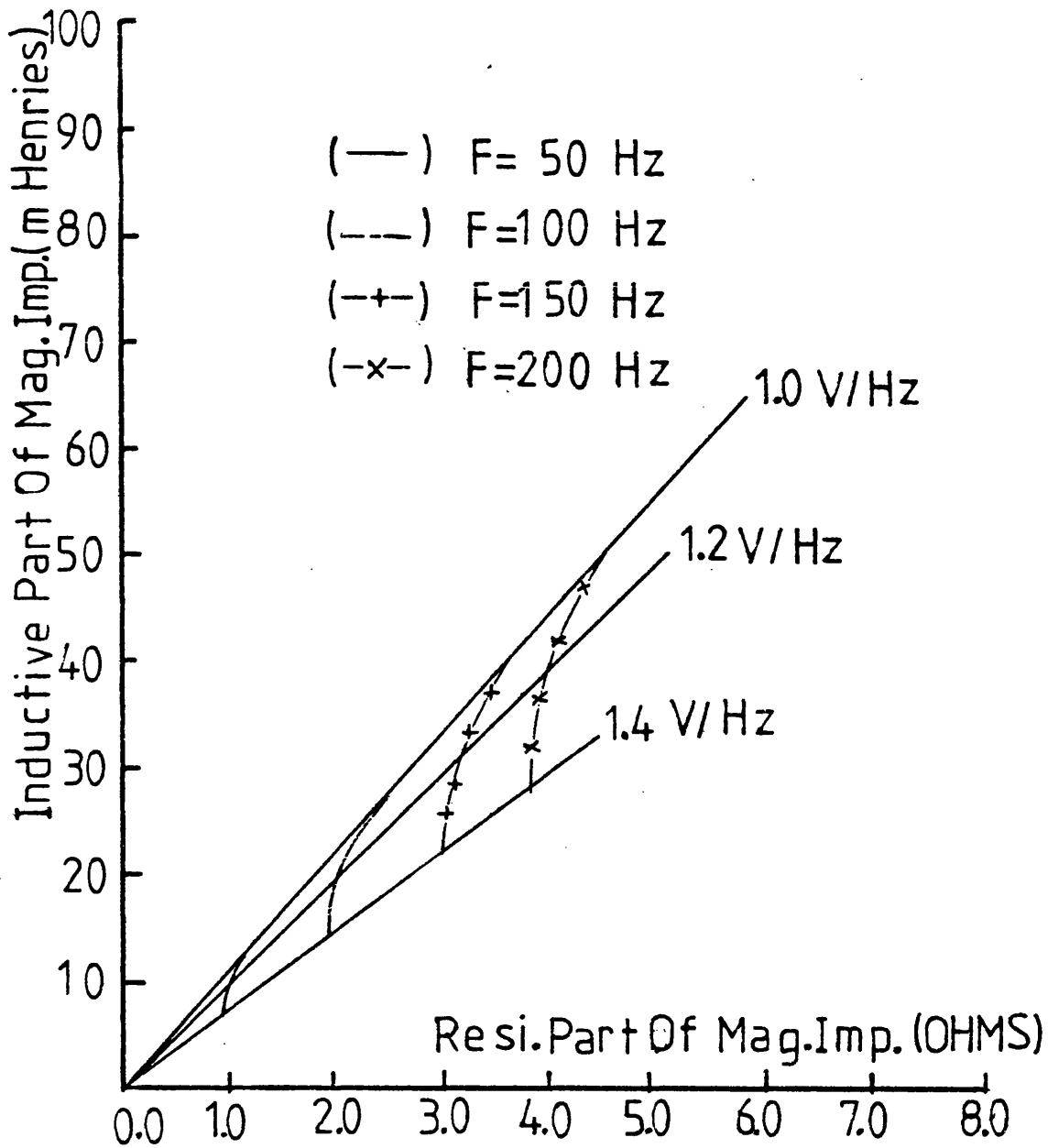


Fig. 3.25 Locus Dia. Of Mag. Branch

Bibliography

- 3.1 ALGER, P.L.: "The nature of induction machines", (Gordon & Breach), New York, 1965.
- 3.2 CHRISTOFIDES, N.: "Origin of load losses in induction motors with cast aluminium rotors", Proc. IEE, Vol. 112, No. 12, December 1965.
- 3.3 CHRISTOFIDES, N. and ADKINS, B.: "Determination of load losses and torques in squirrel-cage induction motors", Proc. IEE, Vol. 113, No. 12, December 1966.
- 3.4 NORMAN, H.M.: "An induction motor locked saturation curve", Trans. AIEE, PAS Vol. 53, 1934, pp. 536-541.
- 3.5 CHANG, S.S.L. and LLOYD, T.C.: "Saturation effects of leakage reactance", Trans. AIEE, PAS Vol. 68, 1949, pp. 1144-1147.
- 3.6 AGARWAL, P.D. and ALGER, P.L.: "Saturation factors for leakage reactance of induction motors", Trans. AIEE, PAS Vol. 80, 1961, pp. 1037-1042.
- 3.7 ANGST, G.: "Saturation factors for leakage induction motors with skewed rotors", Trans. AIEE, PAS Vol. 82, 1963, pp. 716-725.
- 3.8 CHALMERS, B.J. and DODGSON, R.: "Saturated leakage reactances of cage induction motors", Proc. IEE, Vol. 116, No. 8, August 1969.
- 3.9 POHL, R.: "Electromagnetic and mechanical effects in solid iron due to an alternating or rotating magnetic field", Proc. IEE, Vol. 91, Part II, 1944, pp. 239-248.
- 3.10 GIBBS, W.J.: "Induction and synchronous motors with unlaminated rotors", Proc. IEE, Vol. 95, Part II, 1948, pp. 411-420.
- 3.11 McCONNELL, H.M. and SVERDRUP, E.F.: "The induction machine with solid rotor", Trans. AIEE, PAS Vol. 74, Part III, 1955, pp. 343-349.
- 3.12 KESAVAMURTHY, N. and RAJAGOPALAN, P.K.: "Equivalent circuit and evaluation of eddy-current loss in solid cores subjected to alternating and rotating magnetic fields", Proc. IEE, Vol. 107, Part C, 1960, pp. 353-365.

- 3.13 KESAVAMURTHY, N. and RAJAGOPALAN, P.K.: "Eddy currents in solid iron due to alternating magnetic flux", Proc. IEE, Vol. 106, Part C, 1959, pp. 207-213.
- 3.14 ANGST, G.: "Polyphase induction motor with solid rotor - effects of saturation and finite length", Trans. AIEE, PAS Vol. 80, 1961, pp. 902-909.
- 3.15 PILLAI, P.P.: "Part I: fundamental frequency eddy-current loss due to rotating magnetic field", Proc. IEE, Vol. 116, No. 3, March 1969, pp. 407-410.
- 3.16 PILLAI, P.P.: "Part II: fundamental frequency eddy-current loss due to rotating magnetic field", Proc. IEE, Vol. 116, No. 3, March 1969, pp. 411-414.
- 3.17 JAIN, G.C.: "The effect of voltage waveshape on the performance of a three-phase induction motor", IEE Trans. on Power Apparatus and Systems, Vol. 83, 1964, pp. 561-566.
- 3.18 BURBIDGE, R.F. and FRYETT, M.L.: "Synchronous and asynchronous torques in squirrel-cage induction motors", Proc. IEE, Vol. 114 (11), 1967, pp. 1665-1673.
- 3.19 CHALMERS, B.J. and DODGSON, R.: "Waveshapes of flux density in polyphase induction motors under saturated conditions", Trans. IEEE PAS 90, 1971, pp. 564-569.
- 3.20 LEES, M.J. and TINDALL, C.E.: "Field theory analysis of saturation harmonics in induction machines", Proc. IEE, Vol. 121, No. 4, April 1971, pp. 276-280.
- 3.21 ROGERS, G.J.: "Induction motor terminal voltage equations", Proc. IEE, Vol. 123, No. 8, August 1976, pp. 804-810.
- 3.22 ROGERS, G.J. and CAMBRELL, G.K.: "The piece by piece solution of elliptic boundary value problems", J. Phys., Part D, Appl. Phys., 8, 1975, pp. 1615-1623.
- 3.23 HAMMOND, P. and ROGERS, G.J.: "Use of equivalent fields in electrical machines studies", Proc. IEE, Vol. 121, No. 6, 1974, pp. 500-507.

- 3.24 BINNS, K.J.: "Cogging torques in induction machines", Proc. IEE, Vol. 115 (12), 1968, pp. 1783-1790.
- 3.25 BINNS, K.J. and DYE, M.: "Effects of slot skew and iron saturation on cogging torques in induction machines", Proc. IEE, Vol. 117 (7), 1970, pp. 1249-1252.
- 3.26 BINNS, K.J., HINDMARSH, R. and SHORT, P.B.: "Effect of skewing slots on flux distribution in induction machines", Proc. IEE, Vol. 118 (3/4), 1971, pp. 543-549.
- 3.27 BINNS, K.J. and ROWLANDS-REES, G.: "Simple rules for the elimination of cogging torque in squirrel-cage induction motors", Proc. IEE, Vol. 121, No. 1, 1974, pp. 63-67.
- 3.28 BUTLER, O.I. and BIRCH, T.S.: "Comparison of alternative skew effect parameters of cage induction motors", Proc. IEE, Vol. 118, No. 7, 1971, pp. 879-883.
- 3.29 CHALMERS, B.J. and CHANDRA, N.K.: "High frequency no-load losses of cage induction motors", IEEE Trans. on Power Apparatus and Systems, Vol. PAS 89, No. 6, pp. 1043-1048, 1970.
- 3.30 CHALMERS, B.J. and MULKI, A.S.: "Design synthesis of double-cage induction motors", Proc. IEE, Vol. 117, No. 7, 1970, pp. 1257-1263.

CHAPTER 4

COMPARISON AND HARMONIC ANALYSIS OF THE PULSE WIDTH MODULATED INVERTERS WHEN FEEDING INDUCTION MOTORS

Summary

The additional losses due to harmonic frequencies of the predetermined and postdetermined (slit width) PWM techniques are calculated and compared whilst operating under the same given conditions. Using a digital computer, the conditions of the postdetermined PWM technique is set so that there are an integral number of pulses in each half cycle of the supply frequencies. The Fourier series analysis is then applied to calculate the harmonic content and the percentage of the total power distributed in the unwanted harmonics when supplying an induction motor. The predetermined PWM technique is also set to produce the same modulation, fundamental frequency and output power. Its harmonic content and the percentage of unwanted harmonic power are calculated and compared with those obtained from the first technique.

The effect on the additional losses caused by changes in the induction machine parameters due to modulation and harmonic frequencies are also determined. Firstly by using the standard equivalent circuit of the induction motor as the load and secondly by using the new frequency dependent equivalent circuit as the load.

4.1 Introduction

The history of the power converters since the beginning of silicon controlled rectifiers (SCR's) for variable frequency drive systems is reviewed. The application of SCR's in d.c. to a.c. converters resulted in various inverter designs. Each type of inverter has its own advantage and disadvantage. The stepped wave inverters are generally known to produce output voltages with higher harmonic content, yet acceptable for many applications. The pulse width modulated inverter on the other hand, produces output voltages with much less harmonic content, at the cost of circuit complexity ^{4.1}.

Furthermore developments in power transistor technology have made it possible to obtain inverters of up to 20 KW and more outputs ^{4.2,4.3}. In applications such as a.c. electric drive systems for road vehicles, the efficiency of the system is the primary goal of any design engineer. Employing thyristors in such a system would result in a poor efficiency, mainly due to the loss of energy required for commutation circuitry. Obviously the power transistor is best suited to such systems as efficiencies of 95% or more are possible. The harmonic voltages at the inverter outputs give rise to additional losses in the machine. The introduction of these additional losses is one of the factors of the reduction

in the efficiency of the overall system. Various techniques have been developed for eliminating some selected number of harmonics to reduce the additional losses 4.4 - 4.7.

Recent advancements in semiconductor switching devices and the introduction of large scale integration have made it possible to synthesise good sine waveforms at an acceptable cost and with good reliability. A large scale integrated circuit has been developed specifically for use in three-phase induction motor speed control systems 4.8,4.9. These integrated circuits provide three complementary pairs of output drive waveforms which when applied to a six-element inverter (transistor or thyristor) produce a symmetrical three-phase output (120° apart).

The three output waveforms are pulse-width modulated, both edges being modulated such that the average voltage difference between any two of the three output phase (line to line) voltages varies sinusoidally. The relationship between the average voltage and fundamental frequency of this output is inherently linear, but separate control of voltage and frequency is possible if required (eg. to boost motor voltage at low frequencies). These integrated circuits use digital techniques entirely, so the repetition frequency of the PWM signal is always an exact multiple of the fundamental output frequency. This results in excellent phase and voltage balance and consequent low motor losses.

Also the modulation frequency is held within a frequency band of constant width by changing the number of pulses per cycle. This minimises pulsating torque problems at low frequencies ^{4.10}.

In this chapter two popular and highly efficient pulse width modulated inverters which are in wide use in industry are selected for harmonic analysis and comparison of their output efficiency when feeding a variable speed induction motor. The level of power losses in the harmonics are calculated using the frequency dependent model of the induction motor which is obtained in the previous chapters.

The modulation technique involved in the first inverter type is a sine wave envelope and an isosceles triangle waveform, which are mixed by means of comparators to produce a train of pulses whose spacing is equal to, and width proportional to, the integral of the sine wave ^{4.11}. The second method of modulation is slit width, also known as a servo amplifier type inverter. This technique uses a limiting band either side of the sine wave. The current in the power transistors is then forced to follow the sine wave within the band by switching the positive and the negative d.c. supply across the inductive load. These two techniques are capable of producing output waveforms very similar to the sine wave.

A similar Fourier series analysis of references ^{4.5,4.6} is applied to the first inverter type and its output harmonics voltage equations derived and analysed. A new

analysis technique is developed to analyse and determine the harmonic voltage equations of the second type of inverter. The load, time constant and boundary limits, are used to determine the harmonic voltage equations. This is done as follows. The load conditions are assumed to be adjusted so that there is an integral number of pulses in each half-cycle of the supply. The synchronised and locked in phase condition is used so that both techniques are operating under the equal conditions. In the case of non-synchronised systems the pulse repetition pattern over several cycles can still be identified and Fourier series analysis can be applied to determine the output harmonic content. This hardly produces any significant difference in the harmonic content for a given number of pulses per cycle. Therefore, for the simplicity of achieving equal running conditions for the comparison of both techniques, the synchronised and locked in phase case is assumed.

With the aid of a digital computer the models of these techniques are constructed and used to calculate their efficiency in delivering an equal amount of power into a given load under the same conditions. That is the output waveforms of both contain equal numbers of pulses, equal fundamental frequency and produce equal line currents.

All the efficiency calculations are based on the values of the total input power supplied to the machine and power distributed in the harmonics only. The losses

in the inverter system such as switching losses in the power devices, commutation networks etc. are not considered, because these losses have a relation to the nature of the load when delivering a given amount of output power. The normal losses in the machine due to fundamental voltage are not considered either ie. the total losses in the machine if it was running from a pure sine wave supply system.

The new equivalent circuit of the induction motor is used as the load and the efficiencies of both inverter systems are computed and compared.

The additional losses due to harmonic voltages are generally determined from the analysis of the standard equivalent circuit of the induction motors 4.12,4.13. The application of the standard equivalent circuit does not give the correct values of these losses. Because the equivalent circuit parameters change considerably with the order of the harmonics and consequently the magnitude of these losses. Therefore the additional losses are also computed by using the standard equivalent circuit as the load and are compared with those obtained from the new equivalent circuit. The difference between the two sets of results is then used to show the magnitude of the errors involved.

4.2 Literature Review

The announcement of the silicon controlled rectifier ^{4.14} in December 1957, instituted a new area in the field of electric power conversion. Almost immediately attention was focussed on the application of this device in the inversion equipment. In the past induction motors have been considered primarily as constant speed machines, and the great majority of their applications have been in constant frequency systems. The advent of modern-high-current transistors and SCR's and their use in inverters and cyclo converters has brought to an end the time when an induction machine was limited to constant speed service. These solid-state frequency converters supplying power to induction machines are now being used in many applications which previously have been the sole domain of the d.c. machines.

The induction motor is expected to have the following advantages over the commutator motors:

- (a) there are no brushes to change,
- (b) there are no commutators to inspect,
- (c) there are no brush holders and mechanism to check,
- (d) there is more output for the same volume or less weight for the same output, because the induction motor can be driven at high speeds,
- (e) restrictions relating to peripheral speed of the commutator and also the reactance voltages in the rotating windings do not apply.

Commutator motors which are already highly utilized at rated speed can often not supply rated power up to maximum speed because the reactance voltages become too great. There is no such restriction with induction motors. In plants with aggressive atmospheres and liquid chemicals it is preferable to use the squirrel-cage motor instead of d.c. machines. Also induction motors are lighter and their design is considerably less complicated than that of the d.c. motors.

Power inverters can be classified into different categories depending upon the commutation technique used ^{4.15}. They can also be divided into two categories with reference to the output wave shape as "stepped wave inverters" and "multiple pulse width modulated inverters". Each type of inverter has its own advantages and disadvantages. In the case of the stepped wave inverters circuit complexity is less, output voltage is sufficient for many applications, but the total harmonic distortion may be objectionable in some cases. In applications such as communication equipment, the inverter output waveform must be stabilized as well as distortion free ^{4.16,4.17}. The multiple pulse width inverter has credit for low harmonic distortion and on the debit side are the circuit complexity and limited output voltage. The multisteped output waveforms are generally obtained by use of transformers, but this can also be done by simply arranging the control of logic signals ^{4.18}.

There are three methods of modulating the pulse width of inverter output voltage waveforms. Each technique involves the use of one or more synchronised carrier ratios. The ratio referred to is carrier frequency to inverter operating frequency. The three modulation control schemes are:

- (a) fixed ratio,
- (b) variable ratio, and
- (c) adaptive ratio.

In the fixed ratio system the carrier ratio remains constant over the operating range of the inverter, whereas in the variable ratio scheme the carrier steps through a sequence of ratios as the operating frequency increases.

In the adaptive ratio carrier, changes are made on the basis of direct carrier period measurement in the output voltage waveform. The control automatically adjusts the carrier ratio to take care of all possible limiting combinations of pulse width, notch width and carrier frequency. In the process it maintains a high carrier frequency, thereby considerably reducing undesirable harmonics throughout the operating range ^{4.19}.

In applications where low speed operation is not of interest, and power requirements are modest, the square-wave voltage inverter operating from an adjustable d.c. voltage thus continues to have advantages over more sophisticated and hence more complex and costly pulse width modulated designs. Square-wave inverters can be categorized in a number of ways including type

of commutating circuit, single or multiple grouping, type of d.c. power source, fixed or adjustable frequency etc. Although the conduction period of square-wave can be fixed at any interval ranging from less than 90° to 180° , it is particularly advantageous to fix the interval at 120° or 180° . The 120° and 180° square-wave inverters are in wide use. The machines supplied by 120° inverter will run at higher slip than one supplied with 180° inverter from a given d.c. source. Thus for a constant force, power application losses will be high when the machine is fed from a 120° square-wave inverter supply system 4.20.

The conventional three-phase constant frequency source can be inverted directly to variable frequency output, whose frequency becomes the difference between the conventional supply frequency and continuously controlled frequency 4.21.

The rectifier-inverter drive system is generally equipped with a filter between the rectifier and the inverter. Energy can be stored in the inductance and capacitance of the filter. The interchange of energy between the filter component and magnetic field and rotor of the machine can cause the rectifier-inverter induction motor drive system to become unstable at low operating frequencies. From the machine equations, the small-displacement equations can be established, which predict the average value of the converter variables.

(The small-displacement theory has had a long and productive history in analysis of electric machinery. This theory enables one to establish linear equations which describe the operation of a system for small changes about an operating point). Then stability analysis can be performed by employing the Nyquist stability criterion to study the influence of changes in several machine parameters, filter parameters and rectifier commutating reactance^{4.22}. Several instability boundaries for various parameters of the current source inverter using Routh-Hurwitz criterion are also described^{4.23}.

The rectifier-inverter induction motor drive system can be represented in a synchronously rotating frame by neglecting the harmonic component due to switching action in the rectifier. From this simplified representation, the operation of the inverter can be expressed analytically in the synchronously rotating reference frame with the harmonic component due to switching in the inverter included^{4.24}.

With the introduction of cheap high voltage transistors of 10 amp or more rating, it has become feasible to produce a suitable power servo amplifier using the transistors in a switching mode to reduce power dissipation. The time required to switch the power transistors off is considerably less than the SCR's and switching frequencies of up to 10 kHz or more are possible^{4.2,4.3}.

Thus the carrier frequency of the pulse-width modulated inverters can be increased considerably in order to reduce the harmonic content of the output waveform. The applications of the power transistors makes it also possible to employ other methods of pulse modulating such as delta-sigma modulation ^{4.25}. This technique is well known in communication systems and extensively used for the transmission of speech signals. With a sine wave input, the output of a delta-sigma modulation is quantised both in amplitude and in time, and this permits power control to be achieved from a fixed d.c. supply using only a single power controller.

In inverters using SCR's, achieving a reliable commutation is generally one of the most difficult problems associated with inverters. Usually the inverters are classified according to the type of commutation circuit they possess, such as parallel-capacitor commutated, series-capacitor commutated, harmonic-commutated, impulse-commutated etc. ^{4.15,4.26}. Inverters employing self and harmonic commutation, or self controlled with an internal self oscillation circuit, which generates gate triggering signals, operate in the critical commutation region and are generally suited to fixed or moderately variable frequency applications ^{4.27,4.28}. Various commutation circuits have also been developed for different applications, such as providing higher commutation voltages than the d.c. bus for wide ranges of load and speed etc., ^{4.29,4.30,4.31}.

Current source inverters, such as those with a large series inductance in the d.c. bus ^{4.32} have an inherent current limited characteristic. Certain voltage source inverters, such as the d.c. side commutated inverter ^{4.33}, readily handle overloads by simply commutating all load SCR's off whenever the load current approaches the commutation limit. Other voltage source inverters, particularly PWM* inverters using the McMurray-Bedford commutation circuits, cannot rapidly turn all the load SCR's off and on to regulate the peak load current below the commutation limit. These inverters are not inherently current limited but are characterised by a relatively low output voltage response time. This low response time can be used to provide a quasi-inherently current limited or current source characteristic for PWM inverters with induction motor loading ^{4.34}.

The pulse width modulated (PWM) inverter has, for a number of years, offered distinct advantages at the expense of more complex control and power circuit configurations over other inverter types for industrial motor drive systems. With the advent of the fast turn-off thyristor and advances in PWM modulator techniques, the PWM inverter now offers applications up to and above 200 Hz ^{4.35,4.36}. Pulse width modulation essentially involves the sampling of an information signal. This sampled information content is then converted into a series of modulated pulses having pulse widths that reflect the amplitude of the information signal, and it

* Pulse Width Modulation Inverter

is generally recognised as having the following advantages.

- (a) The inherent ability to provide continuous variable-frequency-variable voltage control in a single power stage.
- (b) In contrast to the variable d.c. link inverter, the commutating ability of the PWM inverter remains substantially constant irrespective of the voltage-frequency setting. This is a significant advantage for motor-speed control applications, where it is generally necessary to maintain substantially constant flux conditions over the complete frequency range of operations.
- (c) The control strategy can be programmed to eliminate the significant harmonics in the voltage output. This is a significant advantage for motor applications, where harmonic losses can produce considerable overheating, and where harmonic torques cause instability problems during low frequency operations.

By examination of the frequency-spectra of the PWM and PAM it is apparent that more harmonic distortion occurs with PWM than with PAM for the same frequency ratio and also this distortion and harmonic order decreases with the increasing value of the frequency ratio ^{4.37}.

The complexity of the logic circuit employed to generate sine-weighted pulse trains for PWM control schemes is reduced considerably by the introduction of ROM's (Read Only Memory) ^{4.8}. The memory arrangement is such that four pulse trains, with fixed phase differences between their modulation envelopes, are produced to control single, two or three phase motors.

In general the inverter output waveforms are rich in harmonics. Many techniques have been developed to reduce the harmonics in the inverter output. The pulse width modulation technique is presently the most popular and economical method of voltage and frequency control. Methods employing multiple inverters in parallel have also been developed. Some versions incorporate harmonic elimination schemes to achieve a nearly sinusoidal output ^{4.38 - 4.41}. The output harmonics can also be obtained as a function of pulse width and pulse frequency and output frequency, when they are operating in synchronous mode ^{4.7}, by applying double Fourier series analysis ^{4.42}. The reduction of harmonic components reduces the pulsation torques considerably at low frequency ranges. The presence of these torques becomes troublesome in applications such as machine tool, antenna positioning etc., ^{4.43,4.44}.

Extensive work has been done on the performance analysis of induction motors driven by the square-wave inverter supplies under balanced and unbalanced conditions, techniques of transforming some of the trapped energy in

the commutation circuits, comparison of the changes in the line currents when the machine is supplied with sine wave and square wave, and their various analog model representation forms are available in the literature 4.45 - 4.56. There are also many techniques available to deal with problems arising from miscommutation or SCR failure, without the need for shutdown 4.55,4.56.

During the past several years, interest in the development of a.c. electric drive systems for on-the-road vehicles has increased substantially. Numerous studies have been made of the feasibility of electric propulsion systems, employing power inverters for driving a.c. machines rather than d.c. commutator motors 4.57,4.64. There are two basic types of a.c. motors which could be considered for the transport application - synchronous and induction.

The squirrel-cage induction motor is a proven industrial work force which can be given the required torque/speed characteristic when operated from the variable voltage and frequency of the inverter. The synchronous motor, in a transport application, requires a means to excite the field at all speeds, including zero speed. One method of excitation, which is often used is to excite a coaxial transformer from the stator, or rectify the voltage induced in the secondary with rotating diodes, and to supply the rectified output to the rotating field winding. An alternative method using a solid rotor inductor of Lundell type generator is

sometimes considered because of its stationary field winding, but the greater weight and rotor construction problems usually cause this alternative to be less attractive.

The induction motor is better suited to this application since it provides lower cost, higher reliability and better maintainability for the overall system. The pulse width modulated inverter appears to be the best for this application, because it has the following advantages:- low harmonic content in the output waveform, voltage and frequency control requiring simple control circuitry, the capability of bidirectional power flow without any reconnection ie. power can be caused to flow from d.c. source to the car for acceleration or from the car to the source for deceleration.

4.3 General Technique of Harmonic Analysis for Stepped-Wave Output Inverters

The stepped-wave outputs are generally produced by connecting the load between two basic inverters as shown in figure 4.1(a).

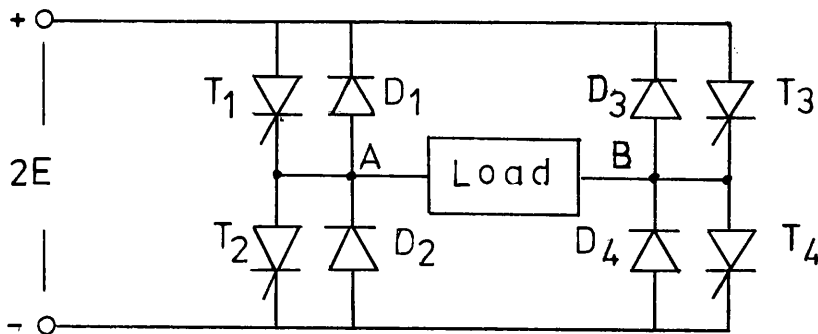


Figure 4.1(a)

The control angles of the corresponding thyristors are arranged such that, they connect two terminals of the load alternatively across the positive and negative supply shown in figure 4.1(b). The harmonic content of the output waveforms can be contracted to a desired value by increasing the number of voltage steps at the expense of using more units.

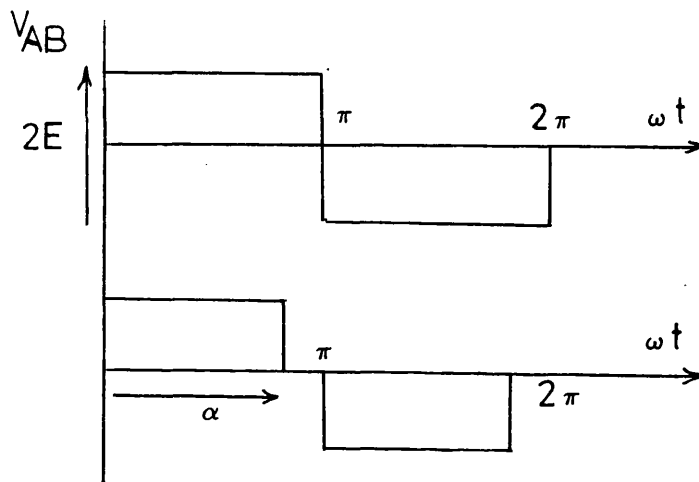


Figure 4.1(b)

Consider the voltages obtained at points A and B shown in figure 4.2 with various control angles (180° , α , $0+\epsilon$) of one unit with respect to the other.

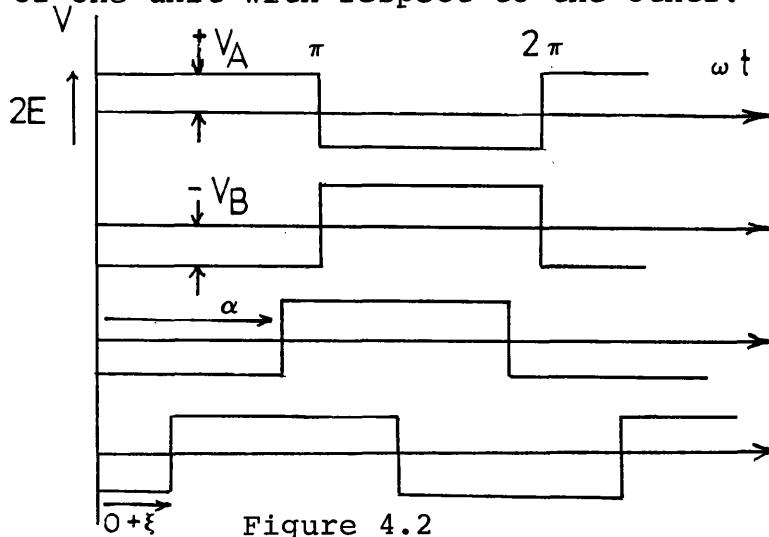


Figure 4.2

Applying Fourier series to V_A waveforms we have.

$$V_A = \frac{4E}{\pi} [\sin \theta + \frac{1}{3}\sin 3\theta + \frac{1}{5}\sin 5\theta + \dots] \quad \text{--- (4.1)}$$

All Cos terms and even values of Sine terms are equal to zero due to a new symmetry of the waveform about $T/2$.

Similarly:

$$V_B = \frac{4E}{\pi} [\sin(\theta - \alpha) + \frac{1}{3}\sin 3(\theta - \alpha) + \frac{1}{5}\sin 5(\theta - \alpha) + \dots] \quad \text{--- (4.2)}$$

Now:

$$\begin{aligned} V_A - V_B &= \frac{4E}{\pi} \left\{ [\sin \theta - \sin(\theta - \alpha)] + \frac{1}{3}[\sin 3\theta - \sin 3(\theta - \alpha)] \right. \\ &\quad \left. + \frac{1}{5}[\sin 5\theta - \sin 5(\theta - \alpha)] + \dots \right\} \\ &= \frac{8E}{\pi} \left[\sin \frac{\alpha}{2} \cos(\theta - \frac{\alpha}{2}) + \frac{1}{3}\sin \frac{3\alpha}{2} \cos 3(\theta - \frac{\alpha}{2}) \right. \\ &\quad \left. + \frac{1}{5}\sin \frac{5\alpha}{2} \cos 5(\theta - \frac{\alpha}{2}) + \dots \right] \end{aligned}$$

In general:

$$V_A - V_B = \sum_n \frac{8E}{(2n-1)\pi} \sin(2n-1) \cdot \frac{\alpha}{2} \cos(2n-1)(\theta - \frac{\alpha}{2}) \quad \text{--- (4.3)}$$

where $n = 1, 2, 3, \dots$

4.3.1 Analysis of Three-Phase Stepped Wave Output Inverters

The three-phase inverter is obtained by employing three basic inverter circuits. The output waveforms of these inverters are made 120° out of phase with each other. The phase to phase voltage relation is obtained by simply equating the phase angle $\alpha = 120^\circ$ in equation (4.3). Thus we have:

$$V_A - V_B = \sum_n \frac{8E}{(2n - 1)} \sin(2n - 1) \frac{\pi}{3} \cdot \cos(2n - 1) \left(\theta - \frac{\pi}{3} \right) \quad \text{--- (4.4)}$$

From the term $[\sin(2n - 1) \frac{\pi}{3}]$ it is evident that all the harmonics of order three and multiples of three become zero.

4.4 Analysis of Inverters with Adjustable Output Voltage by Chopping Technique also known as "Sub-Oscillation"

The output wave from the inverter is modulated by means of chopping with a much higher frequency, and then the width of these chops are varied to obtain the desired output voltage level. The techniques used to modulate the inverter outputs for asynchronous machine applications are normally as follows:

- (a) inverters operating in linear sub-oscillation,
- (b) inverters operating in sinusoidal sub-oscillation,
- (c) inverters operating in non-sinusoidal sub-oscillation.

4.5 Analysis of Inverters Operating in Linear Sub-Oscillation

In the linear sub-oscillation technique the output waveform of the basic inverter shown in figure 4.1(a) is modulated with a constant frequency and variable pulse width. The maximum number of pulses is a compromise between allowable commutation losses in the thyristors and the desired harmonic content of the inverter output waveform. Consider the basic three phase inverter shown in figure 4.3.

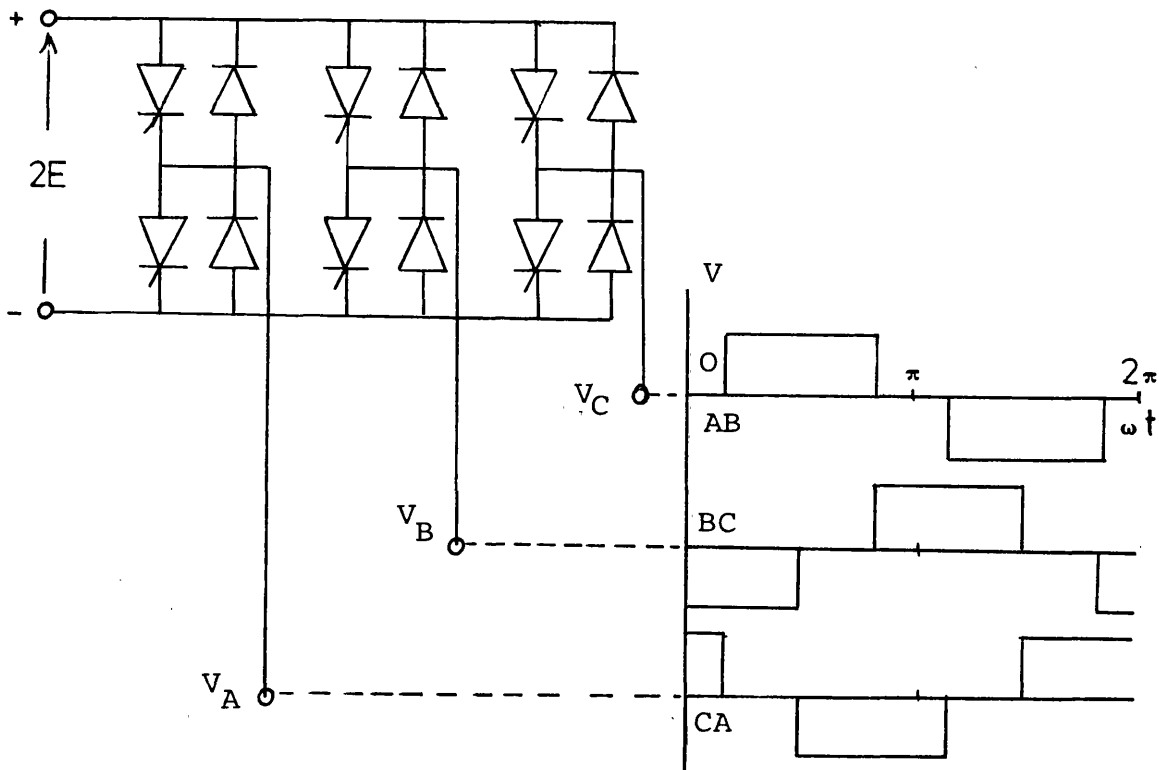


Figure 4.3

Now each basic inverter circuit is modulated with (3S) number of pulses as shown in figure 4.4 overleaf.

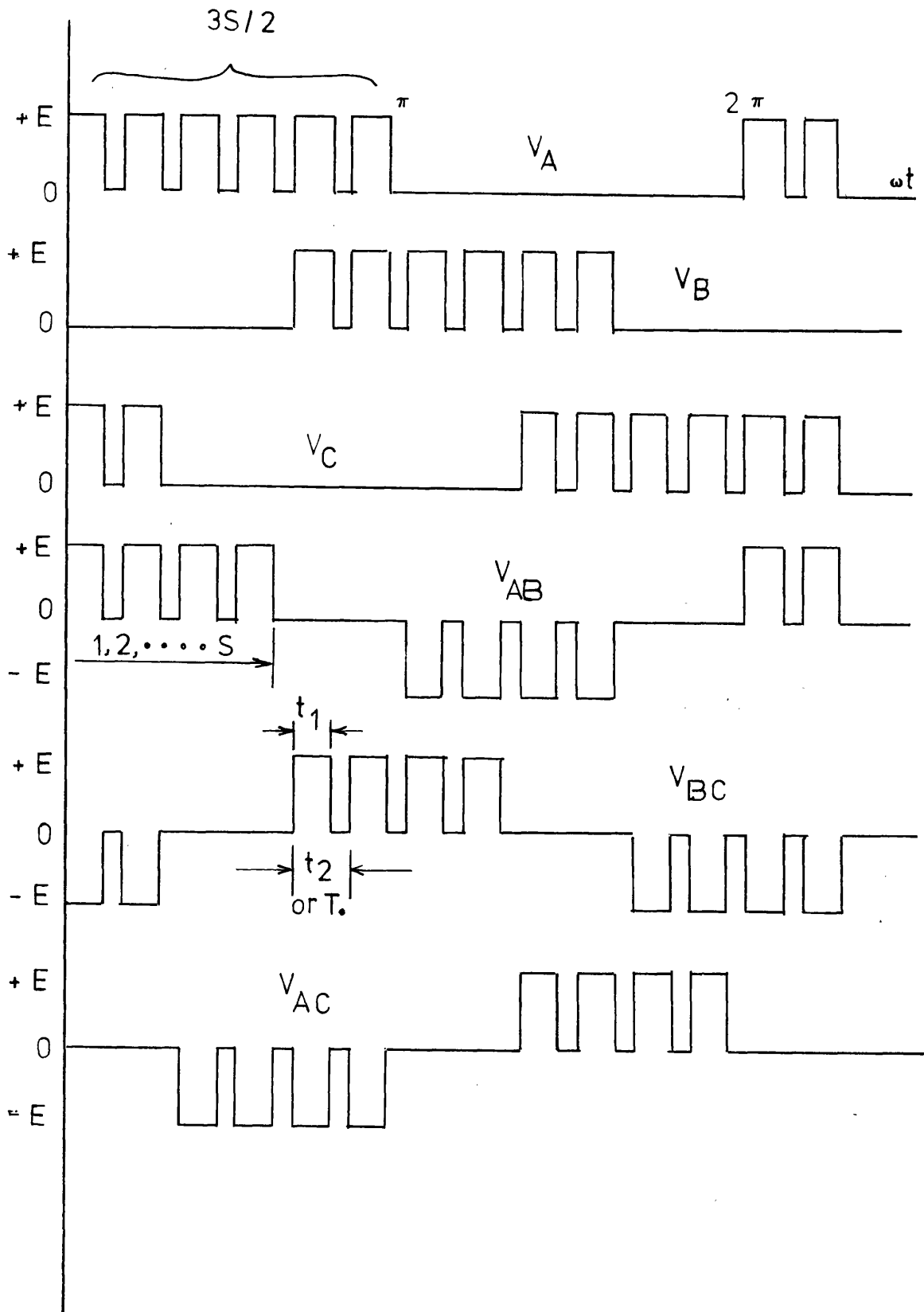


Figure 4.4

Let T_o be the period of sub-oscillation. This period is related to T , the period of main output frequency, by the relation:

$$T_o = \frac{T}{3S} \quad \text{--- (4.5)}$$

Where $3S$ is the number of sub-oscillations within the main period of each inverter, and the value of (S) depends on the range of operating frequency, amplitude of harmonic content etc., let K be the ratio of pulse duration to its period.

$$K = \frac{t_1}{t_2} = \frac{t_1}{T_o} \quad \text{--- (4.6)}$$

Considering the equation (4.3) one can immediately write an expression for V_{AB} as:

$$V_{AB} = \sum_{x=1}^{x=S} \sum_n \frac{8E}{(2n-1)\pi} \sin(2n-1)K\frac{\pi}{3S} \cos(2n-1) \left[\theta - (x-1)\frac{2\pi}{3S} - \frac{K\pi}{3S} \right] \quad \text{--- (4.7)}$$

easily reduced to:

$$V_{AB} = \sum_n \frac{8E}{(2n-1)} \cdot \frac{\sin(2n-1)K\frac{\pi}{3S}}{\sin(2n-1)\frac{\pi}{3S}} \sin(2n-1)\frac{\pi}{3} \cos(2n-1) \cdot \left[\theta + (1-K)\frac{\pi}{3S} - \frac{\pi}{3} \right] \quad \text{--- (4.8)}$$

Thus all harmonics of order 3 or multiples of 3 are equal to zero.

4.6 Analysis of Inverters Operating in Sinusoidal Sub-Oscillations

This technique involves modulating the output waveform with a train of pulses whose width varies in such a manner that their average value follows a periodical sine wave. If this train of pulses is applied to an inductive load such as an induction machine, the current in the stator will be built up while the pulse width increases, falling as soon as the pulse width starts to reduce. Thus, if the width of these pulses is varied proportionately with the amplitude of the reference sine wave, the stator current will also follow the sine wave and hence the machine flux shown in figure 4.5 will result.

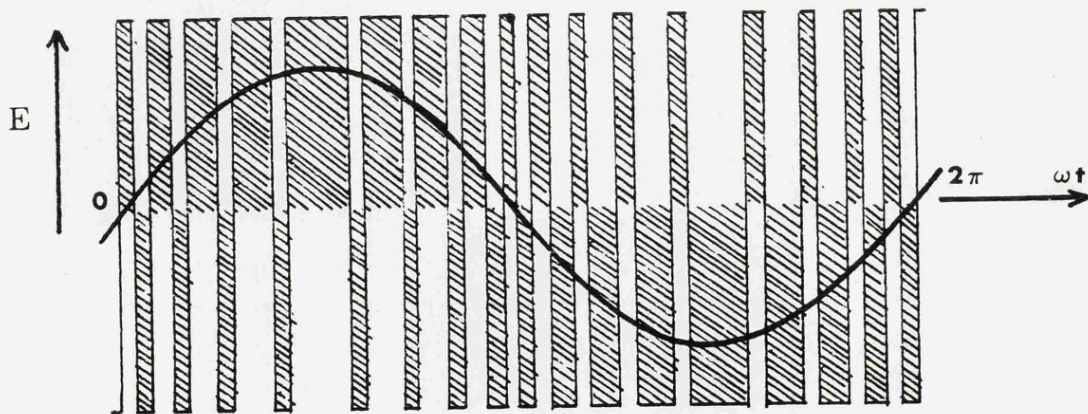


Figure 4.5

There are two popular techniques of modulating the inverter output in this fashion. The first technique involves a sine wave whose frequency determines the inverter output frequency and a triangular wave or saw

tooth with a much higher frequency. The frequency of the sawtooth or triangular waveform is a compromise between the allowable commutation losses and the required reduction in the harmonic content, similar to linear sub-oscillation technique. The comparator is then used to mix an isocetes triangle or sawtooth waveform with the reference sine wave to produce the modulation pulses. The spacing of these pulses are virtually equal ie. their frequency is equal to the frequency of the sawtooth or triangular waveform, and their width is proportional to the integral of the sine wave ^{4.11}.

The second technique involves monitoring the stator current and comparing it with a reference sine wave ^{4.8,} ^{4.9}. This is done by setting boundary limits either side of the sine wave known as the slit width or dead zone. Again comparators are used to switch the positive or negative supply across the input terminals. For example, suppose the machine has just been switched on, the stator or the load current being zero at this instant, the comparator will react to the value of the reference sine wave, and depending on its magnitude will switch a positive or negative supply across the load. This supply will stay across the load until the load current rises outside the slit width. Immediately this happens the comparator senses the difference and switches the load from this supply rail to the other rail. This action continues as long as the reference sine wave is present. The resultant train of pulses are very similar to those

obtained from the first technique, where the widths of the pulses are varied proportionally with reference to the sine wave. But the frequencies of the pulses are no longer equal and their average value depends on many factors such as slit width, load condition and magnitude of d.c. supply etc. Whereas the modulation frequency of the first technique is always equal to the triangular waveform frequency.

4.6.1 Analysis of Inverters Using Triangular Waveforms to Generate the Modulation Pulses

If one considers an inverter of the type shown in figure 4.1(a) and determines the firing angles by comparing the command sinusoidal wave and a reference sawtooth waveform shown in figure 4.6(a), which will produce an inverter output voltage waveform as shown in figure 4.6(b). The output waveform consists of a series of pulses of variable width, whose mean value periodically follows the law of sinusoidal equivalents. The maximum value of the width depends on the magnitude of the fundamental voltage of the inverter output.

Let T'_0 be the period of the sawtooth waveform. This period is related to the period of the output voltage T by the following relation:

$$T'_0 = \frac{T}{S'}$$

where S' is even multiples of three.

The control sine wave can be represented as:

$$V_C = rV_S \sin \theta \quad \text{--- (4.10)}$$

where r is the ratio of the sawtooth amplitude to the sine wave amplitude and its value is always less than or equal to unity $r < 1$, the rectangular pulses appear at the output with instants defined as:

$$\theta_{S_J} = \frac{2\pi}{S^T} + (J - 1) \frac{2\pi}{S^T} \quad \text{--- (4.11)}$$

where $J = 2, 3, 4, \dots$

and they end at instants defined as:

$$\theta_{S_J} + \Delta\theta_{S_J} \quad \text{--- (4.12)}$$

The width of each pulse is defined by the following relationship, see figure 4.6(a).

$$rV_S \sin(\theta_{S_J} + \Delta\theta_{S_J}) = \frac{V_S}{2\frac{\pi}{S}} \cdot \Delta\theta_{S_J} \quad \text{--- (4.13)}$$

This can be reduced as:

$$rV_S \sin\theta_{S_J} \cos\Delta\theta_{S_J} + rV_S \cos\theta_{S_J} \sin\Delta\theta_{S_J} = \frac{V_S}{2\frac{\pi}{S}} \cdot \Delta\theta_{S_J} \quad \text{--- (4.14)}$$

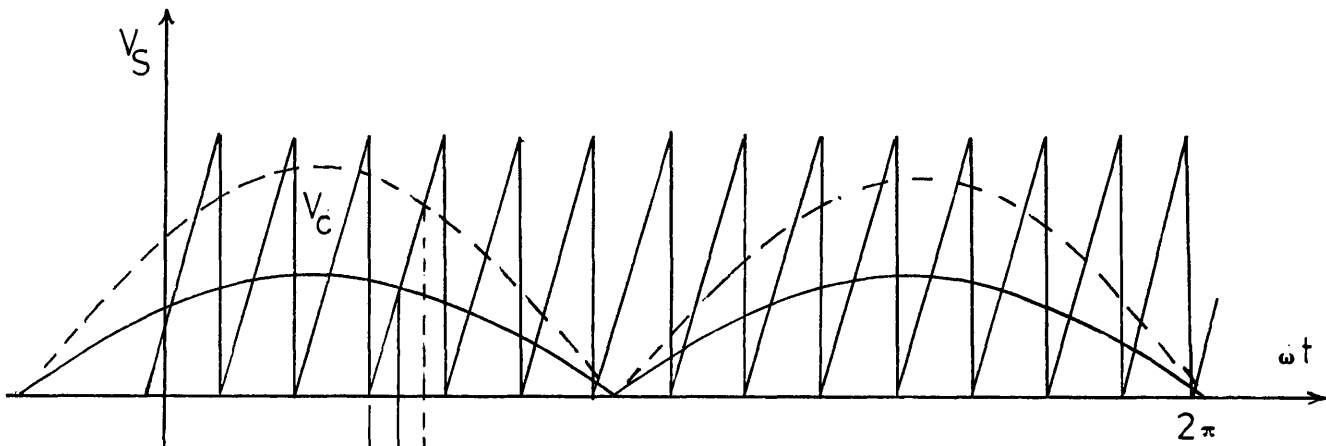


Figure 4.6(a)

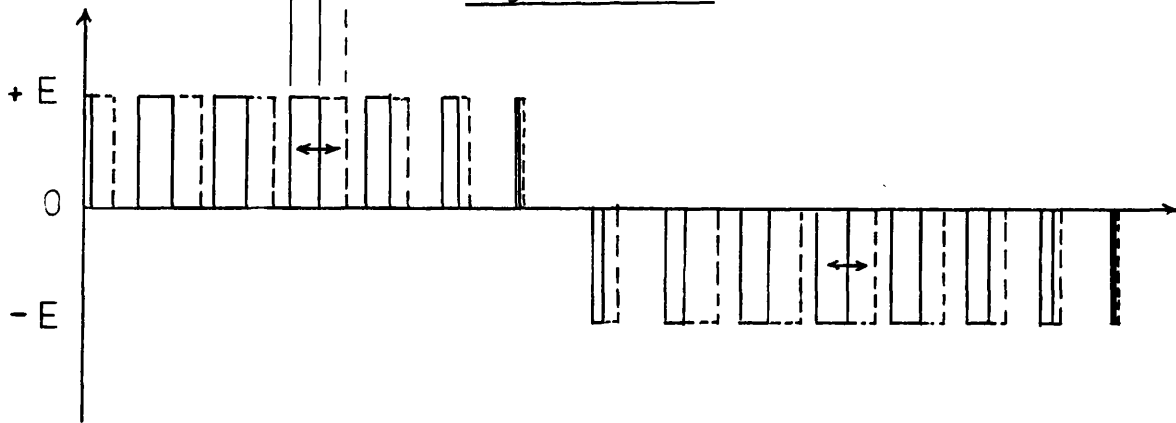


Figure 4.6(b)

If the ratio of $\frac{T}{T_0}$ is very large then the value of $\cos \Delta \theta_{SJ}$ approaches to unity and $\sin \Delta \theta_{SJ}$ approaches to $\Delta \theta_{SJ}$, thus from equation (4.14) we have:

$$\begin{aligned} \Delta \theta_{SJ} &= r \frac{2\pi}{S'} \sin \theta_{SJ} \left[\frac{1}{1 - r \frac{2\pi}{S'} \cos \theta_S} \right] \\ &= r \frac{2\pi}{S'} \sin \theta_{SJ} \left[1 + r \frac{2\pi}{S'} \cos \theta_{SJ} + \left(r \frac{2\pi}{S'} \right)^2 \cos^2 \theta_{SJ} \right. \\ &\quad \left. + \left(r \frac{2\pi}{S'} \right)^3 \cos^3 \theta_{SJ} + \dots \right] \quad \text{--- (4.15)} \end{aligned}$$

Now considering equation (4.7) one can write an expression for the voltage between two phases as:

$$V_{AB} = \sum_{j=1}^{s'} \sum_n \frac{8E}{(2n-1)} \sin \left[(2n-1) \frac{\Delta\theta_{SJ}}{2} \right] \cos(2n-1) \cdot \left[\theta_{SJ} - \frac{2\pi}{4S'} - (J-1) \cdot \frac{2\pi}{S'} - \frac{\Delta\theta_{SJ}}{2} \right] \quad \text{--- (4.16)}$$

The modulation mode shown in figure 4.6 is not the only possible one. This is characterised by a fixed ratio of output voltage frequency to the sub-oscillation frequency, which avoids the introduction of sub-harmonics of fundamental frequency, which can cause machine instability. Furthermore the working condition is limited by maintaining the number of pulses to an acceptable level by taking into consideration the loss that occurs during each commutation.

If the frequency of the reference wave (symmetrical or asymmetrical triangular waveform) is kept constant, and the frequency of the control sine wave is varied, the output voltage will contain these two frequencies. The fundamental will appear in phase with the frequency of the control sine wave and harmonic components whose magnitudes are greatest at frequencies approaching multiples of the reference waveforms (triangular in this case). One can find an expression in general form for the output voltage by considering the asymmetrical

triangular wave; in which the starting point of each ramp constitutes a reference point which repeats periodically; and for the symmetrical triangular wave whose peaks constitute the reference point also repeating periodically (shown in figure 4.7). This allows one to define the reference points shown by dotted lines in figures 4.7(c) and (f).

As shown in figure 4.7(c) the control angle for the asymmetrical case varies between $+\pi$ and $-\pi$ according to the level of control sine wave, and $+\pi/2$ to $-\pi/2$ for one side of the symmetrical reference signal and $-\pi/2$ to $+\pi/2$ for the other side.

For a constant level control signal rV_C for asymmetrical reference we have:

$$2V_r(\theta - \pi) \cdot \frac{1}{2\pi} = rV_r \quad \text{--- (4.17)}$$

where $0 < \theta < \pi$

From equation (4.17) the control angle α is given by:

$$\alpha = \pi(r + 1) - \pi = \pi r \quad \text{--- (4.18)}$$

Thus one can write the following expression in general for the output voltage in terms of its harmonic as:

$$V_A = rE + \sum_{n=1}^{\infty} \frac{2E}{n\pi} \sin(n\theta) + \sum_{n=1}^{\infty} \frac{2E}{n\pi} \cos n\pi [\sin(nr\pi) \cos(n\theta) - \cos(nr\pi) \sin(n\theta)] \quad \text{--- (4.19)}$$

Also similarly for the symmetrical case we have:

$$2V_r(\theta - \frac{\pi}{2}) = rV_r \quad \text{--- (4.20)}$$

where $0 < \theta < \pi$

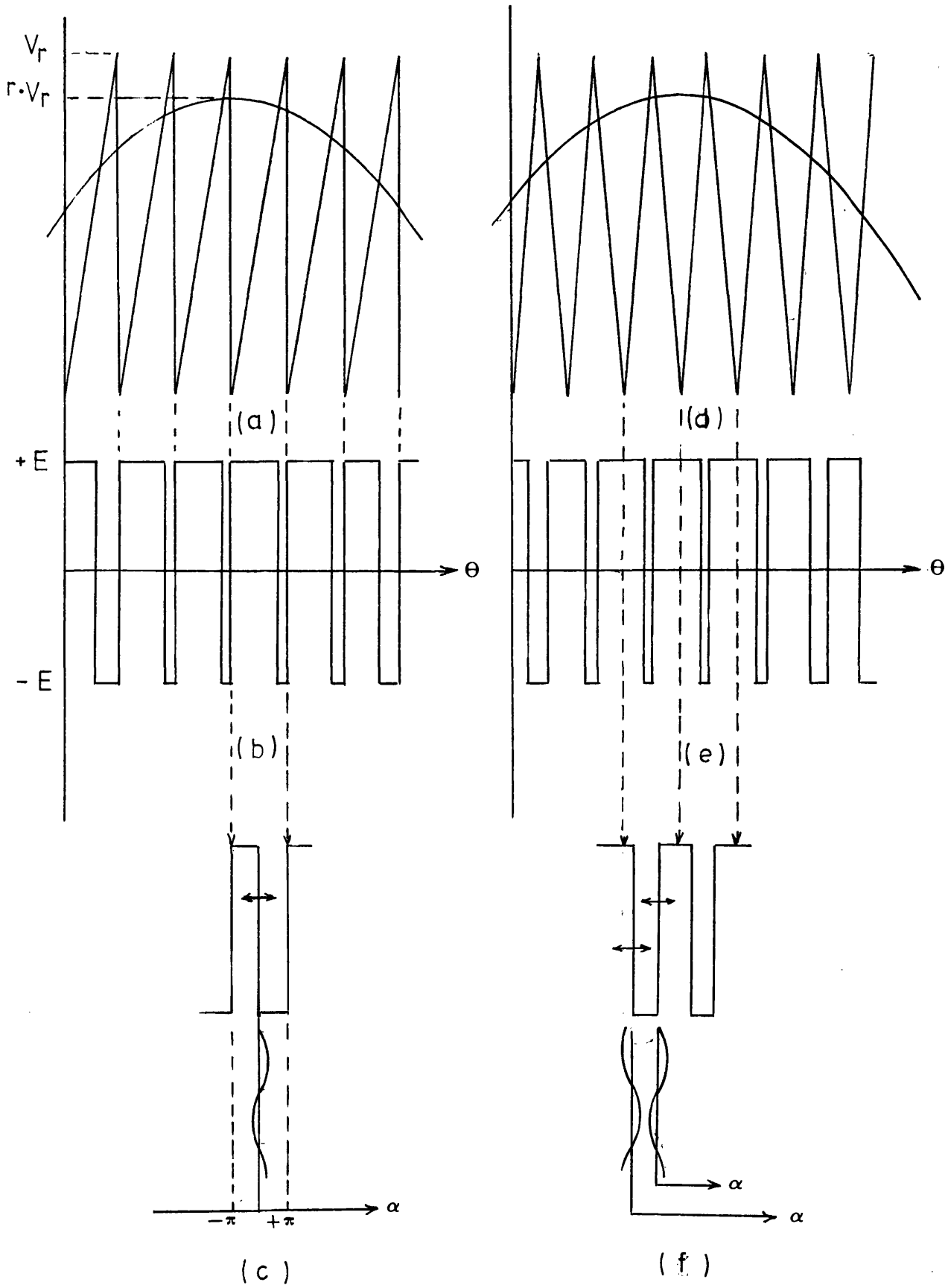


Figure 4.7

Thus the control angle can be defined as:

$$\begin{aligned} \pm\alpha &= (r + 1)\frac{\pi}{2} - \frac{\pi}{2} = r\frac{\pi}{2} \\ \alpha &= \pm r\frac{\pi}{2} \end{aligned} \quad \text{--- (4.21)}$$

in the case considered, positive sign applies for the left side and negative sign for the right side shown in figure 4.7.

Similarly the output voltage can also be written in general form as follows:

$$\begin{aligned} V_A = r \cdot E + \sum_{n=1}^{\infty} \frac{4E}{\pi n} \cos n\theta \sin\theta \left[\sin\left(\frac{nr\pi}{2}\right) \cos\left(\frac{n\pi}{2}\right) - \right. \\ \left. \cos\left(\frac{nr\pi}{2}\right) \sin\left(\frac{n\pi}{2}\right) \right] \end{aligned} \quad \text{--- (4.22)}$$

where $\sin\left(\frac{n\pi}{2}\right) = 0$ for even values of (n)

and $\cos\left(\frac{n\pi}{2}\right) = 0$ for odd values of (n)

But the magnitude of r varies sinusoidally with time.

Thus the control angle for the asymmetrical case becomes:

$$\alpha = \pi r(t) = \pi \cdot r(\theta_S) \quad \text{--- (4.23)}$$

Similarly for the symmetric case reference signal the values of the control angles become:

$$\alpha_1 = +r(t) \cdot \frac{\pi}{2} \quad \text{--- (4.24)}$$

$$\alpha_2 = -r'(t) \cdot \frac{\pi}{2} \quad \text{--- (4.25)}$$

where, in general $|r(t)| \neq |r'(t)|$

or $\alpha = \pi \cdot r \cdot \text{Sin} \theta_S$ asymmetrical reference --- (4.26)

$\alpha = \pm \frac{\pi}{2} \cdot r \text{Sin} \theta_S$ symmetrical reference --- (4.27)

now if we introduce new values of these control angles in equation (4.19) and (4.22) we have:

for the asymmetrical case

$$V_A = r \cdot E \text{Sin} \theta_S + \sum_{n=1}^{n=\infty} \frac{2E}{n\pi} \left\{ \text{Sin}(n\theta) + \text{Cos} n\pi \left[\text{Sin}(nr\pi \cdot \text{Sin} \theta_S) \right. \right. \\ \left. \left. \text{Cos}(n\theta) - \text{Cos}(nr\pi \text{Sin}(n\theta)) \right] \right\} \quad \text{--- (4.28)}$$

for the symmetrical case

$$V_A = r \cdot E \cdot \text{Sin} \theta_S + \sum_{n=1}^{n=\infty} \frac{4E}{n\pi} \text{Cos}(n\pi) \text{Cos}(n\theta) \\ \left[\text{Cos}\left(\frac{n\pi}{2}\right) \text{Sin}\left(\frac{n\pi}{2} \cdot r \cdot \text{Sin} \theta_S\right) - \text{Sin}\left(\frac{n\pi}{2}\right) \text{Cos}\left(\frac{n\pi}{2} \cdot r \text{Sin} \theta_S\right) \right] \\ \text{--- (4.29)}$$

if now Bessel functions of the first order are introduced to the equations (4.28) and (4.29), we have:

$$\text{Sin}(x \text{Sin} \theta) = \sum_{K=-\infty}^{K=+\infty} J_K(x) \text{Sin} K\theta \quad \text{--- (4.30)}$$

$$\cos(x \sin \theta) = \sum_{K=-\infty}^{K=+\infty} J_K(x) \cos K\theta \quad \text{--- (4.31)}$$

for the asymmetrical case one obtains:

$$\begin{aligned} V_A = r \cdot E \cdot \sin \theta_S + \sum_{n=1}^{\infty} \left\{ \frac{2E}{n} \left[1 - (-1)^n J_0(n\pi r) \right] \sin(n\theta) - \right. \\ \left. (-1)^n \frac{2E}{n\pi} \sum_{K=1}^{K=\infty} J_K(n\pi r) \cdot \sin(n\theta - K\theta_S) - \right. \\ \left. (-1)^n \frac{2E}{n\pi} \sum_{K=1}^{K=\infty} (-1)^K J_K(n\pi r) \cdot \sin(n\theta + K\theta_S) \right\} \end{aligned} \quad \text{--- (4.32)}$$

for the symmetrical case one obtains:

$$\begin{aligned} V_A = r \cdot E \cdot \sin \theta_S + \sum_{n'=1}^{\infty} \frac{4E}{\pi(2n')} (-1)^{n'} \sum_{K=1,3,5}^{\infty} J_K(2n' \cdot \frac{r\pi}{2}) \cdot \\ \left[\sin(2n'\theta + K\theta_S) - \sin(2n'\theta - K\theta_S) \right] + \\ \sum_{n'=1}^{\infty} \frac{4E}{n(2n'-1)} (-1)^{(n'-1)} \left\{ J_0 \left[(2n'-1) \frac{r\pi}{2} \right] \right. \\ \cos(2n'-1)\theta + \sum_{K=2,4,6}^{+\infty} J_K \left[(2n'-1) \frac{r\pi}{2} \right] \\ \left. \left[\cos \left[(2n'-1)\theta + K\theta_S \right] + \cos \left[(2n'-1)\theta - K\theta_S \right] \right] \right\} \end{aligned} \quad \text{--- (4.33)}$$

The equations (4.32) and (4.33) are used to calculate the frequency spectrum of both cases with an amplitude ratio of $r = 1$ and a frequency ratio of $\frac{f_r}{f_s} = 18$. This is shown in figure 4.7a, when supplying a balanced three-phase load.

The amplitudes of the lower order harmonics are greater in the asymmetrical case. This is because the asymmetrical modulation technique carries the modulation information by the trailing edge only. Whereas in the symmetrical case the information is carried by the leading and trailing edges of the pulse. The symmetrical case is also used in later sections for comparison with the inverters using the load current for the determination of the modulation pulses.

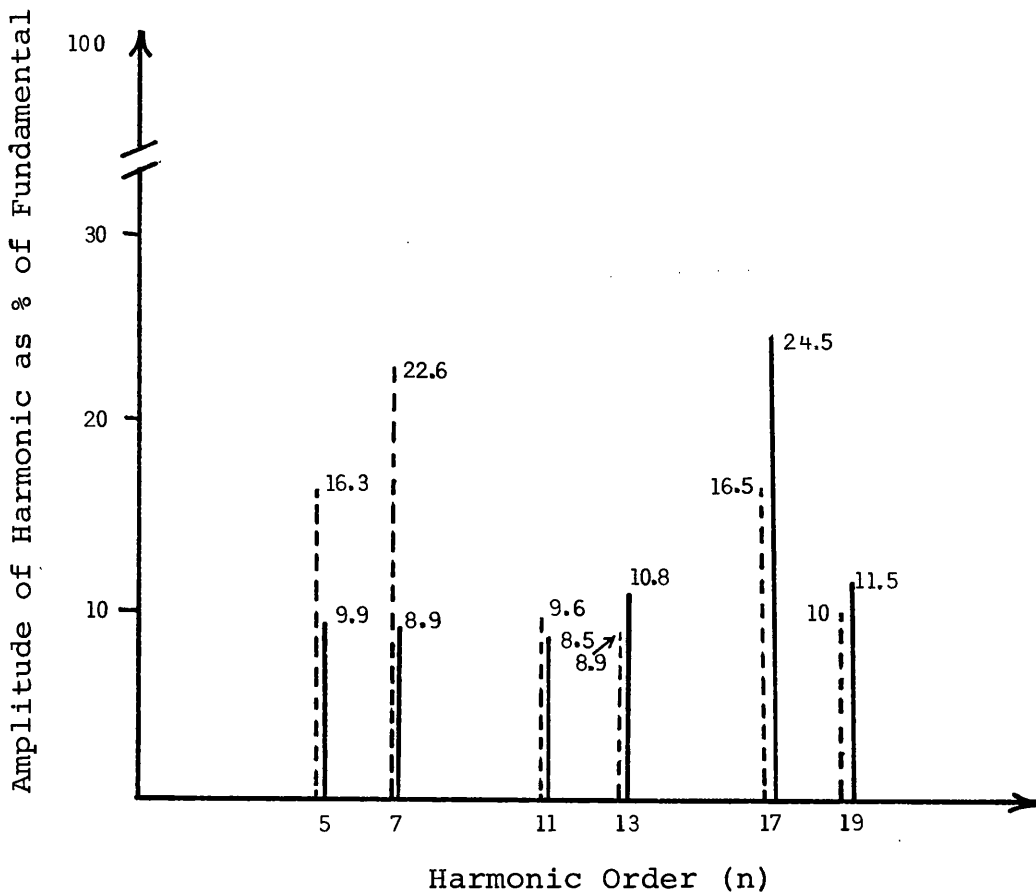


Figure 4.7(a) The Frequency Spectrum of the Symmetrical and Asymmetrical PWM Techniques

- (—) symmetrical
 - (---) asymmetrical
- $\left. \begin{array}{l} f_r/f_s = 18 \\ r = E = 1 \end{array} \right\}$

4.6.2 Analysis of Inverters Using Inductive Load Currents and Boundary Limits to Generate Modulation Pulses

In this technique the width of the modulation pulses are also determined by a sinusoidal law. The inverter switching intervals are determined by comparing the load current with a reference sine wave within a given boundary. Thus, the firing angles of the inverter's switching devices are produced in such a manner that the load current follows the reference waveform. Usually the power devices switch alternatively between positive and negative supply rails, but this is not the only case, and it depends on the type of logic arrangement that is used to determine the firing angles.

In the previous technique the triangular waveform is compared with a sine wave to determine the firing pulses. The width of the pulses are varied according to sinusoidal law, but pulse repetition frequency is always constant and equal to the reference triangular wave frequency. But in the inverter of this type, also known as a slit width amplifier, the pulse width and pulse repetition frequency are varied and their value depends on the magnitude of the reference waveform and boundary limits, also known as the slit width or dead zone, shown in figure 4.8 overleaf.

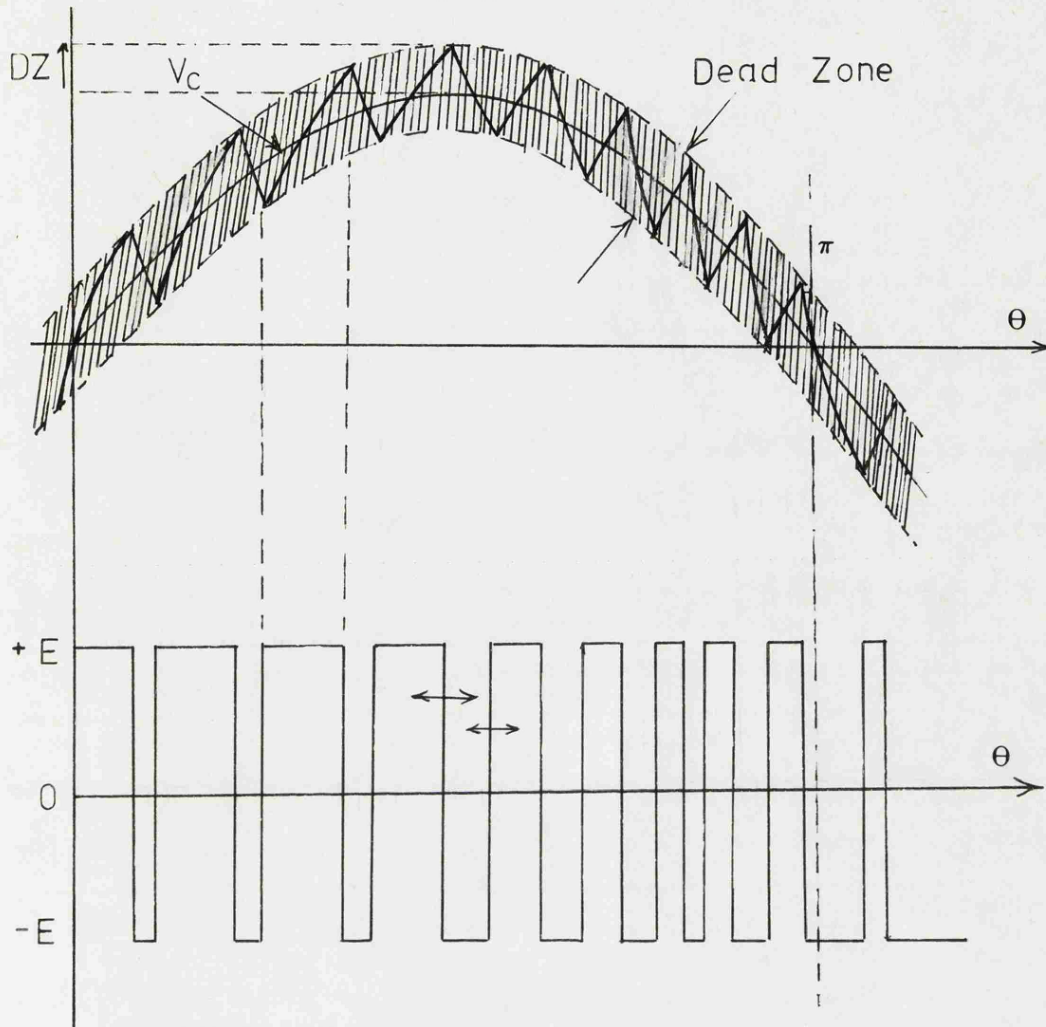


Figure 4.8

In general the value of θ can be determined by the following equation:

$$I_{L(0)} \left[e^{-\frac{T_L}{t}} \right] \pm \frac{E}{R} \left[1 - e^{-\frac{T_L}{t}} \right] = I_c \sin \theta \pm DZ \quad \text{--- (4.34)}$$

where T_L is the load time constant and is given by $T_L = \frac{R}{L}$

and t at any instant is given by: $t = \frac{\theta}{2\pi f}$ --- (4.36)

I_c is the magnitude of the reference current, D_z is half the value of the dead zone and $I_{L(0)}$ is the initial value of the load current.

Suppose that the value of the dead zone is such that it produces an integer number of pulses per cycle such as the one shown in figure 4.8. Thus when θ is equal to zero the initial value of the load current is also zero.

Therefore we have:

$$\frac{E}{R} \left[1 - e^{-\frac{T_L}{t}} \right] = I_c \sin \theta + D_z \quad \text{--- (4.37)}$$

$$\frac{T_L}{t} = \frac{R/L}{\theta/2\pi F} = \frac{K'}{\theta}$$

where K' is constant and equal to $T_L \cdot \omega$

Substituting $\frac{T_L}{t}$ by $\frac{K'}{\theta}$ and expanding equation (4.37) in series form we have:

$$\frac{E}{R} \left[K'/\theta + \frac{K'^2/\theta^2}{2!} + \frac{K'^3/\theta^3}{3!} + \dots \right] = I_c \left[\theta - \frac{\theta^3}{3!} + \frac{\theta^5}{5!} + \frac{\theta^7}{7!} + \dots \right] + D_z \quad \text{--- (4.38)}$$

In general, equation (4.38) has an infinite number of roots. Depending on the accuracy required, the higher orders of the θ can be neglected to reduce it to some manageable form. It must be remembered that the value of θ has an appreciable effect on the order of the series. Thus at any instant the magnitude of the load

current can be found as an initial value for the next switching point (θ).

Hence the load current and its harmonics in general can be determined from the expression:

$$V_A = \frac{E}{\pi} \sum_{m=1}^m \left\{ (\theta_{2m} - \theta_{2m-1}) + \frac{2}{n} \sum_n^{\infty} \left[\sin(n\theta_{2m} - n\theta) + \sin(n\theta_{2m-1} - n\theta) \right] \right\} \quad \text{--- (4.39)}$$

where m is the number of switching points per cycle.

4.7 Program Description of Inverters Using Triangular Waveform as Reference

The majority of power inverters employed in the industry today are based on the technique of comparing triangular waveform with a sine wave to produce the necessary switching angles. To study the behaviour of such systems the following digital computer program is developed to produce the necessary characteristics. The flow diagram of the system is shown in figure 4.9. The program consists of three main parts. The first part of the program takes two reference waveforms (triangular and sine wave) and compares them to produce the switching points. The Newtons' formula (4.40) with a higher degree of accuracy is used to calculate the common root of the two waveforms in time axis.

$$\text{Newtons formula} \rightarrow x_{n+1} = x_n - f(x_n)/f'(x_n) \quad \text{--- (4.40)}$$

Then by applying Fourier series analysis, the resultant switching points over a cycle are analysed in the second part of the program and the amplitude of all the harmonics are computed.

The third part of the program computes the amount of power distributed in each harmonic, when supplied across the terminals of an induction motor. Finally the percentage of the total power distributed in each harmonic plus the efficiency of the system is computed.

The program also includes the following facilities:

- (a) it can compute the efficiency of the inverter using the standard induction motor equivalent circuit or the variable frequency equivalent model obtained in the previous chapter,
- (b) it can compute all the necessary characteristics at any supplied frequency and any number of pulses per cycle. Also the amplitude of the reference wave which determines the amplitude of the fundamental frequency can be set at any value to control the amplitude of the fundamental output voltage and compute the necessary characteristics.

4.7.1 Discussion of Results

The ratio of fundamental output voltage to reference sine wave approaches to unity as the number of pulses per cycle increase ie. for infinite number pulses per cycle, the level of fundamental output voltage is equal to reference sine wave. There is a linear relationship between the amplitude of the reference sine wave with any value of the amplitude of the fundamental output voltage. The ratio of the two amplitudes becomes greater than unity as the number pulses per cycle are reduced and also this ratio becomes even greater as the amplitude of the reference sine wave becomes smaller than the amplitude of the triangular waveform shown in figure 4.10. The relationship between the number of pulses per cycle and the amplitude of the fundamental waveform (in dB's) is also shown in figure 4.11 and approaches to unity (0 dB) as the number of pulses per cycle increases. This is due to the reduction in the number of pulses per cycle, which results in greater harmonic content at the output voltage, and the poorer efficiency shown in figures 4.12 and 4.13.

Thus for a given fundamental output power, the inverter output contains more power in the pulses over a cycle, the fewer the number of pulses, see figure 4.14. The level of the unwanted harmonics remains almost constant for all values of the reference sine wave amplitude as shown in figure 4.15; consequently the power contained in

the fundamental output voltage becomes proportionally less of the total inverter output power as the amplitude of the reference sine wave is reduced. This results in a reduction in the efficiency of the inverter.

4.8 Program Description of Inverters Using Load Current and Boundary Limits to Generate the Modulation Pulses

The digital program of this inverter involves the switching of the supply rails across an inductive load (equivalent circuit of the induction motor) where the polarity of the supply depends on the previous value of the load current. The program starts with a reference sine wave of rotational angle at zero degrees radians and zero initial load current. The inverter switches positive and negative supplies across the load in such a way that the load current rises exponentially towards the value of the reference sine wave plus the value of the dead zone. As soon as both magnitudes become equal, the supply rails are reversed across the load. Now the load current falls exponentially until the magnitude equals the reference sine wave minus the value of the dead zone. Switching of the polarities across the load continues and the load current is forced to follow the reference sine wave within the dead zone limits.

For a given load condition the dead zone is varied step by step until identical switching points over 0° - 180° and 180° - 360° are obtained. (The number of pulses from the positive supply during the first half cycle equals

the number of pulses from the negative supply during the next half cycle). This ensures that the number of pulses per cycle are constant and locked in phase ie. identical patterns of modulation pulses are repeated over each cycle. Since the previous inverter operates with a constant number of pulses per cycle for any given condition it is essential to obtain a constant number of pulses per cycle, so their output harmonic content and efficiency can be compared when operating under the same conditions. There is a unique value of the dead zone for a given number of pulses over a cycle and given operating conditions. Once the required value of the dead zone is determined for any operating condition, the Fourier series is applied to compute the magnitude of the harmonic content of these switching points over a complete cycle. The power contained in each harmonic is also calculated and the total value over a large order of harmonics is used to compute the percentage of the input power in each harmonic. The percentage of input power contained in the fundamental frequency is the efficiency of the inverter operating under that given condition for harmonic losses only.

This digital program has also similar facilities as in the previous type such as changing supply frequency, load condition etc. The flow diagram consists of two parts. Part one searches for a value of the dead zone which produces a constant number of pulses per cycle and is locked in phase for a given load condition (flow

diagram shown in figure 4.16). Part two uses the same input data as part one, the corresponding value of the dead zone, to compute all the required output data (flow diagram shown in figure 4.17).

4.8.1 Discussion of Results

For constant flux applications when supplying an induction machine with constant slip (shown in figure 4.18) the amplitude of the fundamental voltage is linearly proportional to its frequency. Since for a given operating condition, the load time constant remains constant, the number of pulses per cycle falls, as expected, with an increase in the supply frequency. Their relationship with a constant dead zone of about 10% of the load current is represented in figure 4.18. The reduction in the number of pulses per cycle at higher fundamental frequencies increases the level of the harmonic content at the inverter output as shown in figure 4.19. The consequent reduction in efficiency is shown in figure 4.20.

For any given operating condition the number of pulses per cycle increases exponentially with the reduction of the dead zone. Similarly with any other technique as the number of pulses per cycle increases the magnitudes of the harmonics falls and the total power contained in the pulses over each cycle approaches that of the power contained in the sine wave voltage. These characteristics are represented in figures 4.21 to

4.23. If the system is designed such that changes in the load current result in proportionate changes in the dead zone; the number of pulses per cycle remain constant for any changes in the load. The efficiency of the inverter system remains constant for any value of the rotor slip when feeding an induction motor, so long as the width of dead zone follows the line current proportionally as represented in figure 4.24.

4.9 Effect of a Variable Frequency Induction Motor Equivalent Circuit on the Inverter Efficiency Calculations (Harmonic Losses are Considered Only)

The overall efficiency of any inverter type is mainly governed by the level of harmonic content at the output. The nature of the load also has an important part in the efficiency of the system, ie. if the load was pure resistance the efficiency of the inverter supplying such a load is only governed by the harmonic contents. But as in loads such as induction motors, whose equivalent circuit contains reactance as well as resistance, the amount of power distributed in each harmonic becomes smaller as the order of the harmonics increases with non-frequency dependent resistive and inductive parts.

In general:

$$P_n = \frac{V_n^2 R_L}{R_L^2 + (n.X_L)^2} \quad \text{--- (4.41)}$$

where P_n = power in the nth harmonic

V_n = amplitude of the nth harmonic

n = order of the harmonic

R_L = resistive part of the load

X_L = reactive part of the load at fundamental
frequency

For a given operating condition of an induction motor fed from any inverter type the resistive and inductive part of the input impedance seen at the input terminals are frequency dependent (as given in the previous chapters). Employing standard equivalent circuit parameters rather than frequency dependent parameters results in a considerably different distribution of power in each harmonic. In the following sections, the efficiency of two main inverter types are calculated, with constant load parameters (standard induction motor equivalent circuit) and frequency dependent load parameters (frequency dependent induction motor model).

4.9.1 Efficiency Calculation of Inverter Type Using Triangular Waveforms as Reference

The digital program described in Section 4.7 is used to compute the percentage of the total output power in the fundamental voltage when feeding an induction motor. The efficiency of the system is calculated firstly using a standard induction motor equivalent circuit, and secondly using a variable frequency dependent model as the load. In both cases the induction motor is kept running with rotor slip at 10% and the results are shown in figure 4.25. The frequency of

the triangular waveform is kept constant and the frequency of the sine wave which determines the main fundamental output frequency is altered from 50 up through 300 Hz. There is a consequent reduction in the number of modulation pulses per cycle as the fundamental frequency is increased under the same operating conditions (ie. slip is kept at 10% throughout all the supply frequencies) using standard induction motor equivalent circuits. The efficiency of the inverter system is high at the lower end of the supply frequency, falling at the higher end due to an increase in the harmonic content. But using the variable frequency model, the overall efficiency is reduced and maximises at the mid-frequency. The reduction in the overall efficiency is because of the increasing value of the resistive part of the variable frequency model with the order of harmonics; it maximises as the resistive and reactive parts of the load at the fundamental frequency become equal.

Using either of the equivalent circuits as the load, the overall efficiency remains very high. The standard model leads to some higher results than those obtained in real life. Since the losses due to switching devices etc. are common for any model being analysed, they have been omitted in the analysis.

In addition since the level of the reference sine wave is used to control the amplitude of the fundamental output voltage, the efficiency of the inverter system

(operating with constant slip and fundamental frequency using variable frequency model) with various magnitudes of the reference sine wave differing number pulses per cycle are computed and shown in figure 4.26.

As the amplitude of the sine wave becomes smaller compared with the triangular waveform, the fundamental output voltage follows linearly whilst the level of harmonic content remains roughly constant represented in Section 4.7. Thus efficiency decreases for smaller values of amplitude of the reference sine wave. This effect becomes more serious with the reduction of the number of pulses per cycle.

4.9.2 Efficiency Calculation of Inverter Type Using Load Current as Reference

The digital program of Section 4.8 is used to compute the efficiency of this inverter type similarly to that of the previous one. The dead zone is kept at 10% of the load current throughout the main supply frequencies ie. with reference to sine wave frequency of 50 up to 300 Hz. Thus, the number of pulses per cycle lessen as the fundamental frequency approaches 300 Hz. Using the standard induction motor as the load, the efficiency of the inverter remains almost constant (shown in figure 4.27). When the variable frequency model is used as the load the inverter efficiency falls at the lower range and peaks at the mid-frequency point similarly to the previous type. However at the higher

end of the frequency range, the efficiency does not fall as it does with the previous type. This is because this inverter type contains much less harmonic content when there are a reduced number of pulses per cycle.

4.10 Comparison of Inverters Using Triangular Waveform and Load Current as the Reference Signals

As indicated in the two previous Sections, these inverters are highly efficient systems. The comparison between them can only be justified when they are both operating under exactly the same conditions ie. both systems are delivering the same amount of power into a given load and contain an equal number of pulses per cycle. The variable frequency model is employed with constant rotor slip as the load, and the efficiency and load currents are computed. The number of pulses per cycle are kept constant at each step of fundamental frequency and are both supplied with the same positive and negative power rails. The load current of the triangular system is slightly higher than that of the other type considered, and the differences between them at the lower end of the supply frequency range are shown in figure 4.28. The amplitude of the reference signal should therefore be reduced to equal the line currents of both systems at low frequency range. This increases the output harmonic content as shown in figure 4.15. However, the required amount of reduction in the amplitude of the reference signal is very small and has virtually no effect

on the output efficiency. The efficiency of both systems operating under the same conditions are then calculated and shown in figure 4.29. Thus, the inverter type, using load current as a reference, is marginally more efficient. This difference is not a significant factor in selecting the type of inverter for the majority of applications. The significant factor in selecting any technique is the desired complexity of circuitry employed.

4.11 Conclusions

The inverters which sense the load current to determine the modulation pulses, contain less harmonic content at the output and consequently are more efficient than the inverters employing the predetermined modulation techniques, operating with a given number of pulses per cycle. However, the difference in the efficiencies is not significantly large. Therefore, when selecting the modulation technique, other factors such as the complexity of the control circuitry, cost and kind of application should be considered.

The voltage control of the predetermined modulation technique is normally achieved by control of the reference sine wave amplitude. This increases the proportion of harmonic content in the output voltage considerably at lower voltages. It also makes the relationship between the fundamental voltage amplitude and the reference sine wave amplitude non-linear. In order to

establish a linear relationship and reduce the harmonic content at low voltages, the number of pulses per cycle should be increased.

The slit width modulation technique compares the load current with the reference signal to determine the number of pulses per cycle. The magnitude of the line current is normally controlled by controlling the amplitude of the reference signal. For a given slit width the number of pulses per cycle reduces at lower voltages of the line currents. This is also similar to the predetermined modulation technique which results in higher harmonic content. To achieve lower harmonic content at lower power levels the slit width should be related to the amplitude of the reference signal. In this way the number of pulses per cycle can be maintained constant and hence the harmonic content.

The frequency control of both techniques is also achieved by the control of the reference signal frequency.

In the predetermined modulation technique the pulse repetition frequency should be related to the reference signal frequency. This can ensure constant harmonic content at any operating fundamental frequency. Similarly in the slit width modulation technique, the ratio of the slit width to the reference signal amplitude should be reduced, to keep the harmonic content constant at higher frequencies. The control circuitry required for both techniques appears to involve similar

complexities to achieve the best results. Therefore, inverters sensing the load current to determine the modulation frequencies are the most efficient systems for controlling the output voltage levels as well as the fundamental frequency. The overall efficiencies of the machine fed by the inverter systems are not considered.

The normal losses in the machine for given conditions and fundamental voltages are constant and irrespective of the modulation technique employed. The fundamental voltage amplitudes can be kept constant instead of the total inverter output powers. However, the ratio of the total output power to the power distributed in the harmonic voltages remains constant as does the efficiency.

The application of the standard equivalent circuit of the induction motor for the determination of additional losses results in serious errors. The magnitude of the error becomes larger in the power distributed in the higher order harmonics. This is because the inductive part of the machine's impedance reduces, and the resistive part increases, with the order of harmonics. Therefore the proportion of power distributed in the harmonic voltages increases with the order of the harmonics. The application of the standard equivalent circuit is no longer correct for the determination of additional losses in the machine due to harmonic frequencies. This

is one of the advantages of the new equivalent circuit for the induction motors fed from variable frequency inverter supplies.

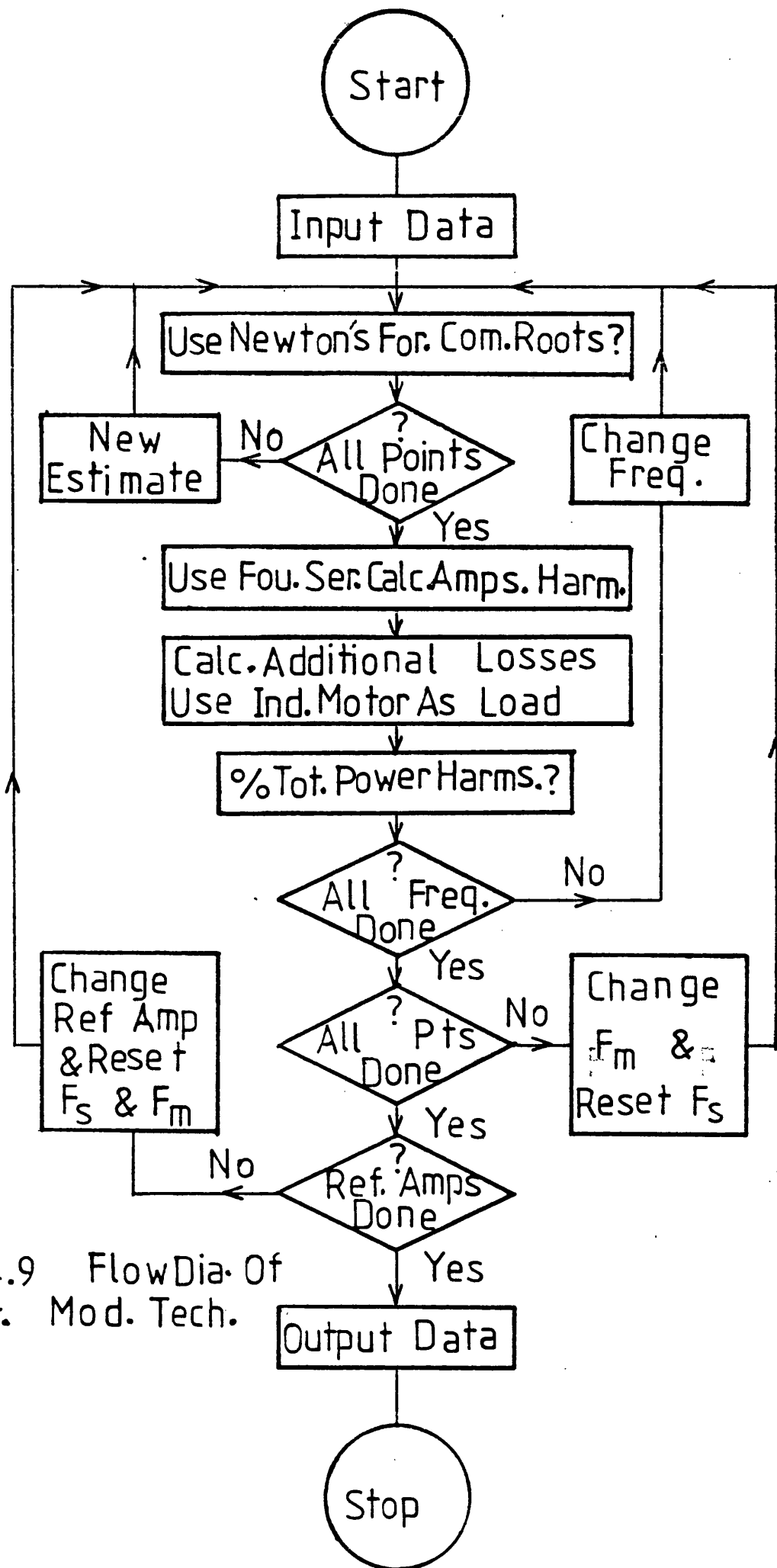


Fig. 4.9 FlowDia. Of
Predet. Mod. Tech.

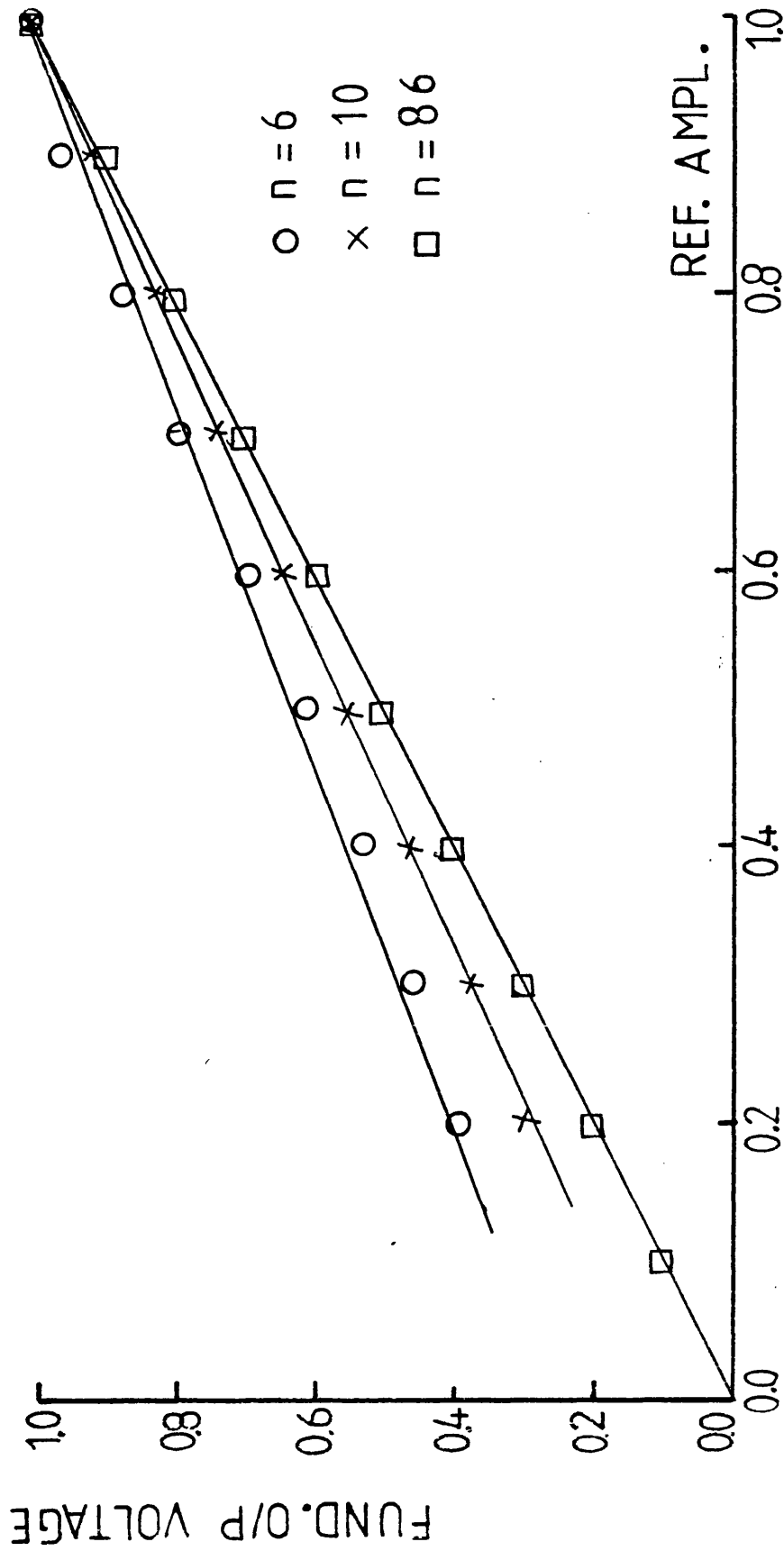


Fig. 4.10 FUND. O/P VOLT. V REF. SINE WAVE
INV. USING TRI. WAVE AS REF.

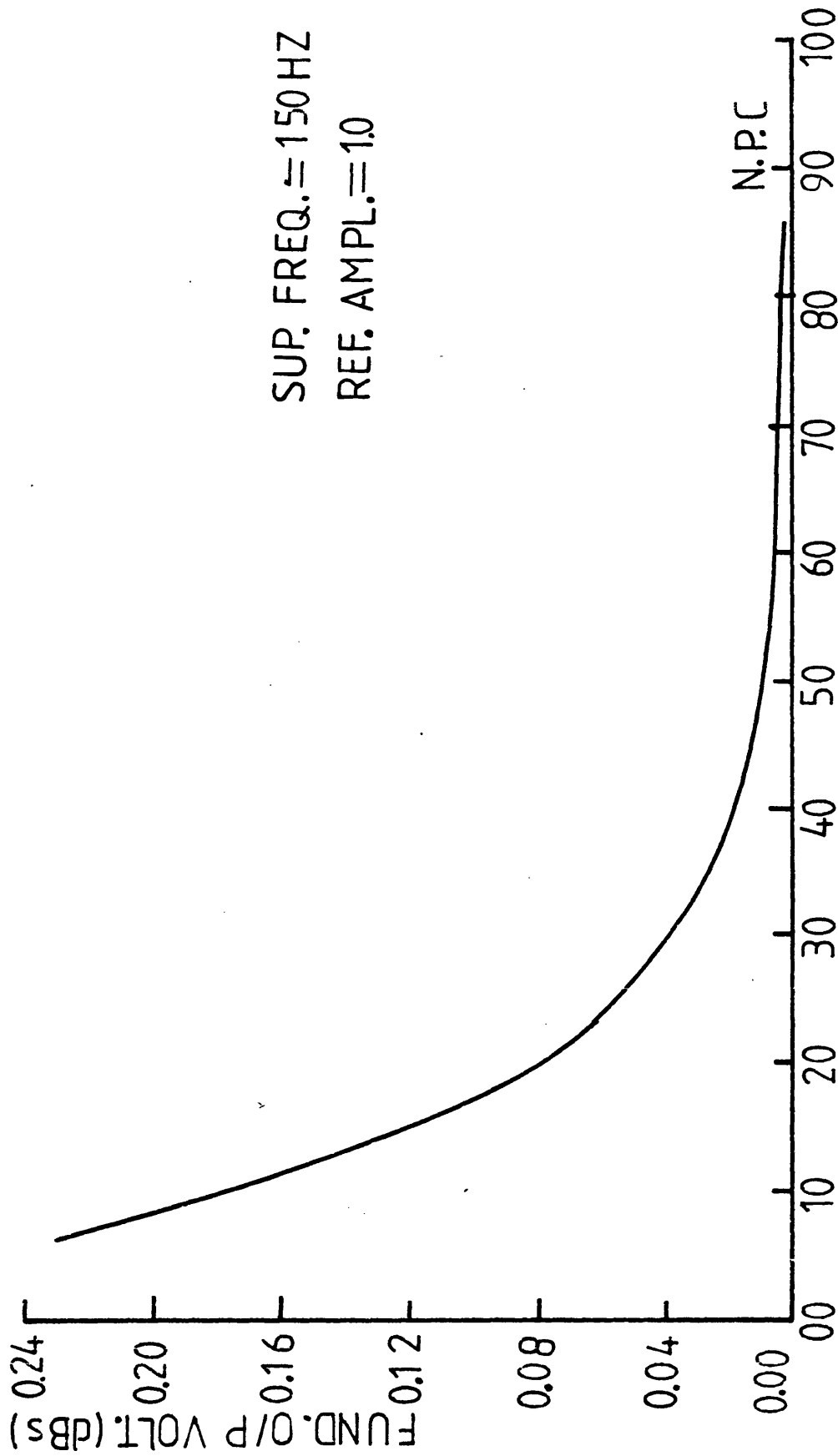


Fig. 4.11 FUND. O/P VOLT. V NO. PULSES PER CYCLE

INV. USING TRI. WAVE AS REF.

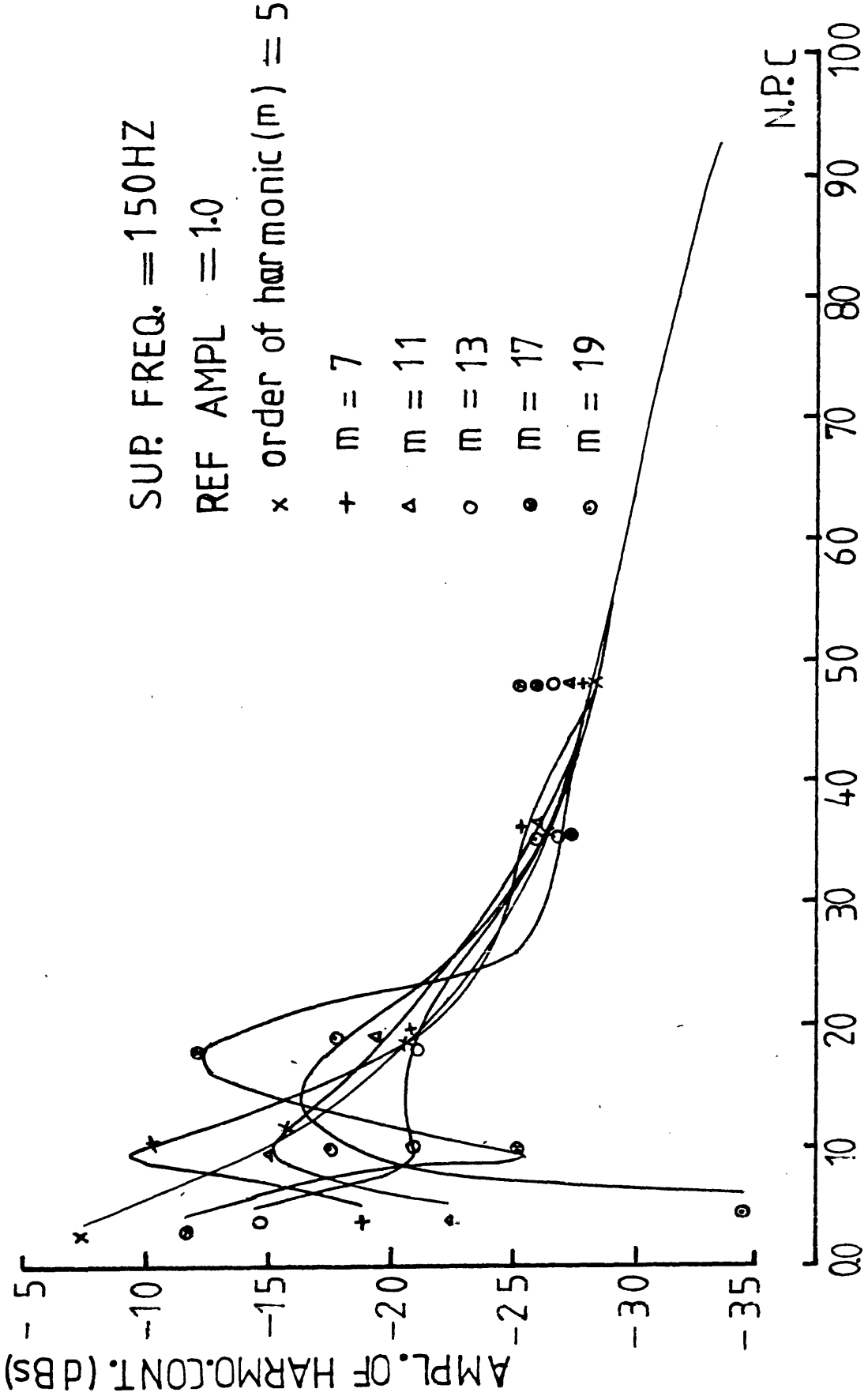


Fig. 4.12 LEVEL OF HARM.CONT. V NO.OF PULSES PER CYCLE
 INV. USING TRI.WAVE AS REF.

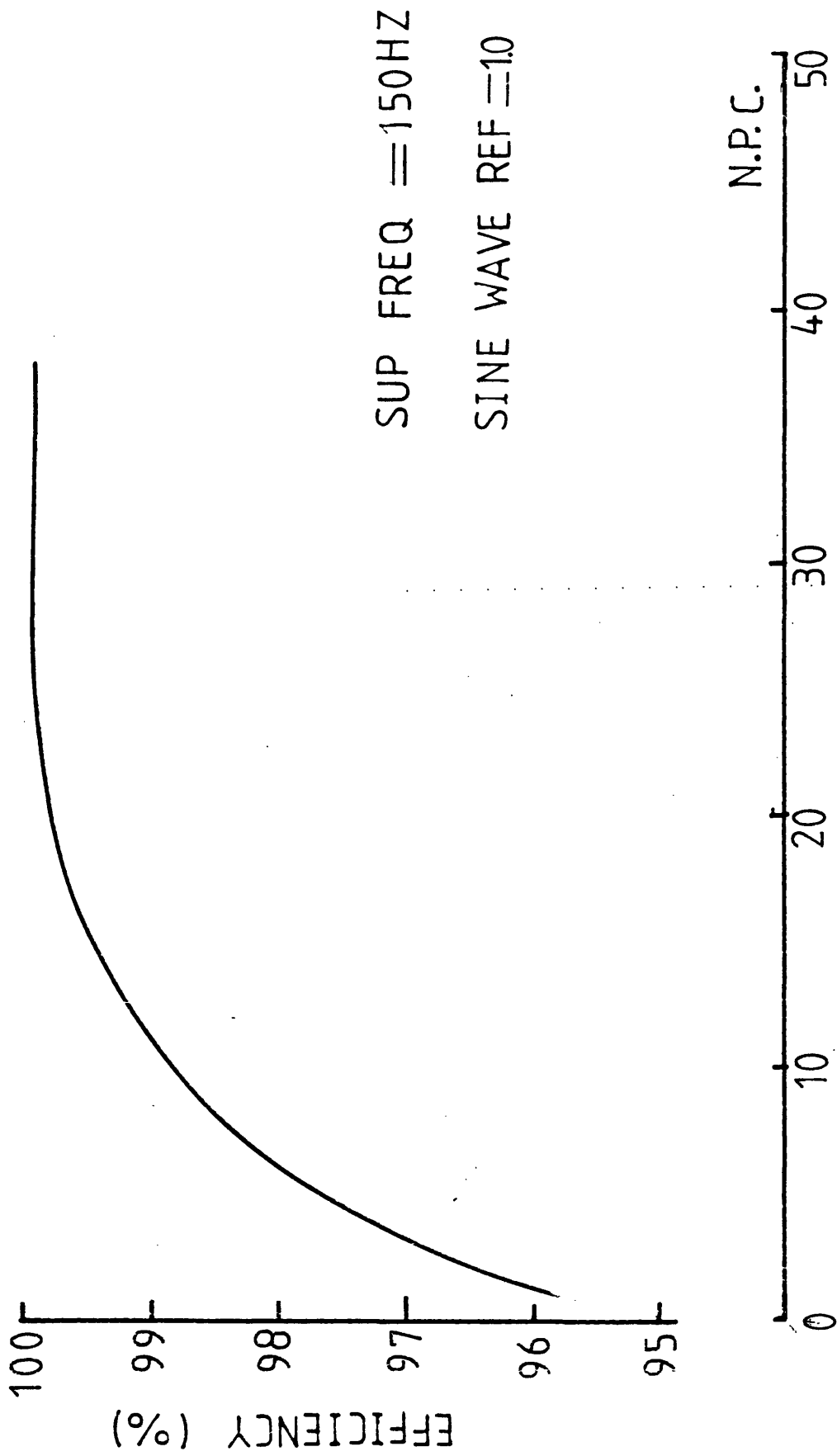


Fig.4.13 EFFICIENCY V NO. OF PULSES PER CYCLE
INV. USING TRI. WAVE AS REF.

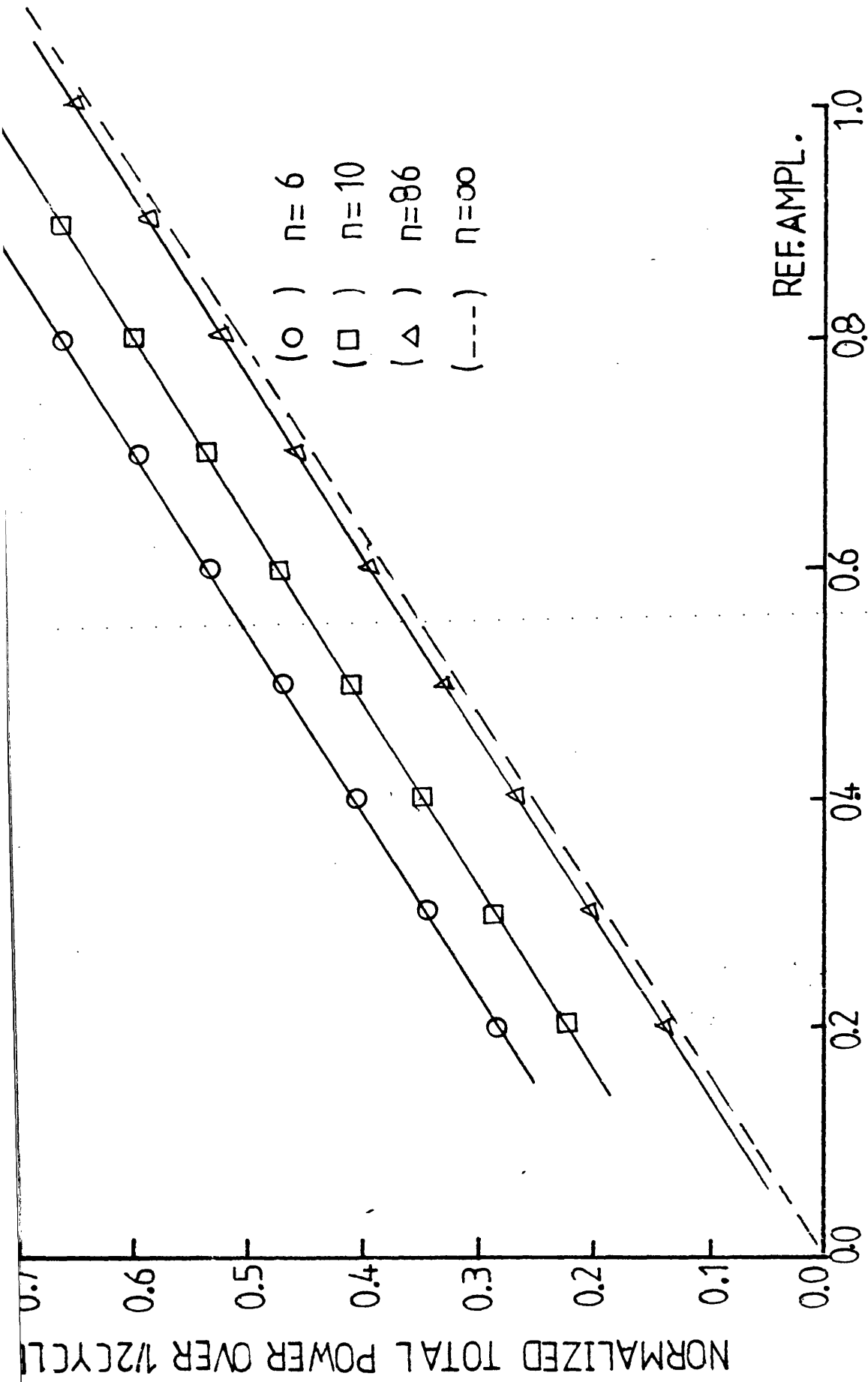


Fig. 4.14 TOTAL POWER IN PULSES OVER 1/2 CYCLE
 REF. SINE WAVE AMPL.

INV. USING TRI. WAVE AS MODU. REF.

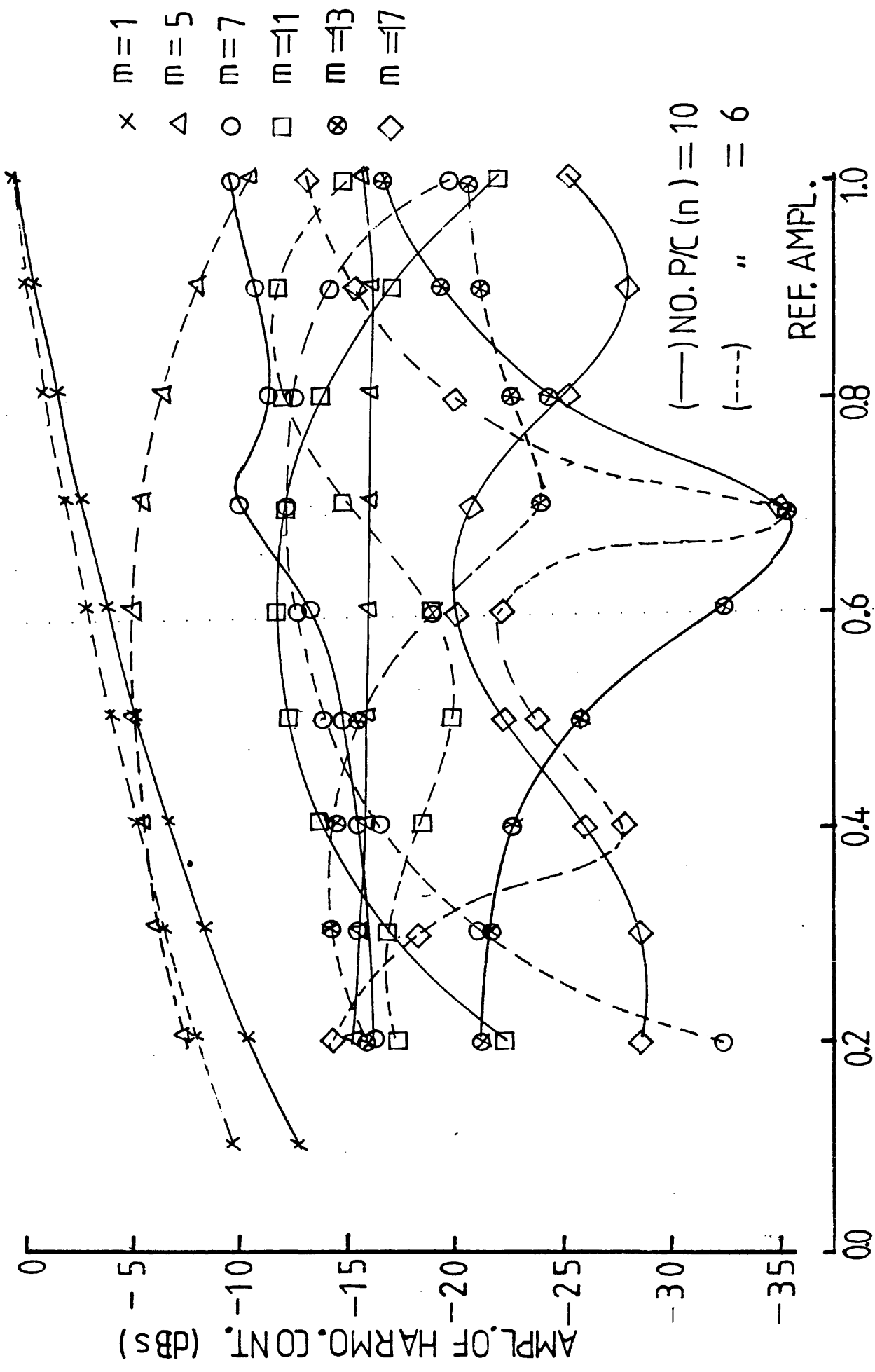


Fig. 4.15 HAPMO. CONT. V REF. SINE WAVE AMPL.
INV. USING TRI. WAVE AS REF.

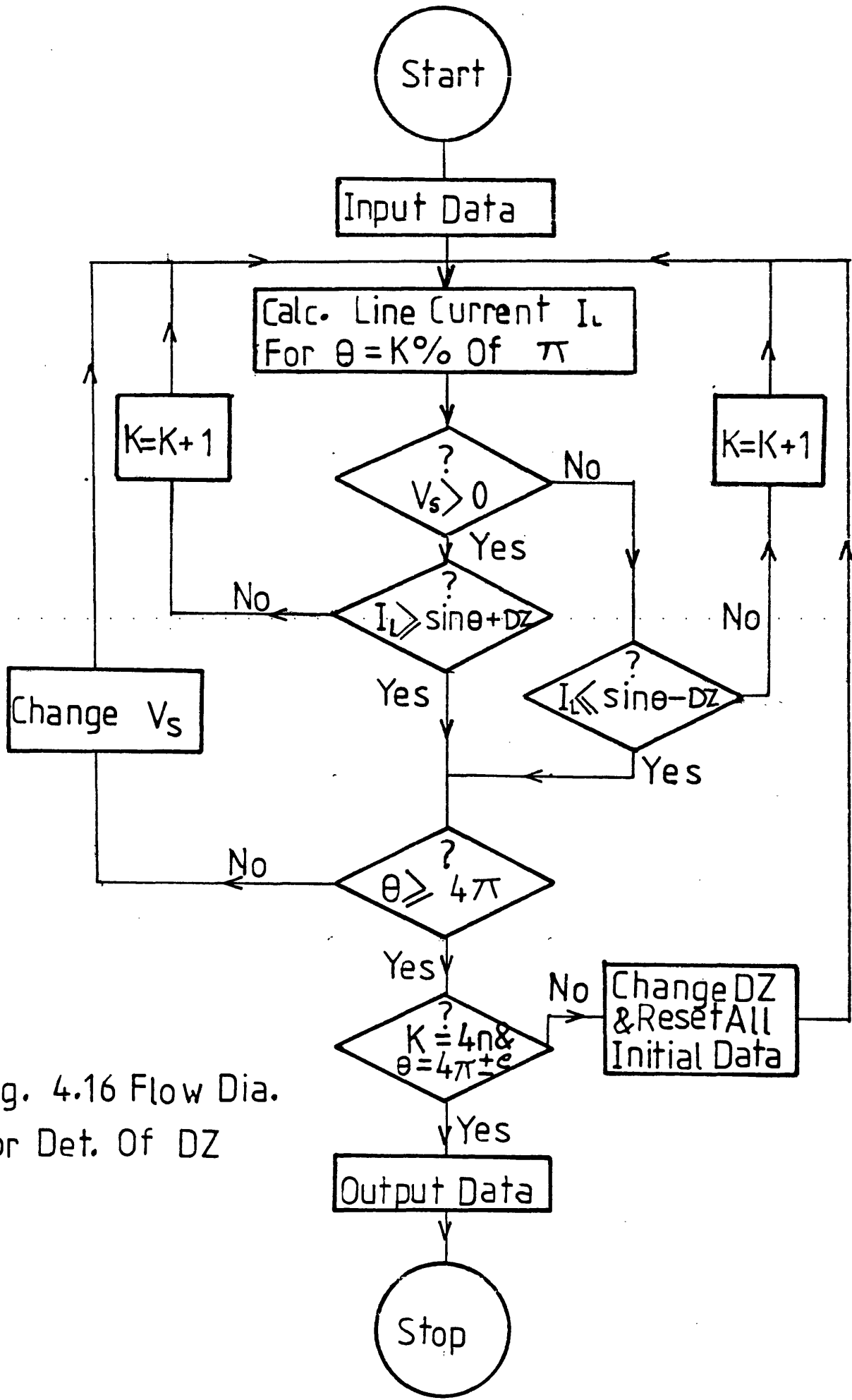


Fig. 4.16 Flow Dia.
For Det. Of DZ

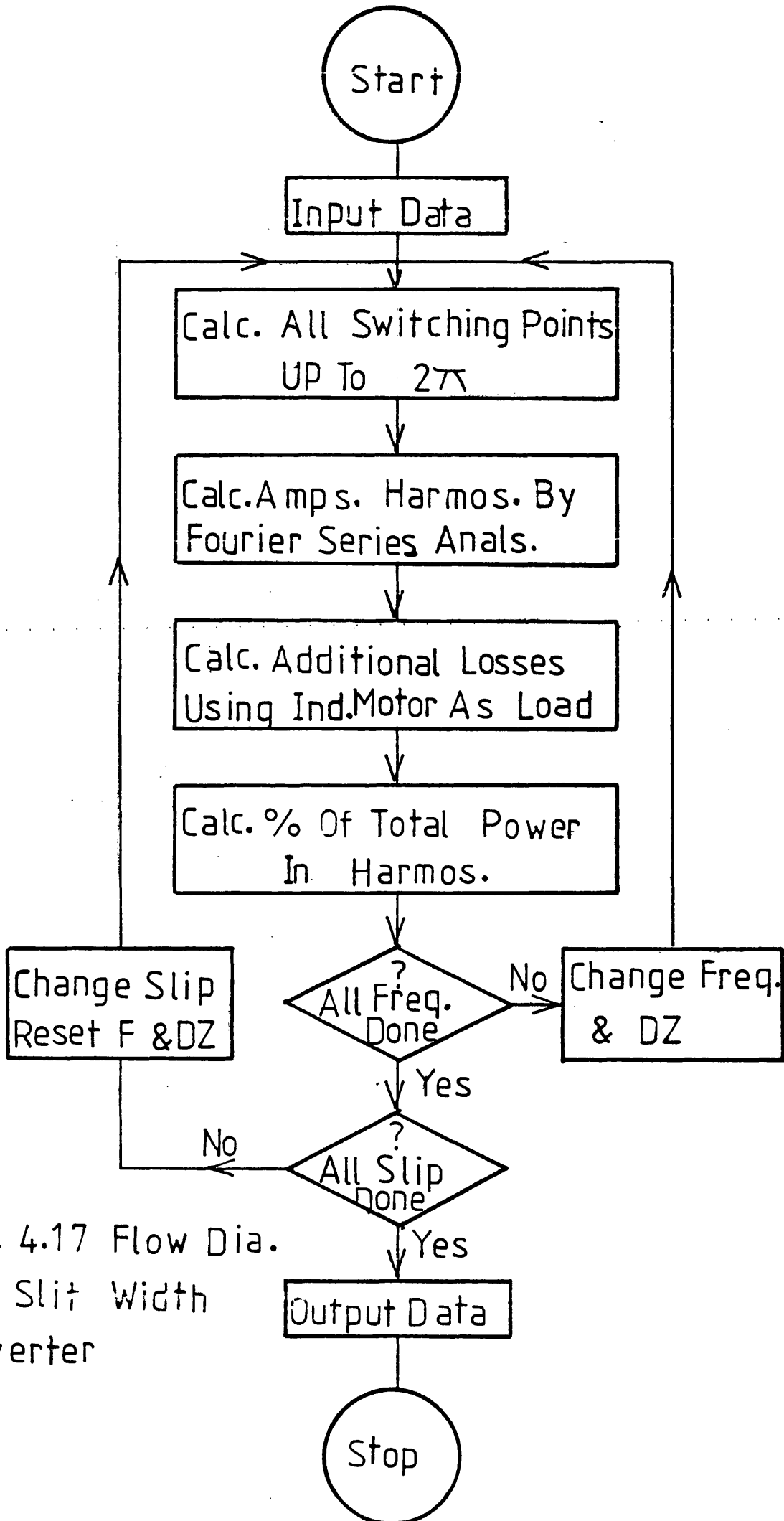


Fig. 4.17 Flow Dia.
Of Slit Width
Inverter

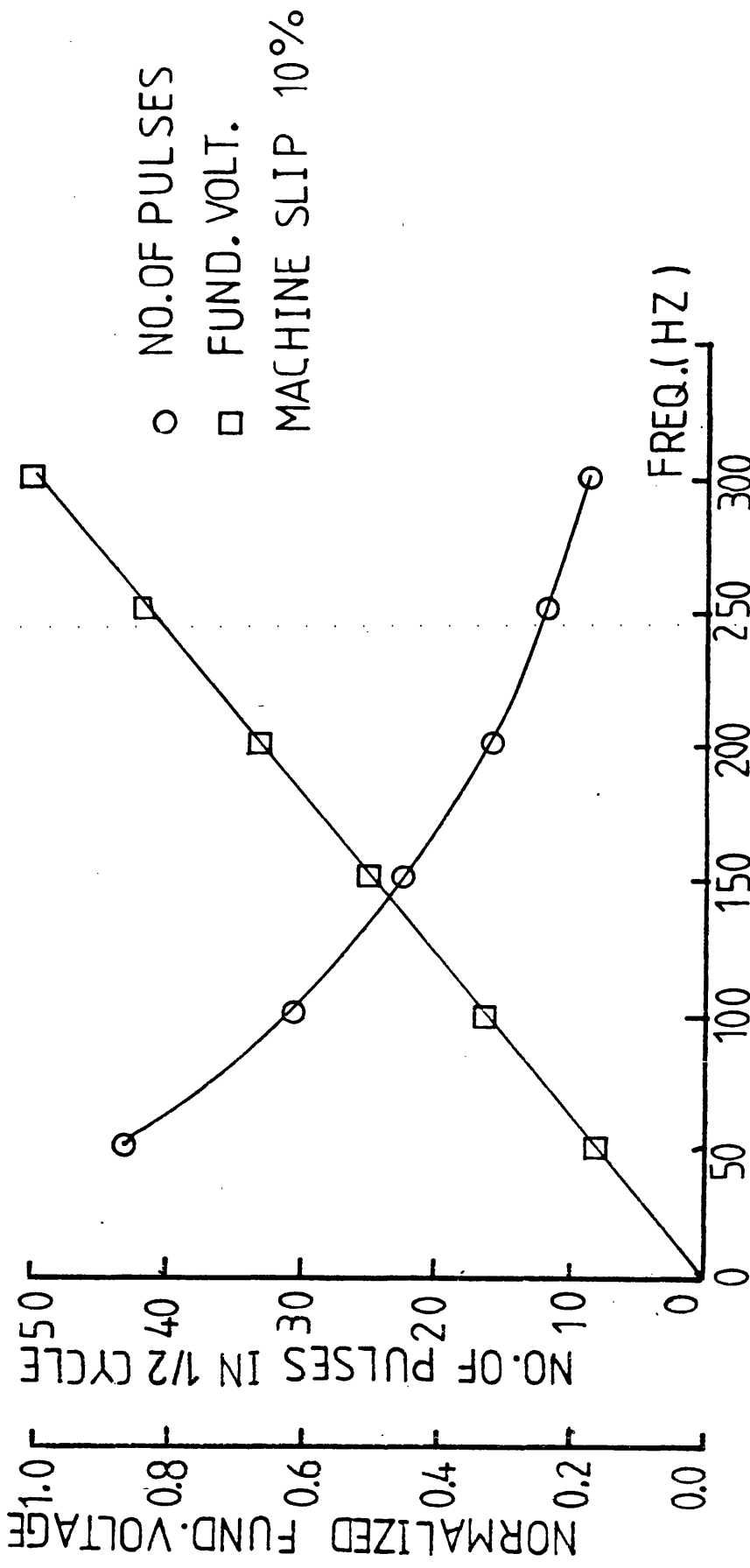


Fig.4.18 FUND. FREQ. V NO.OF PULSES IN 1/2
 CYCLE & NORMALIZED FUND. VOLTAGE
 IN V. USING SLIT WIDTH TECH.

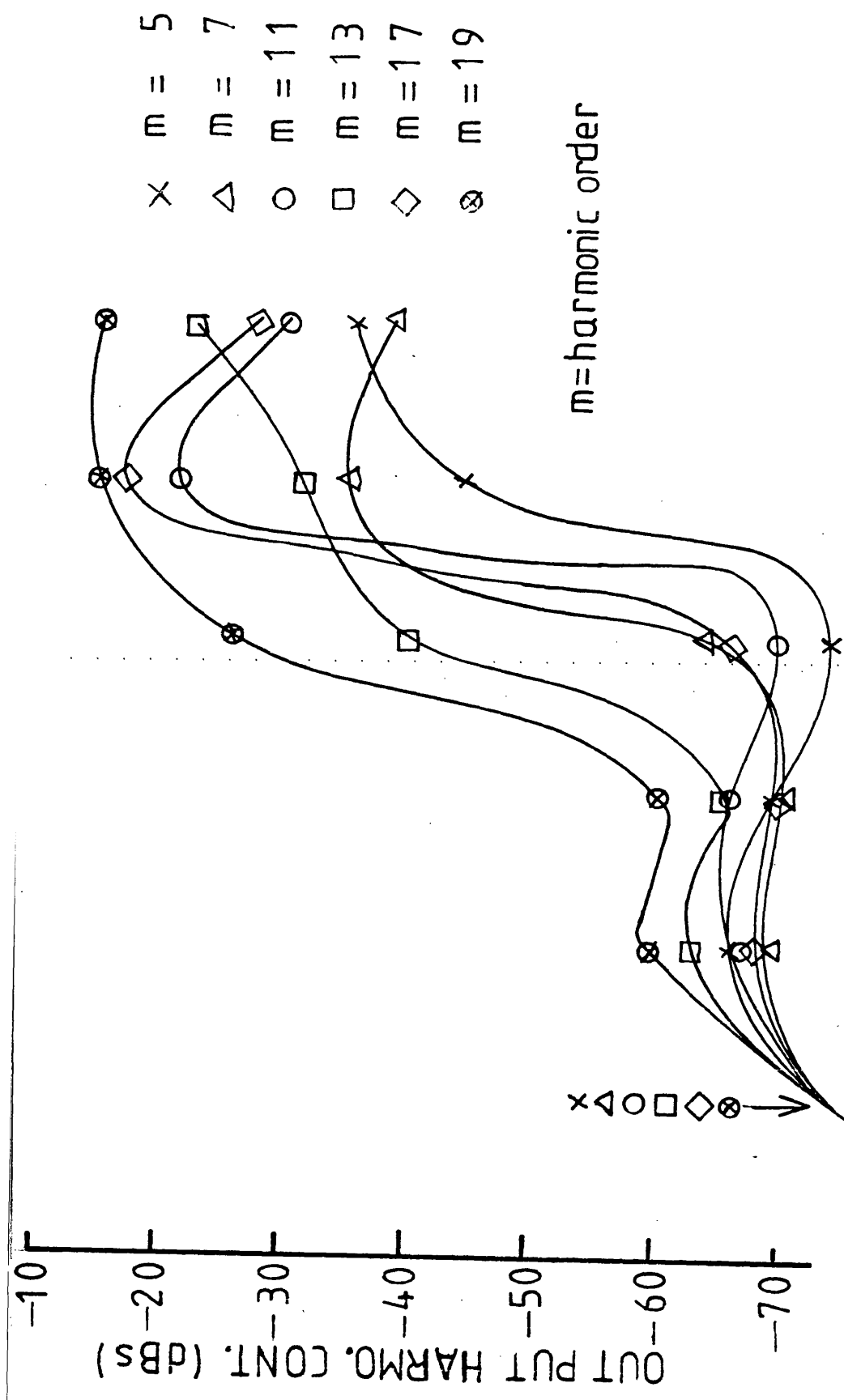


Fig. 4.19 INV. O/P FREQ. V O/P HARMO. CONT. CONT.
INV. USING SLIT WIDTH TECH.

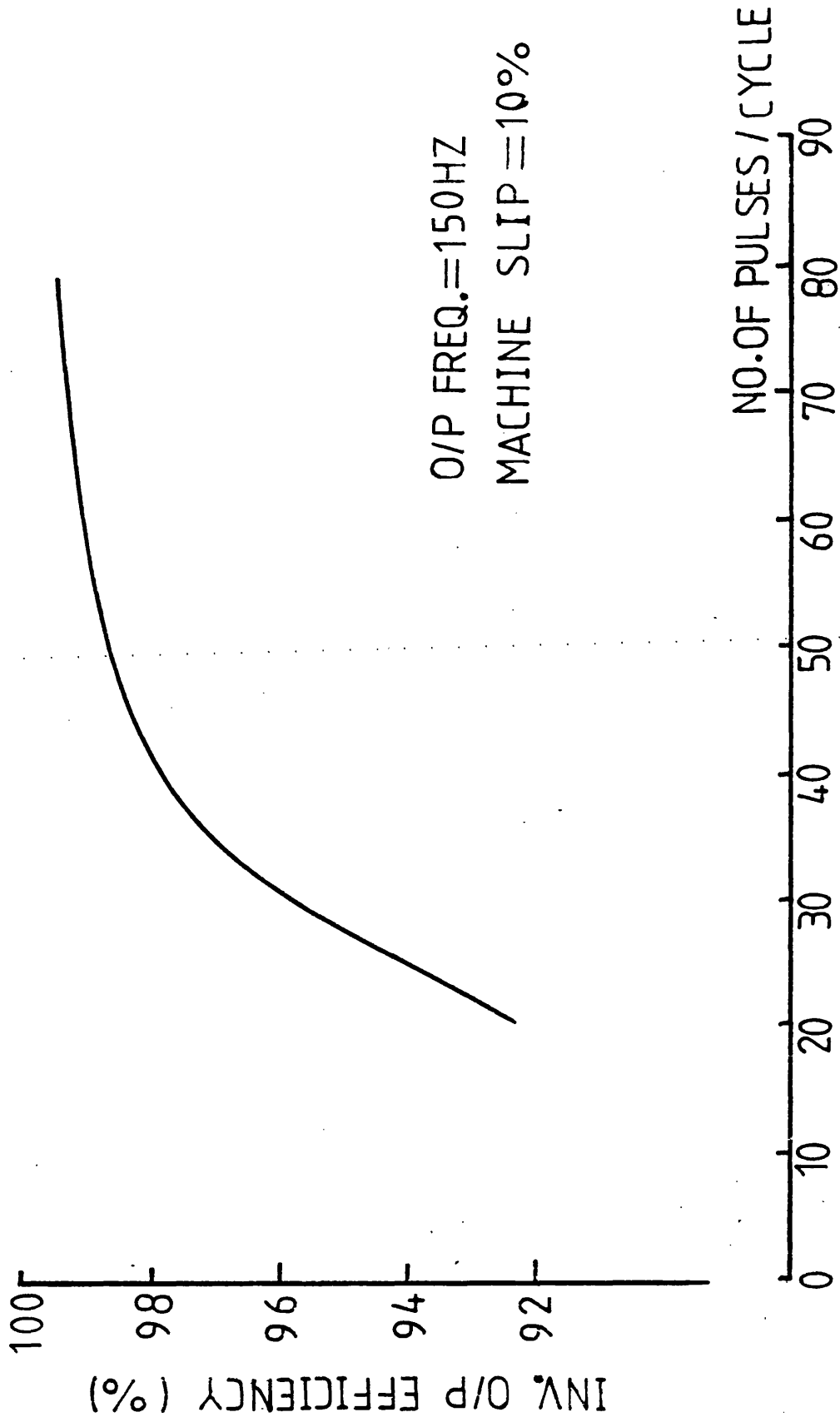


Fig. 4.20 EFFICIENCY V NO.OF PULSES PER CYCLE

INV. USING SLIT WIDTH TECH.

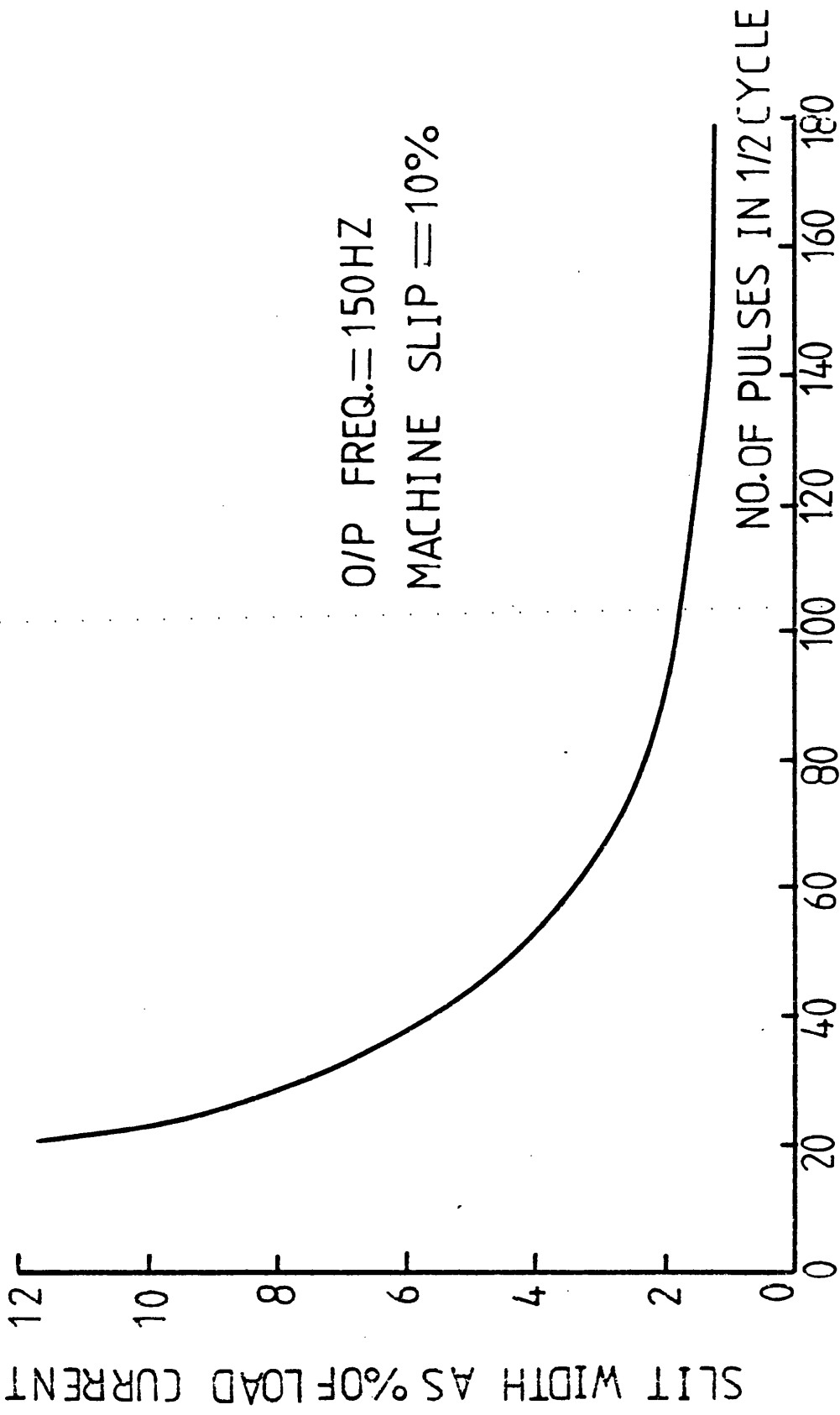


Fig. 4.21 SLIT WIDTH V NO. OF PULSES

INV. USING SLIT-WIDTH TECH.

O/P FREQ. = 150HZ

MACHINE SLIP = 100%

+ order of harmonics = 19

o " " 17

Δ " " 11,13

x " " 5,7

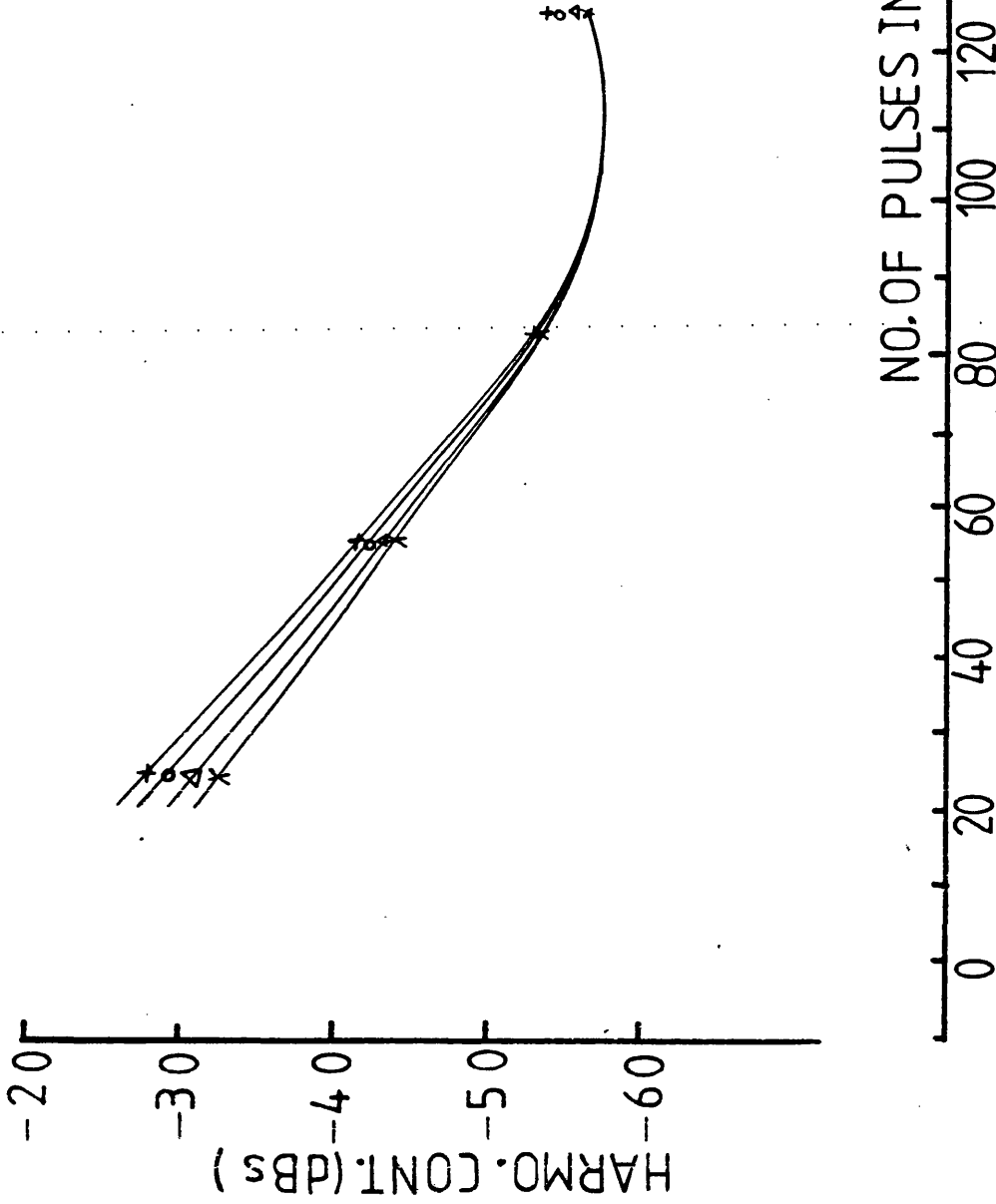


Fig. 4.22 HARMO. CONT. V NO. OF PULSES
INV. USING SLIT WIDTH TECH.

O/P FREQ =150HZ
MACHINE SLIP =10%

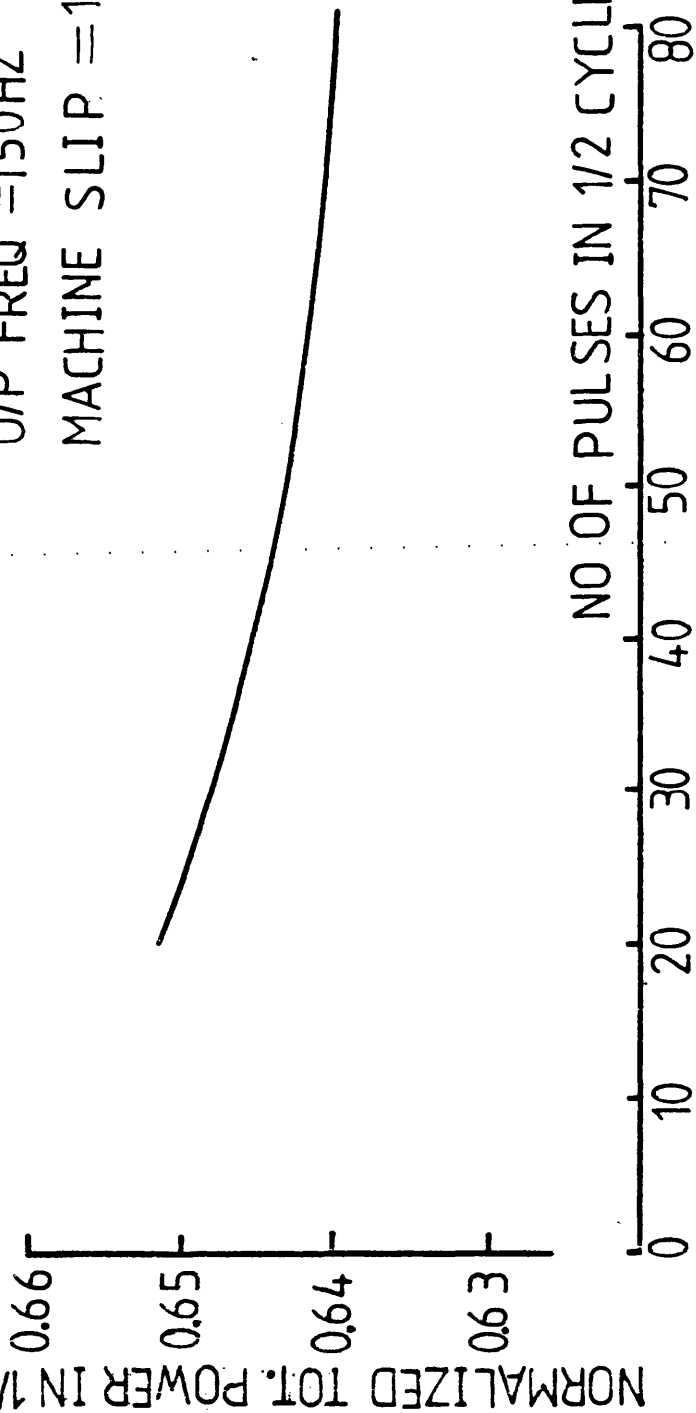


Fig. 4.23 TOTAL POWER IN PULSES OVER 1/2

CYCLE V NO.OF PULSES

INV. USING SLIT WIDTH TECH.

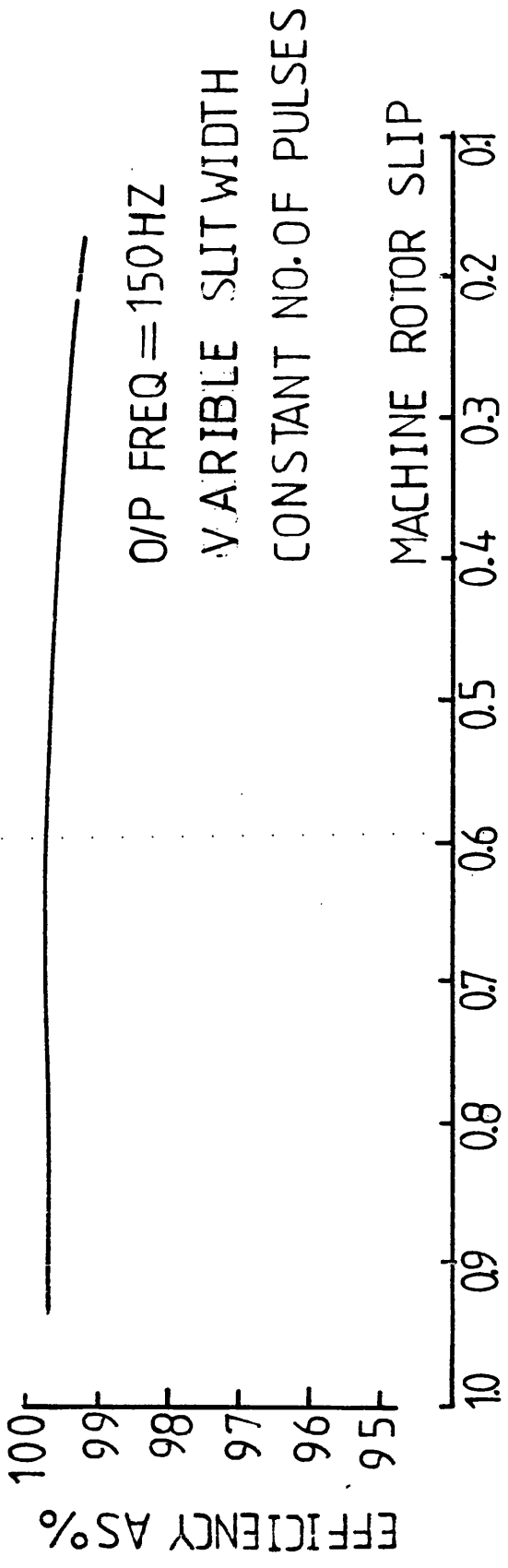


Fig. 4.24

○ FREQ. INDEP. MODEL AS LOAD

□ " " " " " "

NO OF PULSES AT a=86

b=60

c=48

d=32

e=24

f=18

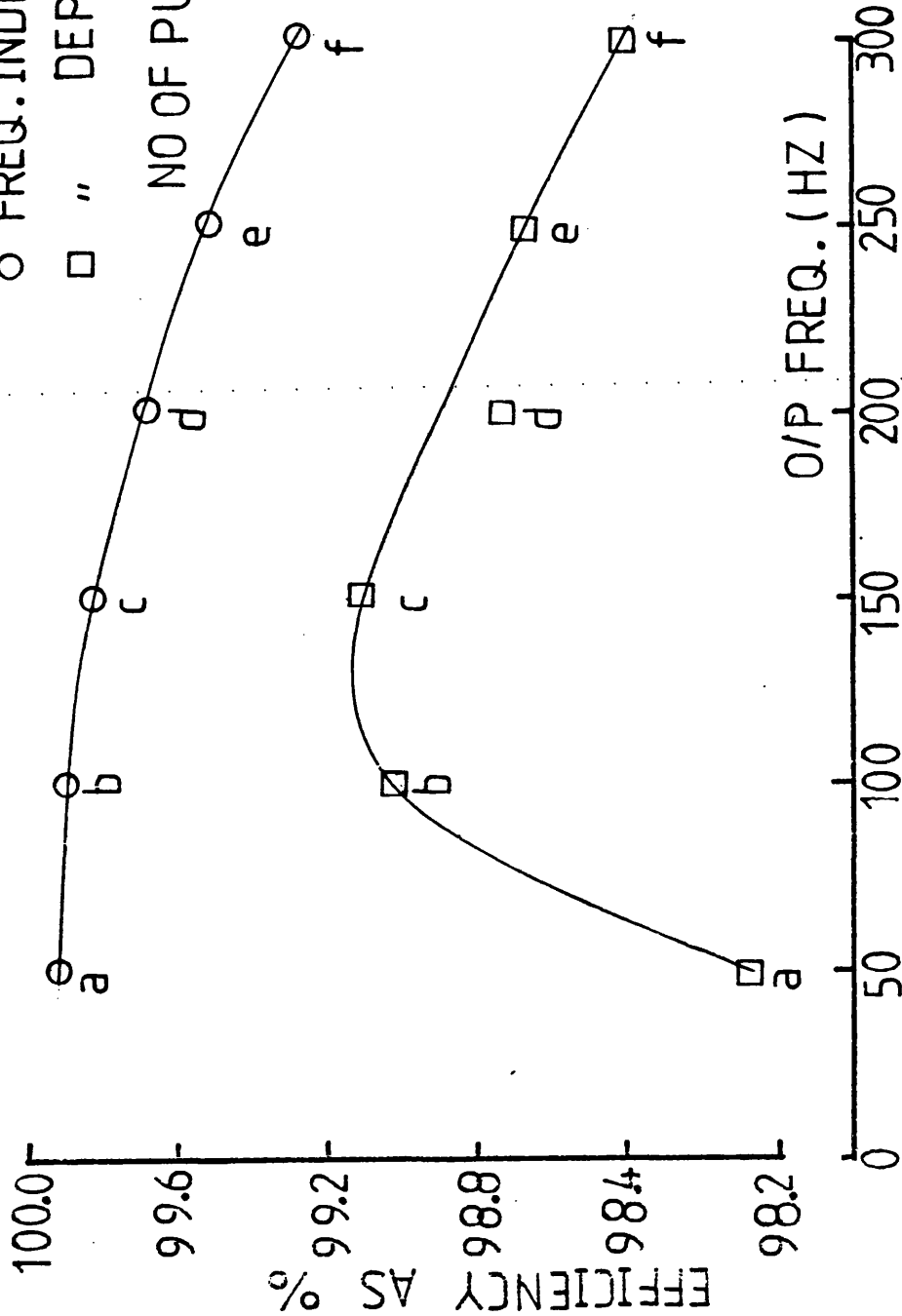


Fig. 4.25 INV. EFFICIENCY (HARM LOSSES ONLY)

V O/P FUND. FREQ.

INV. USING TRI.WAVE AS REF.

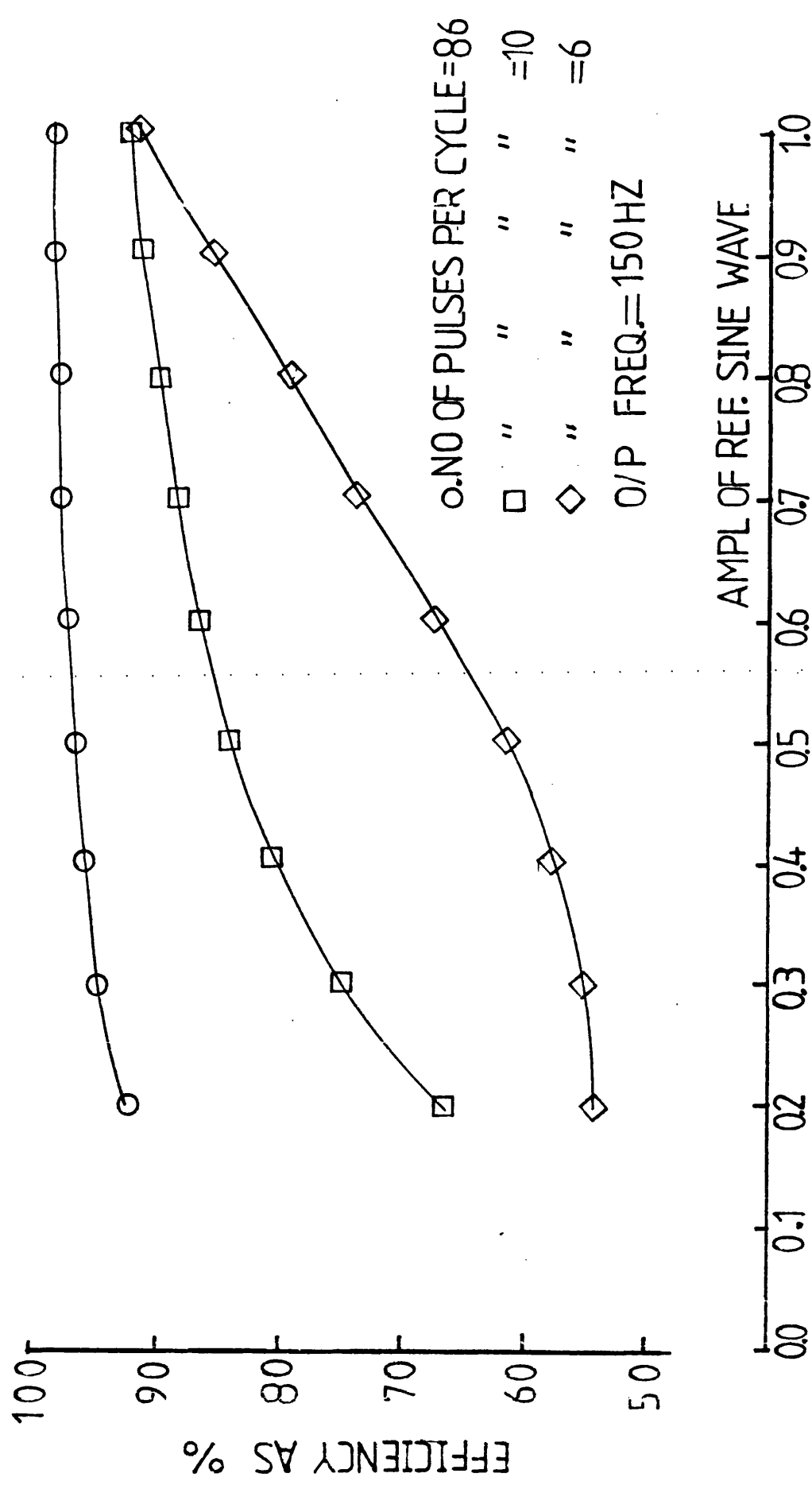


Fig. 4.26 INV. EFFICIENCY (HARM. LOSSES ONLY) V AMPL. OF REF. SINE WAVE WITH FREQ. DEPT. MODEL AS LOAD

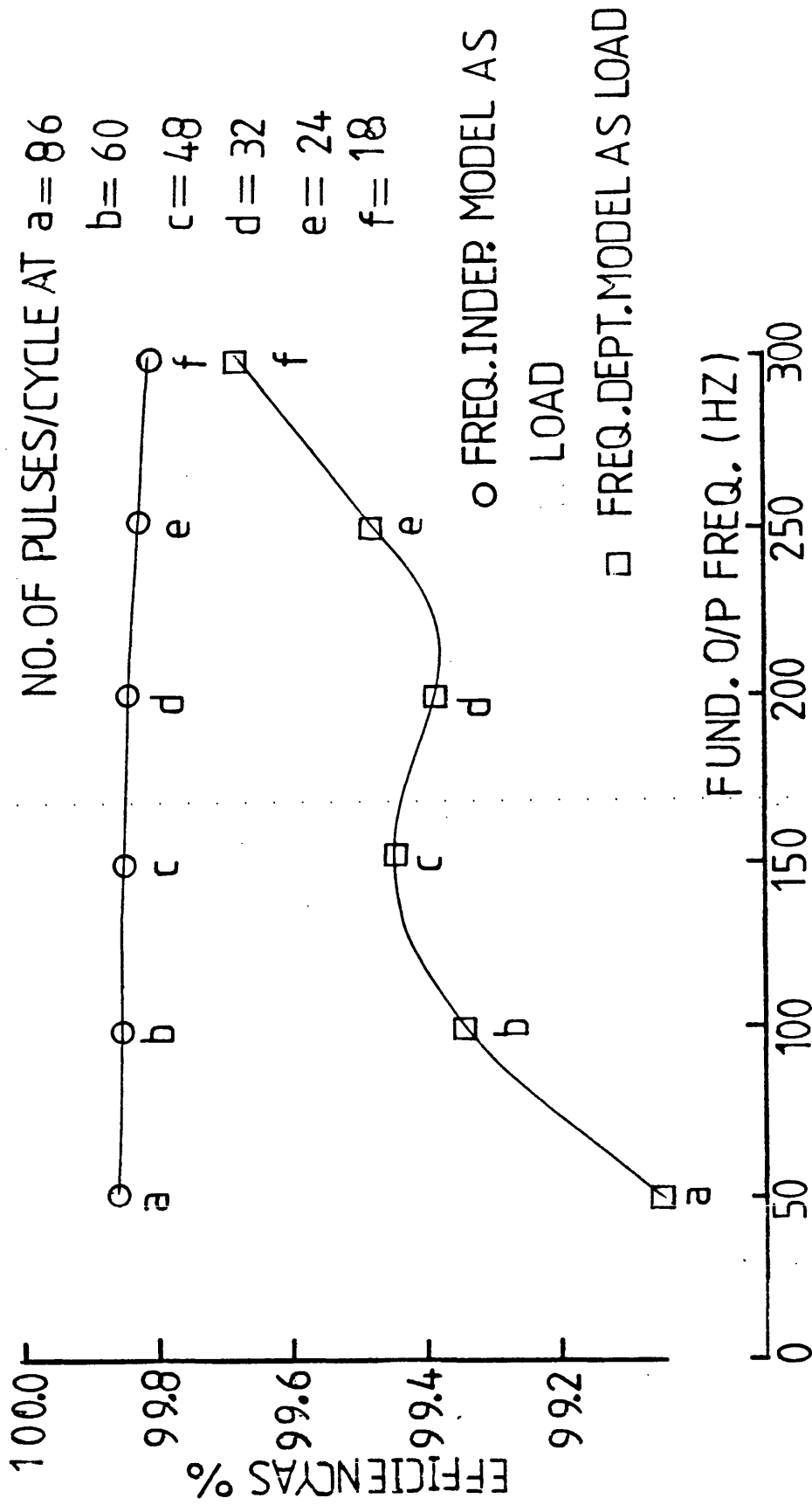


Fig. 4.27 INV. EFFICIENCY (HARM. LOSSES ONLY)

V FUND. O/P FREQ.

INV. USING SLIT WIDTH TECH.

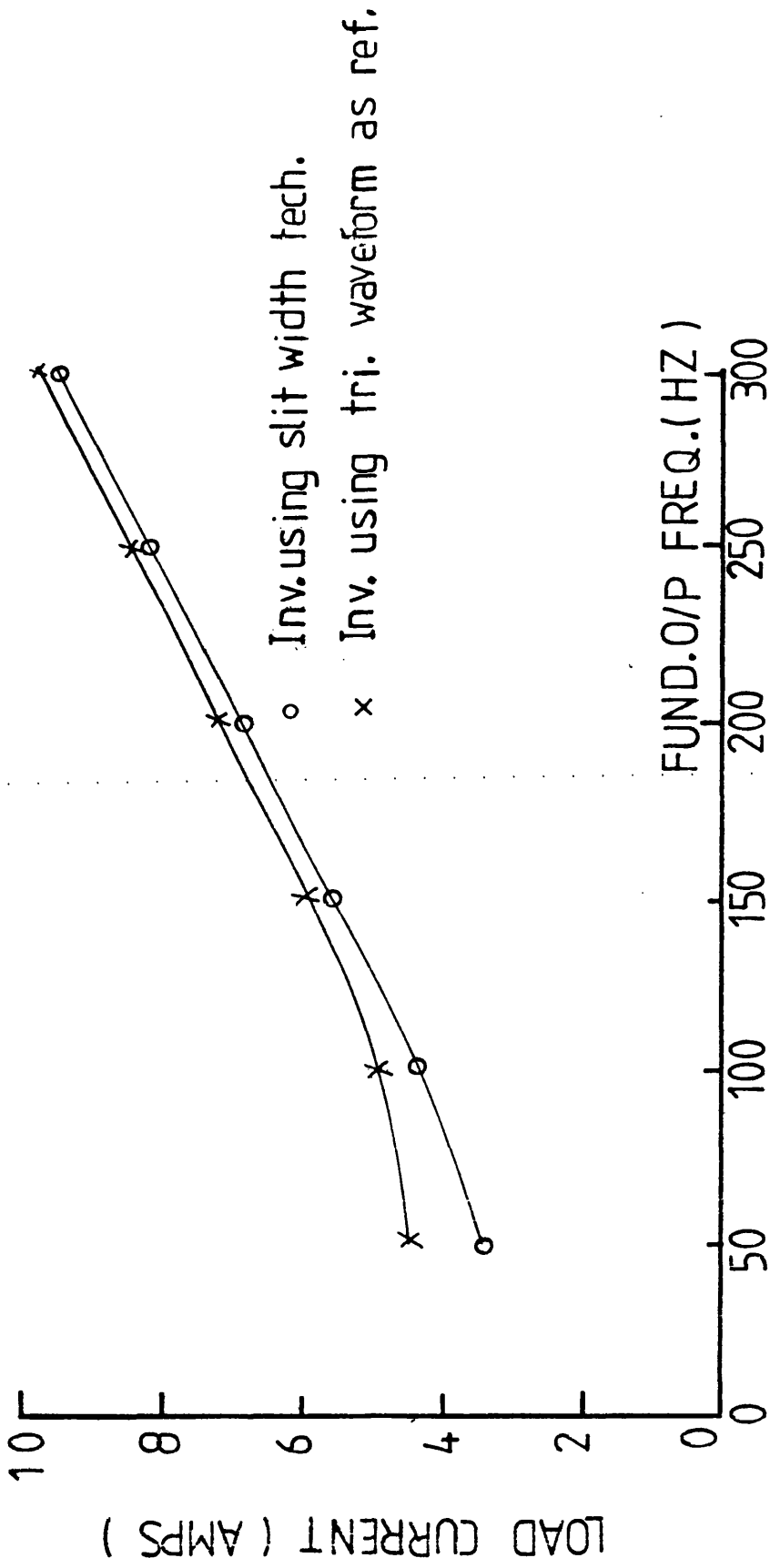


Fig. 4.28 LOAD CURRENT V FUND. O/P FREQ.
 BOTH INVERTERS DRIVING THE SAME
 LOAD

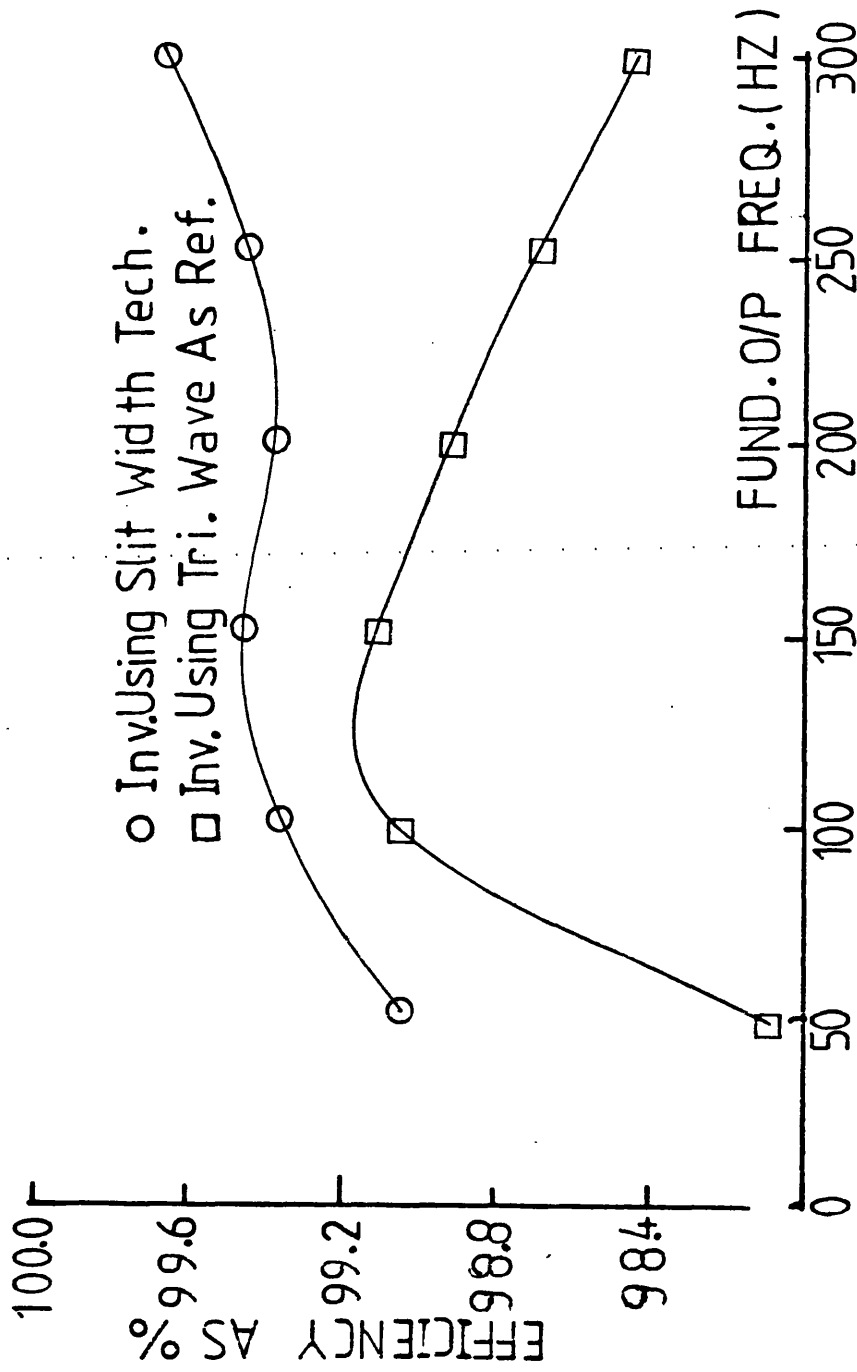


Fig. 4.29 EFFICIENCY OF BOTH TYPE OF INVERTERS

WHEN SUPPLYING THE SAME LOAD V

FUND. O/P FREQ.

Bibliography

- 4.1 MOKRYTZKI, B.: "Pulse width modulated inverters for a.c. motor drives", IEEE Trans. on Ind. Gen. App. Vol. IGA-3, No. 6, Nov/Dec 1967, pp. 493-503.
- 4.2 BOWLER, P.: "A wide band width servo amplifier", IEE Power Electronics - Power Semiconductors and their Applications, Conf. publication No. 123, Dec. 1974, pp. 122-126.
- 4.3 DANIELS, A.R. and SLATTERY, D.T.: "New power converter technique employing power transistor", Proc. IEE, Vol. 125, No. 2, February 1978, pp. 146-150.
- 4.4 TURNBULL, F.G.: "Selected harmonic reduction in static d.c.-a.c. inverters", IEEE Trans. Commun. Electronics, July 1964, pp. 374-378.
- 4.5 PATEL, H.S. and HOFT, R.G.: "Generalised techniques of harmonic elimination and voltage control in thyristor inverters, Part I - harmonic elimination", IEEE Trans. on Ind. App., Vol. 1A-9, No. 3, June 1973, pp. 310-317.
- 4.6 PATEL, H.S. and HOFT, R.G.: "Generalised techniques of harmonic elimination and voltage control in thyristor inverters, Part II - voltage control technique", IEEE Trans. on Ind. App., Vol. 1A-10, No. 5, October 1974, pp. 666-673.
- 4.7 DEWAN, S.B. and FORSYTHE, J.B.: "Harmonic analysis of a synchronized pulse-width-modulated three-phase inverters", IEEE Trans. on Ind. App., Vol. 1A-10, No. 1, February 1974, pp. 117-122.
- 4.8 MAZUR, T.: "A digital logic PWM speed control for simple and polyphase a.c. motors", Motorola Inc., Semiconductor products division, Annual Meeting of the IEEE, Ind. App. Soc., October 1973, pp. 1-9.
- 4.9 HOULDSWORTH, J.A.: "Recent developments in PWM inverter systems", IEE Discussion Paper, October 1978.
- 4.10 LIPO, T.A., KRAUSE, P.C. and JORDAN, H.E.: "Harmonic torque and speed pulsations in a rectifier-inverter induction motor drive", IEEE Trans. on Power App. and Sys., PAS Vol 88, No. 5, May 1969, pp. 579-587.

- 4.11 SCHONUNG, A. and STEMMLER, H.S.: "Static frequency changes with sub-harmonic control in conjunction with reversible variable-speed a.c. drives", The Row Boveri Review, Vol. 51, No. 89, September 1964, pp. 555-577.
- 4.12 JACOVIDES, L.J.: "Analysis of induction motor drives with a non-sinusoidal supply voltage using Fourier analysis", IEEE Trans. on Ind. App., Vol. 1A-9, No. 3, December 1973, pp. 741-747.
- 4.13 JAIN, G.C.: "The effect of voltage wave shape on the performance of a three-phase induction motor", IEEE Trans. on Power App. and Sys., PAS Vol. 84, June 1964, pp. 561-566.
- 4.14 BISSON, D.K. and DYER, R.F.: "A silicon controlled rectifier", AIEE Trans. Part I - Communication and Electronics, Vol. 78, May 1959, pp. 102-106.
- 4.15 BEDFORD, B.D. and HOFT, R.G.: "Principles of inverter circuits", (Wiley), New York, 1964.
- 4.16 ZAKHAR, Y.K. and TVERDOV, I.V.: "High power thyristor inverters for guaranteed supply systems, Telecommunications and Radio Engineer, USSR, 26, 1973, pp. 48-53.
- 4.17 CHAUPRADE, R.C.: "Inverters for uninterruptible power supplies", IEEE Trans. on Ind. App., Vol. 1A-13, No. 4, August 1977, pp. 281-292.
- 4.18 UDAYAGIRI, M.R. and SHEKHAWAT, S.S.: "A novel stepped wave thyristor inverter", IEE, Power Electronics - Power Semiconductors and their Applications, Conference Publication, No. 123, December 1974, pp. 152-159.
- 4.19 ADAMS, R.D. and FOX, R.S.: "Several modulation techniques for a pulse width modulated inverter", IEEE Trans. on Ind. App., Vol. 1A-8, No. 5, October 1972, pp. 636-643.
- 4.20 LIPO, T.A. and TURNBULL, F.G.: "Analysis and comparison of two types of square-wave inverter drives", IEEE Trans. on Ind. App., Vol. 1A-11, No. 2, April 1975, pp. 137-147.
- 4.21 BERG, G.J. and DAS, P.K.: "A new three-phase static variable frequency charger", IEEE Trans. on Ind. App., Vol. 1A-10, No. 5, October 1973, pp. 607-611.

- 4.22 LIPO, T.A. and KRAUSE, P.C.: "Stability analysis of a rectifier-inverter induction motor drive", IEEE Trans. on Ind. App., PAS Vol. 88, No. 1, January 1969, pp. 55-56.
- 4.23 KRAUSE, P.C. and LIPO, T.A.: "Analysis and simplified representation of a rectifier-inverter induction motor drive", IEEE Trans. on Power App. and Sys., PAS Vol. 88, May 1969, pp. 588-596.
- 4.24 SAWAKI, N. and SATO, N.: "Steady-state and stability analysis of induction motor driven by current source inverter", IEEE Trans. on Ind. App., Vol. 1A-13, No. 3, June 1977, pp. 244-253.
- 4.25 AKSEL, A. and SMITH, I.R.: "A delta-sigma modulated speed-control system for induction motors", 12th Universities Power Engineering Conference Proc., April 1977, pp. I-A1.3/1-6.
- 4.26 McMURRAY, W. and SHATTUCK, D.P.: "A silicon-controlled inverter with improved commutation", AIEE, November 1961, pp. 531-542.
- 4.27 THORBORG, K.: "A three-phase inverter with reactive power control", IEEE Trans. on Ind. App., Vol. 1A-9, No. 4, August 1973, pp. 473-481.
- 4.28 MARUHASHI, T.: "Series inverters without external gate triggering circuits", Elec. Eng. in Japan, Vol. 91, No. 1, 1971, pp. 156-164.
- 4.29 KUME, T. and HOFT, R.G.: "Thyristor d.c. switch inverter", IEEE Trans. on Ind. App., Vol. 1A-8, No. 3, June 1972, pp. 257-268.
- 4.30 HUNG HO, H.: "A new and simple three-phase thyristor inverter for variable frequency operation", IEEE Trans. on Ind. App., Vol. 1A-10, No. 6, December 1974, pp. 787-792.
- 4.31 NELSON, R.H. and RADOMSKI, T.A.: "Design methods for current source inverter/induction motor drive systems", IEEE Trans. on Ind. Elec. and Cont. Ins., Vol. IEZ1-22, No. 2, May 1975, pp. 141-145.
- 4.32 PHILLIPS, K.P.: "Current source converter for a.c. motor drives", IEEE Trans. on Ind. App., Vol. 1A-8, No. 6, December 1972, pp. 679-683.

- 4.33 BRADLEY, D.A., CLARKE, C.D., DAVIS, R.M. and JONES, D.A.: "Adjustable frequency inverters and their applications to variable speed drives", Proc. IEE, Vol. 111, No. 11, November 1964, pp. 1833-1846.
- 4.34 FORSYTHE, J.B. and DEWAN, S.B.: "Output regulation with PWM inverter-induction motor drives", IEEE Trans. on Ind. App. Vol. 1A-11, No. 5, October 1975, pp. 517-525.
- 4.35 POLLACK, J.J.: "Advanced pulse width modulated techniques", IEEE Trans. on Ind. App., Vol. 1A-8, No. 2, April 1972, pp. 145-154.
- 4.36 PEDERSEN, N.P.: "Pulse width modulated inverters in man-made fibre industries", IEEE Trans. on Ind. App., Vol. 1A-10, No. 1, February 1974, pp. 128-130.
- 4.37 BOWES, S.R. and BIRD, B.M.: "Novel approach to the analysis and synthesis of modulation processes in power converters", Proc. IEE, Vol. 122, No. 5, May 1975, pp. 507-513.
- 4.38 BEDFORD, B.D. and HOFT, R.G.: "Principles of inverter circuits", (Wiley), New York, 1964.
- 4.39 PATEL, H.S. and HOFT, R.G.: "Generalised techniques of harmonic elimination and voltage control in thyristor inverters, Part I - harmonic elimination", IEEE Trans. on Ind. App., Vol. 1A-9, No. 3, June 1973, pp. 310-317.
- 4.40 GIUSEPPE, B.S.: "Optimal pulse width modulation for feeding a.c. motors", IEEE Trans. on Ind. App., Vol. 1A-13, No. 1, January 1977, pp. 38-44.
- 4.41 SHERLOCK, J.: "An inverter system with elimination of low order harmonics", 12th Universities Power Engineering Conference Proc., April 1977, pp. V-A5.6/1-6.
- 4.42 BLACK, H.S.: "Modulation theory", (Van Nostrand), New York, 1953, pp. 266-276.
- 4.43 SAWAI, Z., HARASHIMA, F. and KAYA, K.: "Analysis of induction motors driven by multiphase and multiple-pulse inverters", Elec. Eng. in Japan, Vol. 90, No. 6, 1970, pp. 196-205, translated from D.G. Zasshi, Vol. 90, No. 12, December 1970, pp. 2523-2531.

- 4.44 CORNELL, E.P.: "Modelling and design of controlled current induction motor drive systems", IEEE Trans. on Ind. App., Vol. 1A-13, No. 4, August 1977, pp. 321-330.
- 4.45 DE CARLI, A., MURGO, M. and RUBERTI, A.: "Speed control of induction motors by frequency variation", Istituto Di Electrotecnica Dell 'Universita' Roma, Italy, Section 4, Paper 4C, June 1966, pp. 4C.1-4C.11.
- 4.46 KRAUSE, P.C. and WOLOSZYK, L.T.: "Comparison of computer and test results of a static a.c. drive system", Conf. Proc. record of 2nd Ind. and Gen. App. Group, Pittsburgh, October 1967, pp. 455-462.
- 4.47 JORDAN, H.E.: "Analysis of induction machines in dynamic systems", IEEE Trans. on Power App. and Sys., PAS Vol. 84, No. 11, November 1965, pp. 1080-1088.
- 4.48 KRAUSE, P.C. and THOMAS, C.H.: "Simulation of symmetrical induction machinery", IEEE Trans. on Power App. and Sys., PAS Vol. 84, No. 11, November 1965, pp. 1038-1065.
- 4.49 MOKRYTZKI, B.: "The controlled slip static inverter drive", IEEE Trans. on Ind. and Gen. App., Vol. IGA-4, No. 3, May 1968, pp. 312-317.
- 4.50 VERHOEF, A.: "Basic forced-commutated inverters and their characteristics", IEEE Trans. on Ind. App., Vol. 1A-9, No. 5, October 1973, pp. 601-606.
- 4.51 BOWLER, P. and CHAN, T.Y.K.: "An efficient high frequency inverter for a.c. drives", IEE Power Electronics - Power Semiconductors and their Applications Conference Publications, No. 123, December 1974, pp. 127-132.
- 4.52 HANSEN, A. and HAVEMANN, H.: "Analysis of a forced commutated inverter and comparison with other inverters", Conf. Proc., 12th Universities Power Engineering Conference, April 1977, pp. III-A3.7.
- 4.53 NEHRIR, M.H.: "Speed control of three-phase induction motor by stator voltage control", IEEE Trans. on Ind. Elec. and Cont. Ins., Vol. IECl-22, No. 2, May 1975, pp. 127-175.
- 4.54 ABBONDANTI, A. and WOOD, P.: "A criterion performance comparison between high power, power inverter circuits", IEEE Trans. on Ind. App., Vol. 1A-13, No. 2, April 1977, pp. 154-160.

- 4.55 CRAF, C E, SKOGSHOLM, E.A. and VOLKMANN, W.K.:
"Practical design consideration for inverter drives", IEEE Trans. on Ind. App., Vol. 1A-9, No. 5, October 1973, pp. 593-600.
- 4.56 STENGEL, R.F.: "SCR inverter survives mis-commutation", Design News, 1973, pp. OEM.4-9-73/69.
- 4.57 AGARWAL, P.D.: "The GM high-performance induction motor drive system", IEEE Trans. on Power App. and Sys., PAS Vol. 88, No. 29, February 1969, pp. 86-93.
- 4.58 JOHNSTON, R.W.: "Modulating inverter system for variable speed induction motor drive (GM electrovair II)", IEEE Trans. on Power App. and Sys., PAS Vol. 88, No. 2, February 1969, pp. 81-85.
- 4.59 LARGIADER, H.: "Design aspects of induction motors for traction applications with supply through static frequency changes", Brown Boveri Rev. 4, 1970; pp. 152-167.
- 4.60 MURPHY, G.J.: "The design and development of a van with a.c. electric drive", Proc. 2nd International Electric Vehicle Symposium, Atlantic City, November 1971.
- 4.61 BETKE, A.C.: "Special-purpose a.c. converter systems for constant horsepower applications", IEEE Trans. on Ind. App., Vol. 1A-8, No. 2, April 1972, pp. 126-135.
- 4.62 MURPHY, G.J.: "Consideration in the design of drive systems for on-the-road electric vehicle", Proc. of IEEE, Vol. 60, No. 12, December 1972, pp. 1519-1533.
- 4.63 WAKEFIELD, E.H.: "An a.c. electric vehicle", IEEE Trans. on Ind. App., Vol. 1A-10, No. 5, October 1974, pp. 544-552.
- 4.64 PLUNKETT, A.B. and PLETTE, D.L.: "Inverter-induction motor drive for transit cars", IEEE Trans. on Ind. App., Vol. 1A-13, No. 1, February 1977, pp. 26-36.

CHAPTER 5

5.1 Conclusions

It has been shown that the frequency-dependent equivalent circuits of the induction motors can be constructed from simple test results. All the changes in the equivalent circuit parameters at different supply frequencies can therefore be related to the output performance characteristics.

In applications with limited speed range requirements the effect of the parameter changes with frequency are negligible and need not be included in the performance equations. However, when the changes in the speed range requirements are from standstill to well outside the design frequency, serious errors, especially in the starting data, would result if the parameter variations were neglected.

The control circuitry required for precise control of the shaft torque must also be related to these parameter variations. This can be achieved by determining the control requirements directly from the frequency dependent equivalent circuit of the machine.

The non-linearities of the machine operating above the rated applied volts-per-hertz are mainly due to the saturation of the machine yoke. This results in a reduction in the output torque, particularly at low values of motor slip and at high supply frequencies.

In the linear operating region the machine equivalent circuit parameters behave in the same manner for both the supply and modulation frequencies. The impedance seen across the machine input terminals by the modulation frequency can therefore be determined directly from the frequency dependent equivalent circuit.

The changes in the machine impedance have a significant effect on the additional harmonic losses due to switching frequencies. The exact value of these additional losses can therefore be determined and used to calculate the efficiency of the system.

The PWM modulation technique which forces the load current to follow the reference sine wave signal within given boundary limits, produces less harmonic content compared with the other techniques operating under the same conditions. This kind of modulation technique should be considered for applications where the overall efficiency of the inverter system feeding induction motors is the important factor.

5.2 Suggestions for Further Work

The application of the microprocessor in control systems in industry has increased considerably in the passed few years. Now it is economically viable to consider the facilities offered by this device for the design and construction of efficient inverter systems. For applications with wide speed range requirements the machine characteristic can be programmed into a PROM so

that the processor unit can determine the modulation pulses according to the required data.

The post determined (slit width) modulation technique generally forces the load current to follow the reference signal in a given band. The width of this band is constant irrespective of the amplitude of the load current. This results in a reduction in the modulation frequency at lower values of the load current for a given fundamental frequency and therefore increases the output harmonic content. Using the microprocessor facilities, the width of the boundary limits can also be related to the load current which can produce a constant number of pulses over a cycle, irrespective of the load current changes. Therefore application of the microprocessor technology can increase the efficiency of the inverter systems considerably.

APPENDIX A

A.1 Part One

A.1.1 Checking the Meter Readings at Different Frequencies

The changes in the resistive part of the machine impedance with the locked rotor for frequency ranges of 50 Hz to 400 Hz are about one ohm. To make sure that this increase in resistance is only due to some changes in the machine parameters, the following method is used to check whether there are any constant or frequency dependent errors in the obtained results.

Consider the two-wattmeter method; this is the commonest method of measuring three-phase power; it is particularly useful when the load is unbalanced. The connections for the measurements of power in the case of a star connected three-phase load are shown in figure A(1).

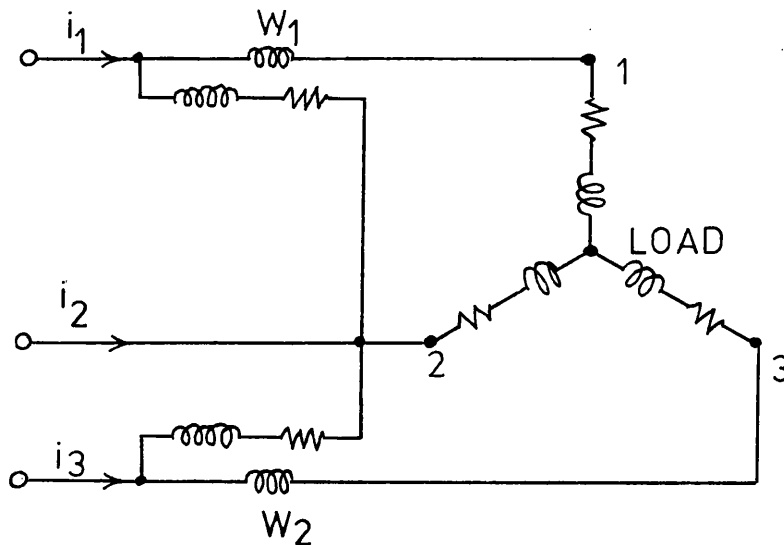


Figure A(1) Two-Wattmeter Method of Measuring Three-Phase Power

The current coils of the wattmeters are connected in lines (1) and (3), and their two pressure coils between lines (1) and (2) and (3) and (2) respectively.

Figure A(2) gives the vector diagram for the load circuit, assuming a balanced load, ie. the load current and power factors are the same for all three phases.

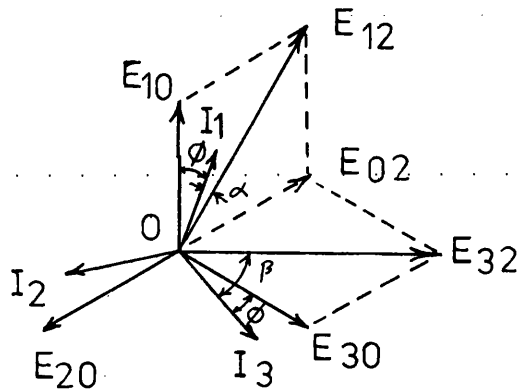


Figure A(2) Vector Diagram of the Two-Wattmeter Method

E_{10} , E_{20} and E_{30} are the vectors representing the phase voltages and are supposed to be equal, while I_1 , I_2 and I_3 are vectors representing the line currents. The voltages applied to the pressure coil circuits of the wattmeters are E_{12} and E_{32} , which are the vector sum of the phase voltages as shown. Then, total instantaneous power in the load

$$= e_1 i_1 + e_2 i_2 + e_3 i_3 \quad \text{--- (A.1.1)}$$

where e_1 , e_2 and e_3 are the instantaneous phase voltages and i_1 , i_2 and i_3 are the instantaneous line currents.

Since:

$$i_1 + i_2 + i_3 = 0$$

$$i_2 = -i_1 - i_3 \quad \text{--- (A.1.2)}$$

Therefore total instantaneous power

$$= e_1 i_1 + e_2 (-i_1 - i_3) + e_3 i_3$$

$$= i_1 (e_1 - e_2) + i_3 (e_3 - e_2) \quad \text{--- (A.1.3)}$$

Now, $i_1 (e_1 - e_2)$ is the instantaneous power deflecting wattmeter W_1 and $i_3 (e_3 - e_2)$ is the deflecting wattmeter W_3 . These wattmeters measure $I_1 E_{12} \cos \alpha$ and $I_3 E_{32} \cos \beta$ respectively. Where α and β are the phase angles between I_1 and E_{12} and between I_3 and E_{32} . The sum of the wattmeter readings thus gives the mean value of the total power in the load.

Now $\alpha = 30 - \phi$

and $\beta = 30 + \phi$

also $E_{12} = E_{32} = 3E$

where E is the phase voltage.

Therefore, the sum of the wattmeter readings

$$W = 3IE \cos(30 + \phi) + 3IE \cos(30 - \phi)$$

since $I_1 = I_2 = I_3 = I$

$$W = 3IE \cos(30 + \phi) + \cos(30 - \phi)$$

$$= 3IE(2\cos 30 \cos \phi)$$

Therefore $W_1 + W_2 = 3IE \cos \phi$ --- (A.1.4)

Similarly $W_1 - W_2 = 3IE \sin \phi$ --- (A.1.5)

Since wattmeters are very expensive and accurate instruments, the possibility of obtaining any frequency dependent error is very small. So if there is any frequency dependent error in the instruments used, it would be in the voltmeter or the ammeter. Therefore, on the assumption that wattmeters do not introduce any frequency dependent errors, the other instrument readings can easily be checked by using the following relationship at any applied frequency, ie.

$$(W_1 + W_2)^2 + 3(W_1 - W_2)^2 = K_2 (3IE)^2 \quad \text{--- (A.1.6)}$$

where E and I are the line voltage and current taken by the voltmeter and ammeter, and K_2 is the value of the error introduced by any of the measuring instruments.

Therefore:

$$K_2 = \frac{(W_1 + W_2)^2 + 3(W_1 - W_2)^2}{3IE} \quad \text{--- (A.1.7)}$$

The value of K_2 remains constant and equal to 1.05 units within the operating frequency range. It suggests that there is a constant error introduced by one of the instruments, but there is no indication of frequency dependent error involved in the readings.

A.1.2 Examination of the Sensitive Phase Meter Readings

The sensitive phase meter readings for frequencies up to 10 kHz are also examined to make sure that there are not any serious errors at certain frequencies. This is done by producing the complex frequency response of a known circuit shown in figure A(3) with values of R_1 , R_2 and C , 3.2 ohms, 25 ohms and $4\mu\text{F}$ respectively.

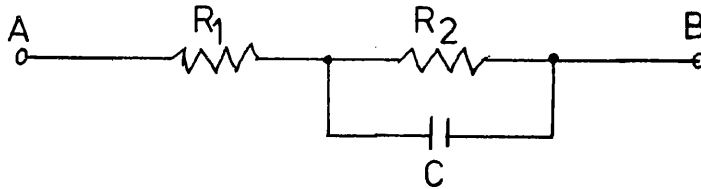


Figure A(3) Series Parallel RC Network

A similar method of measuring the voltage and phase angle across a series resistor is also employed. The complex frequency response is plotted in figure A(4). Since all the values of the input impedance up to frequencies of 10 kHz lie on the expected circular diagram shown in figure A(4), this confirms that all the readings obtained within that frequency range are well within the required accuracy.

A.2 Part Two

A.2.1 Determination of the Rated Applied Volts-Per-Hertz

The rated line to line voltage is normally the maximum value of the voltage just before the machine goes into the saturation region. The value of this would occur at the knee point of the open circuit characteristic curve of the line voltage versus line current.

To obtain the various open circuit values of line voltage and current, the rotor speed is kept at synchronism by means of another d.c. machine. While the rotor is running at synchronous speed, the values of the line voltages and their corresponding line currents are plotted in figure A(5). This open circuit characteristic of the machine shows that saturation occurs at a line voltage of 61 volts. Since this open circuit characteristic is obtained with the supply frequency of 50 Hz, line voltage should be kept at 1.22 V/Hz for the constant flux operation at any supply frequency.

A.2.2 Calculations of the Equivalent Circuit Parameters

Consider the per-phase induction motor equivalent circuit shown in figure A(5a).

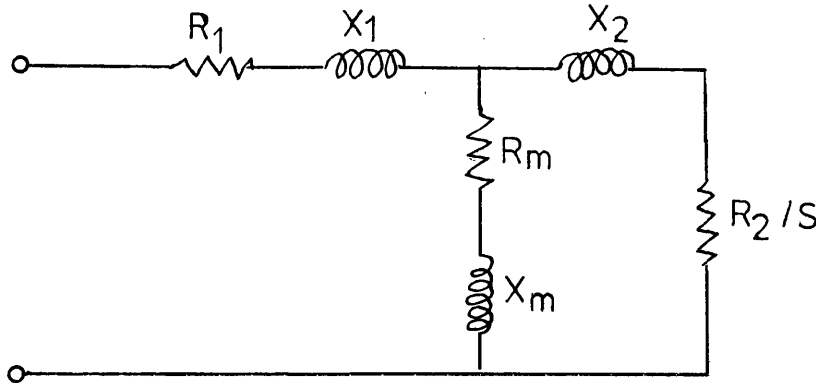


Figure A(5a) Per-Phase Equivalent Circuit

When the motor is running at its synchronous speed the value of secondary resistance R_2/S becomes almost infinity. Since there is no current flowing in the secondary circuit, the total input power must be dissipated in R_1 and R_m .

ie.

$$\text{Therefore } R_1 + R_m = \frac{P_{o/c}}{(I_{o/c})^2} \quad \text{--- (A.2.1)}$$

$$Z_{o/c} = \frac{V_{o/c}}{I_{o/c}}$$

$$\begin{aligned} &= \left[(X_1 + X_m)^2 + (R_1 + R_m)^2 \right]^{\frac{1}{2}} \\ \text{hence } X_1 + X_2 &= \left[(Z_{o/c})^2 - (R_1 + R_m)^2 \right]^{\frac{1}{2}} \quad \text{--- (A.2.2)} \end{aligned}$$

and
$$R_m = \frac{P_{o/c}}{(I_{o/c})^2} - R_1 \quad \text{--- (A.2.3)}$$

Since in the locked rotor test, the value of the magnetising branch is very large compared with rotor circuit parameters, then by neglecting the magnetising branch parameters we have:

$$R_1 + R_2 = \frac{P_{s/c}}{(I_{s/c})^2}$$

$$R_2 = \frac{P_{s/c}}{(I_{s/c})^2} - R_1 \quad \text{--- (A.2.4)}$$

where the value of R_1 is usually taken to be equal to its d.c. resistance.

Similarly we have:

$$Z_{s/c} = \frac{V_{s/c}}{I_{s/c}}$$

$$= \left[(X_1 + X_2)^2 + (R_1 + R_2)^2 \right]^{\frac{1}{2}}$$

and
$$X_1 + X_2 = \left[(Z_{s/c})^2 - (R_1 + R_2)^2 \right]^{\frac{1}{2}}$$

also
$$X_m = X_{o/c} - X_1$$

X_1 and X_2 are usually taken to be equal, but the exact ratio of X_1 and X_2 can be obtained from design data. For this particular motor under the test, values of X_1 and X_2 equal 2.3 and 1.2 mH respectively. The method used for the separation of these reactances is given in Section 2.5.1.

A.3 Part Three

A.3.1 Evaluation of Equivalent RL Network from Frequency Response, Using Circle Fit Technique

Consider the circuit diagram shown in figure A(6).

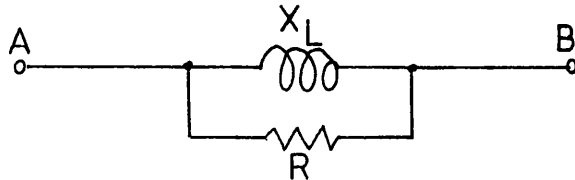


Figure A(6) Parallel RL Circuit

The impedance across terminals A and B is:

$$Z(AB) = \frac{RX_L^2}{R^2 + X_L^2} + j \frac{X_L R^2}{R^2 + X_L^2} \quad \text{--- (A.3.1)}$$

substituting X_L into $\omega \cdot L$ gives:

$$Z(AB) = \frac{R}{1 + (\frac{R}{\omega L})^2} + j \frac{\omega \cdot L}{1 + (\frac{R}{\omega L})^2} \quad \text{--- (A.3.2)}$$

The limits of this impedance as the frequency changes from zero to infinity are:

$\omega = 0$	$Z(AB) = 0$
$\omega = R/L$	$Z(AB) = \frac{R}{2}(1 + j)$
$\omega = \infty$	$Z(AB) = R$

Therefore as frequency changes from 0 to infinity the locus of $Z(AB)$ on the complex frequency plane lies on a circle whose diameter is equal to R , as shown in figure A(7).

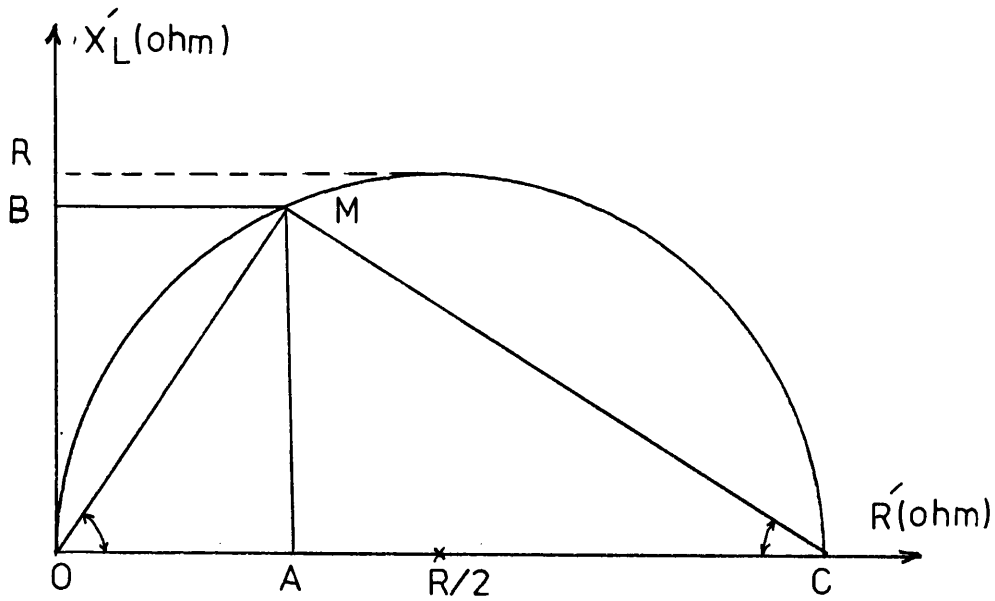


Figure A(7) Locus Diagram of Parallel RL Circuit

To determine the diameter of this circle, consider the point M in figure A(7). The real and imaginary parts of point M are OA and OB respectively.

In triangle OMA we have:

$$\cos MOA = \frac{OA}{OM} = \frac{R'}{(R'^2 + X_L'^2)^{\frac{1}{2}}} \quad \text{--- (A.3.3)}$$

where

$$R' = \frac{R}{1 + \left(\frac{R}{\omega \cdot L}\right)^2} \quad \text{and} \quad X' = \frac{\omega \cdot L}{1 + \left(\frac{\omega \cdot L}{R}\right)^2}$$

In triangle OMC we have:

$$\sin MCO = \frac{MO}{OC} \quad \text{--- (A.3.4)}$$

Substituting the value of MO and OC as diameter (d) we have:

$$\sin \text{MCO} = \frac{(X_L'^2 + R'^2)^{\frac{1}{2}}}{d} \quad \text{--- (A.3.5)}$$

But

$$\cos \text{MOA} = \sin \text{MCO} \quad \text{--- (A.3.6)}$$

Thus equating (A.3.5) and (A.3.6) and solving for d we have:

$$d = \frac{R'^2 + X_L'^2}{R'} \quad \text{--- (A.3.7)}$$

Once it is certain that the locus diagram belongs to a part of the circle, the value of the parallel resistance which is equal to the diameter of the circle can easily be found from the real and imaginary parts of the impedance at any frequency.

A.4 Part Four

A.4.1 Modulation Technique

This technique involves injecting and extracting the modulation signal into the main line current which is supplying the machine load. Since the object of this experiment is to observe the behaviour of the machine parameter with respect to modulation frequency, the effect of source impedances must be minimised. The

impedance of the main supply source seen by the modulation frequency is minimised by decoupling all the phases with very large capacitors. See figure A(8).

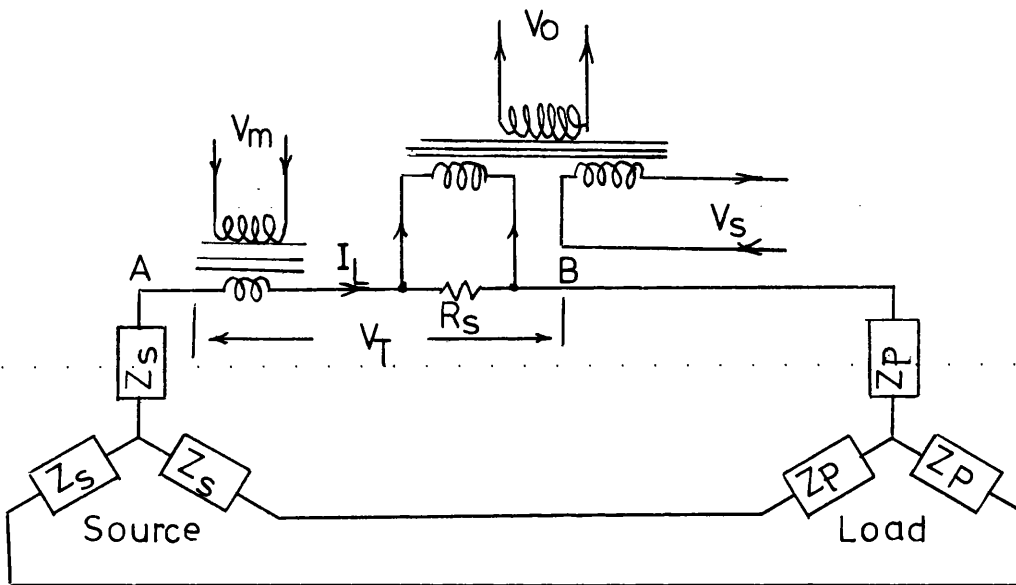


Figure A(8) Circuit Diagram of the Modulation Technique

The modulation signal is injected into the line via a transformer which has very low secondary impedance. The signal is extracted by simply inserting a small resistor in series in the same line. The voltage across this resistor is then fed into a high input impedance transformer as shown in figure A(8).

In addition, the main supply frequency is fed via a phase shifter in anti-phase into another winding of the same transformer. The phase and amplitude of this

signal is adjusted until the main supply frequency at the secondary of the transformer is cancelled out. A low pass filter at the transformer secondary output is also used to reject the possible supply frequency harmonics. The equivalent circuit of figure A(8) for modulation frequencies becomes that shown in figure A(9).

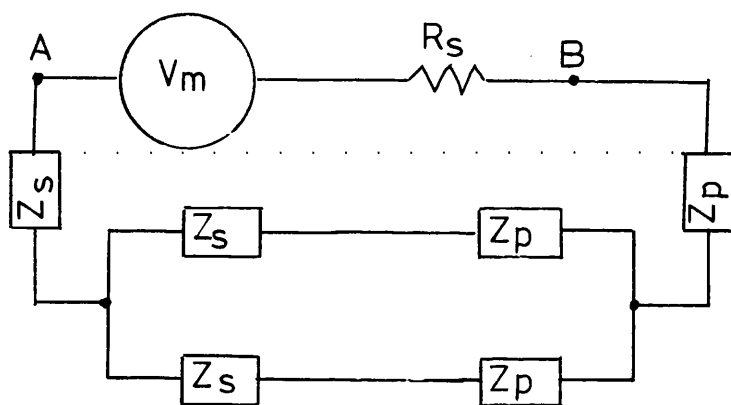


Figure A(9) Equivalent Circuit Seen by the Modulation Signal

The impedance at terminals A and B is:

$$\begin{aligned} Z(AB) &= Z_p + Z_s + \frac{1}{2}(Z_p + Z_s) \\ &= \frac{3}{2}(Z_p + Z_s) \end{aligned} \quad \text{--- (A.4.1)}$$

Thus the impedance of one of the phases of the machine is:

$$Z_p = \frac{2}{3}Z(AB) - Z_s \quad \text{--- (A.4.2)}$$

where Z_s is the impedance of the large capacitors used across the mains three phase supply.

The sensitive phase meter is used both to provide and to measure the necessary voltages and phase angles of the injected and extracted modulation signals. These results are then used to find the value of the $Z(AB)$ and hence phase impedance Z_p for modulation frequencies up to 3kHz.

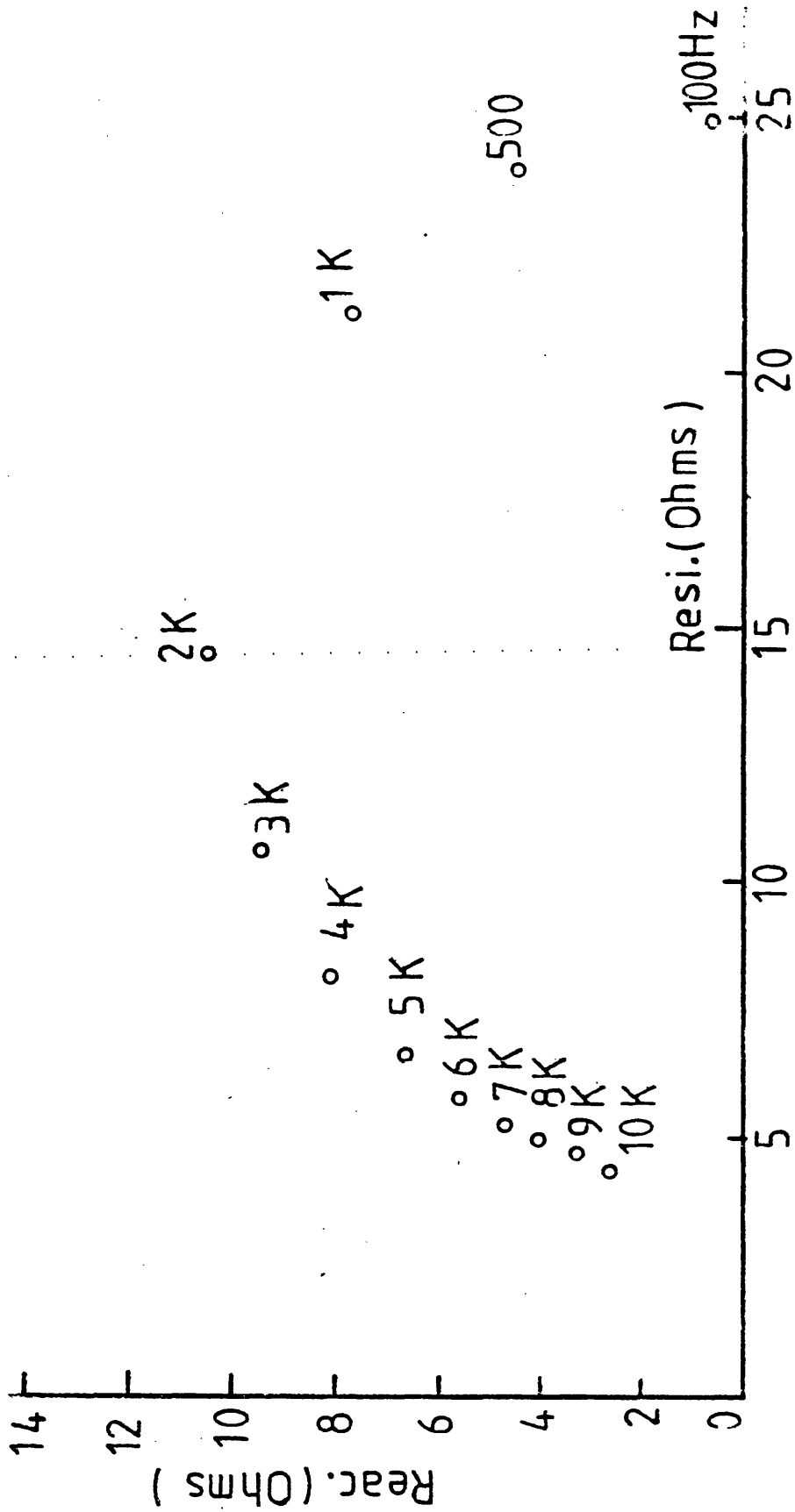


Fig.A(4) Locus Dia. of RL Network

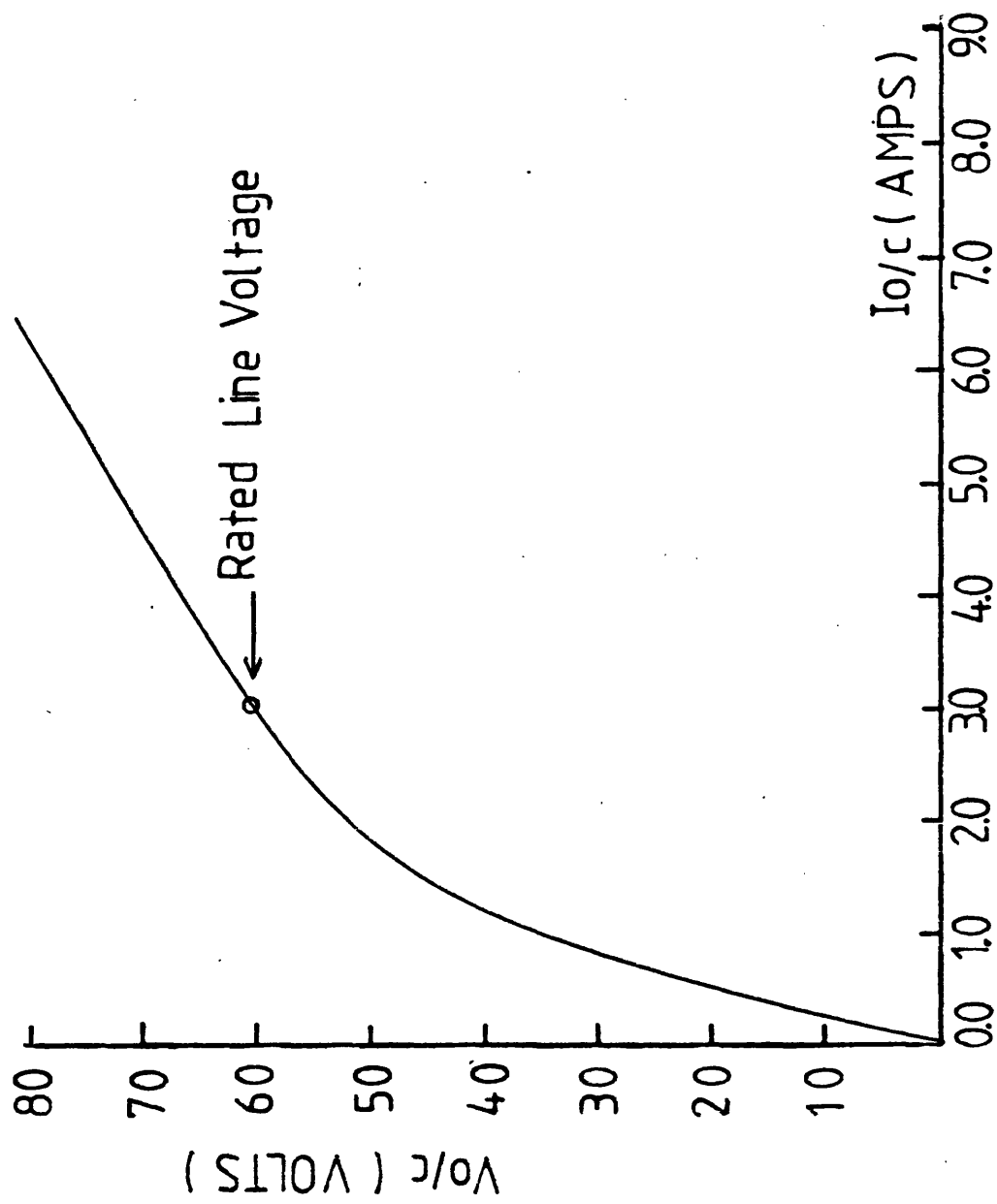


Fig.A(5) Open Circuit Char. at 50Hz

APPENDIX B

Design Details of the Inertia Machine for Plotting the Torque Speed Characteristics of High Speed Induction Motors

B.1 Introduction

To investigate the performance characteristics of this particular high speed induction machine it is necessary to obtain the torque-speed characteristics at various supply frequencies. A simple method of obtaining these characteristics is to plot the shaft torque versus the speed while the machine is accelerating a given inertia mass from zero to maximum velocity. A similar machine has already been designed and constructed by the University of Bristol for speeds of up to 10,000 r.p.m. This machine consists of a standard torque transducer type +2/4/AA using the strain gauge bridge principle, coupled to an inertia mass and an a.c. tachogenerator. The twist in the shaft due to the machine torque is then converted proportionately to d.c. volts by the transducer during the acceleration period. The a.c. tachogenerator also produces an a.c. output signal directly proportional to shaft speed, which is then converted to a d.c. signal and fed together with the transducer output to an X-Y plotter unit. This machine is modified to house the induction machine under experimentation for plotting the necessary characteristics. However due to lack of lubrication

the modified coupler seized up at 6,000 r.p.m. and consequently damaged the torque transducer. Thus it was necessary to design a better inertia machine, which not only had to be robust, but also had to be 100% safe through all speeds up to 18,000 r.p.m., the speed range of this particular machine. For the simplification of bearing design, an a.c. Electrolux commutator motor type KS 5832-100 was employed to carry the inertia disc. The Electrolux motor designed to cope with speeds of up to 20,000 r.p.m., also offers additional advantages in that it can be used as a variable load, as well as keeping the induction motor at synchronous speed if required. In addition, the machine shaft carries a slotted disc, which passes through an infra red photo cell to produce d.c. pulses proportional to shaft speed. These pulses are then converted into an analog voltage, representing the rotor speed.

The application of transducers used in the load shaft to measure the rotor torque is avoided, mainly because of the complexities involved in transducer design at such high speeds. For reasons of economy the application of load cells is not considered either. Instead the case of the main drive induction motor is supported by means of two additional bearings, such that it can rotate in either direction independent of its rotor. Then it is spring loaded such that if it is turned in any direction, it will return to its original position

as soon as it is released, as shown in figure B(1). An a.c. servo motor is also coupled to the machine case which measures degrees of rotation in either direction. The a.c. servo motor output signal is converted to d.c. voltage representing the angle rotation in analog form. The a.c. Electrolux commutator machine which carries the inertia disc is coupled to the main induction motor by special high speed couplers.

As soon as the three phase supply is switched on the case of the machine rotates through an angle proportional to the shaft torque. The angle of rotation then follows the shaft torque until the inertia disc reaches maximum speed. The analog outputs of the torque and speed transducers are then fed to (X) and (Y) inputs of an X-Y plotter, to plot the required torque speed characteristic.

B.2 Design of the Inertia Disc

In general the total deflection time of X-Y plotting units are limited within a few hundred milliseconds. Therefore the value of the second moment of inertia of the disc must be such that it produces an acceleration period at least equal or greater than the deflection period. The acceleration period of the inertia disc from zero to maximum velocity is directly proportional to the speed range, and inversely proportional to the shaft torque.

Therefore by considering the minimum value of the shaft torque and the lower speed range, the second moment of inertia of the disc is estimated. At maximum speeds the shape of the inertia disc has a very important role. This is because the frequencies of the transverse vibration and whirling speeds are directly related to the mass of the disc. Therefore the mass is kept to a minimum, without reducing the second moment of inertia, in order to achieve higher frequency margins. This is done by concentrating the mass mainly on its rim by gouging out the centre of the disc.

Because the disc is physically supported by one end of the a.c. Electrolux commutator motor, the cutting out operation is carried out from one side only and is mounted to reduce the distance from the centre of the mass to the nearest bearing. This results in an increase in the transverse vibration and whirling frequencies. Taking all the above conditions into consideration, two inertia discs, one for lower speeds and one for higher speeds are designed and constructed and are shown in figure B(2).

B.3 Transverse Vibrations and Whirling Speeds

However carefully a shaft may be balanced and assembled, some out of balance forces due to rotation must be present. In rotation, the associated centripetal action is supplied by the elastic resistance of the shaft, which must therefore have lateral deflection.

As a result the deflection form of the shaft "whirls" like a skipping rope at the shaft speed. In general the radius of whirl is finite, but at particularly critical speeds the whirl radius tends to become infinitely large. Thus the rate of growth of elastic resistance exactly matches the rate of growth of centripetal action required ^{B4}.

Similarly if the shaft is carrying two concentrated masses either side of supporting points, a transverse vibration will set up along the shaft. If the operating frequency coincides with this frequency it will increase the oscillation amplitudes and consequently lead to failure in the system. If the concentrated masses carried on the shaft are assumed to be particles, then the critical whirling speeds in radians per second are equal to the circular natural frequencies of transverse vibrations. Where concentrated masses of considerable dimensions are carried, gyroscopic effects appear due to the effect of slope. These effects have no counterpart in transverse vibrations, but can increase the whirling speed considerably. Thus any machine designer must make sure that these critical speeds are well outside his safety margins, if the critical speed has to lie within the operating range under this estimation. The machine must always accelerate through this critical speed as rapidly as possible.

The necessary calculations and estimations are made to ensure that the critical speeds of these particular discs lie well outside the safety margins ^{B2, B6}.

The theory and technique of determining the critical frequencies of these inertia discs are derived and presented in the following sections.

B.4 The Transverse Vibration of a Beam with Two Concentrated Masses

Let us now consider the case of figure B(3a) in which a massless beam supports concentrated masses m_1 and m_2 , at the same instant when the beam is vibrating. Let the deflection under these masses be y_1 and y_2 and let the forces acting on the beam at these points to cause these deflections be f_1 and f_2 , where m_1 and m_2 are armature and inertia disc masses respectively and a , b and c are the respective distances from the bearings as shown in figure B(3b). The reactions on the masses will be $-f_1$ and $-f_2$ and we can assume as usual that the motion is in simple harmonic with a radiancy ω_n . So we can write down these restoring forces as:

$$-f_1 = -m_1 \omega_n^2 y_1 \quad -f_2 = -m_2 \omega_n^2 y_2 \quad \text{--- (B.1)}$$

Clearly we can determine y_1 and y_2 in terms of f_1 and f_2 by applying the method normally used in strength of materials ^{B2,B3}, and so obtain equations which in conjunction with those for f_1 and f_2 will enable us to determine the quantity ω_n ^{B4}.

Resolving vertically we have:

$$f_1 + f_2 = R_{v_1} + R_{v_2} \quad \text{--- (B.2)}$$

taking moments about point (a) we have:

$$f_2 \cdot c + R_{v_1} \cdot a = f_1 \cdot b \quad \text{--- (B.3)}$$

from (B.3) we have:

$$R_{v_1} = (f_1 \cdot b - f_2 \cdot c) / a \quad \text{--- (B.4)}$$

substituting (B.4) in (B.2) we have:

$$R_{v_2} = f_1 \left(\frac{a-b}{a} \right) + f_2 \left(\frac{a+c}{a} \right) \quad \text{--- (B.5)}$$

Now considering the bending moment at a distance x from point (b) and taking Young's Modulus as E and the second moment of area about the neutral axis as I we get:

$$EI \cdot \frac{d^2 y}{dx^2} = R_{v_1} \cdot x + f_1 \cdot [x - (a-b)] + R_{v_2} \cdot [x - a] \quad \text{--- (B.6)}$$

therefore:

$$EI_Y = -R_{v_1} \cdot \frac{x^3}{6} + \frac{f_1}{6} [x - (a-b)]^3 - \frac{R_{v_2}}{6} [x - a]^3 + C_1 X + C_2 \quad \text{--- (B.7)}$$

at $x = 0$ the deflection $y = 0$. Therefore $c_2 = 0$.

(Note: for calculation of $EIy(x)$ substituting the value of x , if inside [] it is negative and should be left out, only positive values should be added).

Also $y = 0$ at $x = a$, so we have:

$$0 = -\frac{R_{v1} a^3}{6} + \frac{f_1}{6} \cdot [a - (a - b)]^3 + 0 + c_1 a$$

therefore:

$$c_1 = \frac{R_{v1} a^2}{6} - \frac{f_1 b^3}{6a} \quad \text{--- (B.8)}$$

To reduce the long formulas, substituting the actual values of a , b and c in equations (B.4) and (B.5)

we have:

$$R_{v1} = 0.416 f_1 - 0.166 f_2 \quad \text{--- (B.9)}$$

$$R_{v2} = 0.583 f_1 + 1.166 f_2 \quad \text{--- (B.10)}$$

$$\text{thus } c_1 = 810 \times 10^{-6} f_1 - 398 \times 10^{-6} f_2$$

Now substituting values of c_1 and c_2 in equation (B.7) and values of f_1 and f_2 from equation (B.1) and taking $x = a - b$ for EIy_1 and $x = a + c$ for EIy_2 , the system equations become:

$$EIy_1 \times 10^6 = 30.14m_1 \omega_n^2 y_1 - 15.95m_2 \omega_n^2 y_2 \quad \text{--- (B.11)}$$

$$EIy_2 \times 10^6 = -15.95m_1 \omega_n^2 y_1 + 16.13m_2 \omega_n^2 y_2 \quad \text{--- (B.12)}$$

In matrix form we have:

$$\begin{bmatrix} (30.14m_1\omega_2^2 - EI \times 10^6) & -15.95m_2\omega_n^2 \\ -15.95m_1\omega_n^2 & (16.13m_2\omega_n^2 - EI \times 10^6) \end{bmatrix} \begin{bmatrix} Y_1 \\ Y_2 \end{bmatrix} = 0$$

The transverse vibration resonance frequency occurs when the coefficient matrix of $\begin{bmatrix} Y_1 \\ Y_2 \end{bmatrix}$ becomes zero.

$$238.45m_1m_2\omega_2^4 - \omega_n^2(16.13m_2 + 30.14m_1)EI \times 10^6 + E^2I^2 \times 10^{12} = 0 \quad \text{--- (B.13)}$$

Substituting values of the armature, high speed inertia disc masses ($m_1 = 0.8575$ kg, $m_2 = 2.205$, EI of shaft = 21.467 g Nm²) and solving equation (B.13) for ω_n we have:

$$\omega_{n_1} = 1.986 \text{ K rad/sec} \rightarrow 317.7 \text{ Hz} \rightarrow 25062 \text{ r.p.m.}$$

$$\omega_{n_2} = 4.96 \text{ K rad/sec} \rightarrow 790 \text{ Hz} \rightarrow 47400 \text{ r.p.m.}$$

The safety margin between the lower resonance frequency and the maximum operating frequency does not appear to be very large, but in fact the armature mass is uniformly distributed along the shaft, and is not concentrated

at one point. This increases the shaft stiffness even further and, hence, the natural vibration frequencies.

B.5 The Determination of Whirling of the Circular Shaft with Gyroscopic Effects

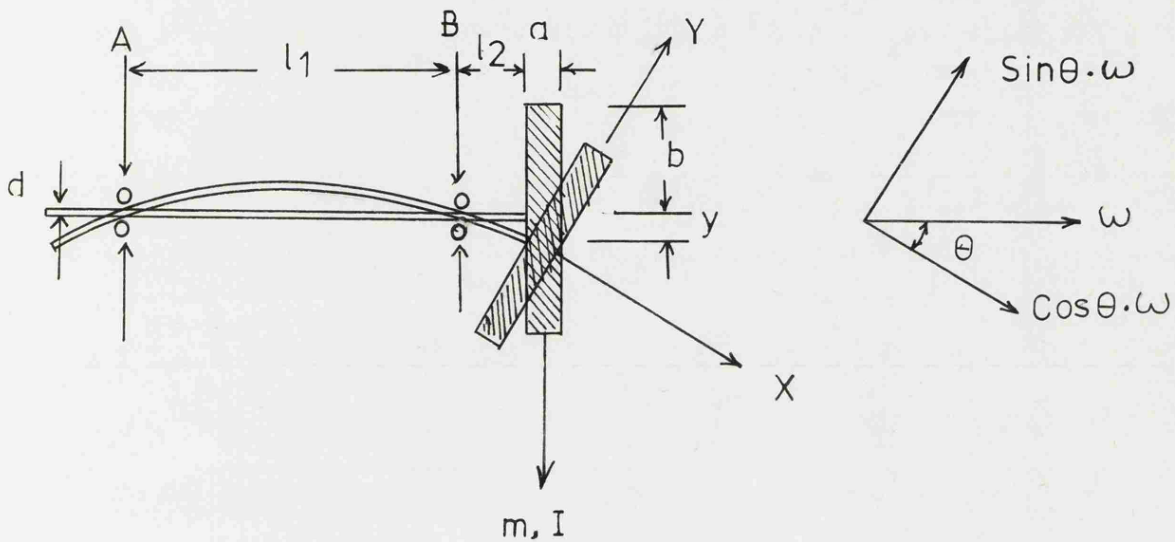


Figure B(4)

$m = 2.205 \text{ kg}$	$l_1 = 11.43 \text{ cm}$	$I_{xx} = m \cdot \frac{b^2}{2}$
$b = 6.63 \text{ cm}$	$l_2 = 1.905 \text{ cm}$	
$a = 2.85 \text{ cm}$	$d = 1.2 \text{ cm}$	$I_{yy} = m \cdot \frac{3b^2 + a^2}{12}$

I_{xx} (2nd moment of inertia in x axis) = $5766.82 \times 10^6 \text{ kg m}^2$

I_{yy} (2nd moment of inertia in y axis) = 3029.3 kg m^2

If the rotational speed of the shaft is ω , the angular momentums along the polar axis are $\omega I_{yy} \sin\theta$ and $\omega I_{xx} \cos\theta$. Resolving these vectors along the direction of ω and perpendicular to ω we have:

$$H_n = (I_{xx} \cos\theta \sin\theta)\omega - (I_{yy} \sin\theta \cos\theta)\omega$$

$$H_n = \omega(I_{xx} - I_{yy}) \sin\theta \cos\theta \quad \text{--- (B.14)}$$

$$\text{But } M = -H_n \omega_1 = -(I_{xx} - I_{yy}) \omega \omega_1 \cos\theta \sin\theta$$

for small values of θ , $\cos\theta \approx 1$ and $\sin\theta \approx \theta$

$$\text{Thus } M \approx -(I_{xx} - I_{yy}) \omega \omega_1 \theta$$

hence at whirling speeds $\omega = \omega_1$

$$\text{therefore } M \approx (I_{xx} - I_{yy}) \omega^2 \theta \quad \text{--- (B.15)}$$

The equations of deflection and slope at the end of the shaft are in general:

$$\begin{cases} y = f \cdot L_{11} + L_{12} M \\ \theta = f \cdot L_{21} + L_{22} M \end{cases}$$

where L_{11} is the maximum deflection at the end of the shaft due to force f ,

L_{12} is the maximum deflection at the end of the shaft due to moment M ,

L_{21} is the maximum slope at the end of the shaft due to force f ,

L_{22} is the maximum slope at the end of the shaft due to moment M ,

$$\text{and } f = m \cdot \omega^2 \cdot y.$$

B.5.1 Determination of L_{11}

The deflection at the end of the shaft due to force f ^{B.4}, is:

$$Y = f \cdot \frac{l_2^3}{3EI_s}$$

where I_s is the second moment of inertia of the shaft and E is the elastic modulus.

Now if point A was free to deflect, the deflection

$$Y_a = f' \cdot \frac{l_1^3}{3EI_s}$$

where $f' = f \cdot \frac{l_2}{l_1}$

but the reflected value of y_a at the other end of the shaft is

$$Y_a \cdot \frac{l_2}{l_1}$$

thus the reflected deflection

$$= \frac{l_2}{l_1} \cdot \frac{l_2}{l_1} \cdot \frac{l_1^3}{3EI_s}$$

where $I_s = \text{the second moment of area} = \frac{d^4}{64}$
and $E = \text{elasticity modulus} = 21.467 \times g \text{ Nm}^2$.

Therefore the total deflection at the end of the shaft due to force f is:

$$L_{11} = \frac{l_2^2}{3EI_s} \cdot [l_2 + l_1] \quad \text{--- (B.16)}$$

B.5.2 Determination of L_{12} and L_{21}

Consider figure B(3).

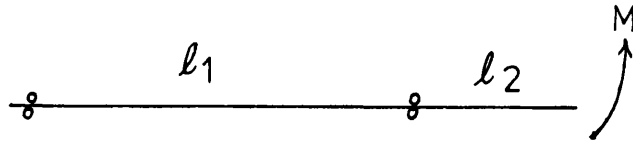


Figure B(3)

The deflection y due to moment M , applying Castigliano's* first theorem is:

$$y = \frac{1}{EI_s} \cdot \left[\int_0^{l_1} f \cdot \frac{df}{dM} \cdot dx + \int_0^{l_2} M \cdot \frac{dt}{dM} dx \right]$$

$$= \frac{1}{EI_s} \cdot \left[\int_0^{l_1} M \cdot \frac{x}{l_1} \cdot \frac{x}{l_1} \cdot l_2 \cdot dx + \int_0^{l_2} M \cdot x \cdot dx \right]$$

therefore:

$$y = M \cdot \frac{l_1 l_2 / 3 + l_2^2 / 2}{EI_s} \quad \text{--- (B.17)}$$

* The displacement corresponding to any f , say, of a system of forces $f_1, f_2 \dots f_n$ can be found by forming an expression for the total elastic strain energy in terms of the forces, and taking its partial differential coefficient with respect to f_r in Castigliano's first theorem.

thus

$$L_{12} = \frac{2l_1l_2 + 3l_2^2}{6EI_s} \quad \text{--- (B.18)}$$

Also the slope at the end of the shaft is in general,
when substituting the value of y from equation (B.17):

$$\theta = \frac{M}{l} \cdot \frac{2l_1l_2 + 3l_2^2}{6EI_s}$$

but $F = \frac{M}{l}$

Therefore the slope at the end of the shaft is given by:

$$\theta = F \cdot \frac{2l_1l_2 + 3l_2^2}{6EI_s}$$

thus

$$L_{12} = L_{21} = \frac{2l_1l_2 + 3l_2^2}{6EI_s} \quad \text{--- (B.19)}$$

B.5.3 Determination of L_{22}

Applying Castigliano's first theorem for the slope due
to moment M at the end of the shaft, in general we have:

$$\theta = \frac{1}{EI_s} \int_0^l M \cdot \frac{dM}{df} \cdot dx$$

in this case

$$\theta = \frac{1}{EI_s} \cdot \left[\int_0^{l_1} M \cdot \frac{x}{l_1} \cdot \frac{x}{l_1} \cdot dx + \int_0^{l_2} M \cdot 1 \cdot dx \right] = M \cdot \frac{l_1/3 + l_2}{EI_s}$$

thus

$$L_{22} = \frac{l_1/3 + l_2}{EI_s} \quad \text{--- (B.20)}$$

now the system equations become:

$$Y = \frac{l_2^2}{3EI_s} \cdot [l_2 + l_1] M \cdot \omega^2 \cdot Y - \left[\frac{l_1 l_2/3 + l_2^2/2}{EI_s} \right] (I_{xx} - I_{yy}) \omega^2 \theta$$

$$\theta = \left[\frac{l_1 l_2/3 + l_2^2/2}{EI_s} \right] M \cdot \omega^2 \cdot Y - \left[\frac{l_1/3 + l_2}{EI_s} \right] (I_{xx} - I_{yy}) \omega^2 \theta$$

or

$$\left[\begin{array}{l} Y \cdot \left[1 - \frac{l_2}{3EI_s} (l_2 + l_1) M \omega^2 \right] + \theta \left[\frac{l_1 l_2/3 + l_2^2/2}{EI_s} \right] (I_{xx} - I_{yy}) \omega^2 \\ Y \cdot \left(\frac{l_1 l_2/3 - l_2^2/2}{EI_s} \right) M \omega^2 - \theta \left[1 + \left(\frac{l_1/3 + l_2}{EI_s} \right) (I_{xx} - I_{yy}) \omega^2 \right] \end{array} \right] = 0$$

when $y = \theta = 0$ the system is stable, but when $y \neq \theta \neq 0$, the system equations are satisfied only if we have:

$$\left[1 - \frac{l_2}{3EI_s} (l_2 + l_1) M \omega^2 \right] \left[1 + \left(\frac{l_1/3 + l_2}{EI_s} \right) (I_{xx} - I_{yy}) \omega^2 \right] = \left[\left(\frac{l_1 l_2/3 + l_2^2/2}{EI_s} \right) (I_{xx} - I_{yy}) \omega^2 \right] \left[\frac{l_1 l_2/3 + l_2^2/2}{EI_s} \cdot M \omega^2 \right]$$

substituting the values and simplifying we have:

$$\omega^4 - 56.8 \omega^2 \times 10^6 - 10^{12} = 0 \quad \text{--- (B.21)}$$

This equation has one positive solution only.

ie. $\omega_0 = 7545 \text{ rad/sec}$

or $f = 1200 \text{ Hz}$

or $64,000 \text{ r.p.m.}$

Thus gyroscopic effect has increased the critical frequency considerably.

B.6 The Torque Transducer

The stator frame of the main drive induction motor is coupled to a 400 Hz a.c. servo motor. The rotor winding of the servomotor R_1 and R_2 are used as the field winding and is supplied with a constant amplitude and frequency from a 400 Hz oscillator. The stator of the a.c. servo motor carries three-phase windings two of which S_1 and S_2 are used to produce a signal, which varies in amplitude according to its position with respect to rotor winding. Thus, the servomotor position is set such that the stator output signal of these particular phases is zero when the main drive induction motor is stationary. When the induction motor is driving the load, its case rotates through an angle whose value depends on the shaft torque and stiffness of the counter balanced springs. The stiffness of springs being constant, the angle of rotation is exactly proportional to the shaft torque. To obtain a linear relationship between the torque and servo output, an additional phase rectifier circuit is designed which samples the servo a.c.

output in the linear region of the sine wave and stores it in the form of an analog signal. These narrow sampling pulses are produced everytime 400 Hz a.c. sine wave rises above the zero volts, ie. at the beginning of each cycle. The phase rectifier and sampling circuit is shown in figure B(5).

The amplitude of the a.c. servomotor output signal is dependent on the amplitude of the 400 Hz oscillator which energises the field winding. Therefore to obtain accurate results, the oscillator circuit must be stable in amplitude and frequency. A standard Wien bridge oscillator ^{B.7} shown in figure B(6a) is constructed. To find its temperature stability, a series of experiments are carried out and its voltage variations with temperature are shown by circles in figure B(7). Then the oscillator circuit is modified to produce a better degree of temperature stability and its output response is shown by a continuous line in figure B(7). This is done by simply adding the necessary compensating components in the feedback loop, and the resultant circuit diagram is shown in figure B(6b).

The frame of the induction motor is rotated through angles from -110° to $+110^{\circ}$ C, and the corresponding transducer d.c. output signals are plotted with oscillator outputs of 1, 2 and 3 volts as shown in figure B(8). The stiffness of the counter balance springs are chosen to give one degree of angular rotation for 0.14 Nm of the shaft torque. Choosing an oscillating

output of 2 volts r.m.s. produces linear outputs in a range of ± 40 degrees of angular rotation. This requires a shaft torque of 5.6 Nm which is greater than the rated value of this particular machine. Thus the oscillator output voltage is set for 2 volts r.m.s. throughout all the experiments.

In addition a simple rectifier circuit is built to convert one of the mains supply phases to a d.c. signal, to plot the changes in supply voltage during starting. The rectifier transfer characteristic is also checked for linear results during all experiments.

B.7 Digital Tacho Design

In order to produce an analog signal proportional to the rotor speed, a slotted disc is mounted on the rotor shaft which interrupts a light beam on a photo-transistor on the other side of the disc. This produces pulses proportional to the rotor speed which are then sharpened by a Schmitt trigger device and divided by two to obtain equal space ratios by a JK flip-flop. To fix the amplitudes of these pulses the JK flip-flop output is then applied to a high gain operational amplifier whose feedback loop contains two 10 volt zener diodes connected back to back. An integrator circuit is then used to convert these pulses to an analog signal whose time constant components R.C, are determined from the relation $V_O = V_{in} \cdot F \cdot R.C$, where V_{in} and F are the amplitude

and frequency of the corresponding pulses and V_0 is the amplifier output. The final circuit diagram is shown in figure B(9).

To achieve smooth analog output signals at low speeds, the number of slots on the disc are chosen as large as possible. Thus when considering maximum and minimum speeds a disc with 20 slots is employed. The machine speed is then varied from zero up to 18,000 r.p.m. and all the corresponding values of the analog signals are monitored for any indication of non-linearities through all the speed ranges of the experiments and are plotted in figure B(10).

The Radio Spares package voltage regulators are used to provide the necessary power supplies.

B.8 Results and Conclusions

The inertia machine was tested several times through different speeds. There was no sign of vibrations at any speeds to indicate the existence of any critical frequency within the operating range.

The torque transducer gave oscillatory responses at starting instances. These could have been reduced by introducing a dashpot in conjunction with the counter balance springs. But this would have produced sluggish responses during starting. Instead the inertia machine was speeded up in the opposite direction to that of the induction motor direction of rotation by means of the a.c. commutator motor. Then the three-phase supply

was switched across the induction motor terminals immediately after the commutator motor was switched off. Thus the transient response of the torque transducer occurred when the inertia machine was switched from a reverse to a forward direction. The X-Y plotter was switched on at the instant of change of direction. This reverse starting is used for plotting all the required torque speed characteristics. Torque speed characteristics shown in figures B(11) to B(31) are plotted with supply frequencies from 10 Hz up through 100 Hz in steps of 10 Hz, and from 100 Hz to 320 Hz inclusive in steps of 20 Hz. In addition at each step of the operation, the machine terminal voltage is kept at the following volts per hertz: 1.34, 1.24, 1.16, 1.1, 1.00, 0.908 (110%, 100%, 97%, 91%, 83%, 75%).

Bibliography

- B.1 "Theory of machines", 2nd Edition, W.G. Green, 1962.
- B.2 "Strength of materials", 11th Edition (Longman), A. Morley, 1954.
- B.3 "Strength of materials", (Arnold), J. Case and A.H. Chilver.
- B.4 "An introduction to the machines of mechanics", 2nd Edition, J.L.M. Morrison and B. Crossland.
- B.5 "Elements of the strength of materials", 5th Edition, S. Timoshenko and D.H. Young.
- B.6 "An introduction to the theory of elasticity for engineers", 2nd Edition, R.V. Southwell.
- B.7 "Electronic circuits manual", (McGraw-Hill), J. Markus, 1971, pp. 531.

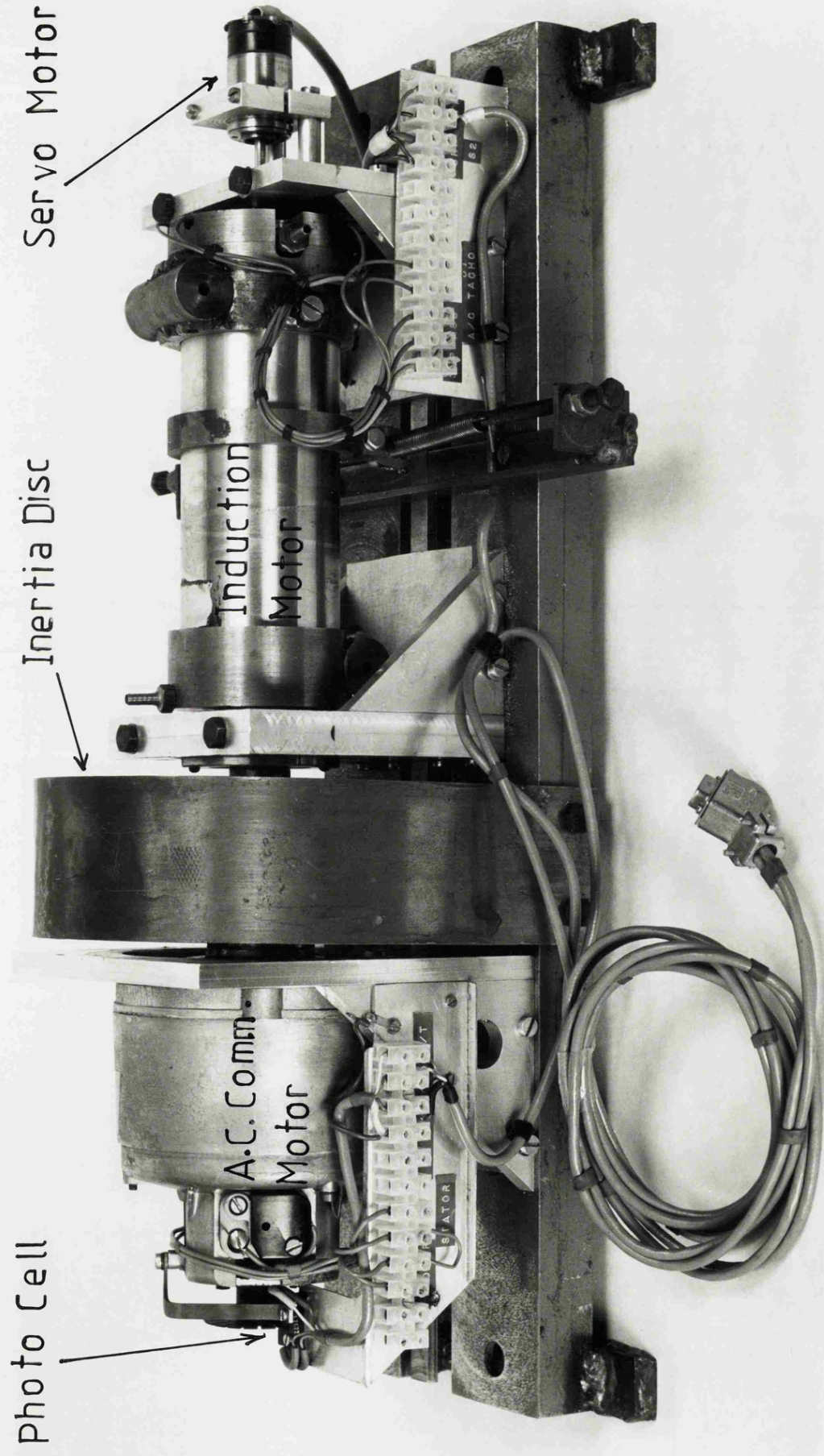
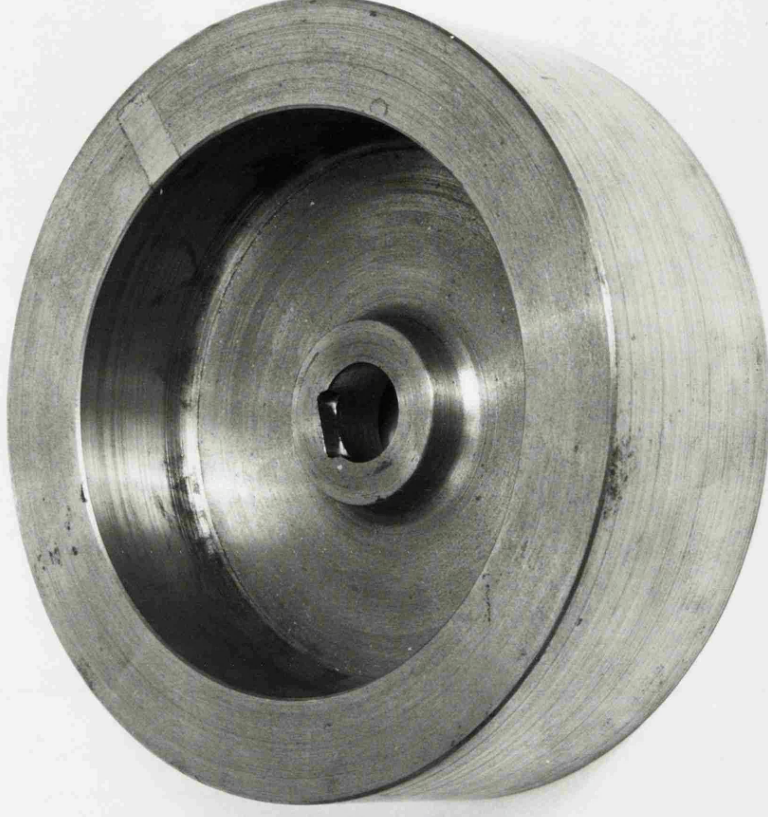


Fig. B.1 The Torque Speed Plotting Machine

Low Speed



High Speed

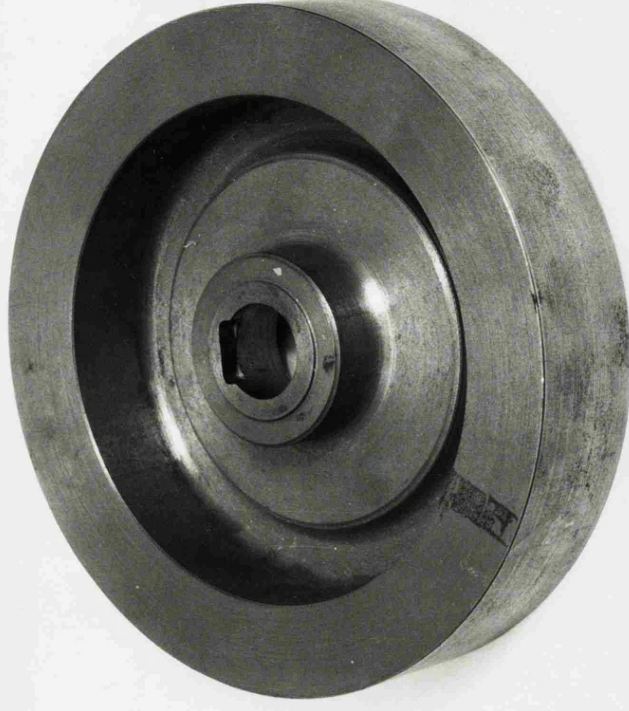
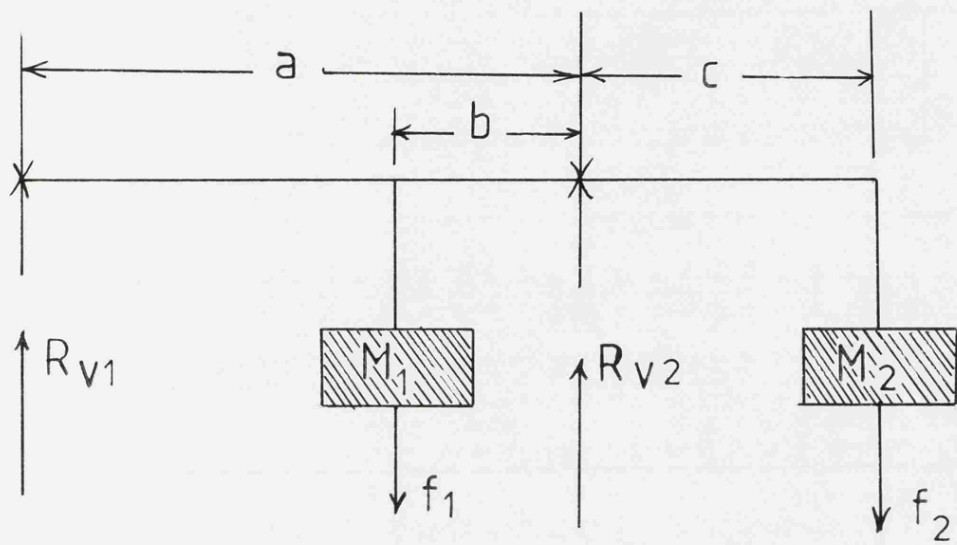
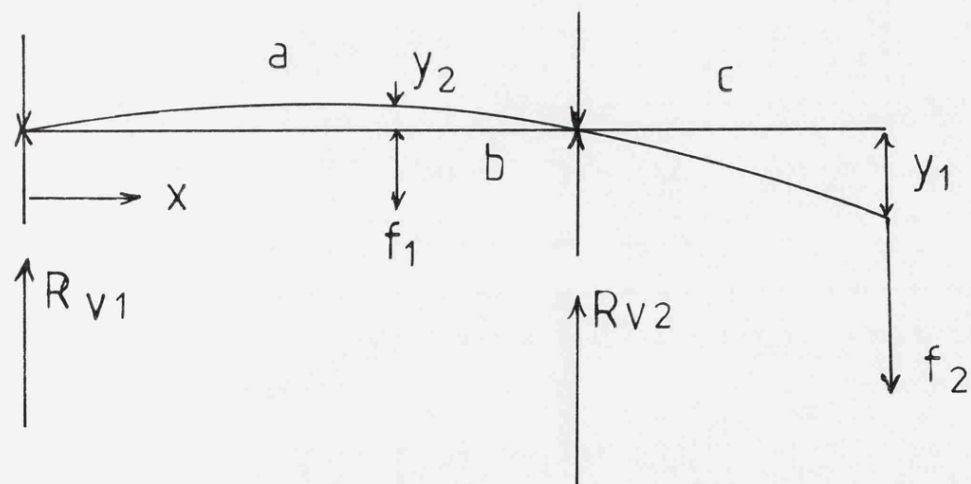


Fig.B. 2 The Inertia Discs



(a)



(b)

Figure B.3

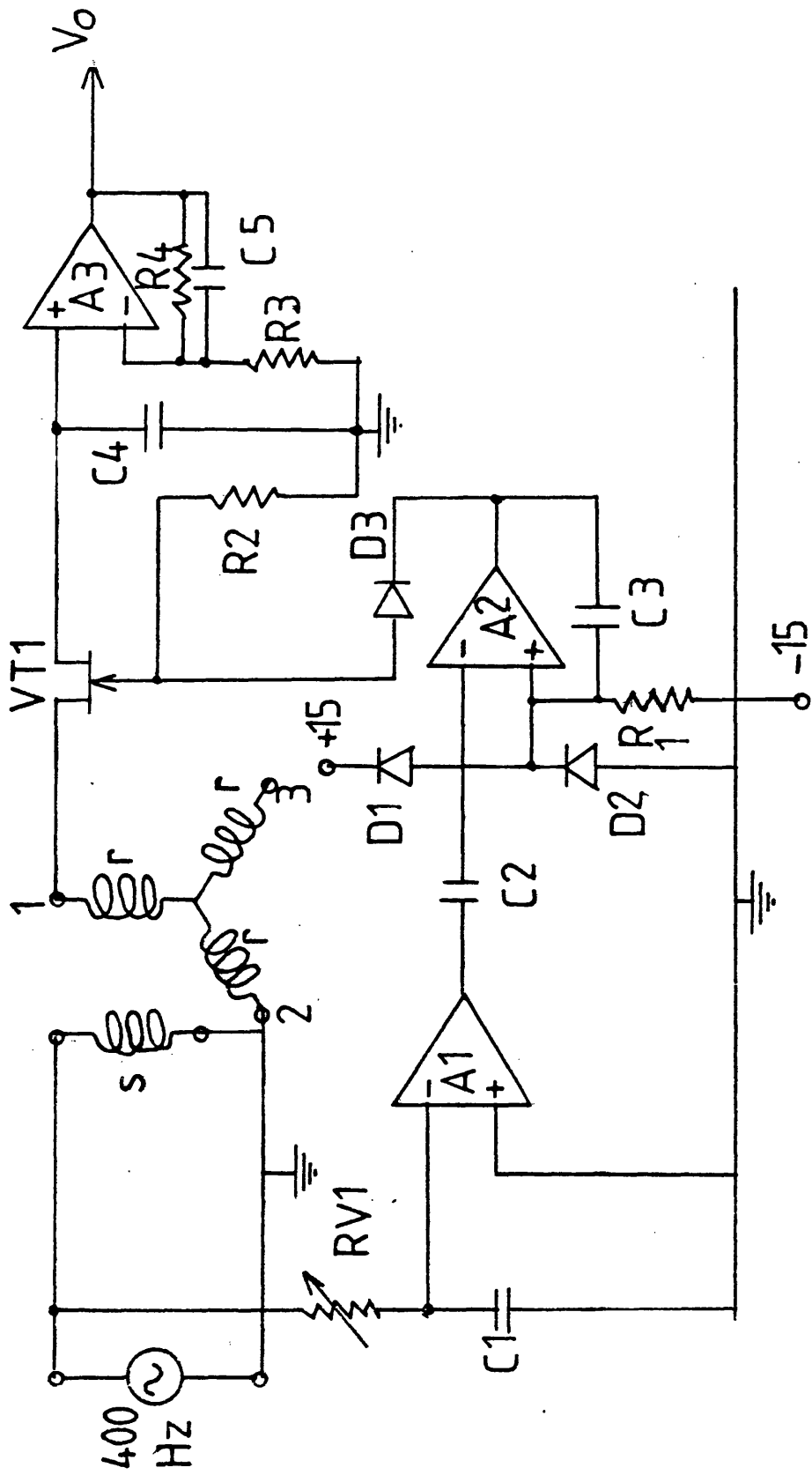
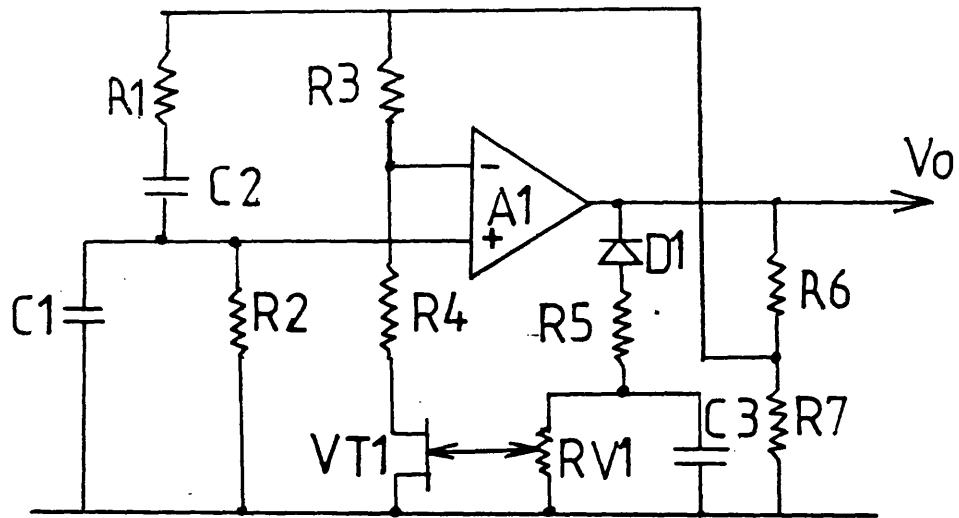


Fig.B.5 PHASE RECTIFIER AND SAMPLING CIRCUIT DIAGRAM



(a) Standard Wein bridge Oscillator

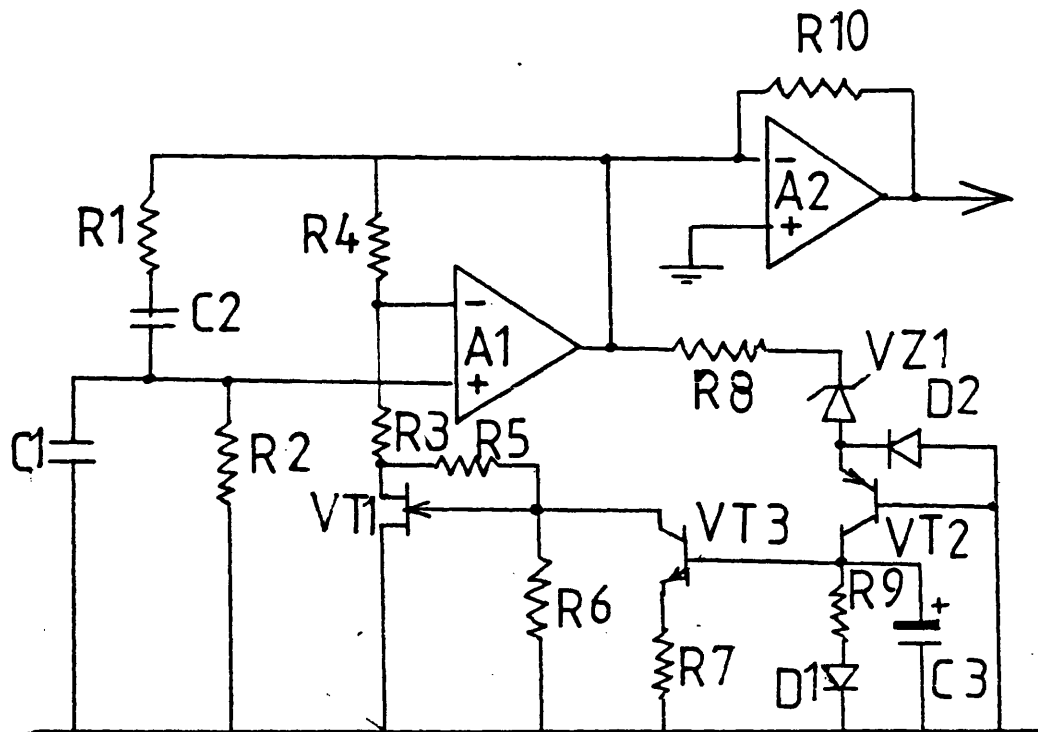
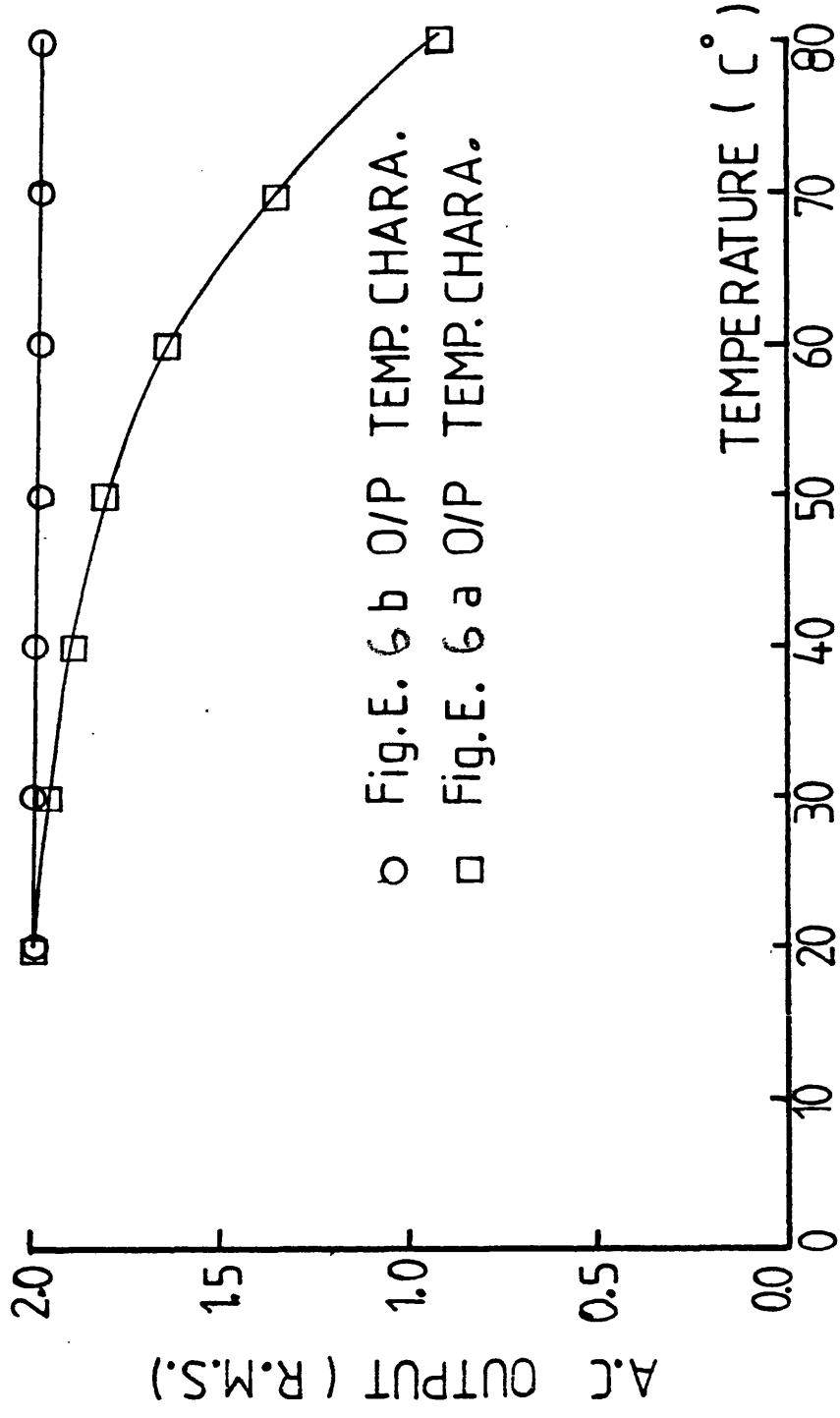


Fig.B.6 (b) Modified Wein bridge Oscillator



○ Fig.E. 6 b O/P TEMP. CHARA.
 □ Fig.E. 6 a O/P TEMP. CHARA.

Fig. B.7 TEMP. CHARA. OF OSCIL.O/Ps (VOLTS AC)

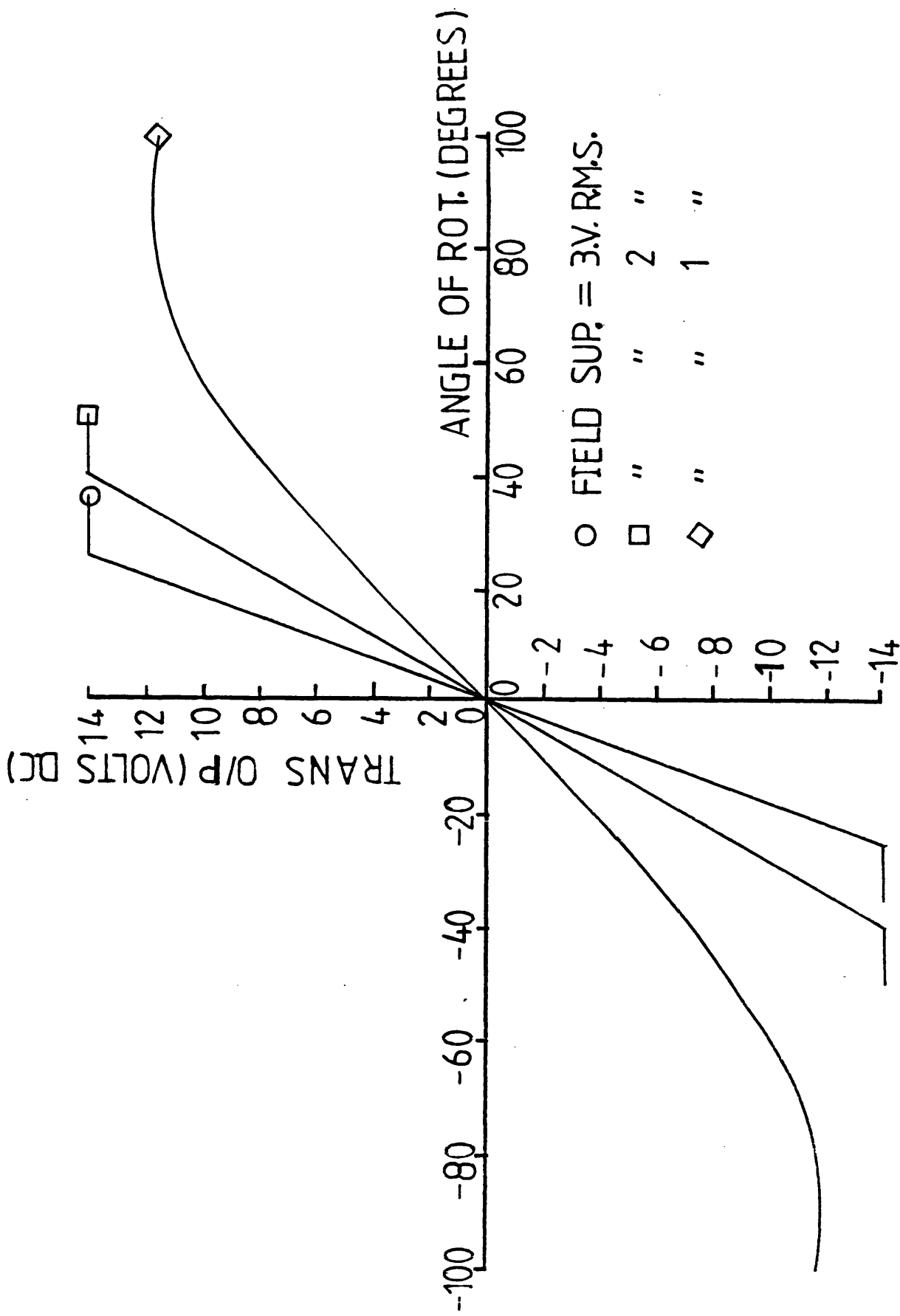


Fig. B.8 TRANSDUCER O/P V ANGLE OF ROTATION

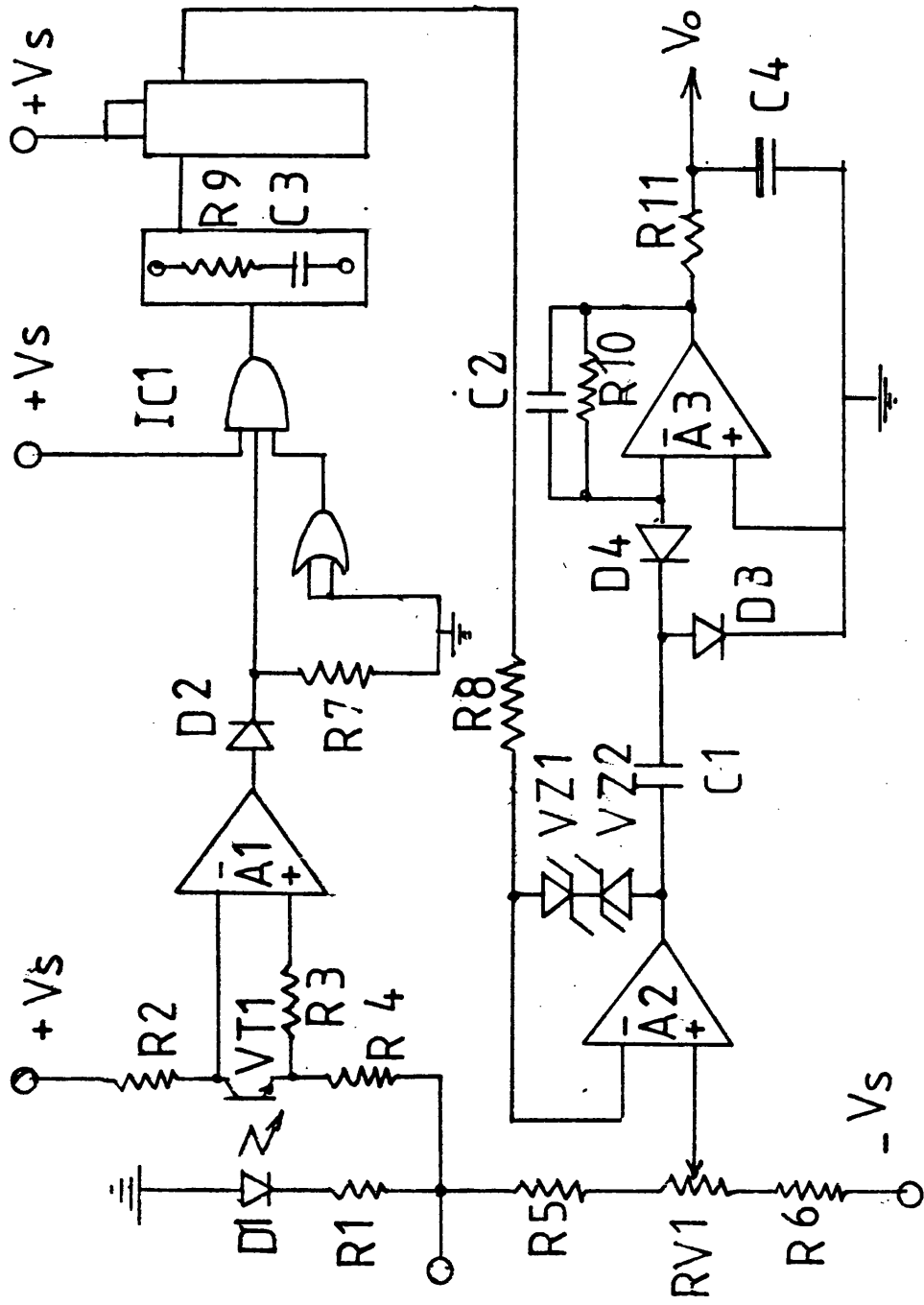


Fig. B.9 CIRCUIT DIAGRAM OF THE DIGITAL TACHO

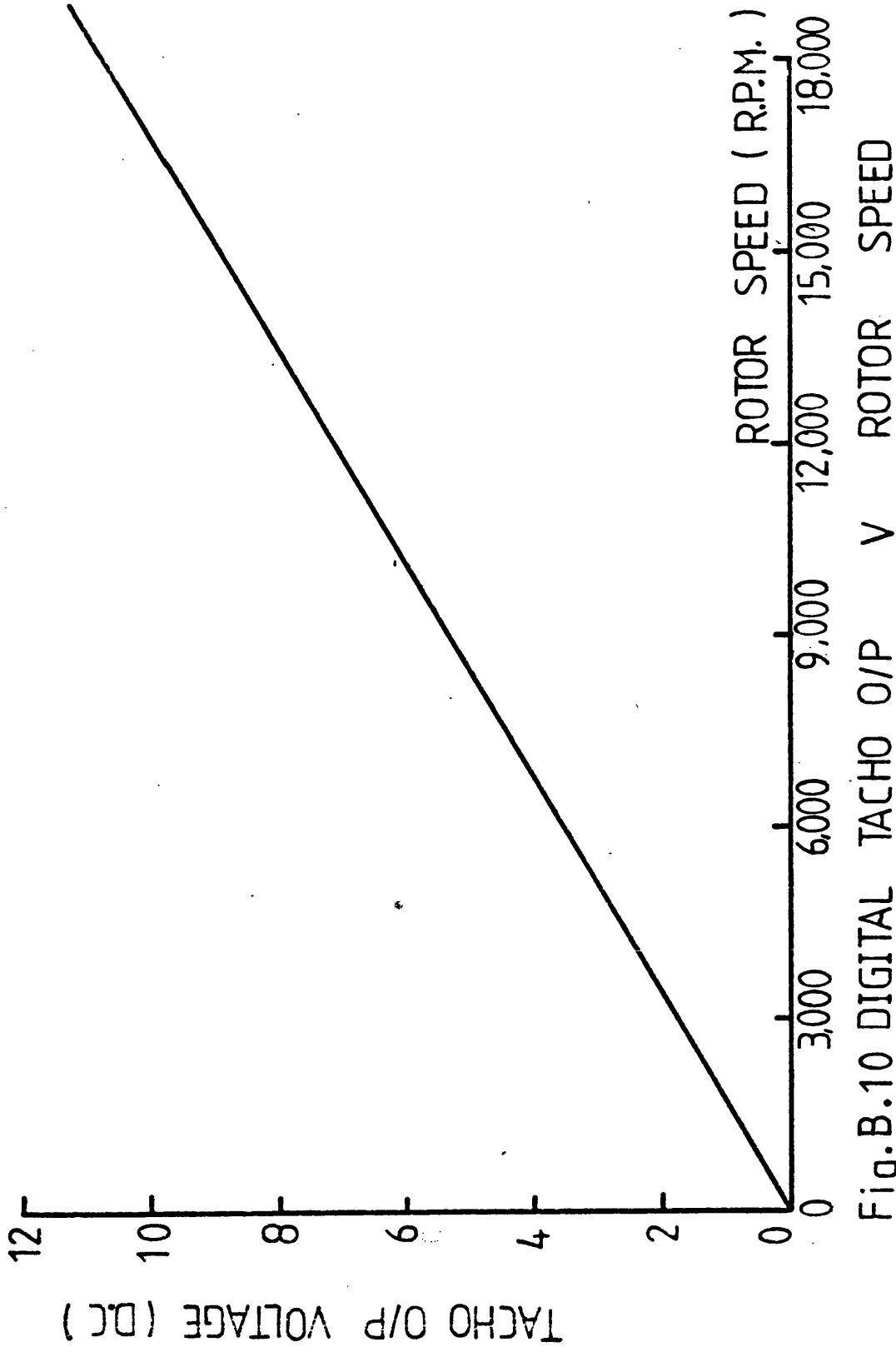


Fig. B.10 DIGITAL TACHO O/P V ROTOR SPEED

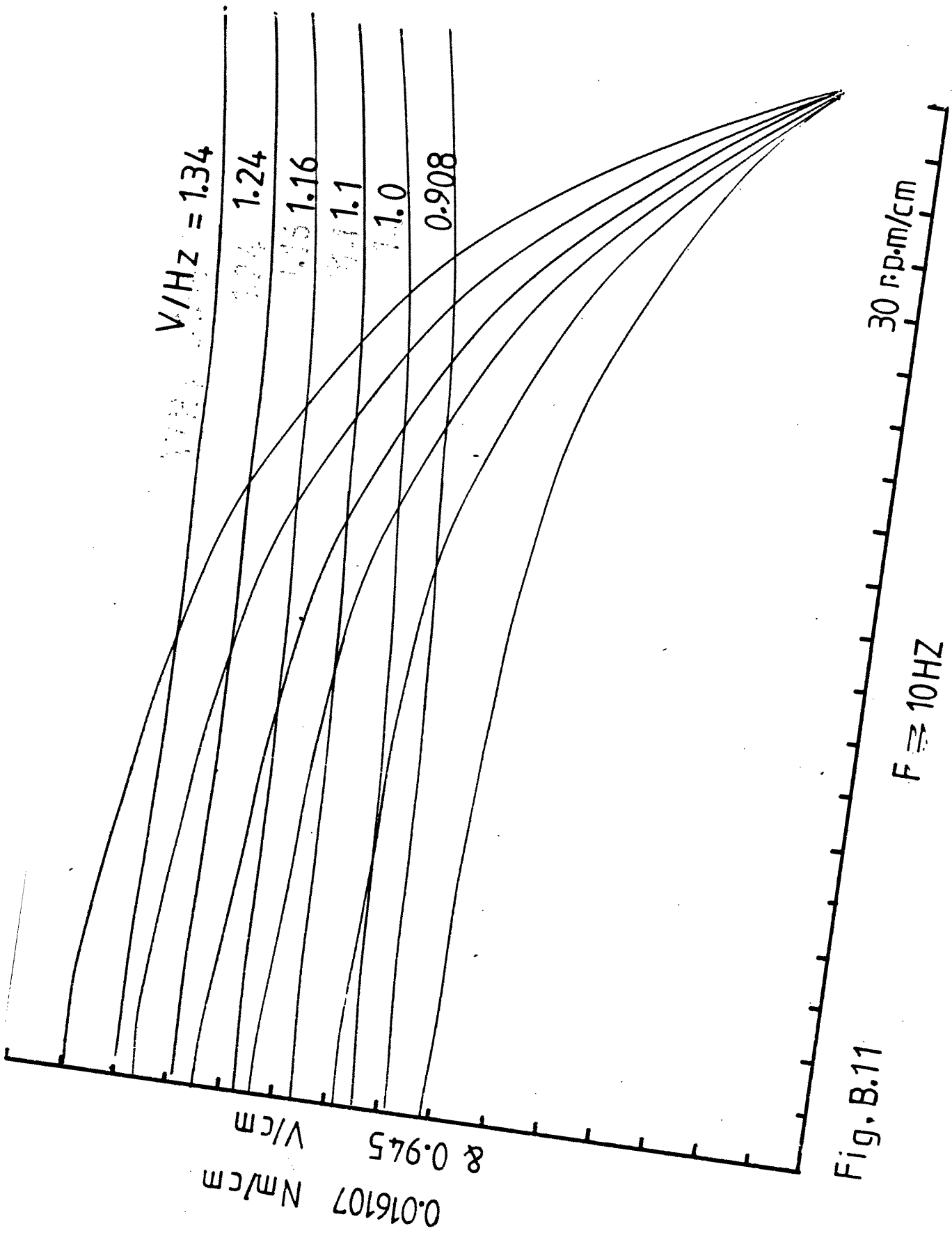


Fig. B.11

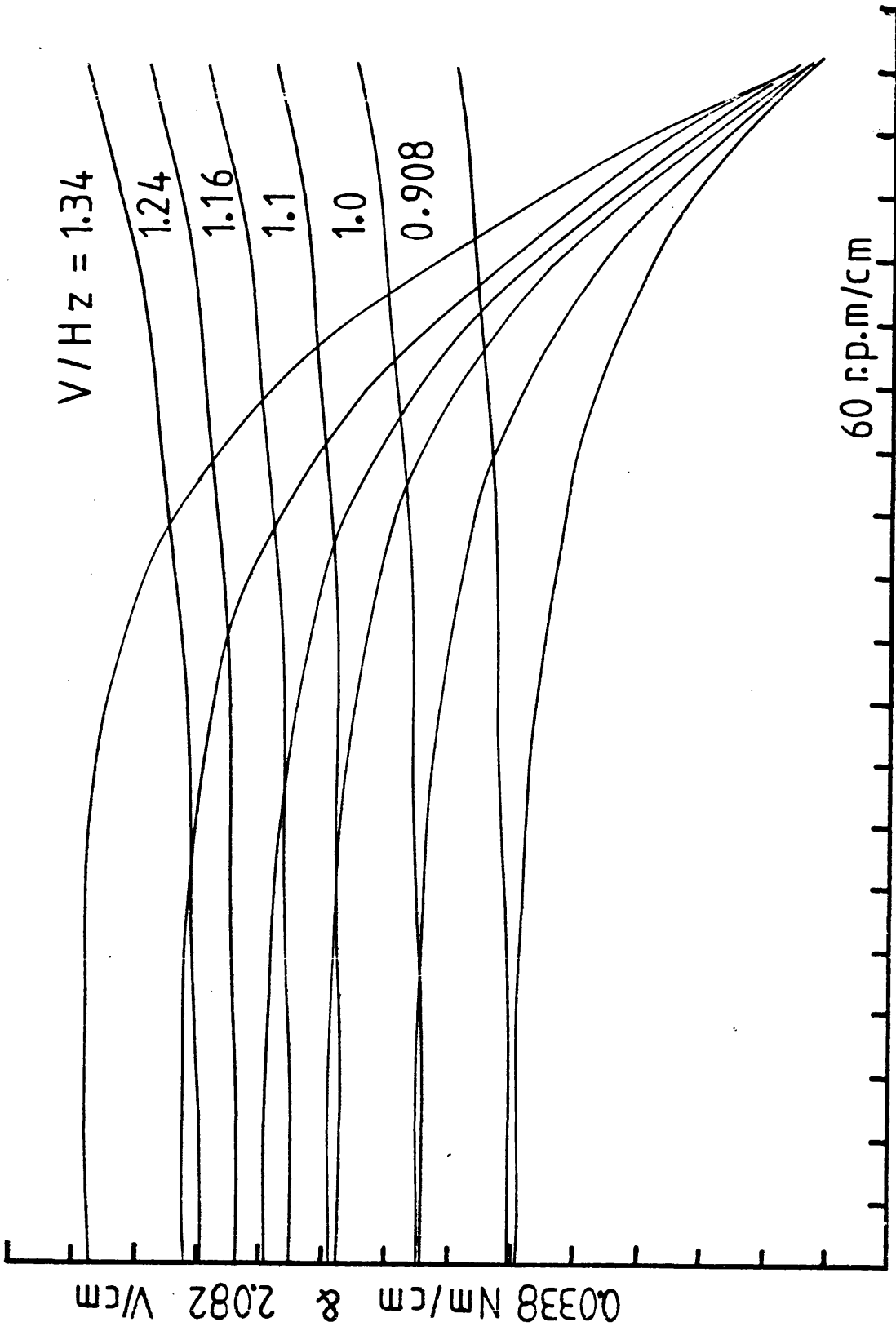


Fig. B. 12 $F \approx 20\text{HZ}$

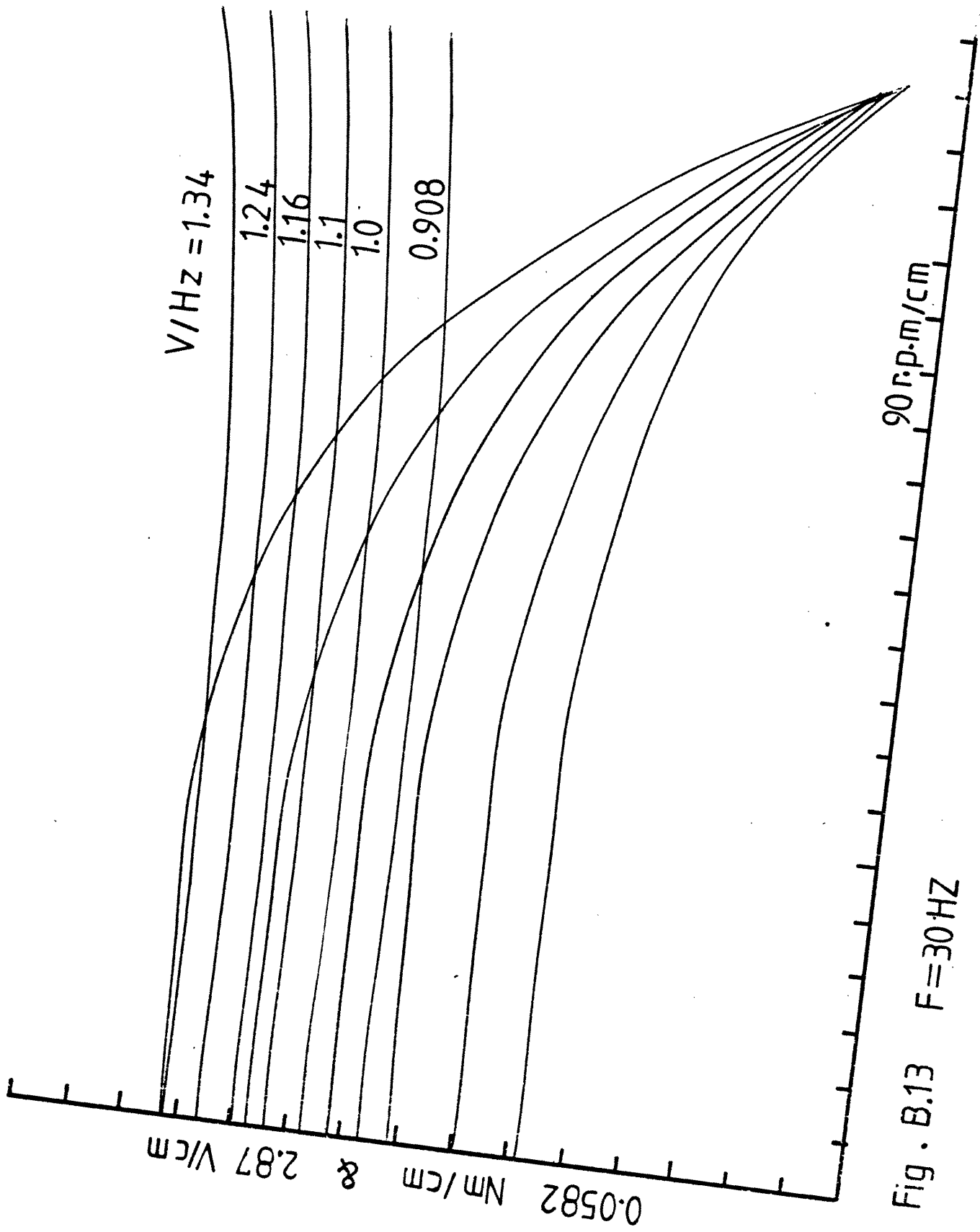


Fig. B.13 $F = 30 \text{ Hz}$

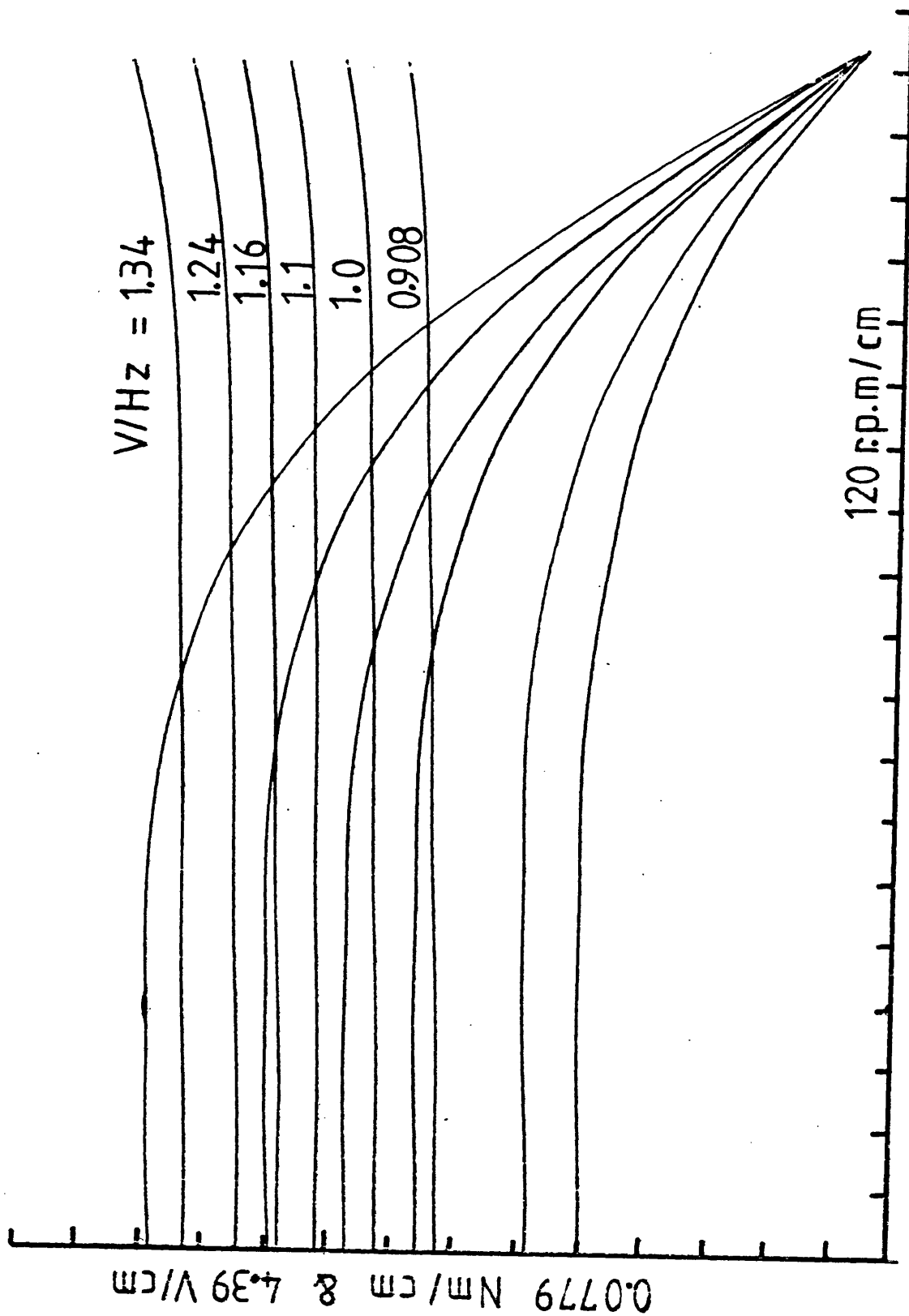


Fig. B.14 $F=40\text{HZ}$

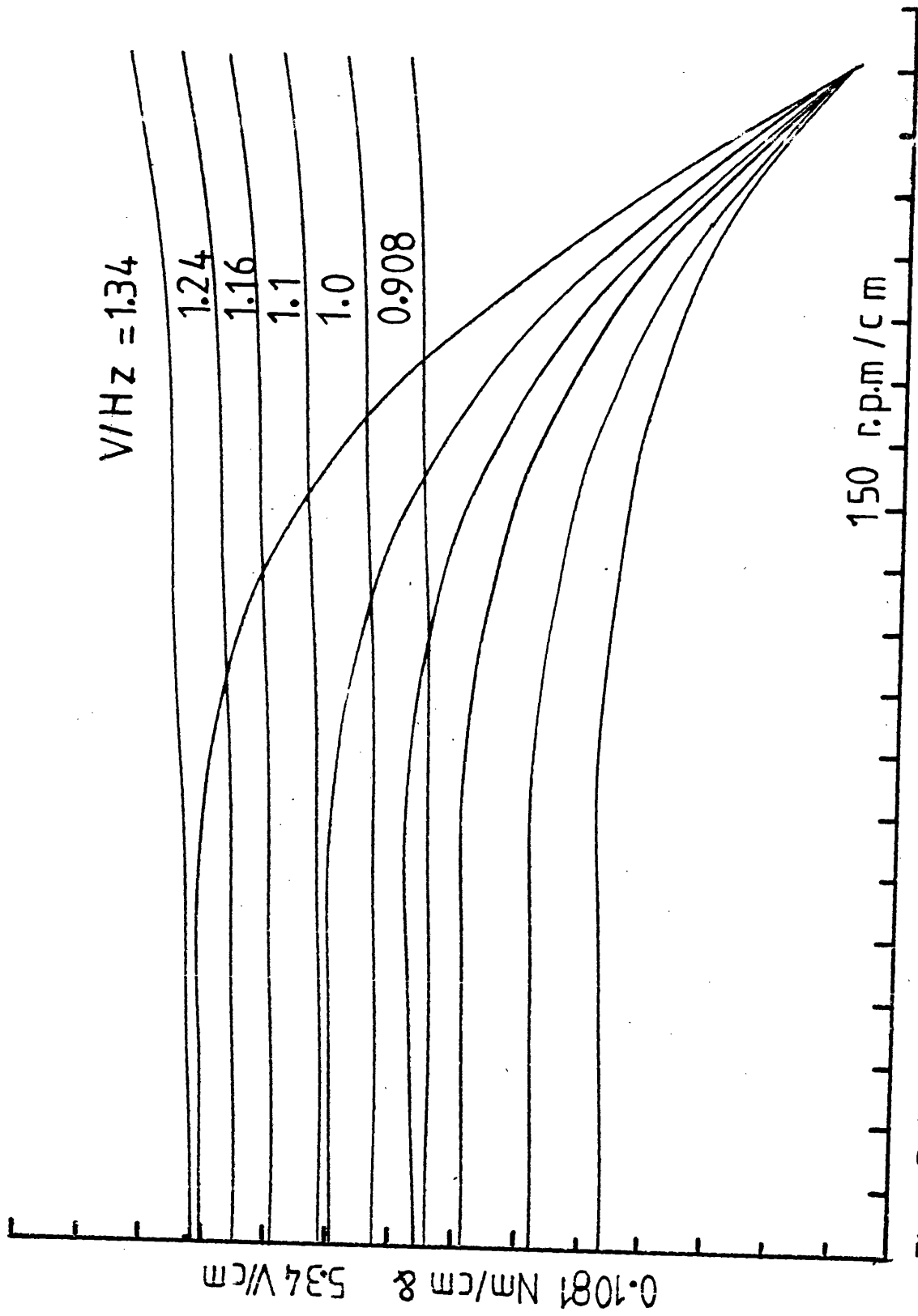


Fig. B.15. $F = 50\text{ Hz}$

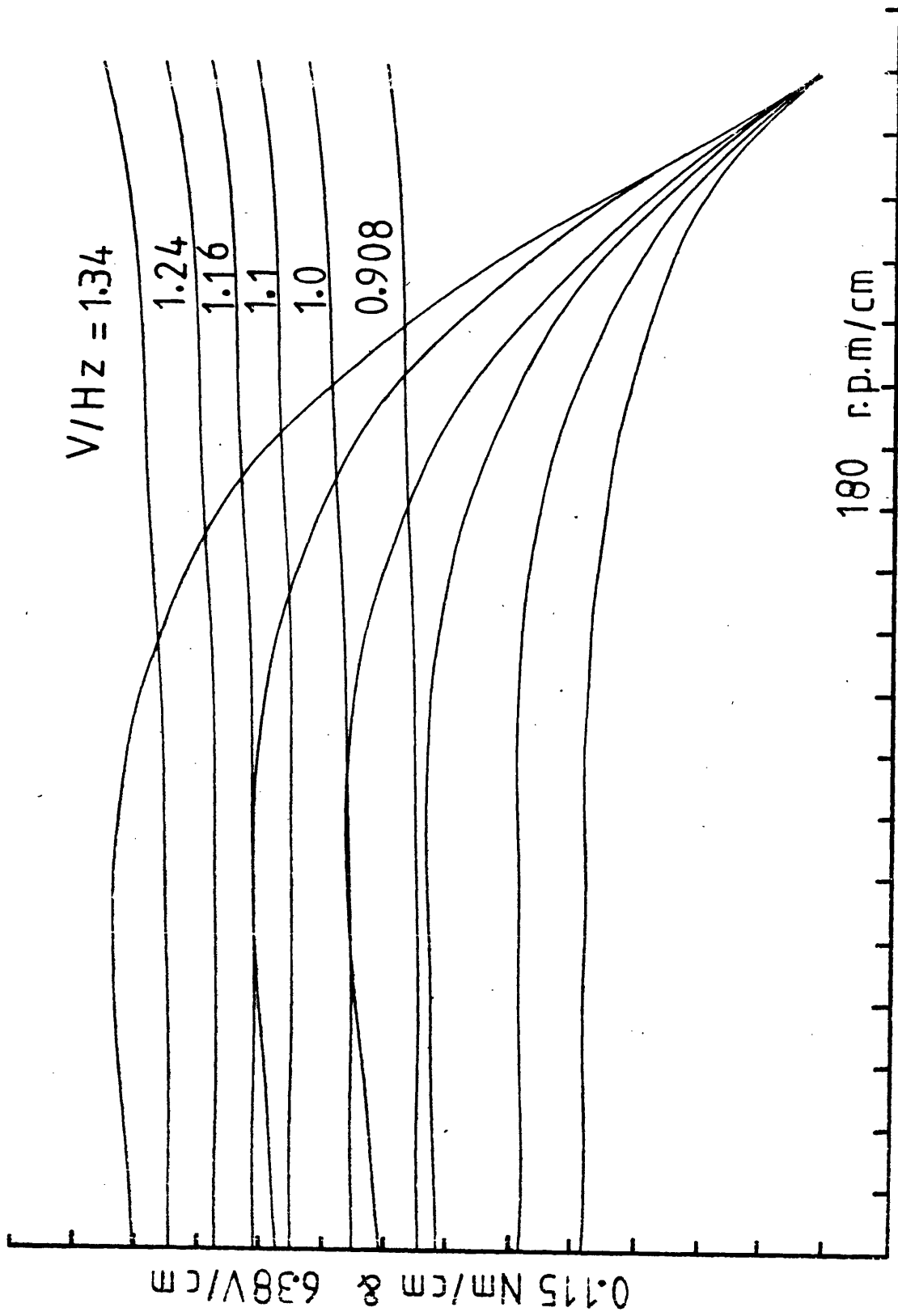


Fig. B.16 $F=60\text{HZ}$

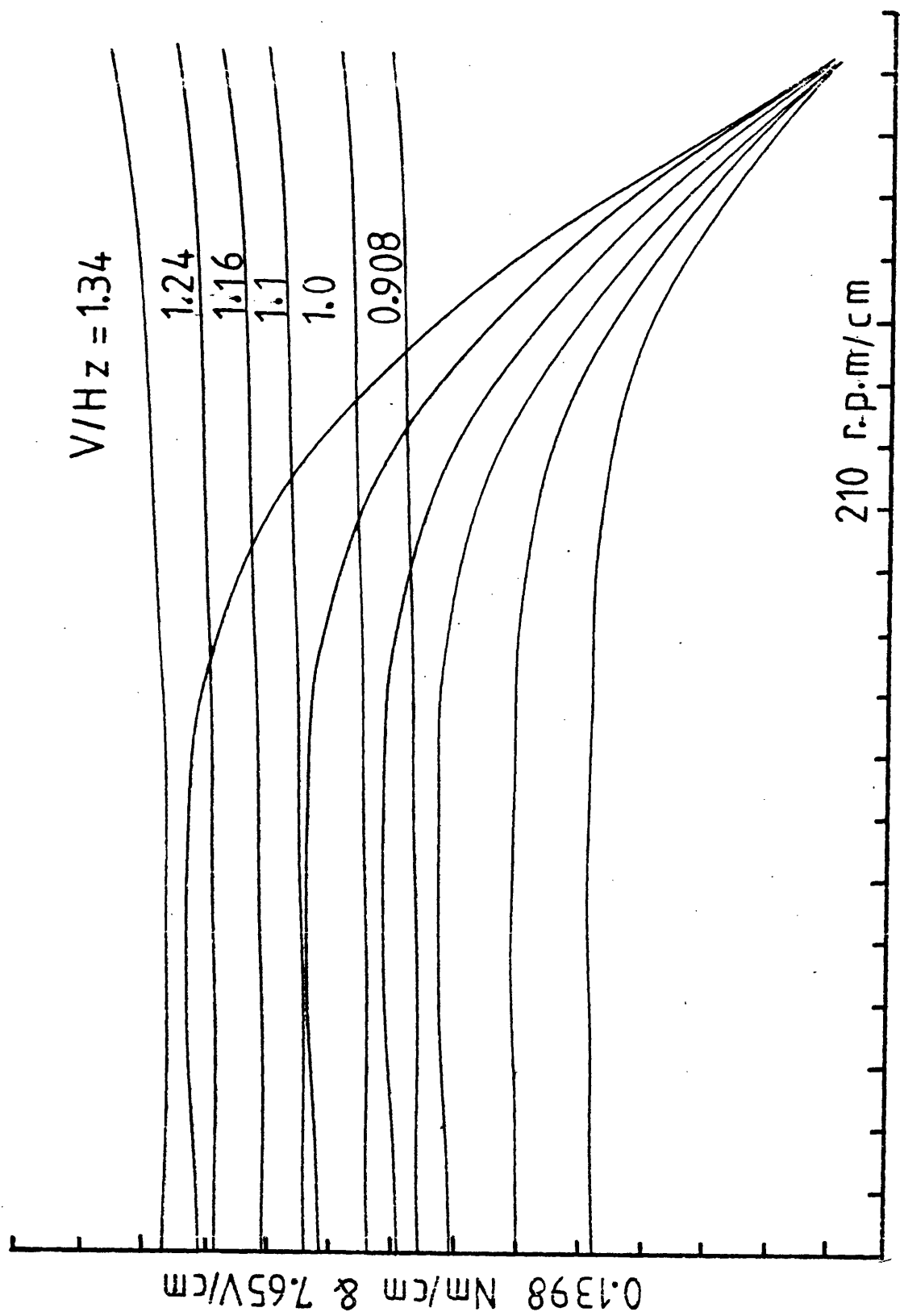


Fig. B.17 $F=70\text{HZ}$

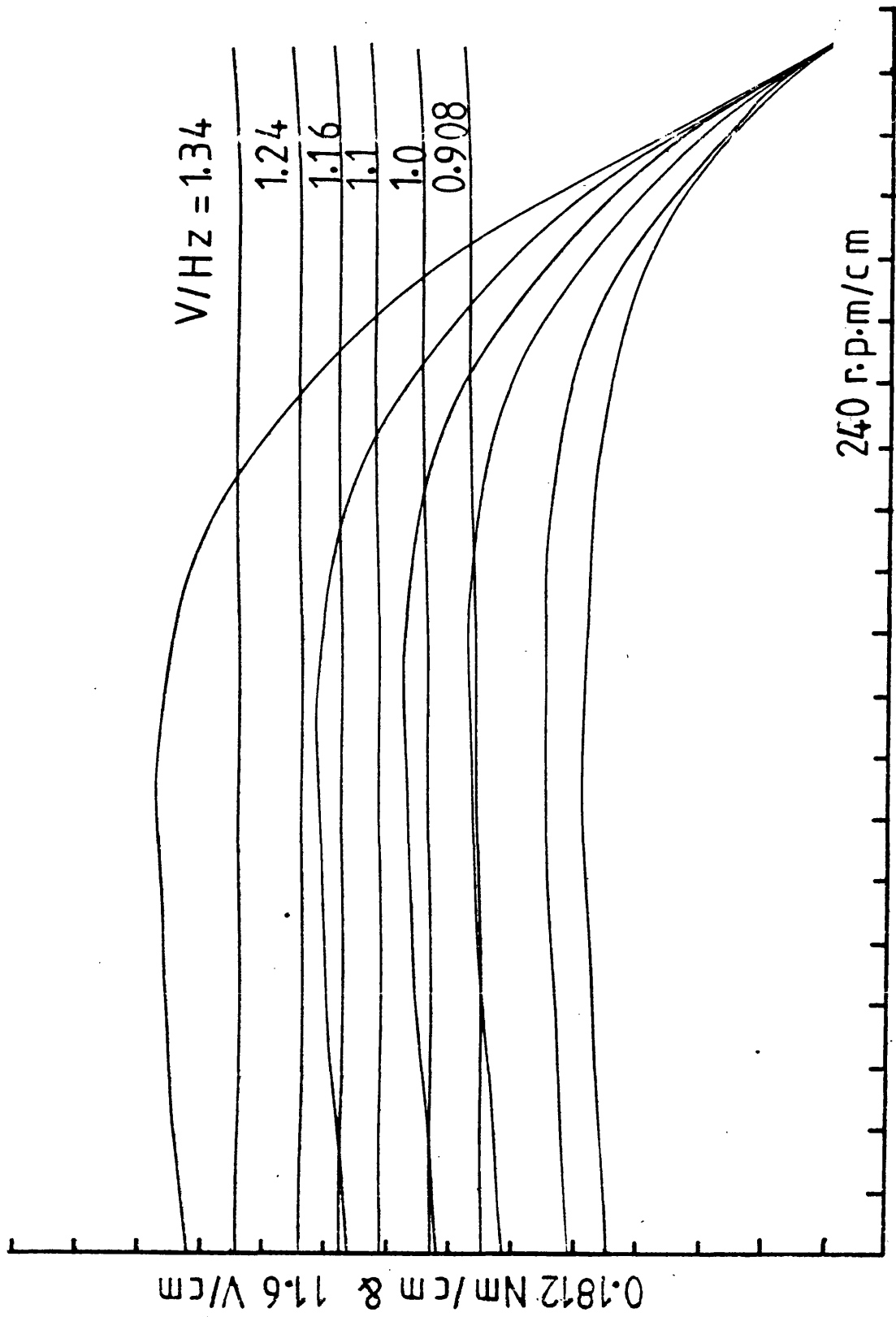


Fig. B.18, $F=80\text{HZ}$

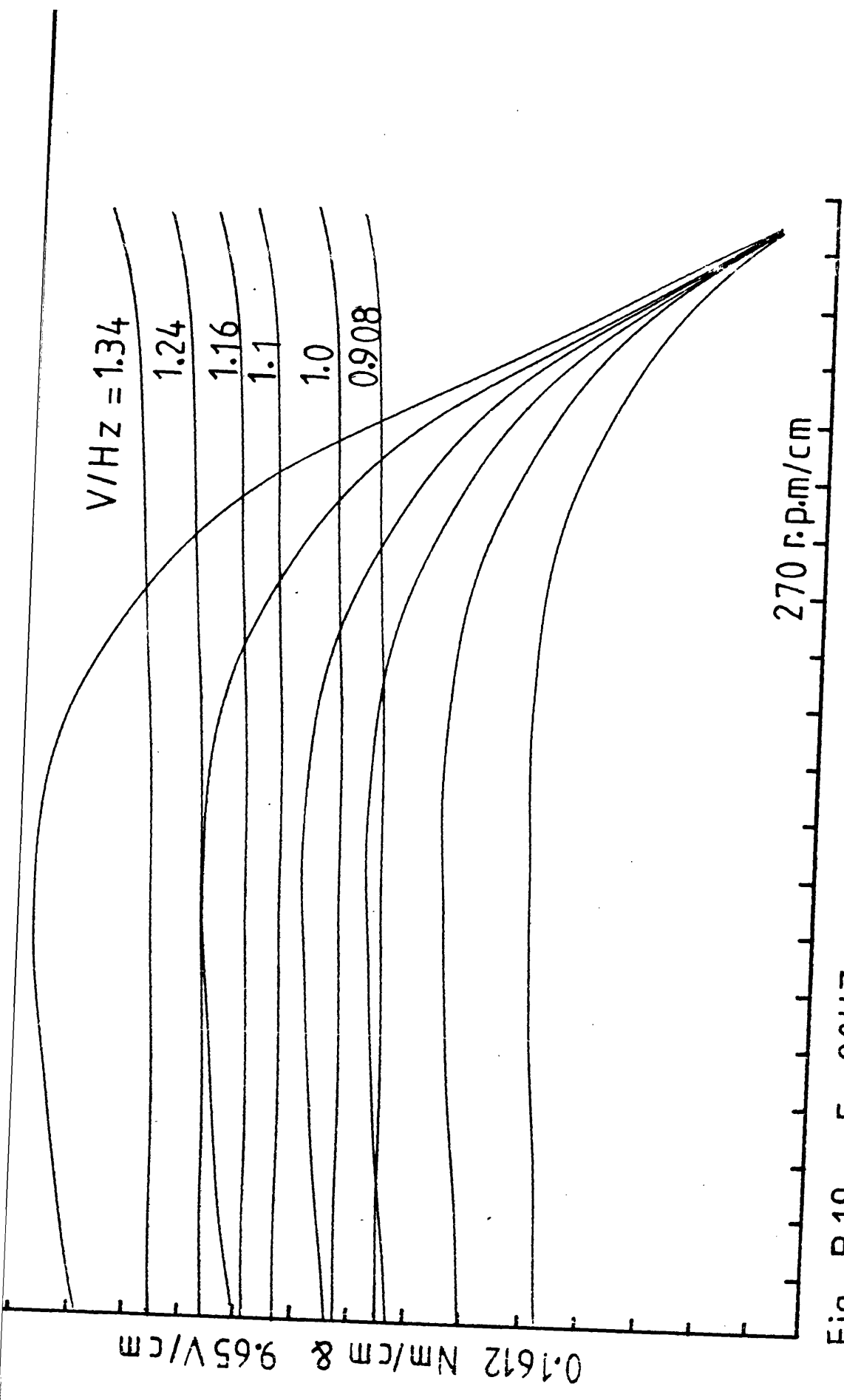


Fig. B.19 $F = 90\text{HZ}$

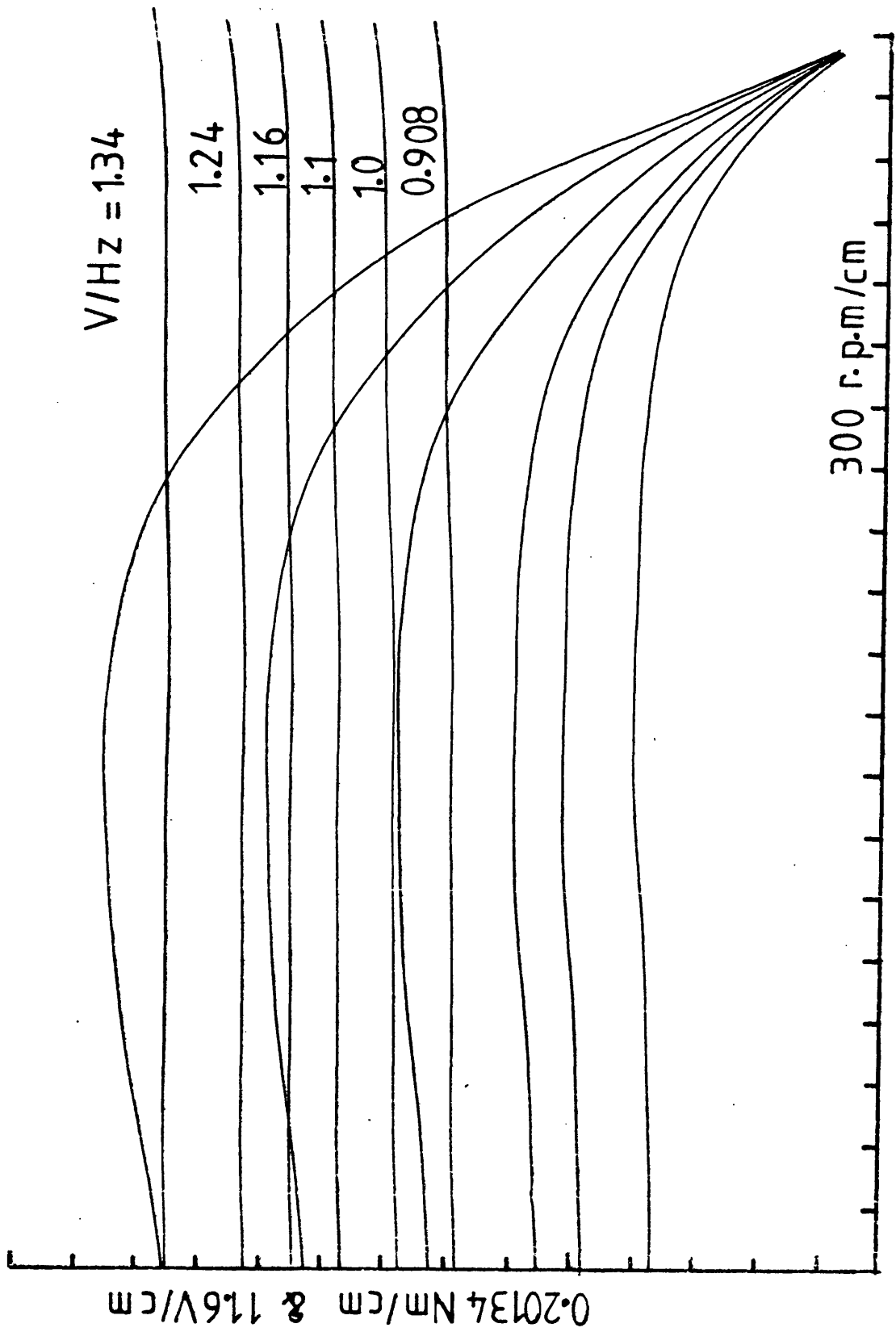


Fig. B.20 $F=100\text{HZ}$

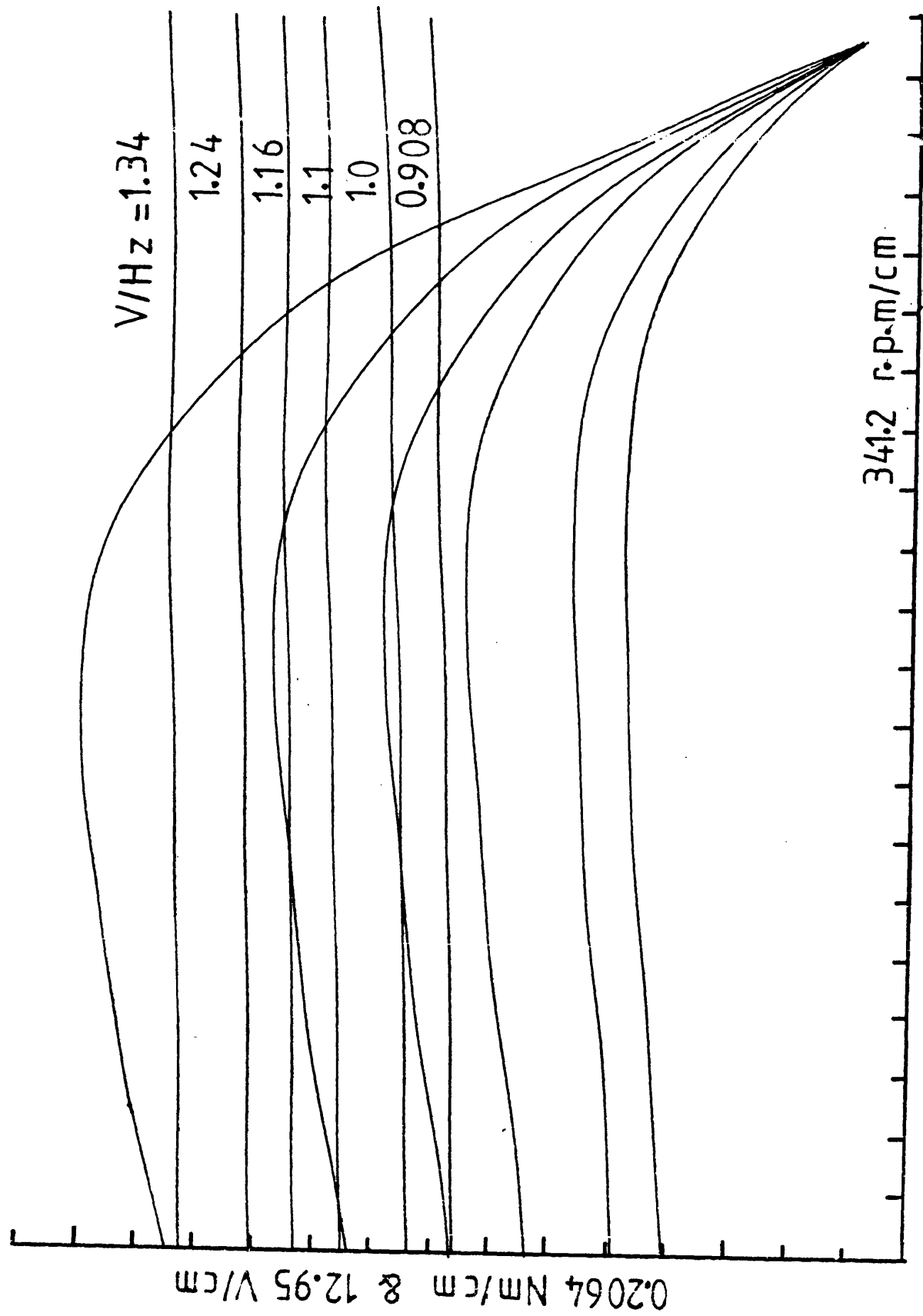


Fig. B.21 $F=120\text{HZ}$

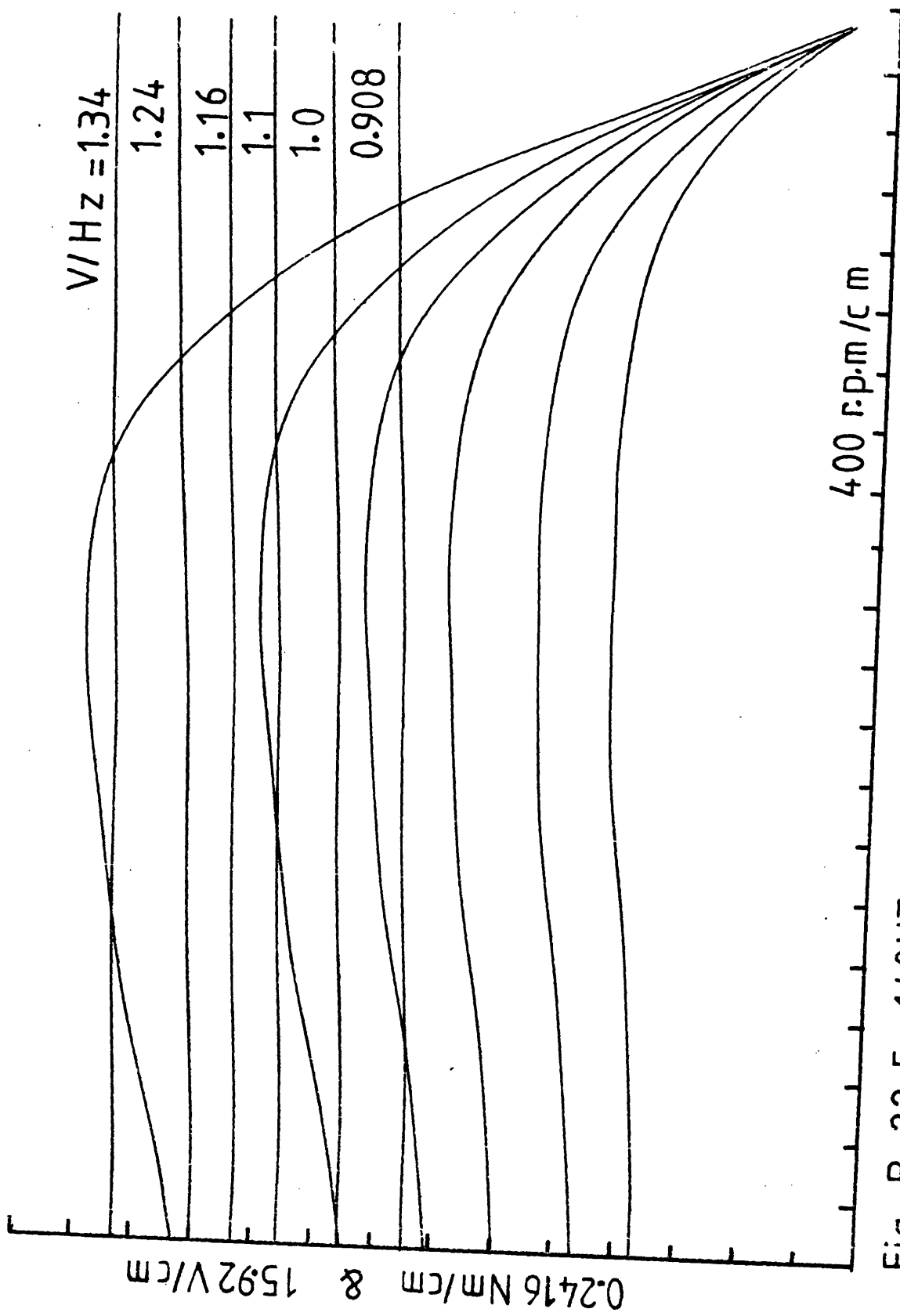


Fig. B. 22 $F = 140 \text{ Hz}$

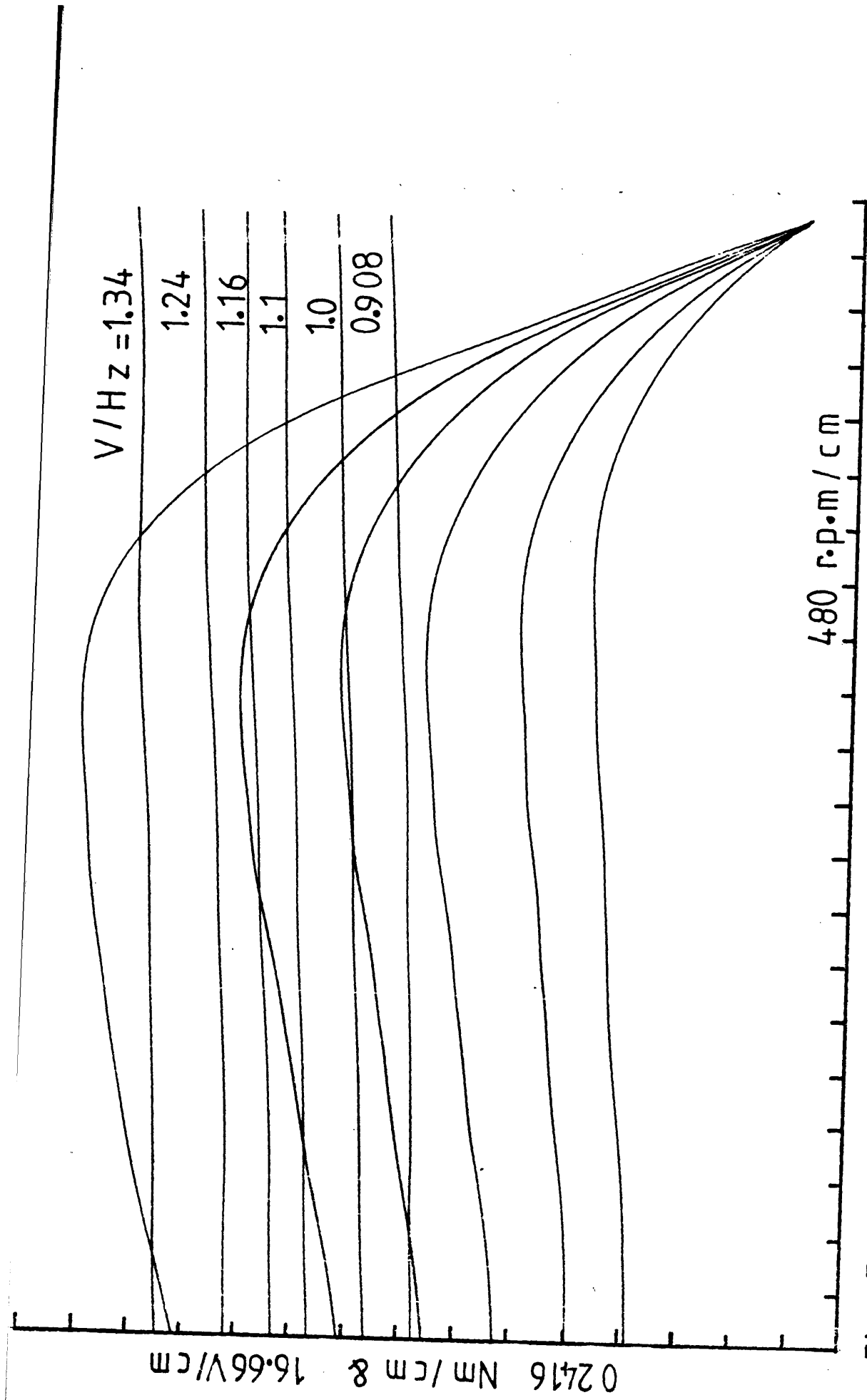


Fig. B. 23 $F=160HZ$

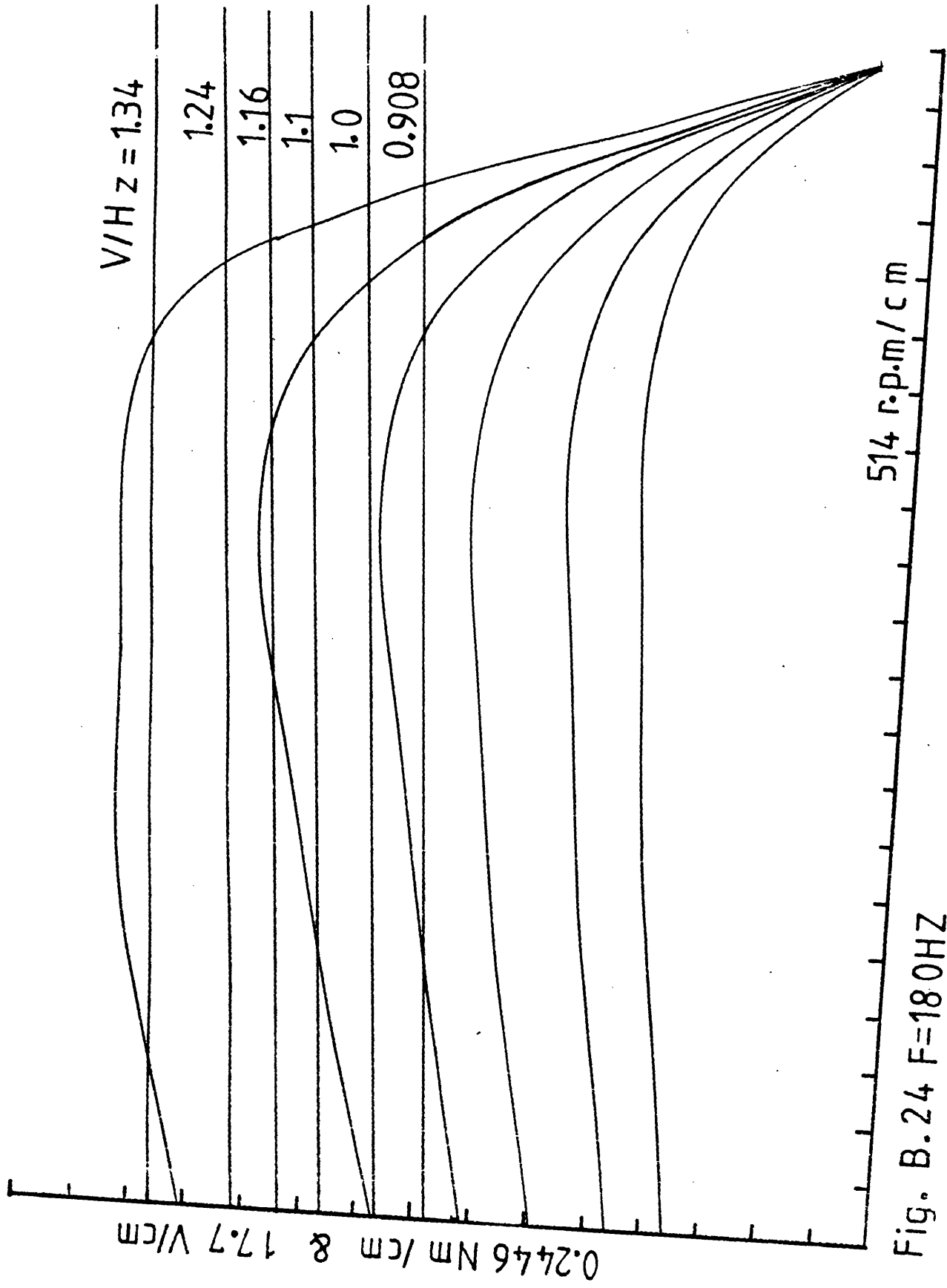


Fig. B.24 $F=180\text{HZ}$

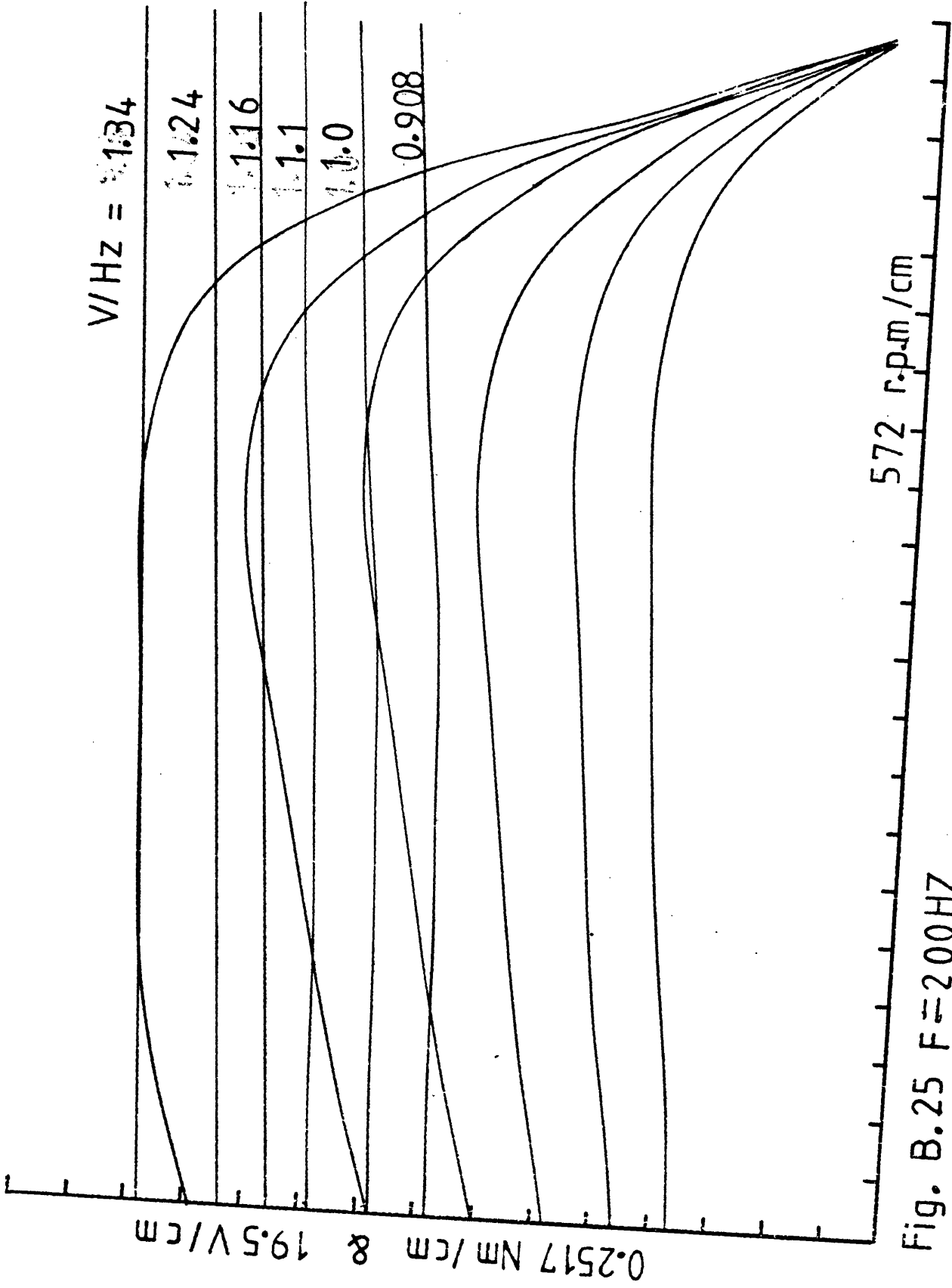


Fig. B.25 $F=200\text{HZ}$

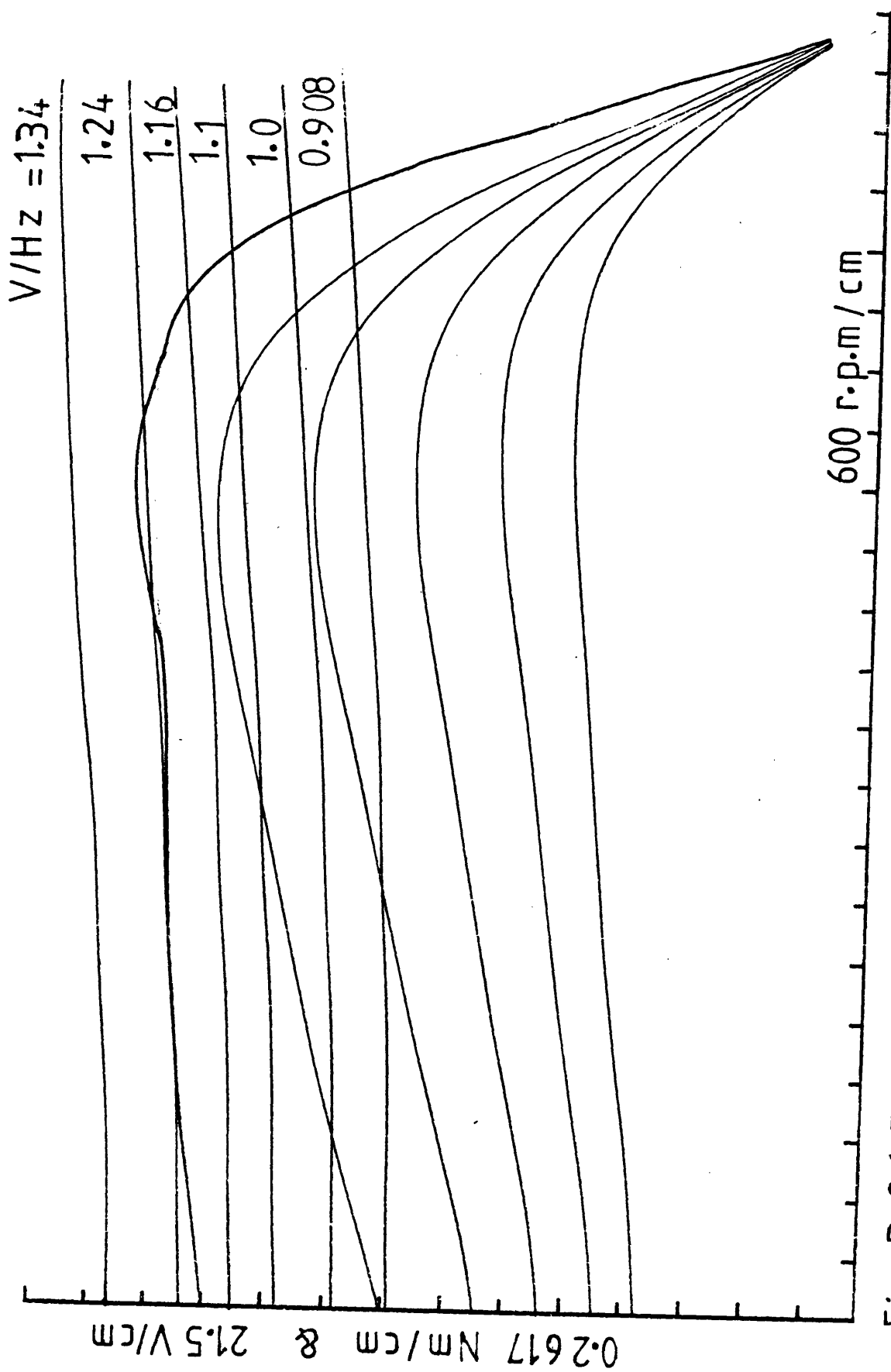


Fig. B.26 $F=220 \text{ HZ}$

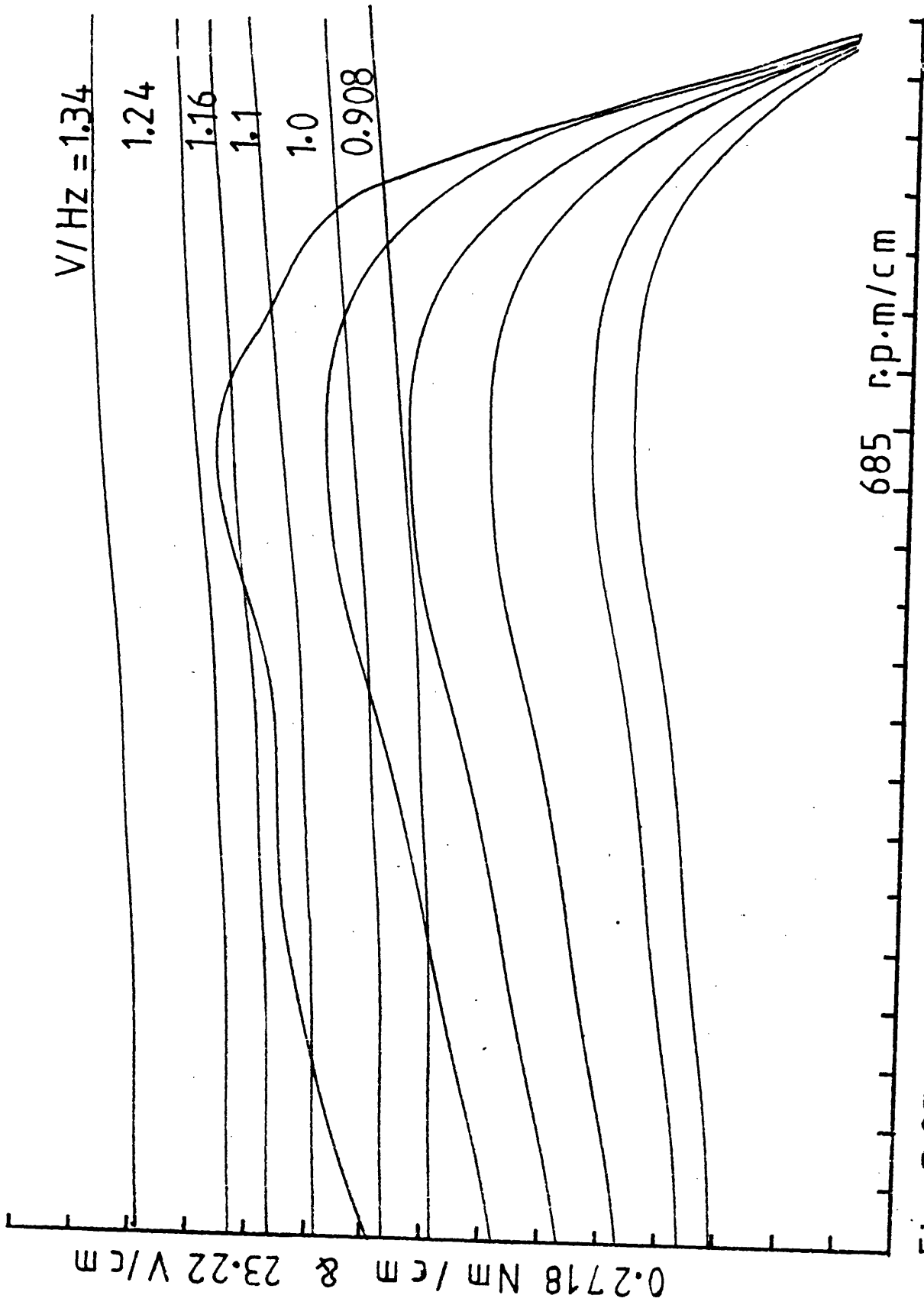


Fig. B.27 F = 240HZ

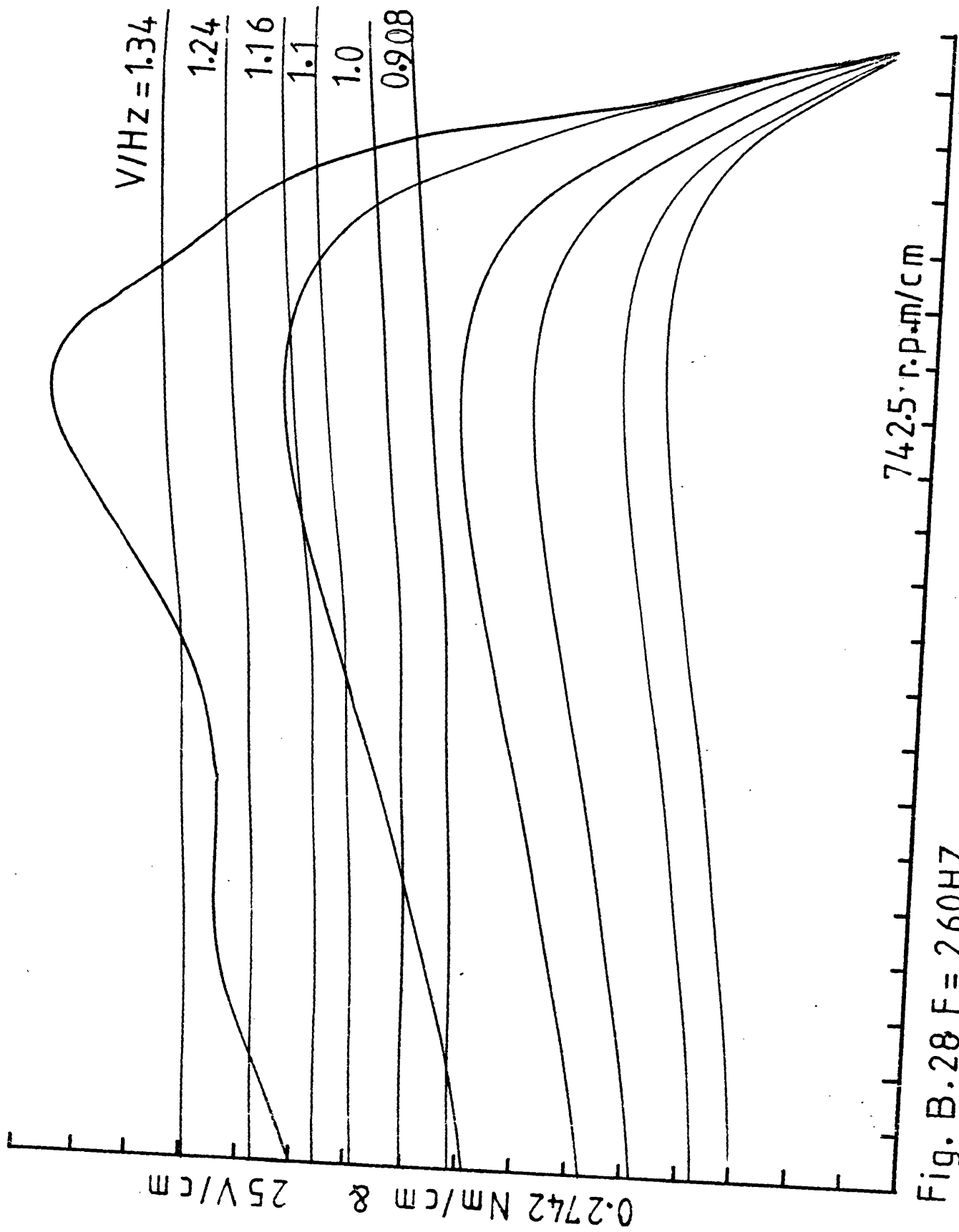


Fig. B.28 F = 260HZ

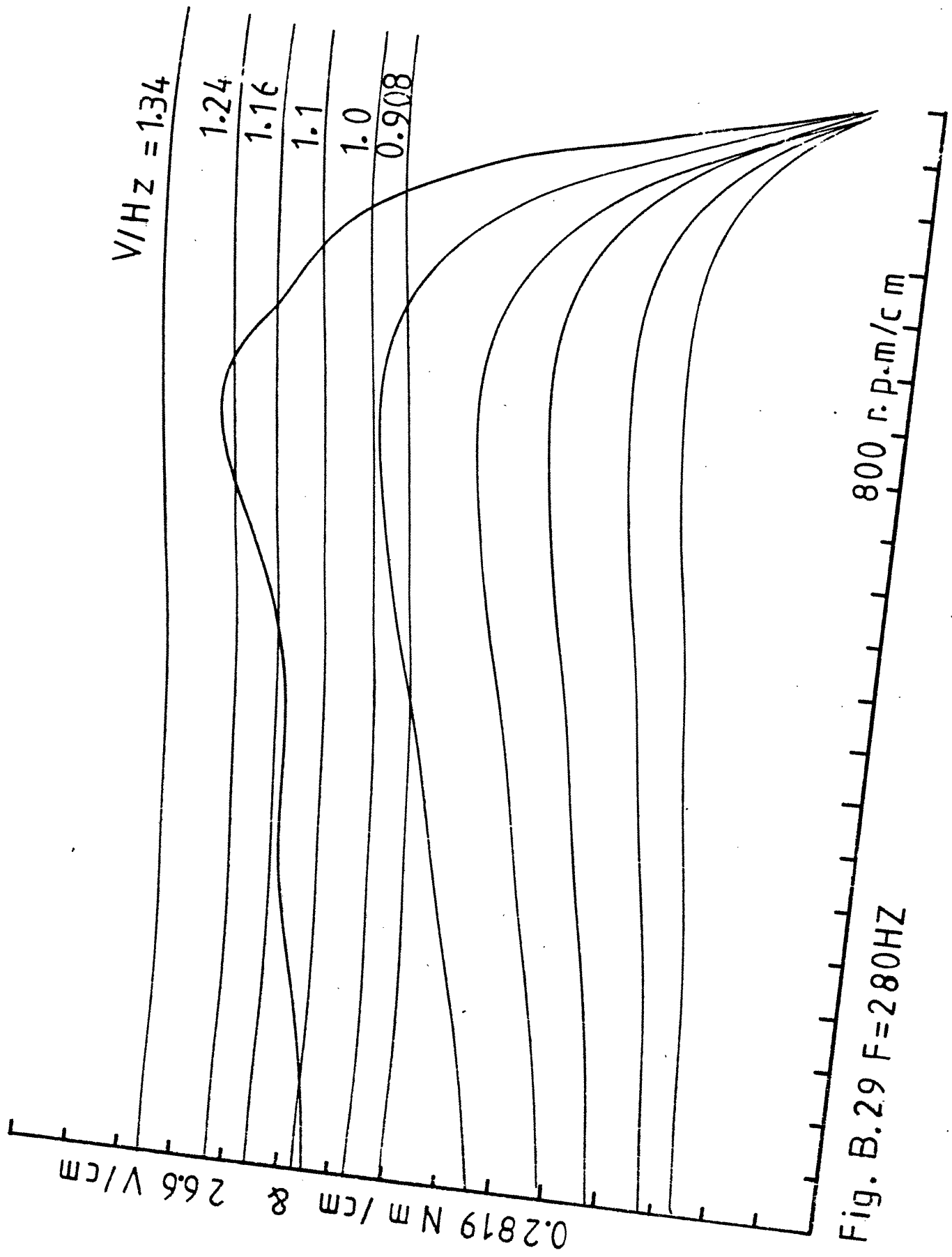
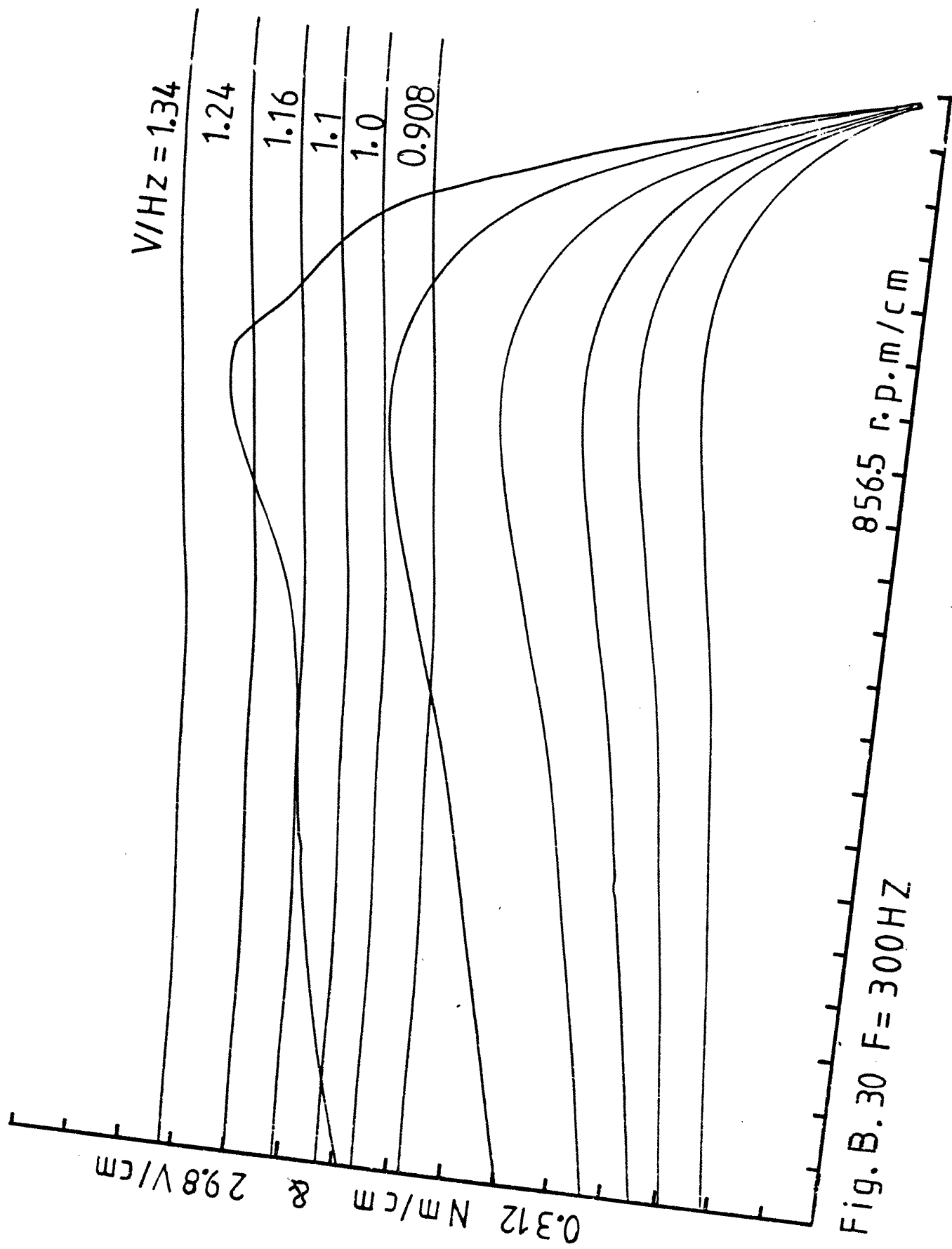


Fig. B.29 $F=280\text{HZ}$



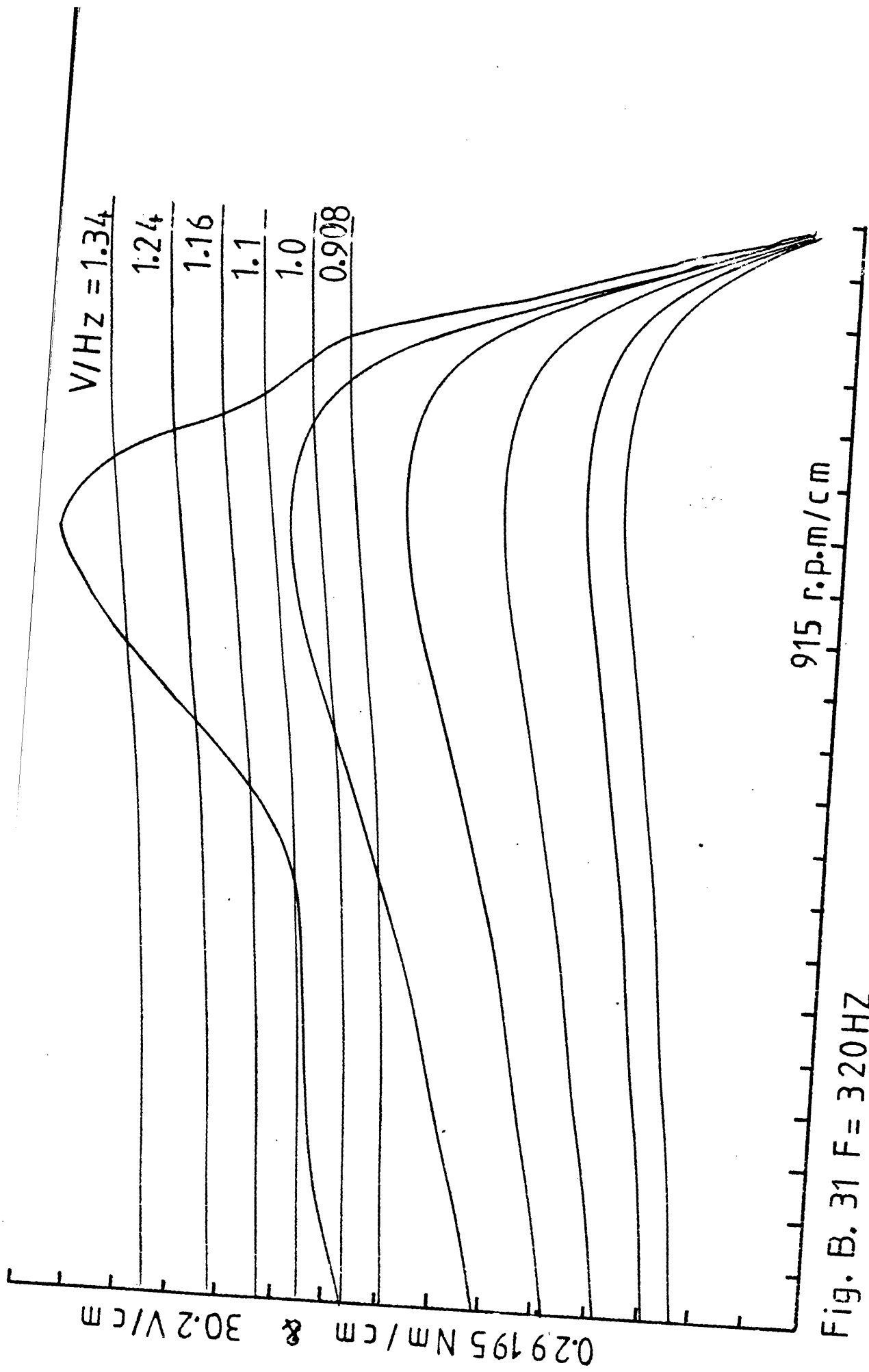


Fig. B. 31 $F = 320 \text{ HZ}$